Wettability Characterization Using Streaming Potential Measurements

Abdulkareem Alroudhan

Imperial College London

Department of Earth Science and Engineering

Supervised by

Prof Matthew D. Jackson

Dr Jan Vinogradov

A dissertation submitted in fulfilment of the requirements for the degree of
Doctor of Philosophy in Earth Science and Engineering of Imperial College London
and the Diploma of Imperial College London
September 2015

Declaration

I declare that this thesis, **Wettability Characterization Using Streaming Potential Measurements**, is entirely my own work under the supervision of Prof Matthew D. Jackson and the co-supervision of Dr Jan Vinogradov. The work was performed in the Department of Earth Science and Engineering at Imperial College London. All published and unpublished material used in this thesis has been given full acknowledgement. This work has not been previously submitted, in whole or in part, to any other academic institution for a degree, diploma, or any other qualification.

Abdulkareem Alroudhan

Department of Earth Science and Engineering

Imperial College London

© 2015 by Abdulkareem Alroudhan.

The copyright of this thesis rests with the author and is made available under a Creative Commons Attribution Non-Commercial No Derivatives licence. Researchers are free to copy, distribute or transmit the thesis on the condition that they attribute it, that they do not use it for commercial purposes and that they do not alter, transform or build upon it. For any reuse or redistribution, researchers must make clear to others the licence terms of this work

Abstract

The surface charge of carbonate minerals, which is also expressed in terms of the zeta potential, plays a key control on reservoir wettability, and changes in the zeta potential have been invoked to explain wettability alteration and the release of previously trapped oil during controlled salinity waterflooding (CSW). We report a method to characterize the zeta potential of carbonates, based on measurements of streaming potential, which can be used to determine the zeta potential of mineral-brine and oil-brine interfaces within the porous medium. The aim of this project was to determine the effect of total salinity, potential determining ion (PDI) contribution, and wetting state on the zeta potential of limestone.

In the first part, we use the streaming potential method to obtain measurements of zeta potential on intact core samples at typical reservoir brine salinity and composition. We determine the impact on zeta potential of varying the total salinity, and the concentration of the PDIs calcium, magnesium and sulfate. The impact of each PDI was determined over a wide range of concentrations naturally found in sea water, formation brines, and typical compositions used in CSW.

We find that the zeta potential varies identically and linearly with calcium and magnesium concentration expressed as pCa or pMg. The zeta potential also varies linearly with pSO_4. The sensitivity of the zeta potential to PDI concentration, and the IEP (iso-electric point) expressed as pCa or pMg, both decrease with increasing NaCl concentration. We report considerably lower values of IEP than most previous studies, and the first observed IEP expressed as pMg. The sensitivity of the zeta potential to PDI concentration is lower when measured using the SPM compared to the EPM, owing to the differing location of the shear plane at which the zeta potential is defined.

In the second part, we use the streaming potential method to investigate how the zeta potential changes when an oil phase is introduced in the rock sample. We establish a relationship between wettability and the zeta potential. This is done for samples that were aged in the presence and

absence of a brine phase, in order to represent mixed-wet and oil-wet cases. In addition, measurements on non-aged samples were conducted in order to represent the water-wet case. We find that the more oil-wet the system is, the more negative the zeta potential gets with the oil-wet case being the most negatively charged. For the crude oil samples, we find that there is a strong correlation between the Amott Index and the zeta potential.

Our findings suggest that the streaming potential method can be used to assess the impact of water chemistry and wetting state on the surface charge of limestone. The results are directly applicable to wettability characterization and understanding of wettability alteration that may take place during CSW.

Acknowledgement

I would like to thank Professor Matthew D. Jackson for his support and guidance throughout my PhD program. My gratitude is also extended to my co-supervisor Dr Jan Vinogradov who has been a great help for me in the laboratory. I thank Saudi Aramco management for sponsoring me in this study.

I would like to thank my wife for bearing with me throughout the program and my daughter and son for being there.

I would like to thank Professors Martin Blunt and Paul Glover for being my examiners and taking the time to evaluate this document.

List of Publications

Peer-Reviewed Journal Articles

Alroudhan, A., Vinogradov, J., Jackson, M. D. "Zeta Potential of Intact Natural Limestone: Impact of Potential-Determining Ions Ca, Mg and SO_4" Colloids and Surfaces A: Physicochemical and Engineering Aspects (accepted)

Alroudhan, A., Vinogradov, J., Jackson, M. D. "Wettability Characterisation in Carbonates using Zeta Potential Measurements" (in preparation)

Conference Proceeding Papers

Alroudhan, A., Vinogradov, J., Jackson, M. D. "Zeta Potential of Carbonates at Reservoir Conditions: Application to IOR" Presented at the 18th European Symposium on Improved Oil Recovery. Dresden, Germany, 14-16 April, 2015.

Table of Contents

List of Tables

List of Figures

Glossary

1/10SW	seawater diluted 10 times (also SW10x)
1/20SW	seawater diluted 20 times
1/2SW	seawater diluted twice
25dSW	seawater diluted 25 times
2SW	seawater with twice the sulfate content (also SW2xSO_4)
3SW	seawater with three times the sulfate content
4SW	seawater with four times the sulfate content
A_k	structural force coefficient
AN	Acid Number
API	America Petroleum Institute (oil gravity)
A_t	adhesion tension
BN	Base Number
C_d	Diffuse layer Capacitance
C_s	Stern layer Capacitance
C_{SPM}	Coupling coefficient for measurement of the Streaming Potential Method
CSW/LSW	Controlled/Low Salinity Waterflooding
DIW	De-Ionized water
DLE	Double Layer Expansion
DP	pressure difference
e	elementary charge
EDL	Electrical Double Layer
EKP	Electrokinetic Potential
EOR/IOR	Enhanced/Improved Oil Recovery

EPM	Electrophoretic Mobility (also u_e)
F	Formation factor
FMB	Formation Brine (also FB)
FMT	Formation Tester
h	film thickness (also x)
I_c	conduction current
ICP-AES	Inductively Coupled Plasma Atomic Emissions Spectrometry
IEP	Iso-Electric Point
IHP	Inner Helmholtz Plane
I_{inv}	inverted Amott index
I_{NMR}	NMR-based wettability index
I_o	Amott index to oil
I_s	streaming current
I_u	USBM index of wettability
I_w	Amott index to water
k	Boltzmann constant
k_w	water permeability
K_{sp}	solubility product (also equilibrium constant)
L	capillary straight length
L_c	capillary actual (tortuous) length
MWL	mixed-wet large pores
MWS	mixed-wet small pores
n^0	number density
NaB	NaCl-EQ at 2 mol/L
NaCl-EQ	NaCl in equilibrium with calcite and atmospheric CO_2
NMR	Nuclear Magnetic Resonance

OHP	Outer Helmholtz Plane
OOIC	Original Oil in Place (also OOIP)
$P_{c,ps}$	pseudo-capillary pressure
PDI	Potential Determining Ion
PS experiment	Pair Stabilization SPM experiment
PV	Pore Volume
PZC	Point of Zero Charge
Q_w	excess charge density transported by the flow
RI	Refractive Index
R_{im}	rate of imbibition
SARA	Saturates, Aromatics, Resins, and Asphaltene
SI	Spontaneous Imbibition
S_{oi}	initial oil saturation
S_{or}	residual oil saturation
SPM	Streaming Potential Method
S_r	remaining oil saturation
SW	Seawater
SW0S	seawater with no sulfate
SW1/2S	seawater with half the sulfate content
S_{wi}	initial water saturation
S_{wirr}	irreducible water saturation
T	temperature
t	tortuousity
T_2	relaxation time distribution
t_D	dimensionless time
USBM	US Bureau of Mines

V	voltage
V_{osp}	volume of oil displaced by spontaneous imbibition of water
V_{ot}	total volume of oil displaced by spontaneous and forced imbibition using water
V_p	pore volume (also PV)
V_{wsp}	volume of water displaced by spontaneous imbibition of oil
V_{wt}	total volume of water displaced by spontaneous and forced imbibition using oil
W_{EDL}	Electrostatic energy of interaction
WI_{CSI}	wettability index based on chromatographic separation
W_R	relative pseudo-work of imbibition ratio
z	valence

Greek Symbols

μ	dynamic viscosity
Δ	distance of the shear plane from the Stern plane
ε	electrical permittivity or the dielectric constant
ϕ	porosity
κ	Debye parameter (inverse of the Debye length)
λ_s	structural force decay length
Π	disjoining pressure
$\rho e\ (z)$	electron density
σ_f	fluid conductivity
σ_{rw}	brine-saturated rock conductivity

σ_s	surface conductivity
σ	Interfacial tension (also IFT)
ζ	zeta potential

1. Introduction

1.1. Overview

The solid/water interface is electrically charged (e.g., Hunter, 1981) and this charge can be characterized in terms of the zeta potential. The surface charge on the interface of natural carbonates plays a role in many subsurface processes. For example, the self-freshening often observed when brackish water invades a freshwater aquifer depends on preferential adsorption of aqueous salt species such as Ca and Mg (e.g., Appelo, 1994), while contaminated carbonate aquifers may be remediated through sequestration of the contaminant by co-precipitation with the mineral phase (Meece and Benninger, 1993). Uptake of contaminants such as heavy metals is related to their reactivity as a function of the ionic strength and pH of the aqueous electrolyte (Reeder et al., 2001). The wetting state of carbonate oil reservoirs is believed to be influenced by the zeta potential (Buckley et al., 1998; Gomari et al., 2006), as is the success of enhanced oil recovery by modification of injection brine composition and/or ionic strength (Zhang and Austad, 2006; Yousef et al., 2010). Moreover, solubility of CO_2 in brine as a trapping mechanism in saline aquifers is an important component of carbon capture and storage (Riley, 2010). Compared to sandstones, aqueous CO_2 solubility is greatly enhanced in the presence of carbonate minerals such as calcite (Rosenbauer et al., 2005). The increase in CO_2 concentration has a profound effect on pH (Pokrovsky et al., 2005), which in turn alters the zeta potential of calcite and leads to its dissolution (Eriksson et al., 2007). The zeta potential is also an important control on the use of self-potential measurements to monitor subsurface fluid flow (e.g. Saunders et al., 2008; Gulamali et al., 2011; Jackson et al., 2012a, b).

The zeta potential governs the electrostatic interactions between mineral surfaces and polar species naturally found in the oil phase or added to the water phase (e.g., surfactants). The electrostatic interaction between mineral/water and water/oil interfaces in turn impacts the wettability of reservoir rocks. This is because the interaction will be repulsive when both interfaces have the same surface charge polarity leading to more water-wet conditions. However, electrostatic attraction will lead to a more oil-wet system if the polarity of the surface charge is different (i.e., one interface is negative while the other is positive).

Another observed impact of the electrostatic interaction is through IOR/EOR processes. For example, Controlled or Low Salinity Waterflooding (CSW or LSW) has been shown to lead to systematic increases in oil recovery. Studies conducting these waterflooding experiments have concluded that the effect results from wettability alteration (Zhang and Austad, 2006; Yousef et al., 2010). However, there is no agreement on the processes at the mineral surface leading to this increased recovery (e.g., Romanuka et al., 2012).

This is due in part to the fact that the Controlled/Low salinity effect in carbonates is much more complex than in clastic rocks. Carbonate rocks are much more reactive than their clastic counterparts as they are more sensitive to the water composition (e.g., Morse, 1986). Also, carbonate reservoirs include minerals such as calcite, dolomite and anhydrite that are much more soluble than quartz; the main mineral in sandstone. Regardless, both the calcite surface charge and the low salinity effect are impacted by the water chemistry. A clean calcite surface should have a charge that reflects the water composition. Thus, if wettability alteration is the responsible mechanism for the low salinity effect, then changes in the water chemical composition must reflect changes to the surface charge.

However, previous zeta potential measurements on calcite were conducted using commercially available zetameters, which employ powdered samples. Most of these reported measurements were done on diluted brines and mostly using synthetic calcite. Hence, the porous medium is lost and representing the distribution of multiphase fluids is not possible. Moreover, zetameter measurements at elevated temperatures are limited to 80^{o}C, which is lower value than most reservoirs (90-110^{o}C).

The advantage of the Streaming Potential Method (SPM) employed here is that it represents the porous medium. A full description of the system‟s surface charge is possible because the SPM can be conducted with the reservoir appropriate pressure, temperature, brine composition, and wetting state. Previous streaming potential measurements were conducted using saline brines (e.g., Vinogradov et al., 2010) but mainly on sandstones. There is a difference between sandstone and limestone rocks, which is that divalent ions (e.g., Ca and Mg) are considered to be potential determining ions (PDIs) as they have the capability to alter the surface charge of limestone but not sandstone where the surface charge is only a function of the pH and total salinity of the brine. In a proof of concept study, Jackson and Vinogradov (2012) showed a relationship between

electrokinetic data obtained using SPM and the wetting state of carbonates suggesting that SPM could be used to study wettability and wettability alteration processes such as low salinity waterflooding. Streaming Potential Method is much quicker in the laboratory compared to traditional methods of wettability characterization (e.g., Amott index).

Given the importance of understanding the surface charge in carbonates for reservoir characterization and EOR processes such as CSW and surfactant waterflooding, it is apparent that there is a need for measurements at reservoir conditions on limestone rocks. In this study, we use the SPM to determine the zeta potential in intact limestone plugs and understand how it is affected by the PDI content of the brine and the wetting state of the mineral surface.

1.2. Aims and Objectives

The broad aim of this study is to develop a better understanding of the electrokinetic behaviour of limestone and how that behaviour is affected by changing water chemistry and the wetting state. The aims are achieved through extensive and systematic streaming potential and brine composition measurements. The specific objectives are to measure the zeta potential of intact carbonate samples saturated with:

1) NaCl-only brines in order to assess the effect of total salinity
2) Brines with only one PDI in order to assess the PDI‟s impact
3) Brines with multiple PDIs in order to assess different compositions, which include:
    a. Typical formation brines found in hydrocarbon reservoirs
    b. Seawater
    c. Brine compositions used in low salinity waterflooding
4) Brine and oil to represent:
    a. Oil-wet conditions
    b. Mixed-wet conditions

1.3. Thesis Organization

Chapter Two starts by briefly reviewing the concept of wettability: its definition and impact on macro-scale fluid flow properties, followed by the classification of wetting systems. Then, the various wettability measurements, including both traditional and non-traditional methods, are described and critiqued. The process of wettability alteration is discussed as a function of the properties of both the oil and water phases considering the resulting interactions between these phases and the rock. The chapter ends with a discussion of the thin wetting film; which includes the components of the disjoining pressure that leads to film stability or the lack thereof.

Chapter Three is dedicated to the theory of the surface charge and streaming potential. It starts by discussing the origin of the surface charge on the calcite-water and oil-water interfaces. Later, the development of the electrical double layer is described. Then, a discussion of the establishment of the streaming potential, its measurement, and the zeta potential interpretation follows. The chapter ends with a review of the published zeta potential measurements for the calcite-water and oil-water interfaces.

Chapter Four reports the results of single-phase brine streaming potential measurements on limestone. These results cover the impact of the total salinity and each PDI on the zeta potential. They also cover the zeta potential for a typical formation brine and natural seawater. Moreover, they include the zeta potential of compositions used in low salinity waterflooding. The chapter conclusions are directly applicable for understanding of the low salinity waterflooding and wettability alteration mechanisms, which include the PDI concentrations needed to reverse the polarity of the calcite surface charge as well as understanding the impact on surface charge of two different reported approaches to CSW.

Chapter Five reports results demonstrating the relationship between wetting state and the zeta potential. These results include synthetic and crude oil. They are of aged samples that represent oil-wet and mixed-wet conditions. The impact of each wetting state is considered and the implications on the electrostatic interaction (and the thin film) are evaluated.

Chapter Six includes the conclusions drawn from this study and recommendations for future work.

2. Wettability Overview

2.1. Introduction

Wettability is one of the main characteristics of the petroleum system influencing hydrocarbon field development, since it governs the distribution of fluids within the porous medium. Some enhanced oil recovery schemes are a good example of this: low salinity water flooding has been suggested to alter the wettability to be more water-wet or mixed-wet, which allows more oil to be released from the rock surface (Morrow and Buckley, 2011).

Wettability has a major impact on fluid flow and electrical properties of the rock-fluids system. It influences the capillary pressure, relative permeability, water flood behaviour, and ultimate oil recovery (Anderson, 1986a). Consequently, the wetting state effectively controls the volumes and ratios of the produced fluids, as well as their residual saturations.

Wettability is defined as the ability of a fluid to spread over the surface of a solid in the presence of another fluid (Craig, 1971). In porous media, the wetting phase will be in contact with the pore surface (rock) while the non-wetting phase will occupy the centre of the pore. Wettability is dependent on the chemical and physical properties of the rock/water/hydrocarbon system such as the brine chemistry, rock mineralogy, oil composition, temperature, and pressure (Anderson, 1986a). The saturation history of the reservoir also impacts the wetting state (Brown and Neustadter, 1980).

An intense debate exists about the wettability condition that yields the highest recovery. Kennedy et al. (1955) reported neutral wettability (very weak water wetness) whereas and Owens and Archer (1971) reported water-wet rocks to correspond to best recovery. However, when considering the ultimate recovery, Salathiel (1973) argued that it is highest in mixed wetting conditions where surface drainage can be maintained. Jadhunandan and Morrow (1995) concluded that weakly water-water conditions result in the highest recovery in a systematic suite of 50 core floods.

There is a general acceptance of the default wetting states of reservoirs worldwide. Carbonate reservoirs, which make more than half of the world‟s oil reserves and considerable gas reserves (Roehl and Choquette, 1985; Akbar et al., 2001) tend to be oil-wet (Chilingar and Yen, 1983;

Okasha et al., 2007; Anderson, 1986a) whereas sandstone reservoirs tend to be water-wet (Anderson, 1986a). In reality, this is not the case as a single reservoir is may have a range of wetting states.

Multiphase flow in subsurface reservoir rock is controlled by the pore-scale distribution of the fluid phases, which in turn depends on the wettability of the rock mineral surfaces. The wettability of reservoir rock is typically characterised in the laboratory using direct measurements of contact angle or adhesion on smooth surfaces of the mineral(s) of interest (e.g., Amyx, 1960; Buckley and Morrow, 1990), although contact angles interpreted from x-ray computed micro-tomography (μ-CT) images of intact rock samples have recently been reported (Andrew et al., 2014). Smooth surface measurements fail to preserve the complex pore and mineral surface topology and their relevance to pore-scale wetting behaviour is not clear (e.g., Morrow, 1975).

Wettability may also be indirectly characterised using measurement of spontaneous and forced displacement of one fluid phase by another, in rock samples recovered from the reservoir and brought to surface (e.g., Anderson, 1986b). Approaches such as the Amott index (Amott, 1959) and the US Bureau of Mines (USBM) method (Donaldson et al., 1969) utilise intact rock samples so the pore and mineral surface topology is preserved, but the pore-scale wetting behaviour is inferred rather than directly quantified (e.g., Amott, 1959; Donaldson et al., 1969). Moreover, the displacement experiments can be time consuming, requiring a complete cycle of drainage and imbibition to characterise the wetting behaviour of each fluid phase. Other indirect approaches include imbibition rate (Morrow et al., 1994; Ma et al., 1999) and chromatographic separation index (Strand et al., 2006).

The key failing of these direct and indirect approaches to characterise reservoir wettability is that the experiments must be conducted in the laboratory; there is no downhole tool that can be used to determine wettability *in-situ*, although some progress has been made in interpreting nuclear magnetic resonance (NMR) logs to determine wettability (Guan et al., 2002; Al-Mahrooqi et al., 2003, 2006). Laboratory experiments often fail to capture properly the wetting state of the reservoir, because sample preservation is challenging and wettability restoration may fail. Moreover, the small number and volume of samples brought to surface results in sparse wettability data that fail to capture spatial variations present within the reservoir (e.g., Anderson 1986a, b;

Hamon, 1997). Such wettability variations can have a significant impact on production (e.g., Parker and Rudd, 2000; Jackson et al., 2005).

In order to develop a better understanding of the wetting phenomenon, factors affecting the ability of competing fluids to wet a certain surface will be discussed. This will be an introduction to the physical mechanisms affecting the wettability since this phenomenon is best described at the microscopic level.

2.2. Physical Controls

2.2.1. Surface and Interfacial Tension

Any wetting state can be described in terms of the relative adhesion of a fluid compared to another fluid on a surface. The adhesion tension originates from the surface tension (ST), which can be described as the tendency of a liquid to occupy a minimum surface area for a given volume. It is a stress at the surface between a liquid and its vapour that is caused by differences in the molecular forces in the vapour and those of the liquid and by an imbalance of these forces at the interface. The interfacial tension (s) is the stress resulting when two immiscible phases are in contact. The surface tension of a pure substance decreases with temperature. The system loses energy through the adhesion work when a fluid wets a solid (Cuiec, 1991).

2.2.2. Adhesion Tension

Adhesion tension, A_t, is the tension between two unlike surfaces and is the difference in tension of each of the fluids to the surface of the solid surface (Amyx, 1960):

$$A_t = \sigma_{so} - \sigma_{sw,} \tag{2.1}$$

where σ_{so} = interfacial tension between solid and oil, σ_{sw}= interfacial tension between solid and water, σ_{wo}= interfacial tension between water and oil. The interface of two immiscible fluids intersects the solid surface, for example, the wall of a capillary tube, at an angle, θ, which is described by the Young-Laplace equation (e.g., Tiab and Donaldson, 2004):

$$\cos\theta = \frac{\sigma_{so} - \sigma_{sw}}{\sigma_{wo}}. \quad (2.2)$$

This angle is called the contact angle and is conventionally measured through the fluid of the higher density (Fig. 2.1a). When $\sigma_{so}>\sigma_{sw}$ and $0< \theta <90^o$, the adhesion tension is positive and the surface is water wet. When $\sigma_{so}<\sigma_{sw}$ and $\theta >90^o$, the adhesion tension is negative and the surface is preferentially wet by oil. The final scenario is when $\sigma_{sw} = \sigma_{so}$, the adhesion tension is equal to zero and the contact angle is 90^o. In this case, the surface is equally wet by the two fluids (water and oil). Table 2.1 shows the range of contact angle for each wetting state. Figure 2.1b shows when $\theta = 0^o$ leading to total spreading of water on the surface.

Table 2.1. Contact angle relation to the wetting state. After Amyx (1960).

Wetting State	Contact angle to water (degrees)
Oil-wet	105-180
Neutral-wet (intermediate)	75-105
Water-wet	0-75

Fox and Zisman (1952) considered a critical surface tension σ_c corresponding to the value of σ_{wo} for which $\cos\theta = 1$ in Equation (2); liquids for which $\sigma_{wo}>\sigma_c$ make finite contact angles with the solid surface, but liquids for which $\sigma_{wo}<\sigma_c$ will spread indefinitely. This critical tension is equal to the adhesion tension of Equation (1), which is the numerator of Equation (2). Irrespective of whether a finite contact angle exists, the wettability can be described as the loss of free energy per unit surface area during wetting (Briant and Cuiec, 1971).

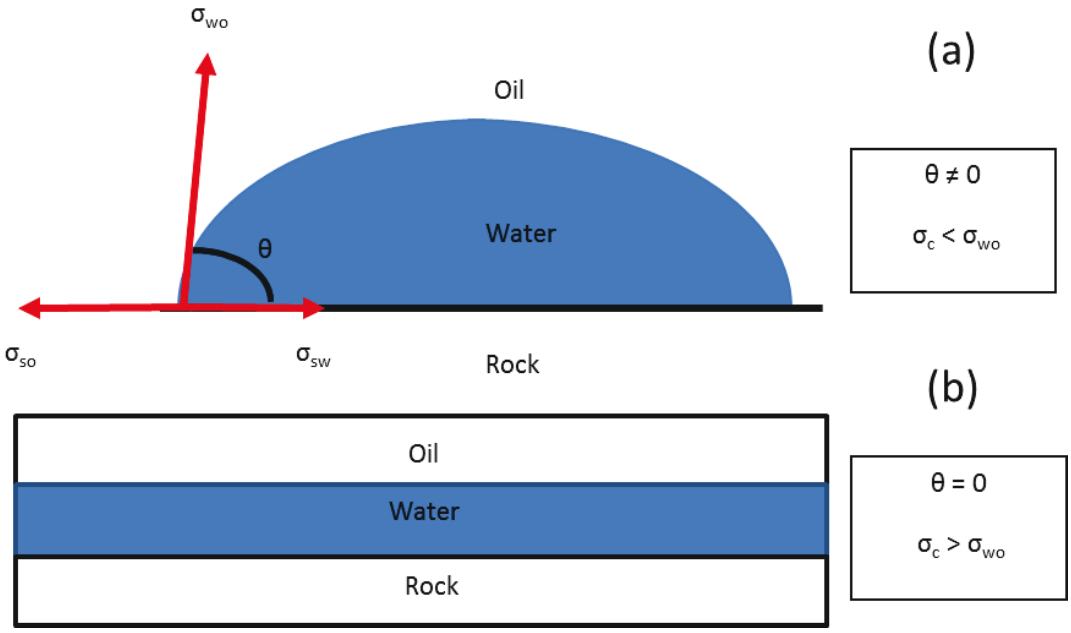

Figure 2.1: The equilibrium of forces at a water-oil-rock interface. The interfacial tension between water and oil is σ_{wo}, oil and rock is σ_{so}, water and rock is σ_{sw}. (a) partial wetting characterized by a contact angle (θ) development. (b) adhesion tension is higher than the (oil-water) interfacial tension leading to complete wetting via the spreading of water over the rock surface. Modified after Amyx (1960).

2.3. Mode of Occurrence

Wettability modes are recognized as either homogeneous or heterogeneous. Homogeneous wetting states have all pores of the same preference to a phase (wetting) in presence of another (non-wetting). Heterogeneous wetting states have pores or parts of pores being wetted with one phase and other pores being wetted with the other phase.

2.3.1. Homogeneous Wetting States

Previously, it was assumed that the wetting state of the reservoir is a water-wet condition (e.g., Anderson, 1986a). This was explained by the fact that the majority of rocks were deposited under water, which means it was the first fluid to contact the grains of the rock before hydrocarbons migrated at a later stage. Later, it was discovered that some reservoirs are strongly oil-wet and the adsorbed hydrocarbon layer, on the rock surface, was only removed by firing, after several solvents could not remove it (Anderson, 1986b).

In a strongly water- or oil-wet system, the wetting phase will coat the grains of the rock and be in contact with most of them at all times while the non-wetting phase is kept away from the rock matrix. Intermediate or neutral wettability is another homogeneous mode. It occurs when all the pores of the rock have equal wetting to both fluids. Weakly wetting states comprise the different shades going from the neutral towards the strongly wetting states, which for the weakly water-wet case will have contact angles range (60^o-90^o) and (100^o-150^o) for the weakly oil-wet case (Suicmez et al., 2007). In oil/gas industry, the use of the neutral and weakly wetting state terms is sometimes interchangeable if the reservoir does not show a strong wetting preference, which reflects the lack of an agreed standard.

It is important to distinguish neutral wettability from the (fractional or mixed) states. Neutral implies the mineral‟s lack of preference to either fluid. Fractional and mixed wetting states refer to the variety of wetting states within the rock porosity framework (Anderson, 1986b).

2.3.2. Heterogeneous Wetting States

Brown and Fatt (1956) introduced fractional wettability, where parts of the pores are water-wet while others are oil-wet, thus, moving away from the simple view that the wettability occurrence is always uniform. They did not assign any pore size cut off for when the pore will be wetted by either phase. Fractional wetting is typical with rocks that have minerals of different surface chemical properties (Bortolotti et al., 2010).

Salathiel (1973) introduced mixed wettability where smaller pores are water-wet and bigger pores become oil-wet and a continuous path for oil flow is established. Thus, it is related to the distribution of connate water within a core. Mixed-wetted rocks have lower irreducible water saturations (S_{wirr}) and residual oil saturations (S_{or}) because flow is allowed for both phases down to very low saturation levels. Another mixed-wetted systems characteristic is that the relative permeability to oil is reasonably high even at low oil saturations (Anderson, 1986a).

Dixit et al. (2000) further divided mixed wettability into two modes. Mixed-Wet Large (MWL) is where the largest pores are oil-wet and the smallest pores are water-wet, as Salathiel (1973) hypothesized. Mixed-Wet Small (MWS) is where the smallest pores are oil-wet. Dixit et al. (2000) modelled an Amott test and a USBM test (see measurements section) for both mixed-wet cases (MWL and MWS) and noticed a discrepancy between both indexes when the assumptions about

the pore size distribution and the strength of wetting within each fraction were changed. Kovscek et al. (1993) introduced the mixed-oil-wet pores, in which within a single pore, parts of it are oil-wet while the corners remain water-wet.

2.4. Methods of Wettability Measurement

There are direct and indirect methods of wettability assessment. There is only one direct method: the measurement of contact angle, but there are a number of ways of measuring it such as the Sessile-Drop and the Wilhelmy plate methods (e.g., Tiab and Donaldson, 2004).

The indirect methods include the Amott and USBM indexes, the imbibition rate, chromatographic separation, and NMR. The Amott and USBM methods are based on measurements of spontaneous and forced imbibition volumes, which are related to the wetting state. The imbibition rate method relates how much a sample spontaneously imbibes water and relates it to the wetting state. The common restrictions of these methods are that they are time consuming and can only be done in the laboratory.

2.4.1. Contact Angle

In the "Sessile Drop Method", the contact angle is measured optically in a system containing a flat surface of the mineral, on top of which a drop of fluid resides within another fluid. Another method is the Wilhelmy plate, which measures the advancing and receding contact angles giving hysteresis information (e.g., Tiab and Donaldson, 2004). The advancing angle represents the waterflooding phase whereas the receding angle represents the oil charging or migration into the reservoir. The plate is dipped in one phase and then lowered into the other phase, and the measured contact angle is the advancing angle. The plate is then moved in the opposite direction and passes through the interface again, giving the receding contact angle (Andersen et al., 1988). These two angles might define a hybrid system when one is higher than 90^o (water-wet) and the other is lower than 90^o (oil-wet).

The main advantage of this method is that it is the only direct method of measuring the wetting state of the mineral surface. The main disadvantage is that it is not representative of the porous media because it does not account for surface roughness (Morrow, 1975). Andersen et al. (1988) suggested the dynamic Wilhelmy plate method to be used for heterogeneous surfaces but it is

difficult to get to equilibrium contact angle on smooth surfaces. Another shortcoming is the rock/brine/oil system cannot be represented by a single angle (Hirasaki, 1991a), since a multitude of them exist in any single reservoir due to heterogeneity in (surface roughness, different mineralogy, gradients in crude oil compositions, etc.), which lead to a range equilibrium contact angles.

2.4.2. Amott Method

The Amott method for wettability evaluation is based on spontaneous imbibition and forced displacement of oil and water from cores (Amott, 1959). It depends on capillary pressure and microscopic displacement efficiency. This method measures how easily the wetting phase spontaneously displaces the non-wetting phase, and then, compares that to the total displacement after forced imbibition is finished (Anderson, 1986b). The test will give the average wettability of the core, after accomplishing the outlined procedure (Amott, 1959):

1. The test starts at the residual oil saturation (S_{or}), this is established by displacement of the oil.

2. The core is immersed in oil for 20 hours, and the amount of water displaced by spontaneous imbibition of oil is considered V_{osp}. (Step 1on Figure 2.2)

3. Then, water is displaced to the irreducible saturation (S_{wirr}), the total amount of water displaced is called V_{ot}, which includes both water volume displaced by imbibition and forced displacement. (This is Step 2 on Figure 2.2)

4. The core is immersed in water for 20 hours, and the amount of oil displaced by spontaneous imbibition of water is considered V_{wsp}. (Step 3 on Figure 2.2)

5. The remaining oil is then displaced by water to S_{or} and the total amount of oil displaced is called V_{wt}, which includes oil volume expelled by both imbibition and forced displacement. (Step 4 on Figure 2.2)

The Amott wettability method is expressed as the ratio of saturation change through spontaneous imbibition to the saturation change by both spontaneous and forced imbibition (Amott, 1959):

$$I_w = \frac{V_{wsp}}{V_{wt}} \tag{2.3a}$$

$$I_o = \frac{V_{osp}}{V_{ot}}, \tag{2.3b}$$

where I_w is the ratio of displacement-by-water and I_o is the ratio of displacement-by-oil. The indices range from 1 for strongly-wetted samples to 0 for weakly-wetted samples. Water-wet cores are characterized by a positive displacement-by-water ratio (I_w), and a zero value for the displacement-by-oil ratio (I_o). Neutral wettability is distinguished by a value of zero for both ratios. Oil-wet cores are characterized by a value of zero for the displacement-by-water ratio (I_w), and a positive displacement-by-oil ratio (I_o). Generally, a strong wetting preference for either fluids is indicated by a ratio approaching one, and a weak preference by a ratio approaching zero. Mixed-wetting conditions (discussed in Section 2.3.2) are characterized by non-zero ratios because usually both phases spontaneously imbibe.

The original Amott method used an arbitrary time period of 20 hours for the spontaneous oil and water imbibition. This time duration is not enough for low-permeability samples or high viscosity systems. Results reported in the literature show that imbibition can take several hours to more than two months to go to completion.

The main disadvantage of the method is its insensitivity near the neutral wetting state. Also, it lumps all systems exhibiting high index to water as very strongly water-wet, not discriminating between what is strongly versus what is weakly water-wet (Ma et al., 1999). This is because in the contact angle range around (60-120^o) neither fluid will spontaneously imbibe in the plug (Anderson, 1986b).

The advantage of this method over other methods is that it is sometimes sensitive to heterogeneous wetting states (fractional and mixed). This is because both water and oil freely imbibe into the sample. This will be reflected by positive displacement-by-water and displacement-by-oil ratios indicating the non-uniform wetting state of the system. The Amott index to water will be used in Chapter 5 to quantify wettability of rock samples.

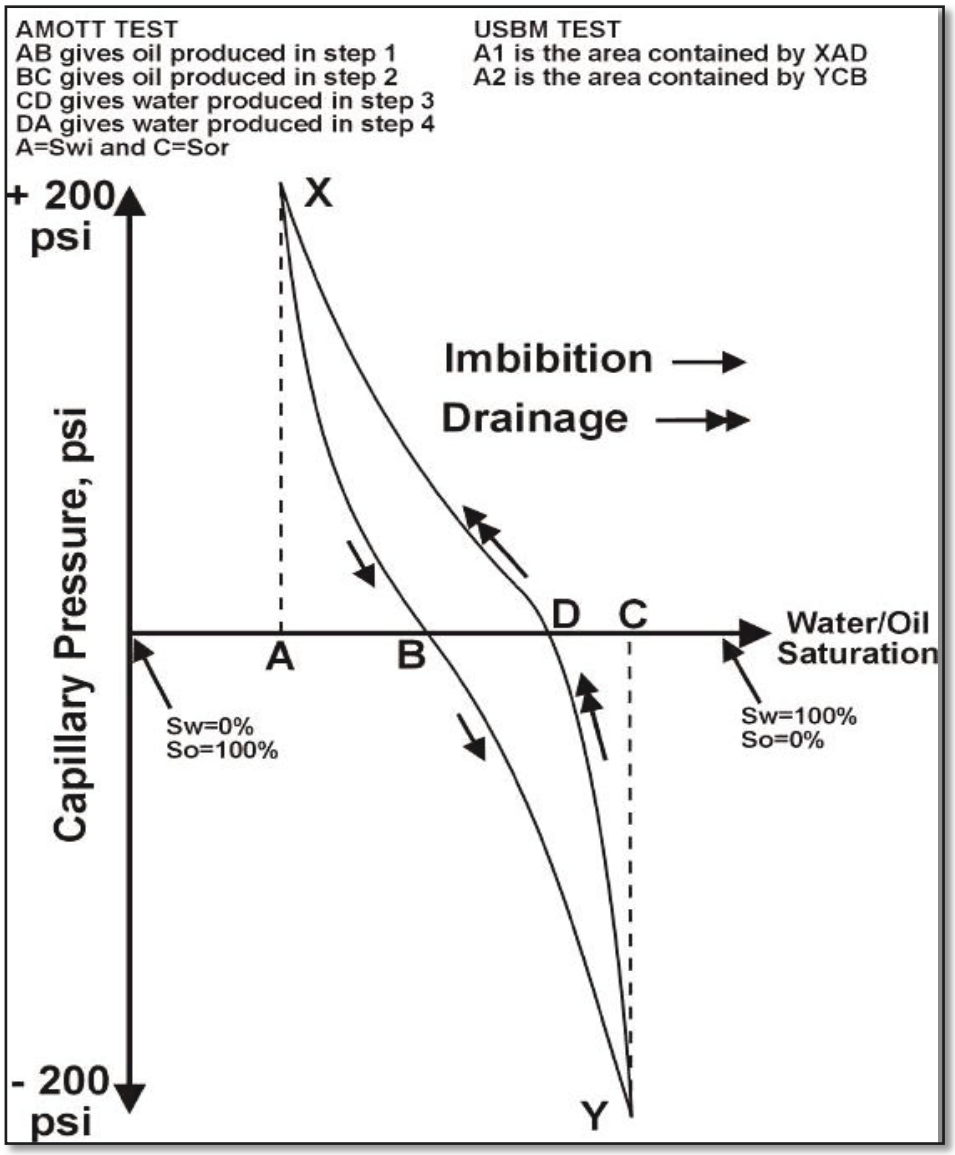

Figure 2.2: Steps for the Amott and USBM tests. (After Core Lab, 1983).

2.4.3. USBM Method

The United States Bureau of Mines (USBM) wettability index also depends on capillary pressure and microscopic displacement efficiency. It is calculated from the areas under the drainage and imbibition capillary pressure curves, which are acquired by alternately displacing water and oil from core plugs at capillary equilibrium (Donaldson et al., 1969). These areas represent the energy needed for fluid displacement. Less energy is needed when a wetting fluid is displacing a non-wetting fluid than the other way around, thus, indicating the wetting state. Thus, these areas under

the curves are a direct indicator of the degree of wettability. This index (I_u) uses the logarithm of the area ratio of oil displacing water, A_1 (from S_{wirr} to S_{or} in Figure 2.3), to water displacing oil, A_2 (from S_{or} to S_{wirr}) as follows:

$$I_u = log \frac{A_1}{A_2}. \tag{2.4}$$

Increasing positive values to +∞, means increasing water wetting to strongly water wet as A_2 has a value of zero. Increasing negative values to -∞ means increasing oil wetting characteristics to strongly oil wet as A_1 value goes to zero. Neutral or equal wettability is represented by a zero value. For a water-wet core, A_1 is greater than A_2, and I_u is positive as can be seen in Figure 2.3. For an oil-wet core, A_1 is smaller than A_2, and I_u is negative.

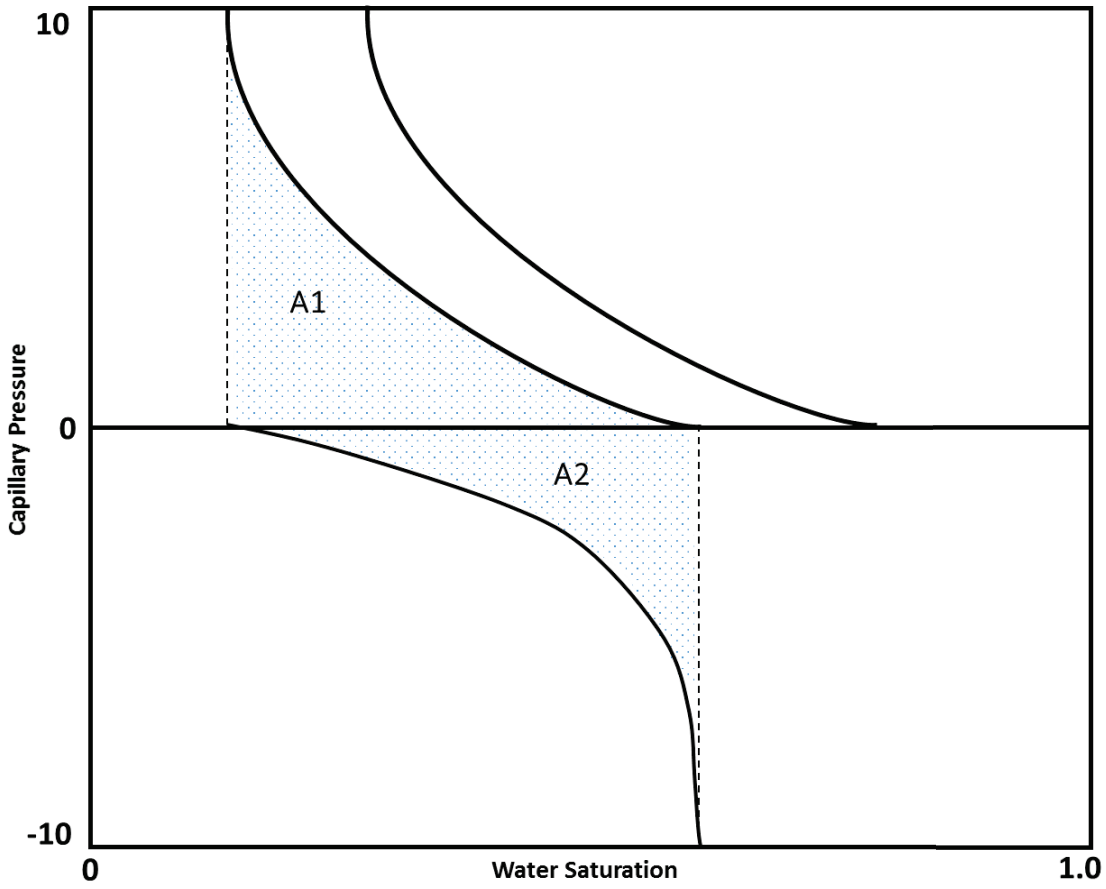

Figure 2.3: Capillary pressure data for the USBM method. (After Core Lab, 1983).

A limitation of the USBM is that only 3 options are available (water, neutral, or oil wetting states) with nothing in between. An advantage that USBM test has is for systems that do not imbibe either oil or water in significant quantities since neither imbibition rate (described below in Section 2.4.4) nor Amott method help in this case (Ma et al., 1999).

2.4.4. Imbibition Rate Method

Morrow et al. (1994) proposed a test that uses the early imbibition rate to characterize core wettability due to the weaknesses of the common Amott and USBM methods. The spontaneous imbibition part of the Amott test is measured by the volume of oil produced without considering the rate of imbibition. The imbibition rate method has the advantage of differentiating the degrees of water-wet systems (Zhou et al., 2000), since samples imbibing water at a faster rate are considered to have higher water-wetness compared to samples with slower rates, which are considered to be of a weaker water-wetness, even when both samples show the same endpoint saturations. The imbibition recovery R_{im} is (Ma et al., 1999):

$$R_{im}(t) = \frac{1}{V_p(1 - S_{wi})} \int_0^t \frac{C}{\sqrt{t}} = \frac{2C\sqrt{t}}{V_p S_{oi}}, \tag{2.5}$$

where C is a constant, V_p is pore volume, and S_{wi} and S_{oi} are the initial saturations of water and oil respectively. Figure 2.4a shows the imbibition recovery for samples that were aged for different amounts of time (Ma et al., 1999). The more water-wet samples (less aging time) showed higher recoveries earlier than more aged samples, i.e., higher imbibition rates.

The authors define a pseudo-capillary pressure curve $P_{c,ps}(t_D)$ as:

$$P_{c,ps}(t_D) = \frac{a}{t_D^b}, \tag{2.6}$$

where a and b are constants and t_D is the dimensionless time defined as:

$$t_D = t\sqrt{\frac{k}{\varphi}}\frac{\sigma}{\mu_w}\frac{1}{L_c^2}, \tag{2.7}$$

where t is time, k is the permeability, φ is the porosity, s is the interfacial tension, μ_w is the viscosity of water, and L_c is the characteristic length of the rock sample.

The area under the $P_{c,ps}$ curve, W, is related to the work done by the system because of the change in surface free energy that accompanies spontaneous imbibition. It would provide a useful measure of wettability, can be obtained directly from measurements of spontaneous imbibition, and is referred to as the pseudo-work of imbibition:

$$W = \int_{S_{wi}}^{1-S_{or,im}} P_{c,ps}\, dS_w \int_{S_{wi}}^{1-S_{or,im}} \frac{dS_w}{t_D^b}, \tag{2.8}$$

where $S_{or,im}$ is the remaining oil saturation after the completion of the imbibition process.

In the strongly water wet systems, the pseudo-work of imbibition (W) is usually the highest and its value can be used to normalize for other wettability states. Thus, a relative pseudo-work of imbibition ratio is defined as W_R:

$$W_R = \frac{W}{W_{sww}}. \tag{2.9}$$

Figure 2.4b shows the correlation between W_R and I_w, as a function of aging time (Ma et al., 1999). The correlation is favourable but is only restricted for neutral to strongly water wetting conditions. As mentioned earlier, the main advantage is the method is helpful in distinguishing between different shades of water wetness.

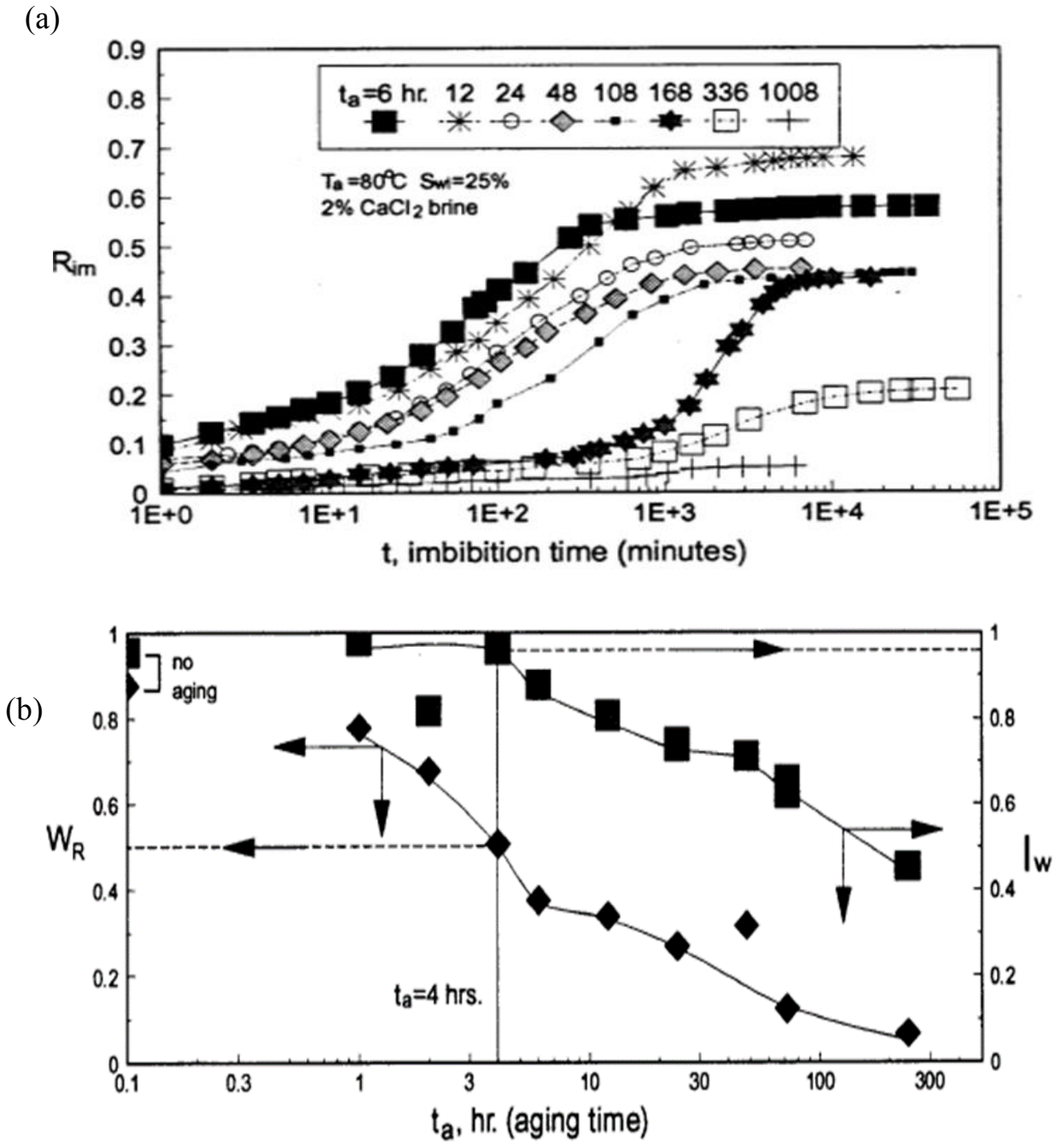

Figure 2.4: a) Samples of altered wettability as a function of aging time (t_a) exhibiting different spontaneous imbibition behaviour, b) A comparison between the Amott index (I_w) in squares and the pseudo-work-of-imbibition based wettability index (W_R) in diamonds as a function of aging time. After Ma et al. (1999).

2.4.5. Chromatographic Separation Index

This measure of wettability was introduced by Strand et al. (2006), where they used the chromatographic separation between a non-adsorbing tracer Thiocyanate, SCN^- , and sulfate, SO_4 , was developed to verify changes in the water-wet fraction after aging the carbonate rock with different oil phases. When plotting the relative concentration of SCN^- and SO_4 versus the injected pore volume, the area between the effluent curves is directly proportional to the water-wet area of the core, because the chromatographic separation only takes place at the water-wet area (Figure 2.5). The new index is then calculated as: (Strand et al., 2006)

$$WI_{CSI} = \frac{A_{Wett}}{A_{Heptane}}, \tag{2.10}$$

where A_{wett} is the area between the non-adsorbing SCN^- and the adsorbing SO_4 curves. The area $A_{heptane}$ is the reference area between SCN^- and SO_4 in strongly water-wet conditions in the presence of heptane.

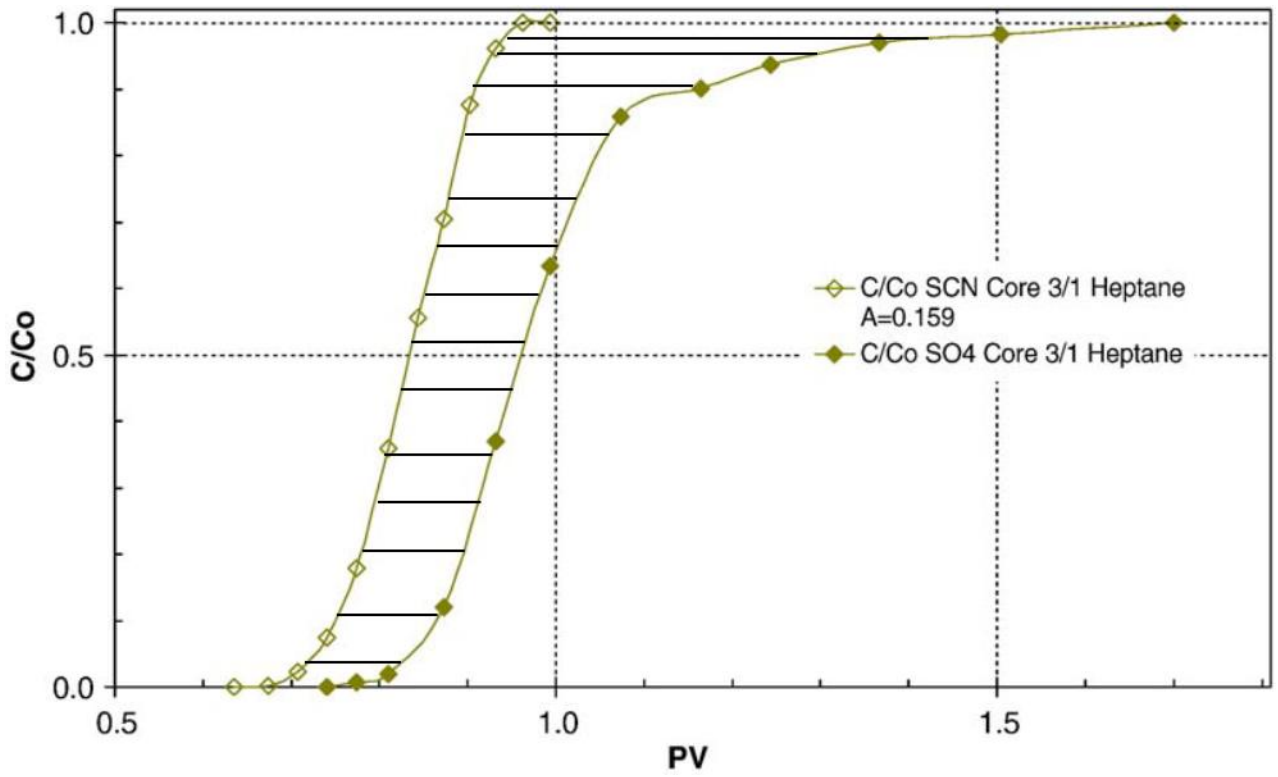

Figure 2.5: Water-wet reference case for the chromatographic separation technique. Effluent profiles for SCN^- and SO_4 in the presence of heptane S_{or}=22%. The striped area between the two curves defines (A=0.159) the adsorption of SO_4 at the clean mineral surface. PV is pore volume and C/Co is the ratio of the effluent concentration of sulfate or tracer to the injected concentration of sulfate or tracer. After Strand et al. (2006).

The water-wet case was a core with residual saturation of heptane and was used as a reference case. Hence, the area between the two curves in Figure 2.5 represent the completely water-wet case. When the rock is aged, an oil-wet fraction is expected, and the resulting area between the two curves should decrease as the case in Figure 2.6. The new index WI_{CSI} runs from 0 (no adsorption in the totally oil-wet case), 0.5 in the neutral case, to 1 in the water-wet case. AN and BN stand for the acid and base numbers, respectively, and will be discussed later (Section 2.5.2).

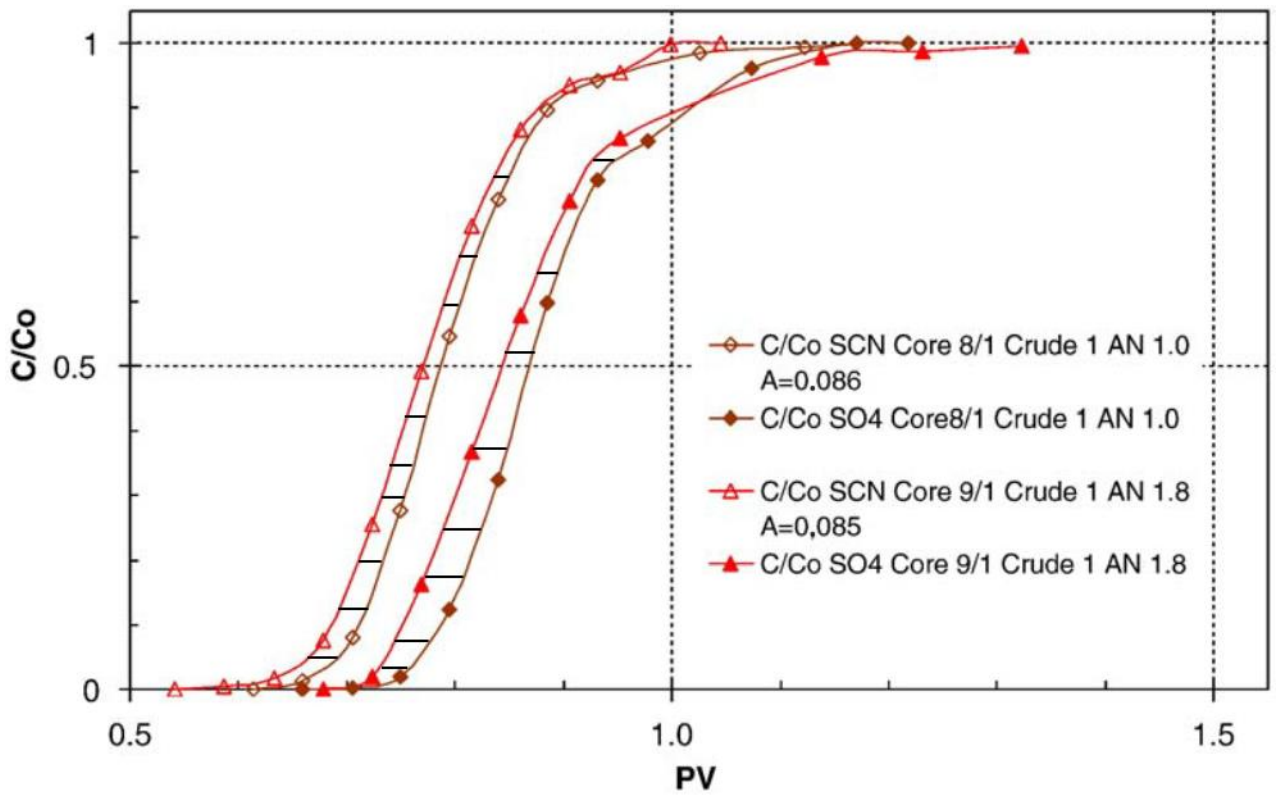

Figure 2.6: Mixed-wet cases for the chromatographic separation technique. Effluent profiles for SCN^- and SO_4 for chalk cores aged with crude oils of different acid number (AN). The striped area between the two curves is smaller than that of the water-wet case (A=0.085 and 0.086 vs. 0.159). After Strand et al. (2006).

The disadvantage of this method is that it is not applicable to minerals on whose surface SO_4 does not adsorb. Even when only considering carbonates, this test was only conducted on the Ekofisk chalk and only conducted at room temperature. Moreover, it has poor correlation to the Amott index, which was not surprising to the authors as they claim that their method is good at neutral conditions, which is where the Amott index fails to discriminate.

2.4.6. Nuclear Magnetic Resonance (NMR)

Nuclear Magnetic Resonance (NMR) is a non-invasive technique that can provide information about the pore structure, the amount of fluids and the interactions between the pore fluids and the rock. The use of NMR measurements to assess the impact of wettability was started by Brown and Fatt (1956) who used sand as water-wet media and Dri-film coated sand as oil-wet media. They found water relaxed faster in the water-wet case when compared to the oil-wet case. Since then,

only a few studies exist on the subject, which tried to correlate NMR measurements to the established indexes of USBM or Amott-Harvey (Guan et al., 2002, Fleury and Deflandre, 2003; Al-Mahrooqi et al., 2003, 2006). The NMR index of wettability is given by (Al-Mahrooqi et al., 2006):

$$I_{NMR} = \frac{T_2^{Swi} - T_2^{Sor}}{T_2^{Sor}}, \tag{2.11}$$

where T_2 is the relaxation time distribution measured at: S_{wi}, which is the initial or the connate water saturation, and S_{or}, which is the residual oil saturation. Figure 2.7 shows an example of a water-wet sample (a) and an aged sample (b) at saturation S_w=1 and at S_{wi}. At S_{wi}, the 2 samples are indistinguishable. However, there is a clear difference in the T_2 distribution at S_w=1 as the aged sample showed a much slower T_2. Figure 2.8 shows the correlation between this index and the Amott-Harvey index of the results of Guan et al. (2002) and Al-Mahrooqi et al. (2006). There is a general correlation that gets much poorer for the two ends (strongly water- and oil-wet cases).

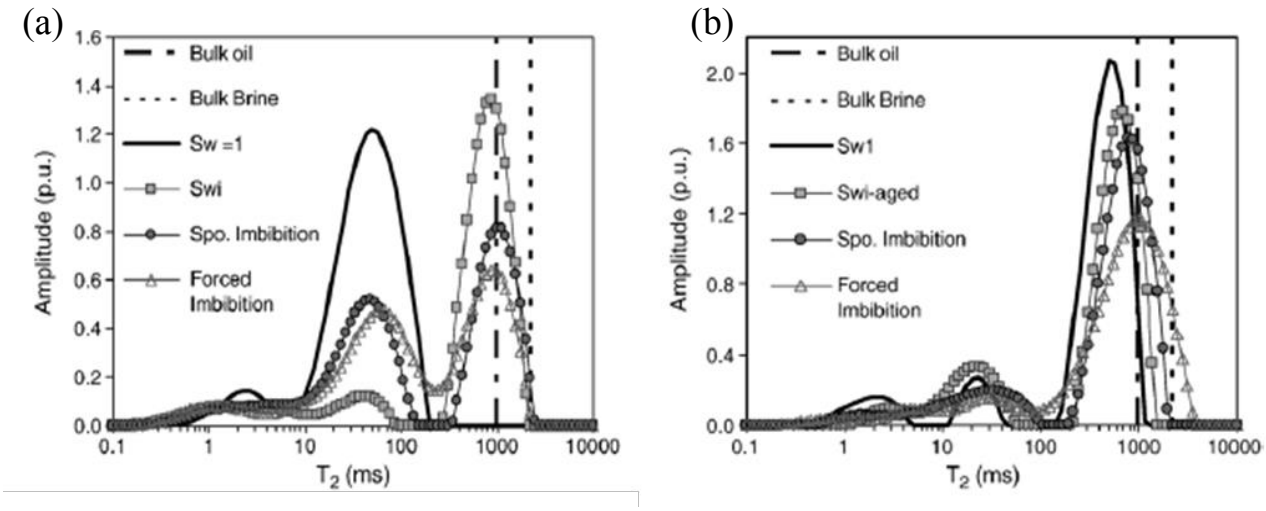

Figure 2.7: Comparison of NMR T_2 distributions to wettability in sandstone. a) water-wet and b) aged with crude oil. After Al-Mahrooqi et al. (2006).

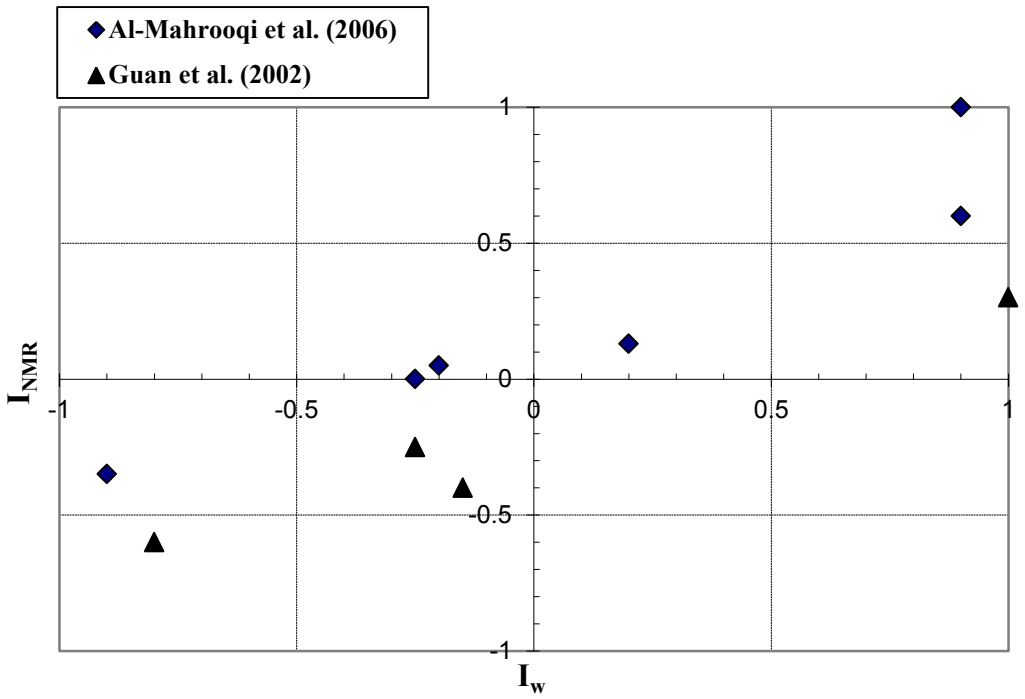

Figure 2.8: Comparison of NMR wettability index (I_{NMR}) to Amott Index (I_w). After Guan et al. (2002) and Al-Mahrooqi et al. (2006).

The problem of the NMR response is its dependence on the saturation of the fluids and the pore-size distribution. So, at different water saturations different NMR T_2 relaxations will result, which is not taking into account the actual surface contacted by the oil phase. Also, the NMR response is a combination of the response of both oil and water, which-in some cases-is indistinguishable (Looyestijn, 2007). Hence, this requires the knowledge of the T_2 distribution of the oil and of the rock at S_w=1.

2.4.7. Flotation Test

This is a simple and qualitative method of measuring wettability in powders. This is done by exposing the powder to an oil phase in a transparent vial either directly or after being suspended in a brine of a certain composition (Wu et al., 2008). Then, the powder would be transferred to another vial filled with brine. The floating fraction of the powder is assumed to represent the oil-

wet part where the volume fraction that deposited at the base of the vial is considered to be water-wet.

This test is done by visual evaluation of the prepared samples and is not applicable to the porous medium. Another problem is that particles of fractional wettability are not distinguishable depending on whether the oil adsorbing on the particle covered enough surface area to allow the particle to float.

2.5. Wettability Alteration

Carbonate rock formations are deposited in sub-aqueous environments (Morse and Mackenzie, 1990), which means the primary porosity was filled initially with brine (typically seawater). Secondary porosity could be created by subsequent diagenetic events that require brines of various compositions to invade the primary porosity leading to the leaching of rock material. Hence, before any hydrocarbon migration event, the total rock porosity was filled with water, which means that the initial wetting state is strongly water-wet (e.g., Morse and Mackenzie, 1990).

This initial state usually changes after the migration of crude oil into the carbonate reservoir. The crude oil contains polar organic compounds such as asphaltenes (Anderson, 1986a), which have the capability to adsorb onto the mineral surfaces, altering the wetting state away from the original water-wet state towards a more mixed- and/or oil-wet state (e.g., Buckley et al., 1998). Understanding of this final wetting state is important as it will be encountered by the oil companies as they execute their field development and production plans.

At later stages of field development, the need for enhanced oil recovery (EOR) processes may arise as the hydrocarbon production rate decreases. This calls for another type of wettability alteration, which requires modifying the wetting state from the current (more neutral to oil-wet) towards wetting conditions that are optimized to increase oil recovery. The aim is to mobilize some of the trapped oil phase by freeing it from the rock surface through a possible wetting state alteration via water chemistry, which can be done in many ways, including changing the brine ionic strength and composition as in the controlled-salinity waterflooding (Zhang and Austad, 2006; Yousef et al., 2010) or by adding surfactants to the water phase during the waterflooding

(e.g., Mannhardt et al., 1993). Another way is to promote more oil-wet conditions compared to the initial wettability of the reservoir. This could lead to improved oil recovery through promoting surface film drainage by creating a continuous path for oil flow along pore surfaces (Salathiel, 1973).

However, changing the water chemistry does not guarantee the success of the wettability alteration process. Oil composition, rock mineralogy, fluids saturation history, pore roughness, initial water saturation, and water chemistry are all important factors affecting wettability alteration (Anderson, 1986a, Morrow et al., 1994; Jadhunandan and Morrow, 1995; Buckley and Liu, 1996). In order to develop a better understanding of how the wetting state might be assessed, the knowledge of such factors and their effect on the wetting state of a system becomes important.

The following discussion will show how wettability alteration is a function of varying parameters such as aging, crude oil chemistry, and water chemistry potential determining ion content of water (PDI). These parameters are the ones of importance especially the water chemistry and PDI content since they have been shown to impact oil recovery (Zhang and Austad, 2006), and the surface charge (e.g., Pierre et al., 1990). Since these factors are not isolated, another discussion will follow on the mechanisms of interaction of all three phases (mineral-brine-oil) within the reservoir.

2.5.1. Relationship to Aging

Variations of this parameter are used to change the wetting state in the laboratory in order to restore the original wettability (e.g., Anderson, 1986a) and to obtain different degrees of a water-wet system (Ma et al., 1999) as was seen in Section 2.4.4. For natural systems, we note that there is always enough time for wettability alteration process to go to completion and the aging discussed related to the laboratory conditions.

Aging is described by the properties of the oil and water phases used, the initial water/oil saturations in the rock sample, and the time and temperature the rock sample experienced. The discussion of aging is included since this will be the way to alter the wetting state of the samples in the laboratory and compare the results to those in the literature, which both are correlated to traditional methods such as the Amott index.

Experimental studies have shown the effect of aging time on wettability. Zhou et al. (2000) observed wettability alteration by systematically varying the initial water saturation (from 15% to 25%) and the aging time (from no aging up to 240 hours) at reservoir temperature. Oil recovery by both spontaneous imbibition and waterflooding was then evaluated as a function of the altered wetting states. They noticed that recovery by spontaneous imbibition passes through a maximum as the wetting state is changed from strongly water-wet (original case) towards neutral-wet, which corresponded to samples aged around four hours. Waterflooding recovery increased as the wetting state moved towards less water-wet (I_w= 0.2 from I_w= 1).

As the aging time of the sample in the crude oil increases, the wetting state becomes less water-wet. Similarly, when the initial water saturation decreases, the system gets less water-wet. The choice of duration of aging (or the aging time) in laboratory experiments is based on the time required to establish an adsorption equilibrium in the system. Theoretically, this equilibrium signifies an altered wetting state, and is commonly reported to be achieved in two to six weeks in the literature (Anderson, 1986b; Cuiec, 1991). Zhou et al. (1995) noticed that increasing the aging time results in an increase in oil recovery by waterflooding but a decrease in the imbibition rate. Increasing the initial water saturation increases the final recovery and rate of imbibition while the oil recovery for waterflooding decreases. The authors also noted that variation of aging time results in graded wetting states that enables oil recovery to be related to wettability.

Jadhunandan and Morrow (1995) experimented with wettability alteration of sandstone by changing the conditions that lead to the adsorption of oil polar molecules onto the mineral surface. They studied systems of different crude oils, brines, initial water saturations, aging temperatures, and rates of flooding, keeping a standard 10-day aging time. An increase in aging temperature combined with lower initial water saturation resulted in a less water-wet state. They related oil recovery to the wetting state, which was measured by the Amott wettability index. The results of more than 50 waterfloods demonstrated that highest recoveries obtained were for the close to or at neutral wetting states.

2.5.2. Relationship to Crude Composition

Crude oils are complex colloidal systems containing hydrocarbons and polar organic compounds of oxygen, sulphur and nitrogen (Anderson, 1986a; Drummond and Israelachvili, 2004). The polar

fraction of the crude oil contains surface-active compounds (such as asphaltenes and resins), which contain both acids and bases.

The crude oil can be divided into different fractions in order to understand the effect of the active components during their interaction with water and rock, which assists in understanding and predicting the ability of different oils to change the wettability. These include physical properties such as density/API grade, viscosity, and refractive index (RI), and chemical properties such as acid and base numbers (AN and BN), SARA components, which is an acronym for saturated hydrocarbons (Saturates), Asphaltenes, NSO-compounds, compounds containing nitrogen, sulphur, and oxygen (collectively referred to as Resins) and aromatics (Aromatic hydrocarbons).

Buckley et al. (1998) introduced the use of the American Petroleum Institute (API) gravity along with acid number (AN) and base number (BN) as properties to evaluate the potential for a particular crude oil to alter wetting behaviour. Acid and base numbers refer to the concentration of proton donating and accepting polar compound within the oil (Cuiec, 1975).

The carboxylic material (carboxyl group, -COOH) in crude oil, as determined by AN (mg KOH/g), is one of the most important wetting parameters for carbonate systems (Speight, 1999). The large molecules will attach to the carbonate surface when the carboxyl group loses a proton and becomes negatively charged. The impact of the AN of the crude oil on the wetting properties of chalk is illustrated by Figure 2.9 showing spontaneous imbibition of water into chalk cores saturated with oils of different AN. The imbibition rate and oil recovery decreased dramatically as the AN of the oil increased (Standnes and Austad, 2000).

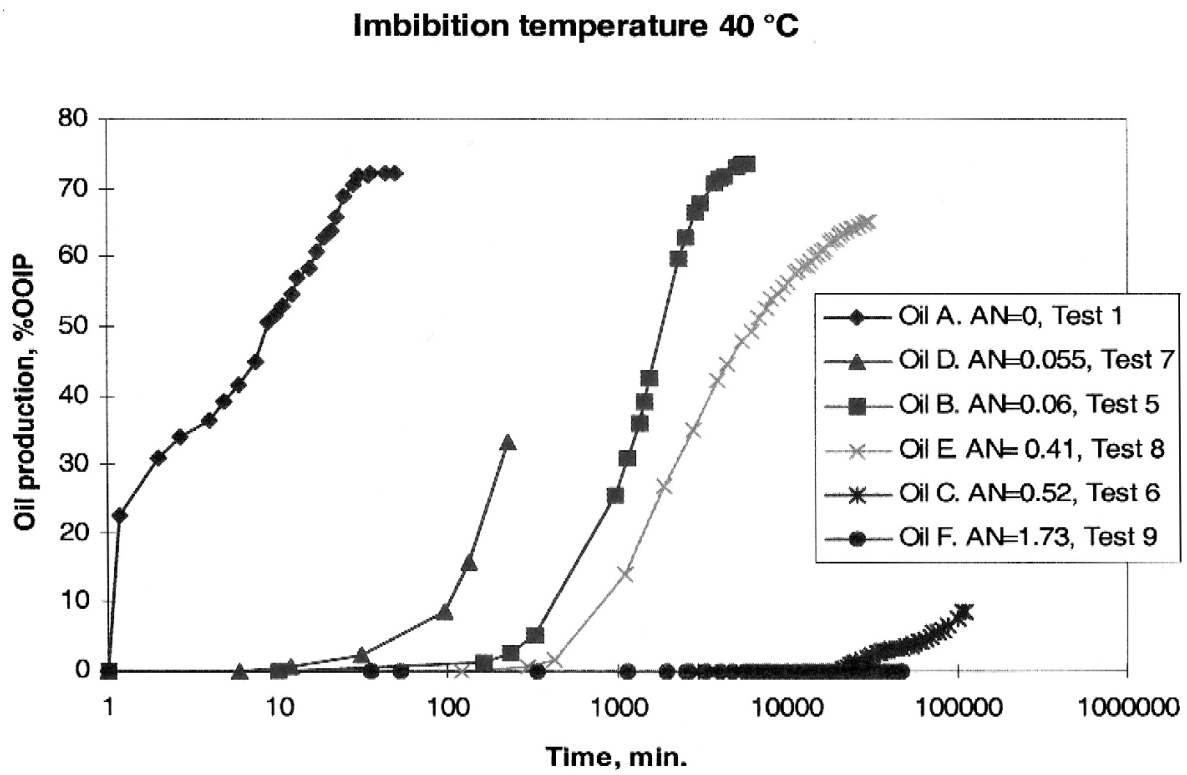

Figure 2.9: Spontaneous imbibition into chalk cores saturated with oils of different acid number AN. After Standnes and Austad (2000).

Wu et al. (2008) studied the effect of using different polar acids on the wettability of powdered calcite. Their work included studying the adsorption of these different acids onto the calcite surface (Fig. 2.10a), the floatation tests of oil-wet powder (Fig. 2.10b), and the effect of each acid on the contact angle (Fig. 2.10c).

Their conclusion was that the contact angle and the floatation test consistently showed that the acids with longer chains resulted in a more oil-wet system. However, the acid adsorption onto calcite (Fig. 2.10a) showed a different trend, which is almost opposite to the trends in Figure 2.10b and 2.10c. For example, cyclohexane-pentanoic acid showed 99% oil-wet powder volume in the flotation test and the highest contact angles to water but showed a very low adsorption ability towards the calcite surface. Wu et al. (2008) concluded that the ability of an acid to alter calcite surface to become oil-wet is not related to adsorption. The structure of the adsorbed carboxylic acid had more effect on wettability than its adsorbed quantity as the authors found that the molecular structure of the organic acids affected the wettability of floated calcite powders more than the quantity used.

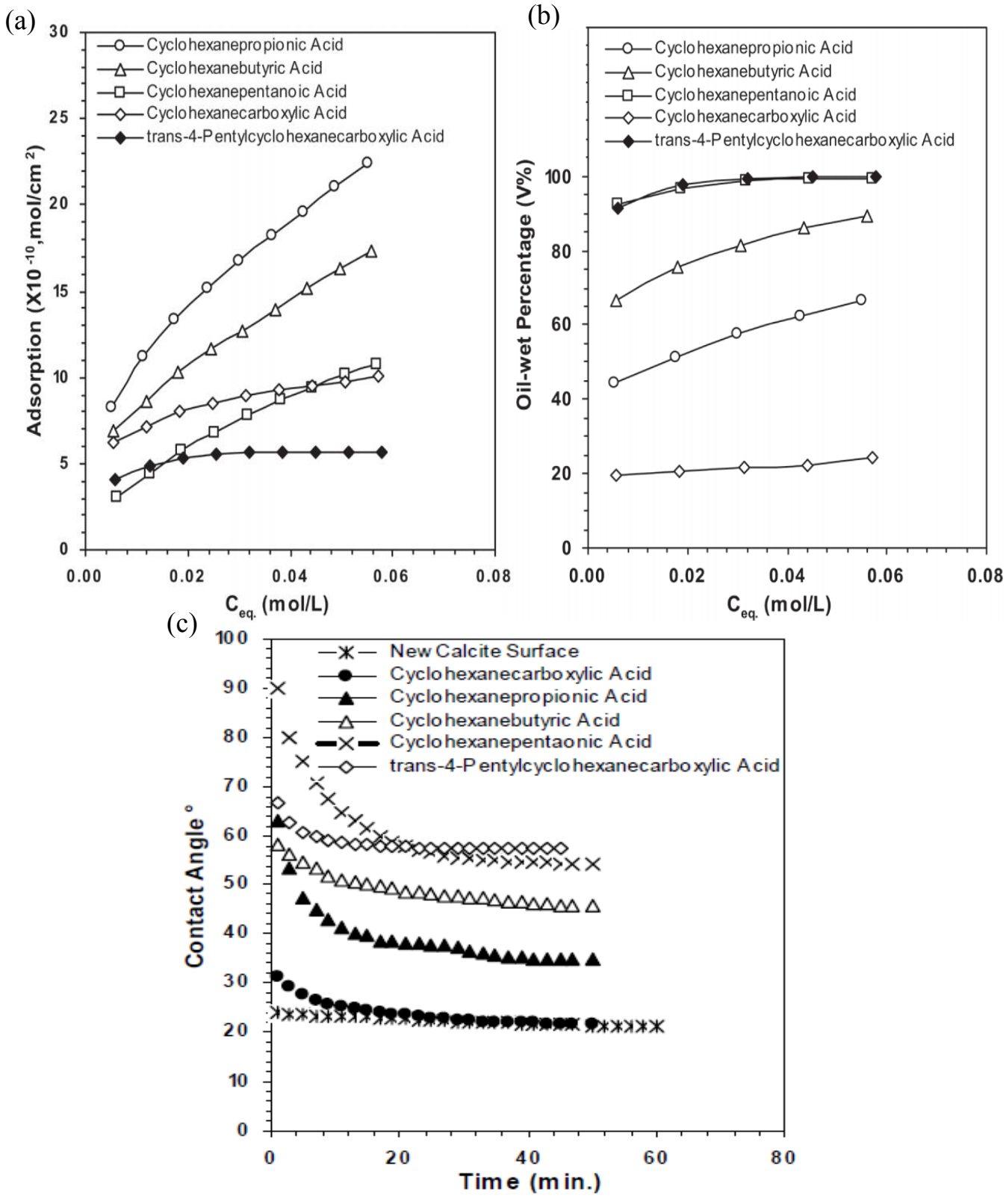

Figure 2.10: The effect of different organic acids on wettability by measuring: a) acid adsorption on calcite, b) volume percentage of floating calcite powder to indicate oil-wetness as a function of the added amount of acid, and c) water contact angle for each acid as a function of time. After Wu et al. (2008).

The basic components in the crude oil, quantified by the base number BN (mg KOH/g), play a minor role as a wetting parameter. However, for a given AN, it was observed that an increase in BN improved the oil recovery, which is assumed to have resulted from a more water-wet chalk (Puntervold et al., 2007). Figure 2.11 shows an increasing oil recovery as a function of an increasing basic crude oil component (BN) when the acid component (AN) is held constant. It was suggested that an acid-base complex could be formed within the oil phase, which might have made the acidic material less active towards the carbonate surface.

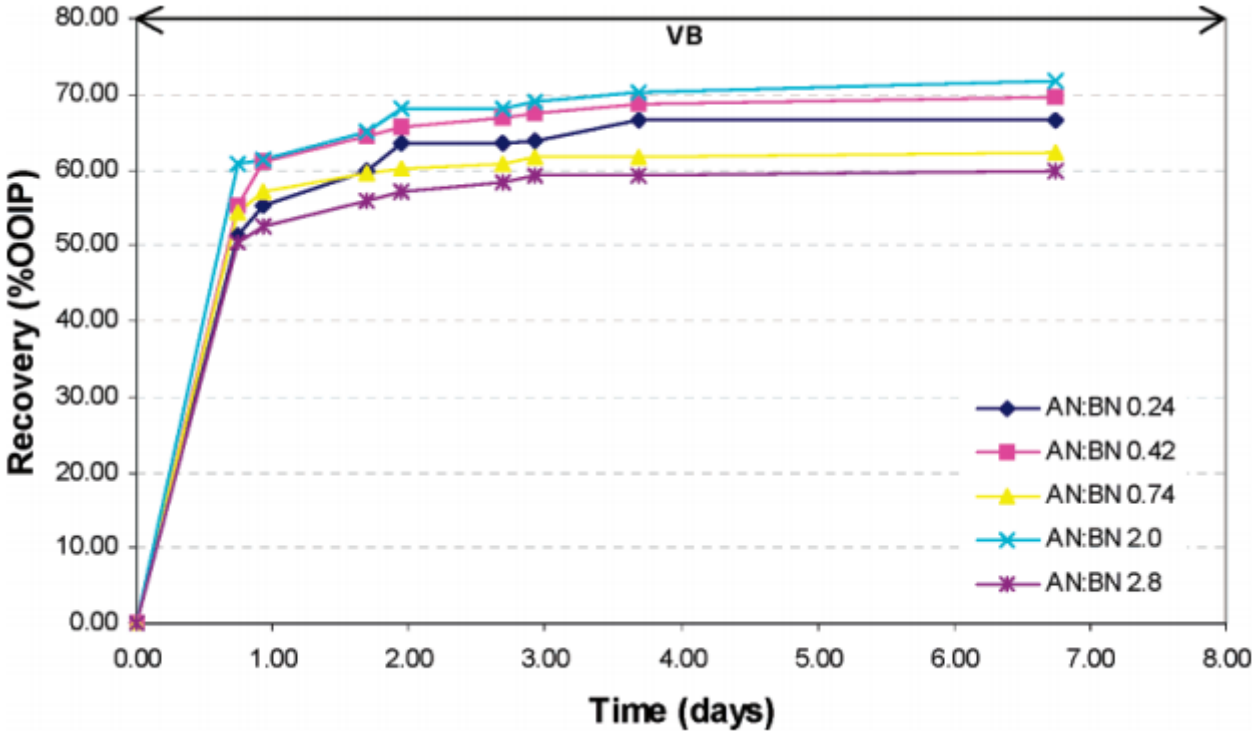

Figure 2.11: The effect of the basic crude oil components as measured by BN on the wetting state and oil recovery. As the acid to base ratio (AN:BN) decreases, the recovery increases as the system is assumed to become more water-wet. VB is the formation brine used in the waterflooding experiments. After Puntervold et al. (2007).

Asphaltenes are high-molecular weight aggregates that are insoluble in light normal alkanes but soluble in benzene, which occurs in relatively large quantities in many crude oils. They are believed to be colloidal poly-dispersions comprising flat, disk-like aggregates (Dubey and Waxman, 1991). They are usually coated with lower-molecular-weight resins (Chung et al., 1991).

Resins adsorbed to the asphaltene surfaces apparently stabilize the asphaltene colloidal dispersions. They can be precipitated from many crude oils when the oil is diluted with a low molecular weight alkane such as pentane or heptane, which is commonly used in the laboratory in order to obtain different wetting states. Using crude oils with different asphaltene content, Al-Maamari and Buckley (2003) showed that more oil-wet conditions result from the precipitation of asphaltene as more heptane is added. This is shown by the sharp increase in the advancing contact angle to water (Figure 2.12), especially, for A-93 and Tensleep crude oils.

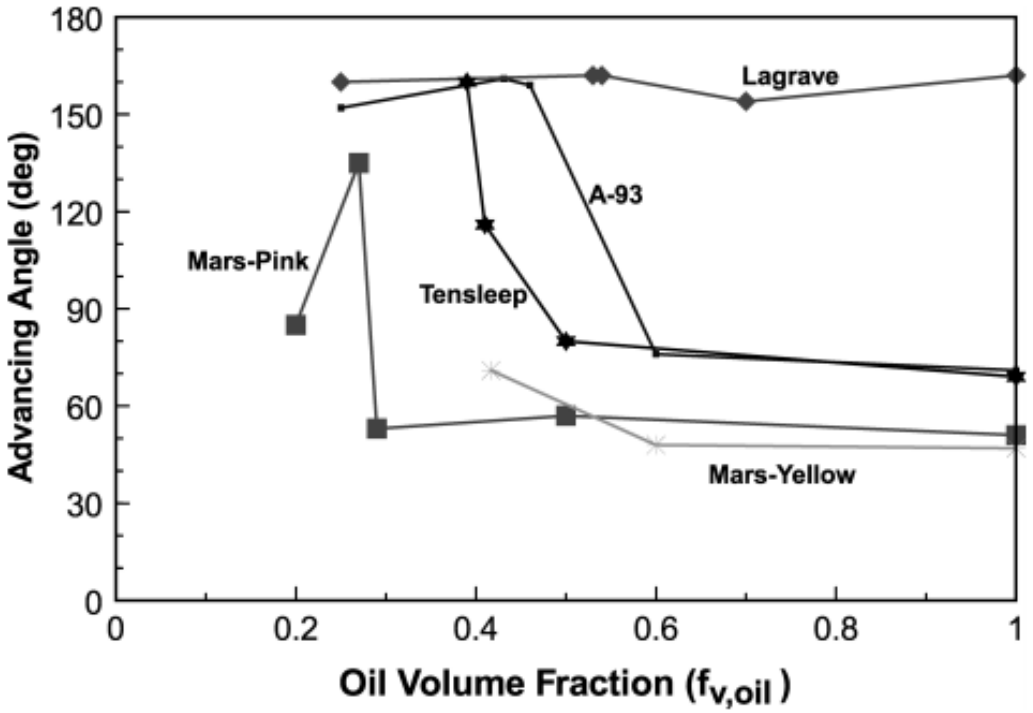

Figure 2.12: Wettability alteration from asphaltene precipitation. Contact angles were measured after exposure of mica surfaces to several crude oils (Mars-Yellow, Mars-Pink, Tensleep, A-93, and Lagrave) diluted with n-heptane to various oil-volume fractions. After Al-Maamari and Buckley (2003).

2.5.3. Mechanisms Leading to Oil-wet conditions

Polar components in a crude oil, such as resins and asphaltenes, may alter the wetting state of the rock (Anderson, 1986a; Buckley and Liu, 1996). Such components can adsorb on the mineral surface through various mechanisms of interaction (Figure 2.13), which include polar interactions, surface precipitation, acid/base interaction, and ion binding (Buckley and Liu, 1996; Buckley et al., 1998).

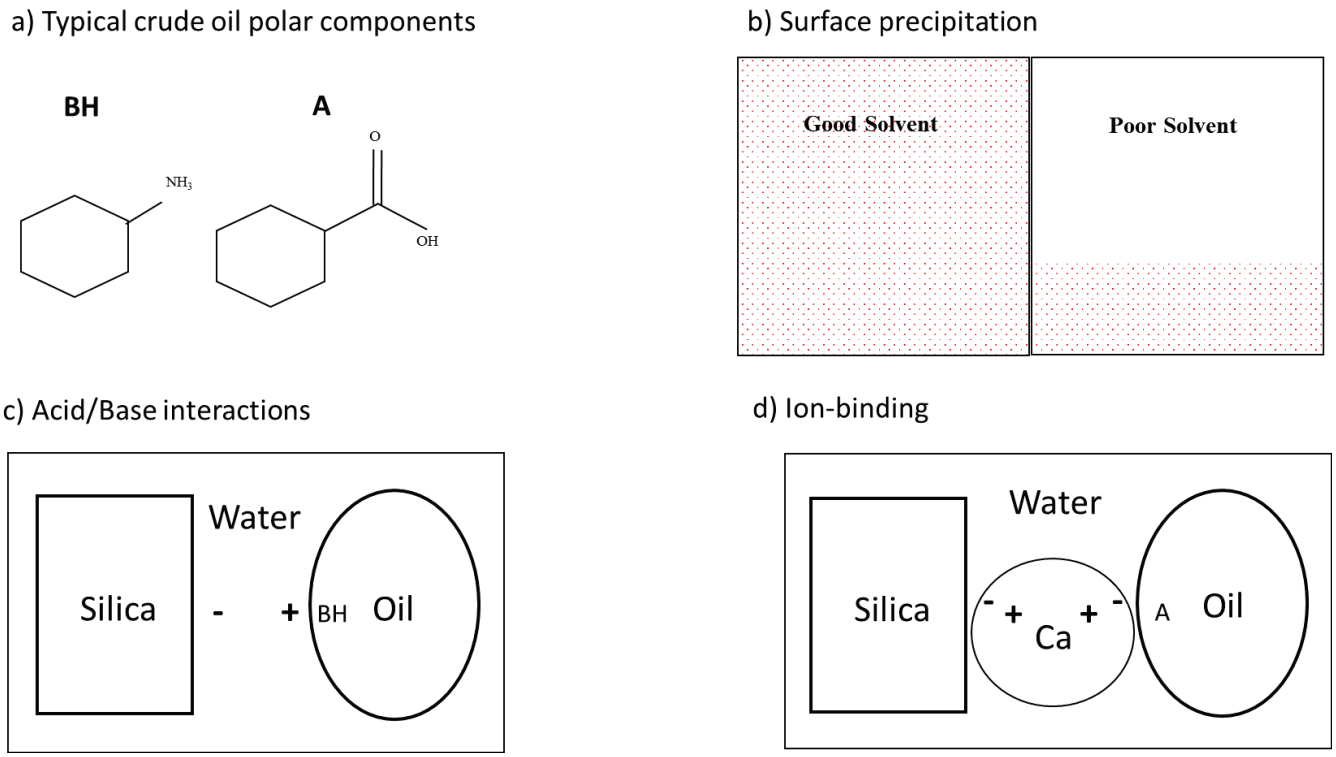

Figure 2.13: The four mechanisms of interaction between crude oil components and the quartz surface. a) shows the structure of a typical base molecule to the left, which is denoted BH in c) and d) and to the right is the structure of a typical acid molecule (denoted A). In absence of water, such molecules are capable of directly adsorbing onto the silica surface via their polar functionality. After Buckley et al. (1998).

In the absence of a water film, which inhibits polar interactions with the surface of the mineral, the polar interactions dominate. A polar compound molecule (Figure 2.13a) and a surface site may take from tens to hundreds of hours to reach equilibrium and complete wetting state alteration (Bortolotti et al., 2010). At equilibrium, the thin water film collapses allowing for completion of

the polar interaction. After the collapse, the polar components directly interact with the polar surface sites on the mineral (Buckley et al., 1998).

Surface precipitation interaction can occur if the pressure and temperature (PT) of the reservoir decreases during oil recovery to a point where the solvent property of the crude oil is compromised (Al-Maamari and Buckley, 2003), causing precipitation in the pores (Bortolotti et al., 2010). Crude oils vary in their ability in acting as a solvent for their asphaltenes and resins and wettability alteration toward a more oil-wet state is promoted when a crude oil is a poor solvent (Figure 2.13b) (Buckley et al., 1998). In the laboratory, surface precipitation can be triggered by diluting the crude oil with heptane (Salathiel, 1973), which contributes to the development of mixed-wetting state (Buckley et al., 1998).

Acid/base interactions are related to the presence of polar compounds in all phases of the oil, water, and mineral system (Buckley et al., 1998; Gomari, 2009). Any of those can behave as acids or bases through losing or gaining a proton (Cuiec, 1975), hence, becoming negatively or positively charged (Figure 2.13c). The magnitude of this charge depends on the extent of the interaction, which itself is dependent on the pH and concentration of the brine (Takamura and Chow, 1985; Hoeiland et al., 2001).

The mineral surface charge and the negatively charged oil/water interface (Buckley et al., 1989) will decide the stability of the water film. If the surface is negatively charged, repulsion will result and the water film is stable. In the calcite case, adsorption of acidic species (e.g., carboxylic acids) is promoted when it is positively charged, which results in the rupture of the water film and wetting state alteration to oil-wet (Buckley et al., 1998). A more detailed discussion about thin water films is in Section 2.6.

The brine pH was shown to affect the wettability when aging a synthetic silica porous sample in crude oil (Buckley et al., 1998). Low pH (around 4) led to a positive charge on the basic (alkaline) groups of the crude's polar component, which lead to a weakly water-wet sample (I_w= 0.5). The positive charge lead to a weaker electrostatic repulsion. Whereas a strongly water-wetting state (I_w= 1.0) resulted when the aging was conducted using a high pH (= 8) brine (Buckley et al., 1995). Thus, at high pH the negative charge adsorbed on both silica and oil interfaces is higher and the electrostatic repulsion is stronger, leading to a more stable water film. It is important to note

that no similar work was conducted on carbonate minerals, which indicates that the electrostatic behaviour might be different.

Ion binding interactions are related to multivalent ions present in the brine, which interfere by masking the on-going acid/base interaction. This masking can occur as the ions bind two sites of the same phase (e.g., oil-Ca-oil) or bridge between sites of different phases (mineral-Ca-oil) as seen in Figure 2.13d. Buckley et al. (1998) stated that this type of interaction can only lead to wetting alteration if the ion is able to bind both the mineral and oil phases together, which was demonstrated in surfactant adsorption experiments (Mannhardt et al., 1993). The effect can be the opposite if the ion binds two molecules of the same phase (i.e., oil-Ca-oil or mineral-Ca-mineral) since this binding reduces the number of available sites at each interface.

Ionic binding can involve multivalent ions of the same polarity as the mineral surface. They are more resistant to desorption than the acid/basic interactions for the same crude oil. Liu and Buckley (1997) made contact angle measurements on aged glass slides where the aging was done in the presence (ionic binding interaction) and absence (acid/base interaction) of an aqueous phase. These measurements were done to evaluate the desorption of the adsorbed polar components of the crude oil. The results showed less desorption of slides that were pre-wetted compared to the slides aged in dry crude oil only.

The discussion above was on measurements conducted on silica while the carbonate minerals did not get as much attention, which might be because of their complex mineral surface (Buckley et al., 1998) or for historical reasons as sandstones were the first reservoirs to be explored (Roehl and Choquette, 1985). Another complexity is that carbonates are overwhelmingly biogenic in origin (Moore, 2001) unlike sandstones, which are of physical origin. This difference in origin results in the development of vastly different porosity networks where in sandstone the pores are only inter-granular while the carbonates contain, in addition to the inter-granular pores, moldic, intra-granular pores and vugs, all directly related to the reactivity of the carbonate minerals (Lucia, 1999).

In the Stevns Klint chalk studied by Strand et al. (2006), calcium is an example of the ionic binding interaction. When the calcite mineral surface is positively charged, the carboxylic acids can adsorb on the surface by their negatively charged part; the hydroxide. This carboxylic molecule orients its non-polar part towards the oil phase and away from the surface (as in Fig.

2.14), to which the calcium ion can attach (Lowe et al., 1973). Since calcium makes up the calcite lattice, it can bridge the polar head of the carboxylic molecule to the surface of the mineral. This linkage makes the calcite‟s surface more oil-wet (Hamuda and Gomari, 2006; Gomari, 2009).

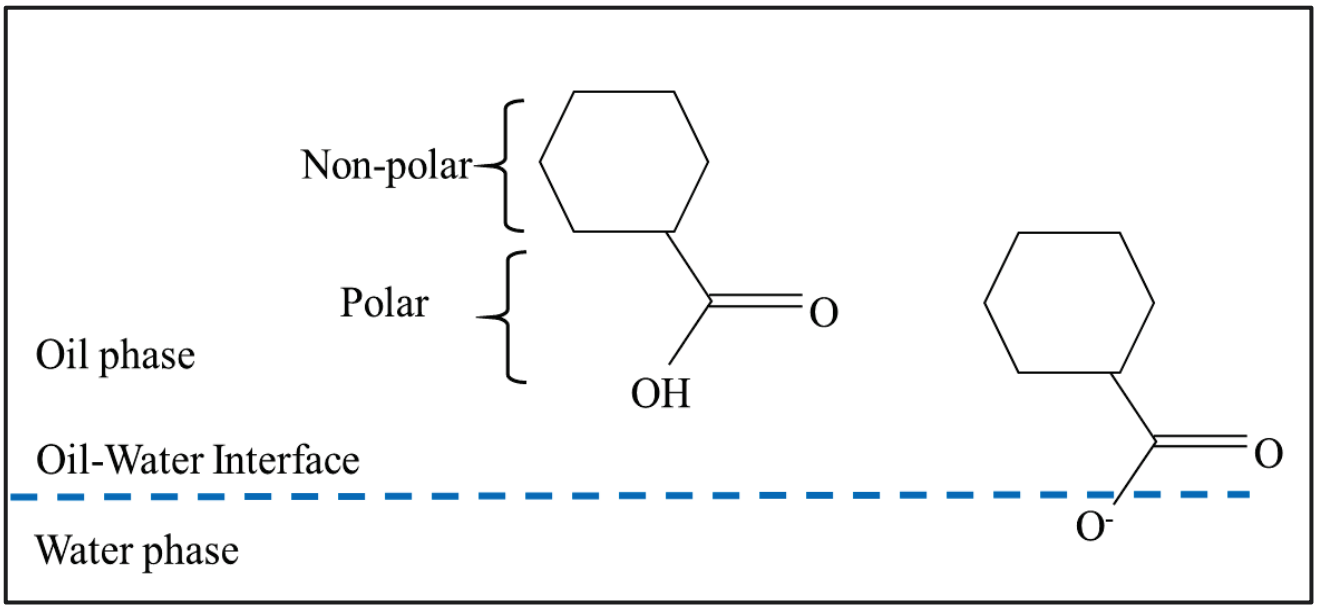

Figure 2.14: Acid/Base interaction at the oil/water interface. As the carboxylic acid molecule orients its polar head into the interface, it loses the proton lead to a negatively charged site.

2.5.4. Relationship to Water Chemistry

We have seen the impact that the properties of oil and water phases have on the wettability of the system, which can cause it to change from an initially water-wet to a more oil-wet state. Let us now consider what changes might be needed to those properties in order to lead the wetting state to revert to its original water-wet state or at least towards it. This is important as this is the goal of many enhanced oil recovery (EOR) processes such as surfactant and controlled salinity waterflooding, which introduce changes to the water chemistry that are expected to lead to improved recovery over conventional waterflooding by possible wetting state alterations. Hence, the impact of brine chemistry on the system‟s wetting state needs to be evaluated by considering the brine‟s composition, ionic strength, and pH.

Two of the most successful examples of changing the water chemistry that leads to increased oil recovery are low or controlled salinity waterflooding (LSW or CSW), which-although not proven,

are still generally believed to result from wettability alteration (Morrow and Buckley, 2011). The first observations of Morrow and workers found that changes in brine composition affected waterflooding oil recovery (Jadhunandan and Morrow, 1991, 1995; Yildiz and Morrow, 1996). This was established for sandstones by Tang and Morrow (1997; 1999) and advanced by BP‟s work (Webb et al., 2004; McGuire et al., 2005).

Observation of similar effects on carbonates followed later, as was shown by Zhang and Austad (2006) for chalks, and by Yousef et al. (2010) for limestone. These two works represents two main approaches to increasing the oil recovery from carbonate reservoirs but both start by replacing the formation brine by seawater. Then, further oil recovery is observed by either increasing the content of sulfate in the seawater as done by the first approach of Zhang et al. (2007) in Figure 2.15. The lowest spontaneous imbibition oil recovery was for the seawater with no sulfate (SW0S) while the highest spontaneous imbibition oil recovery was that of seawater with four times seawater content of sulfate (SW4S).

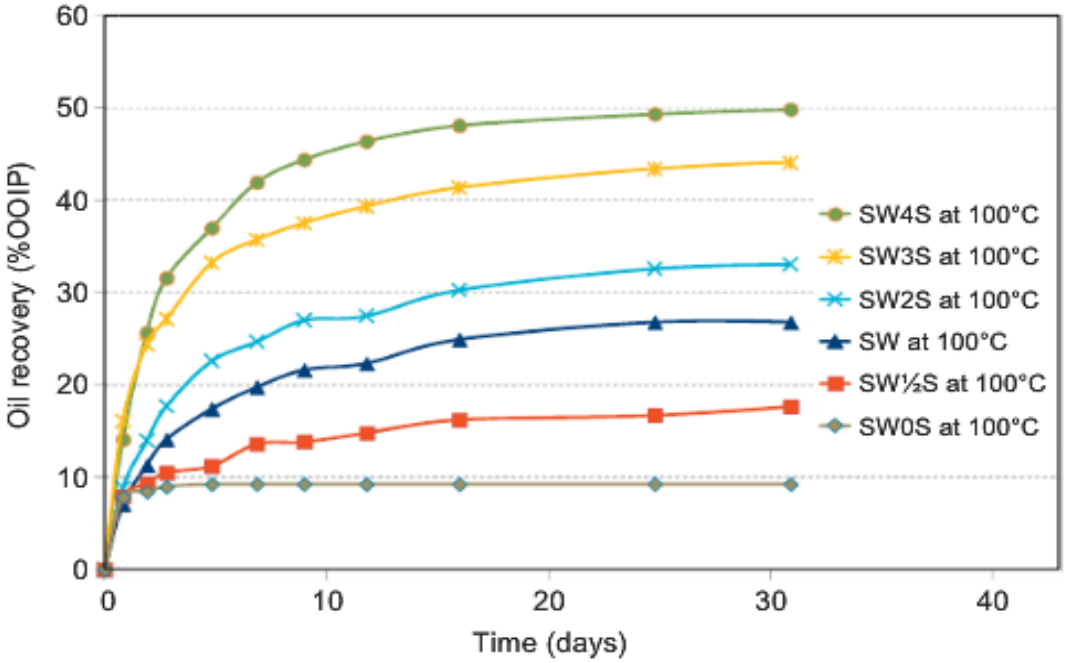

Figure 2.15: Oil recovery by spontaneous imbibition of seawater (SW) and a number of compositions from seawater modified with different sulfate content, into Ekofisk chalk at 100°C. SW0S, refers to seawater without any sulfate content, SW1/2S is seawater with half the content of sulfate of natural seawater, SW2S is seawater with twice the content of sulfate, SW3S is seawater with three times the content of sulfate, SW4S is seawater with four times the content of sulfate. After Zhang et al. (2007).

The second approach is to increase the oil recovery by diluting the seawater as started by Yousef et al. (2010) of the reservoir engineering technology team in Saudi Aramco, which can be seen in Figure 2.16. They consistently show incremental recovery over that of seawater by a total that is around 19-20% for the seawater dilutions for a large number waterflooding experiments of composite core plugs of the same reservoir.

However, an important note to make is that the controlled salinity effect is not as simple as lowering the ionic strength or adding sulfate. Romanuka et al. (2012) have conducted an extensive spontaneous imbibition study that included samples from the Stevns Klint chalk, three different limestone formations, and two different dolomite formations. Their results showed variations in the oil recovery between samples (replicates) from the same carbonate as big as 15% OOIC but on average 3-5% OOIC. Moreover, some of the replicates did not show any increased oil recovery when the formation brine was replaced with brines of lower ionic strength or with higher sulfate

content. Hence, the low salinity effect is not universal and might not work for all rocks, brine compositions, and oil types.

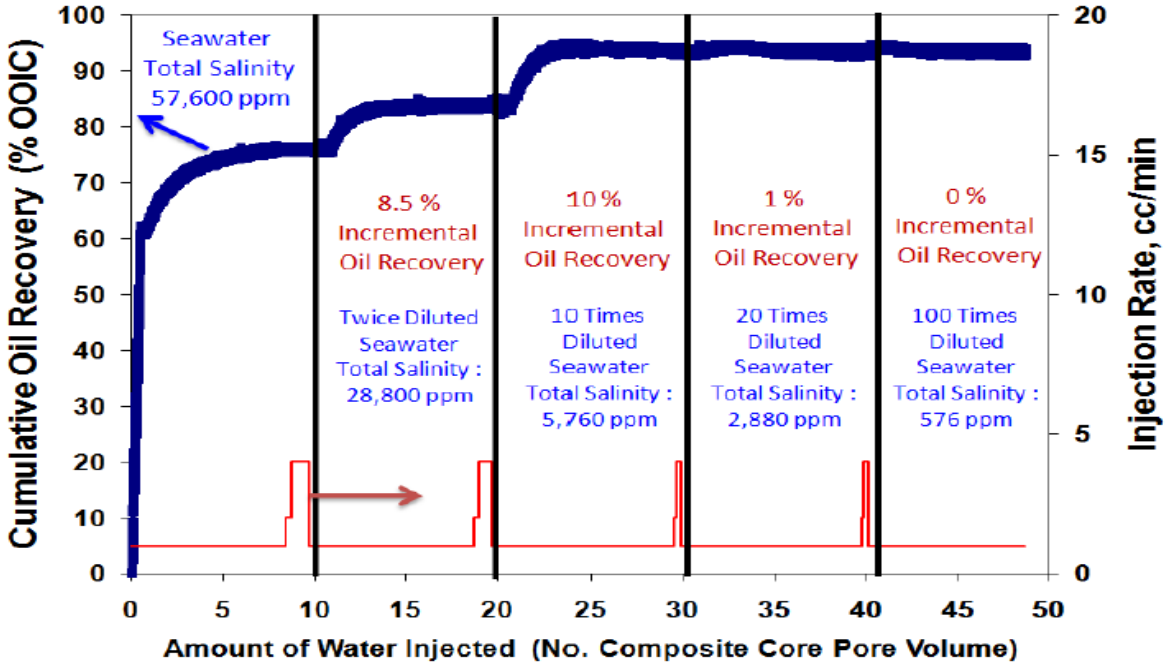

Figure 2.16: Waterflooding incremental oil recovery of seawater and dilutions including twice, 10 times, 20 times, and 100 times. After Yousef et al. (2010).

2.5.5. Mechanisms Leading to Water-wet conditions

We have seen that water chemistry can play a major role in increasing the oil recovery by both spontaneous imbibition and waterflooding processes. Now, we go through the underlying mechanisms that lead to these enhanced recoveries, which are believed to be stemming from wettability alteration. First, we need to define the idea of a potential determining ion (PDI), which is any ion in the water phase that is capable of changing the surface potential/charge of a solid (e.g., mineral surfaces) by specifically adsorbing at the interface (e.g., Hunter, 1993). Potential determining ions can be the crystal lattice ions, the ions H^+ or OH^- of the solution, and/or multivalent ions in solution that might specifically adsorb on a mineral changing its surface charge, which is measured by measuring the zeta potential. For calcite, Ca and SO_4 are strong PDIs towards calcite (Pierre et al., 1990). Their relative concentration dictates the surface charge (Strand et al., 2006).

The suggested mechanism for wettability alteration in chalks using seawater starts by considering the presence of sulfate, which changes the charge of the oil-wet chalk surface by adsorbing at water-wet parts of the mineral and making it less positive (Strand et al., 2006). The electrostatic repulsion between Ca ions and the mineral phase is hypothesized to be reduced because the calcite's positive charge is expected to be lower due to the adsorbed SO_4. Thus, Ca ions are attracted to the mineral surface and they react with the carboxylic material removing them from the surface sites according to (Austad et al., 2009):

$$\mathbf{RCOO^-\text{-}CaCO_3 + Ca^{2+} + SO_4^{2-} \leftrightarrow RCOOCa^+ + CaCO_3 + SO_4^{2-},} \qquad (2.12)$$

where R represents a non-polar hydrocarbon group. As more calcium ions concentrate near the surface, they react with more of the negatively charged carboxylic acids resulting in their desorption. Thus, the sulfate acts as a catalyst to increase the concentration of Ca close to the calcite's surface. However, they did not explain how Ca might be able to adsorb at the positive calcite, which should be electrostatically repelled. Also, the authors suggest that Mg is able to displace Ca ions, which are connected to the carboxylic group in addition to displacing other Ca from the surface. The displacement occurs as (Austad et al., 2009):

$$\mathbf{RCOO^-\text{-}CaCO_3 + Mg^{2+} + SO_4^{2-} \leftrightarrow RCOOCa^+ + MgCO_3 + SO_4^{2-}.} \qquad (2.13)$$

Hence, it is believed that this displacement alters the wetting state of the rock towards more water-wet and causing an increase in oil recovery (Zhang and Austad, 2006; Strand et al., 2006). This process is depicted in Figure 2.17. However, they did not show any surface charge measurements at conditions corresponding to their spontaneous imbibition experiments where the increased oil recovery was observed.

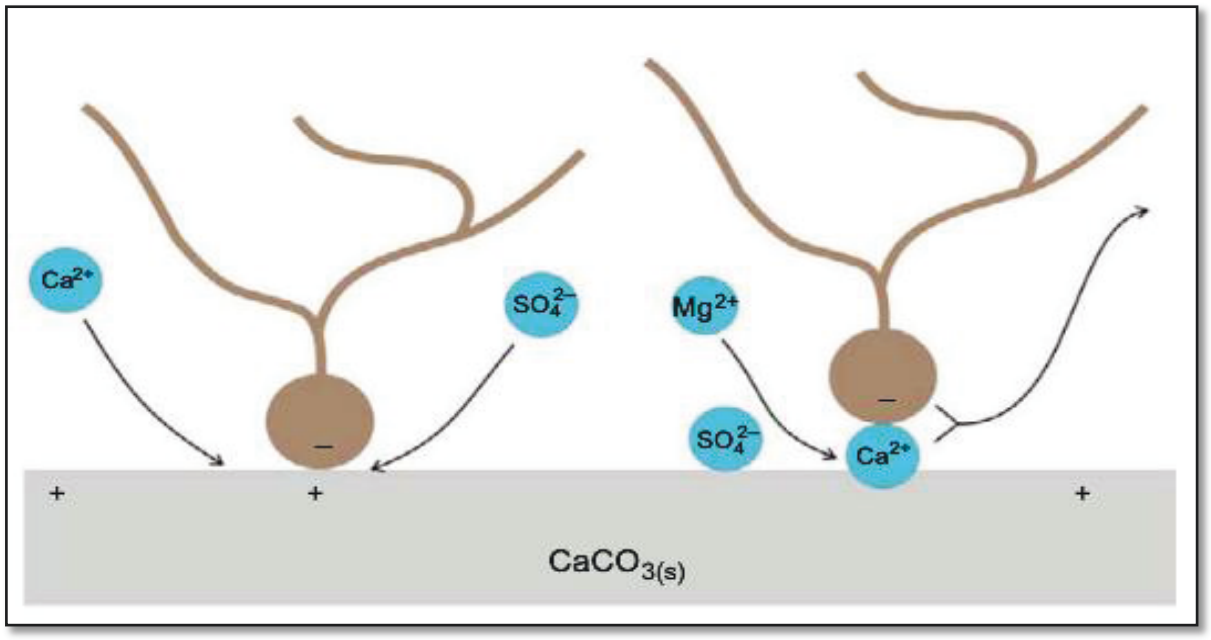

Figure 2.17: Suggested wettability alteration mechanisms, the removal of carboxylic acids adsorbed at the mineral surface by ionic interaction of calcium and magnesium whose catalyst is sulfate. After Strand et al. (2006).

Another suggested mechanism of how the low salinity effect works is the double layer expansion (DLE) (e.g., Nasralla and Nasr-El-Din, 2014). As will be seen in Sections 2.6 and 3.4, the thickness of the electrical double layer (EDL) is controlled by the ionic strength and composition of the brine. For example, a thicker EDL will result when the formation brine is displaced with brines of lower ionic strength, e.g., seawater and seawater dilutions, which in turn is expected to promote a thicker and stable thin film of water. Stable wetting films might lead to a more water-wet system (Buckley et al., 1989) and lead to an increased oil recovery.

The double layer expansion (DLE) would be the suggested mechanism for the enhanced oil recovery in the case of seawater dilutions, which is also known as Smart Water (Yousef et al., 2010, 2011, 2012). Figure 2.18a shows the contact angle of oil increasing as formation (connate) brine is replaced by seawater and seawater dilutions. Figure 2.18b shows the contact angle to water decreasing for the same brine and crossing into the water-wet zone.

(a)

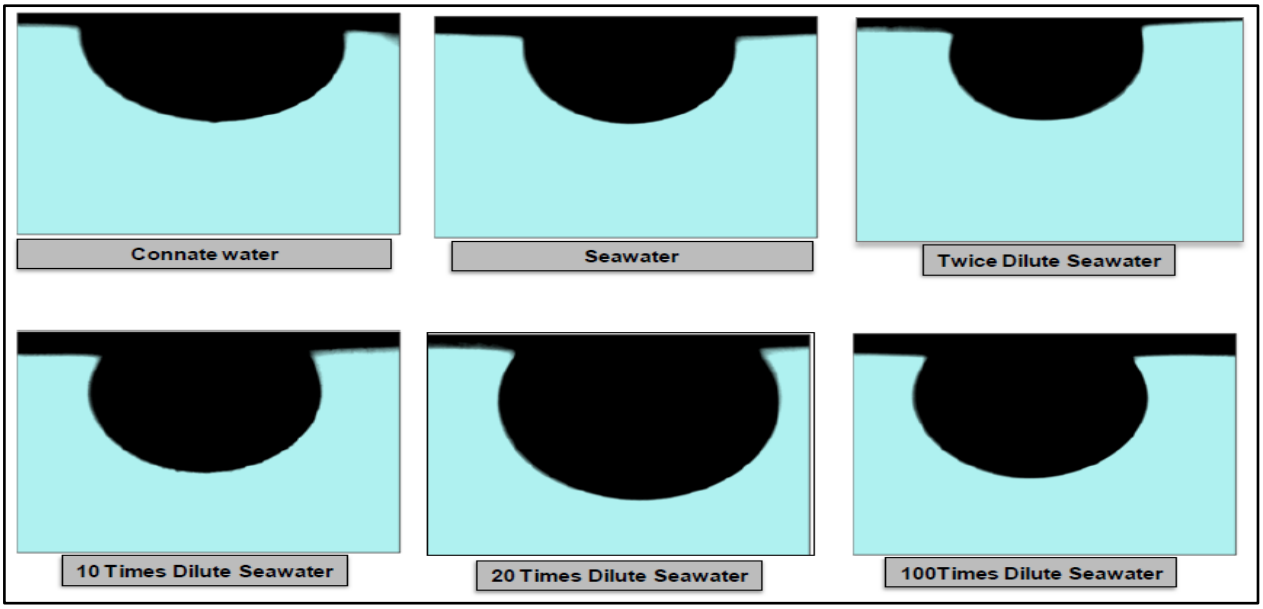

(b)

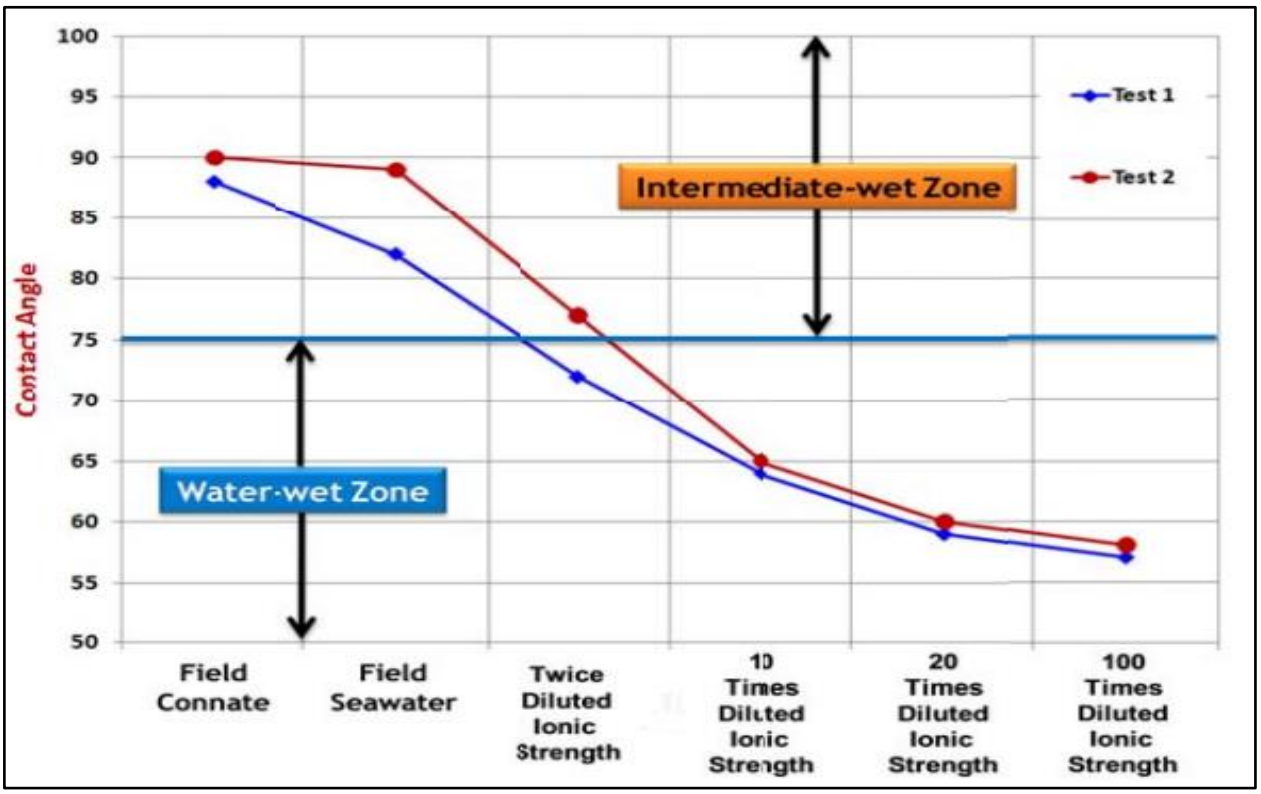

Figure 2.18: Contact angle for different brines showing a trend of more water wet conditions with more dilutions of seawater. a) shows an increase of the contact angle to oil with more dilution while b) shows a decreasing trend for contact angle to water from neutral wetting towards water-wet with more dilution. After Yousef et al. (2010, 2011).

Another aspect of the wettability alteration noticed in Smart Water is the enhancement of the connection between the macro- and micro-pores. This is evidenced by the apparent shift in the position of the NMR T_2 distributions in Figure 2.19. The post-test T_2 relaxation times are faster (shifted towards the left) than prior to the test, which shows a better connectivity between the microscopic and macroscopic pores.

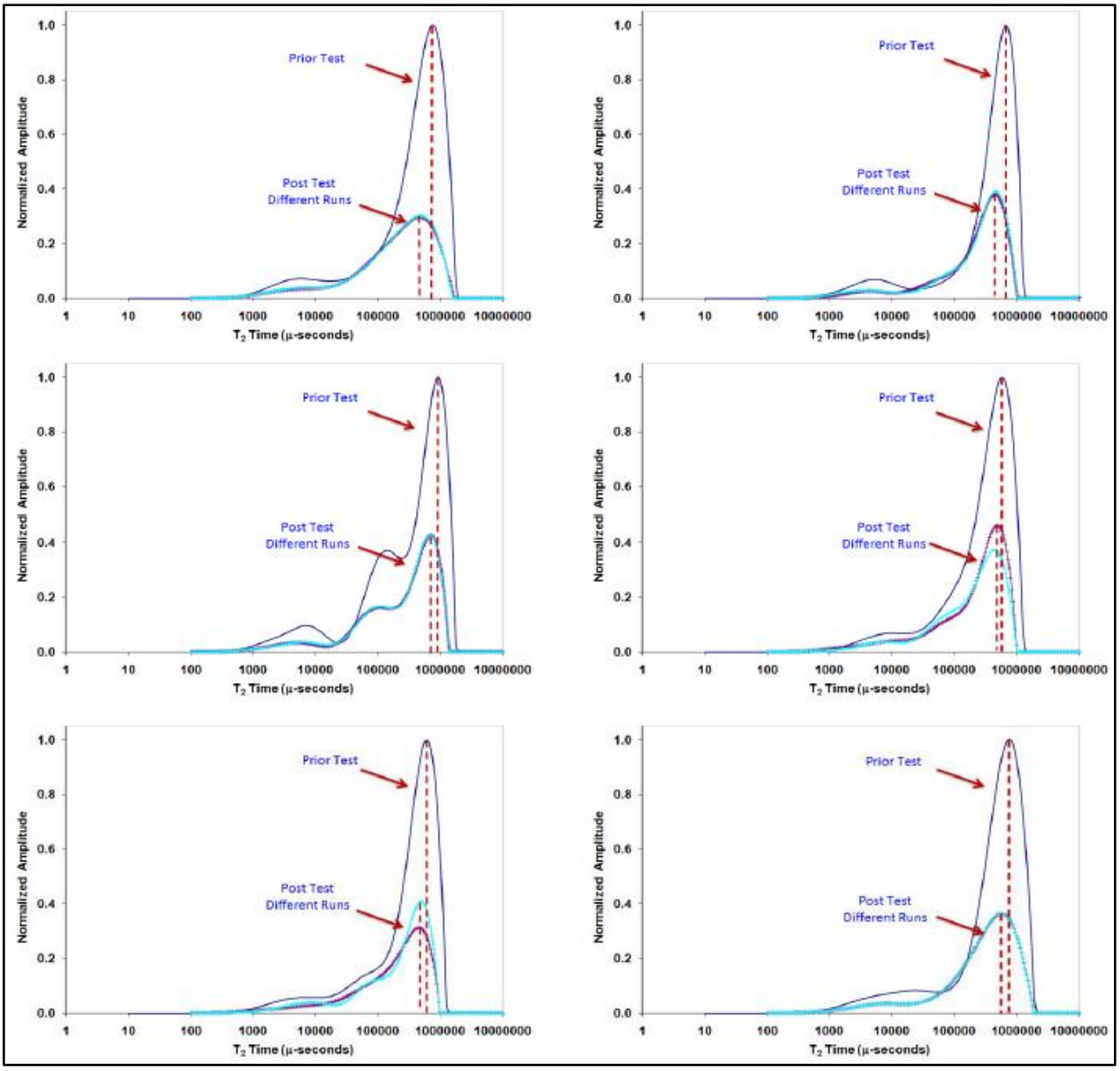

Figure 2.19: NMR measurements for six samples of pre- and post- Smart Water experiment showing a shift in the T_2 suggesting an enhanced connection between the micro and macro porosity. After Yousef et al. (2010).

2.6. Thin Film Overview

The presence of a thin water film, which separates the mineral phase from the oil phase has a vital and decisive role in governing the interactions of the rock/water/oil system on the pore level and the resulting spreading and adhesion (Buckley et al., 1989; Busireddy and Rao, 2004). At the macroscopic scale, the understanding of the contact angle relationship to the wetting is sufficient, but the situation changes when the wetting of surfaces is controlled at the molecular level because the forces involved in maintaining a thin film operate at much smaller distances and their effects might not be reflected in visible changes to the contact angle. Moreover, contact angle measurements do not give any information about what controls the wetting state. As such, it becomes necessary to understand these forces and their impact on the wetting state.

Hirasaki (1991a) observed that the existence and thickness of the water film (thickness ranges 1-100 nm) is related to the wetting state of the system. A thick water film is stable and the system will be water-wet. On the other hand, a thin film is unstable and will rupture (or collapse), which allows the polar components in the oil to interact with the mineral surface in order to change its wetting state. The disjoining pressure describes the state of the wetting film and has three components, which controls the film spreading over the mineral surface as a function of its thickness (h):

$$\Pi_{total}(h) = \Pi_{vdW}(h) + \Pi_{e}(h) + \Pi_{s}(h) \qquad (2.14)$$

where Π_{vdW} is the van der Waals or the molecular component, Π_e is the electrostatic component (between ions), and Π_s is the component of structural forces (hydration) (Hirasaki, 1991a). The thin (<50 nm) water film stability is determined by the balance of these forces within it (Hirasaki, 1991b). The average thin-film thickness is around 10 nm but can be much smaller (~1 nm) (Hirasaki, 1991a; Tokunaga, 2012). The disjoining pressure opposes further thinning of the film, which thins until its disjoining pressure is equal to the applied capillary pressure. Figure 2.20

shows a disjoining pressure isotherm (curve) as total pressure and is broken down into the three components.

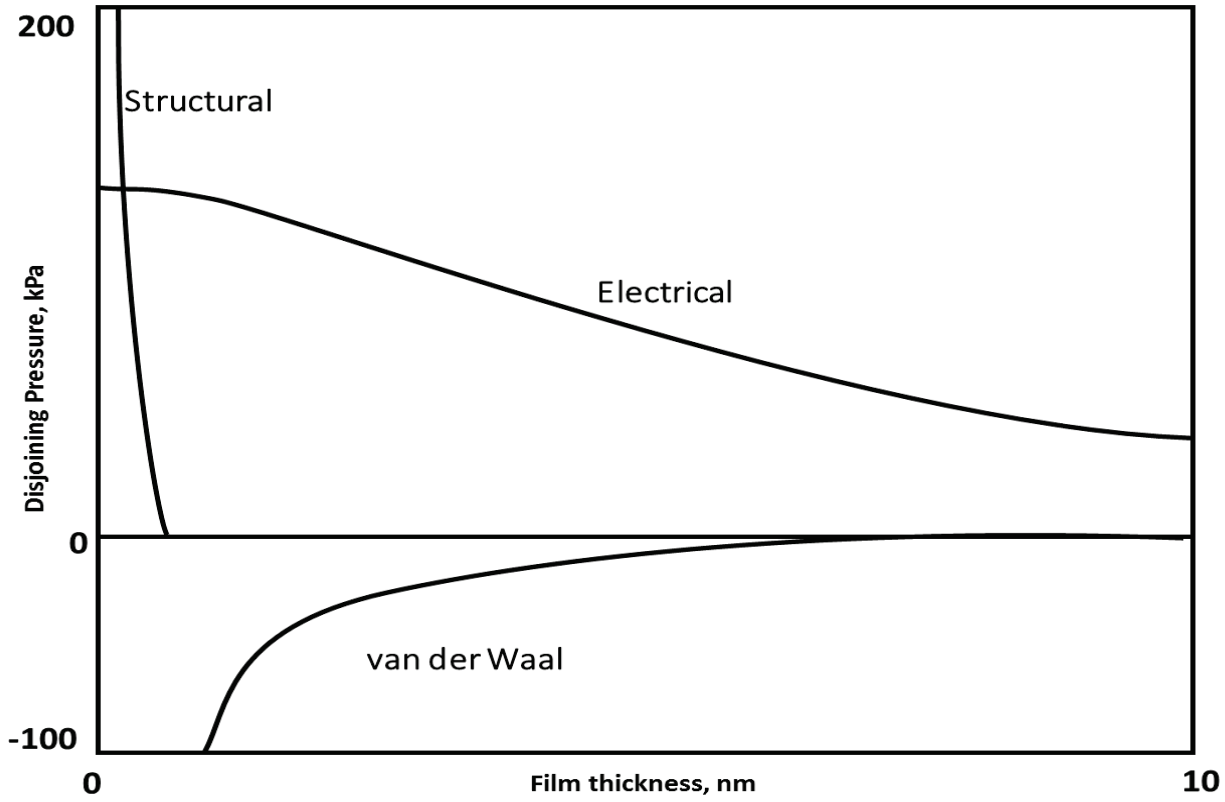

Figure 2.20: Disjoining pressure isotherms, a total isotherm and isotherms of contributing components, namely the Van der Waals, electrical and structural. After Hirasaki (1991a).

The van der Waals dispersion force exists between all matter, which makes it an important component of the intermolecular forces. It has a wide range of distances at which it can be effective from 0.2 nm to >10 nm. It is has a quantum mechanical origin and acts to bring molecules together within the same phase, which means that the van der Waals dispersion force is always attractive. This is reflected by its negative component in the total disjoining pressure (Figure 2.20), which means it leads to the de-stabilization of any thin film. Also, Van der Waals force is not affected by the solvent‟s properties such as the ionic strength and ion valence (Hunter, 1993; Sjostrom, 1999). This force‟s contribution to the disjoining pressure is given by: (e.g., Israelachvili, 2011)

$$\Pi_{vdW} = -\frac{A}{12\pi h^3}, \quad (2.15)$$

where A is the Hamaker constant (Israelachvili, 2011), which is dependent on the interacting media and ranges from 10^{-20}-10^{-21}J. The traditional approach of the Hamaker constant calculation for a thin film is the assumption that the interaction between two different media is the geometric mean of the interactions of each medium with itself (Israelachvili, 2011). Hence, the Hamaker constant for a thin film of Medium 3 (e.g., water) separating Medium 1 and Medium 2 is calculated as:

$$A_{132} = (\sqrt{A_{11}} - \sqrt{A_{33}})(\sqrt{A_{22}} - \sqrt{A_{33}}). \quad (2.16)$$

The electrostatic force is another factor that contributes to the overall change in the disjoining pressure. This is because the zeta potential, which is a reflection of the surface charge, is directly affected by the total ionic strength and composition of the brine.

The electrostatic component of the disjoining pressure can be calculated when the zeta potential at both interfaces (mineral-water and water-oil) and the total ionic strength are known (Israelachvili, 2011):

$$\Pi_{EDL} = 64n^0 kT\, tanh(ze\zeta_1/4kT)\, tanh(ze\zeta_2/4kT)\, exp(-\kappa h), \quad (2.17)$$

where n^0 is the number density, k is the Boltzmann constant, T is the temperature, z is the valence, e is the elementary charge, ζ_1 is the zeta potential at the mineral-water interface, ζ_2 is the zeta potential at the oil-water interface, and κ is the Debye parameter, which is given by (Hunter, 1981):

$$\kappa = \sqrt{\frac{2n^0 z^2 e^2}{\varepsilon kT}}, \quad (2.18)$$

where ε is the permittivity of the electrolyte. The Debye length, which is the inverse of the Debye parameter characterizes the electrical double layer (EDL) thickness. The Debye length decreases with increasing electrolyte concentrations and vice versa.

The structural force, which is also known as the solvation or hydration force, is a short-range (a few molecular diameters) force that arises when liquid molecules are induced to structure into layers as they are restricted between two surfaces. This structuring/ordering in liquids arises from the geometry of molecules, which reflects the (structural) repulsive force between them. (Israelachvili, 2011).

An example of the manifestation of this force is at the interface of water and a solid (e.g., silica) where the draining out of the final layer of water is strongly resisted (Berg, 2010). Hence, the contribution of this force is always repulsive, which is calculated as (Derjaguin and Churaev, 1987):

$$\Pi_s = A_k exp \frac{-h}{\lambda_s}, \tag{2.19}$$

where A_k is the structural force coefficient in the range $1.5x10^7$-$1x10^8$ kPa, and λ_s, a very short characteristic decay length, which ranges between 0.02 up to 0.06 nm (Hirasaki, 1991b). This force provides a lower limit for the thickness of the water film at which the surface is no longer water-wet (Hirasaki, 1991a; Hall et al., 1983). The inclusion of this force in the disjoining pressure calculation is not ubiquitous because of its very short-ranged nature, which makes it negligible (Schembre et al., 1998) when considering thicker EDLs.

Thin films have a physical criteria for their stability, which is in addition to forces mentioned above. Melrose (1982) estimated values of the minimum pore size for film stability, which hints that the water film cannot be stable below a certain pore size due to the rise of a net attractive force. Moreover, the pore shape was found to affect the film thickness for the same conditions, i.e., applied capillary pressure. Kovscek et al. (1993) found that concave surfaces are able to support the thickest wetting films in smaller pores whereas convex pore surfaces supported thick films in the bigger pores.

3. Electrokinetic Phenomena Overview

The electrokinetic phenomenon (EKP) is related to the establishment of an electric potential gradient coupled to a relative fluid motion in the vicinity of a charged surface (Delgado et al., 2007). There are four types of electrokinetic phenomena: electrophoresis, electroosmosis, streaming potential, and sedimentation potential. The first two examples refer to an applied electric force that leads to a mechanical movement of either the solid or the fluid whereas the latter two to refer to a mechanical motion leading to the establishment of an electric force.

The electrokinetic phenomenon (EKP) is only possible because of the existence of an interfacial charge (e.g., mineral/water interface). We first look at the origin of the surface charge, which leads to an establishment of an electrical double layer, that is characterized by the zeta potential, which in turn is measured in this study using the streaming potential method (SPM).

3.1. Surface Charge

A surface charge spontaneously develops at the interface of water and other media (e.g., Hunter, 1981; Hunter, 1993). Understanding this surface charge in terms of polarity and magnitude is beneficial for many geological applications. As was seen in Section 2.6, two approaching charged surfaces interact at close separations. This interaction is the electrostatic component of the disjoining pressure, which might contribute to the stability or instability of the wetting film and therefore the wettability (Buckley et al., 1989; Hirasaki, 1991). Alteration of electrical surface charge is hypothesized to be one of the dominant mechanisms for improving oil recovery since it impacts the wettability alteration process, which can be established by altering the injected water chemistry (Zhang and Austad, 2006; Strand et al., 2006; Yousef et al., 2011). However, we note that none of these previous studies measured the surface charge at the reservoir conditions, i.e., using intact porous medium, formation brine salinity and in the presence of an oil phase. We now look at the origin of the surface charge at the two interfaces of interest in this study: calcite-water and oil-water.

3.2. The Origin of Calcite/Water Interfacial Charge

There are several mechanisms by which a solid surface immersed in a liquid can attain an electric charge. These include the difference in electron/ion affinity at the interface (differential adsorption and desorption of ions), ionization of the surface groups, isomorphous substitution (Riley, 2005), and physical entrapment of immobile charge in one phase (Hunter, 1981).

The electrical charge at the interface of the calcite surface and water might be caused by structural defects of the surface crystals that are observed where random substitutions or omissions of lattice ions occur. In the presence of water this leads to a residual electric charge since electrical neutrality is only attainable with perfectly stacked crystals with no defects (Moulin and Roques, 2003).

Also, the surface structure of carbonate minerals is different from the bulk structure of calcite or dolomite. This relates to the crystal's surface rearrangement when it is exposed to water over time (Stipp et al., 1994). The structure of the surface of calcite is relaxed compared to the bulk part of the crystal, which refers to the difference in the angle at which Ca and CO_3 are oriented for both surface and bulk. This is shown by the electron density response derived from X-ray reflectivity measurements shown in Figure 3.1 (Fenter et al., 2000). There are differences in the atomic distribution in the bulk structure of the mineral. Oxygen atoms are either bridging as in the bulk of the mineral (shared by two calcium atoms) or non-bridging as on the mineral surface (bonded to one calcium atom). The latter represents the edge of the lattice surface where protonation occurs giving a charge to the calcite surface (Mao and Siders, 1997).

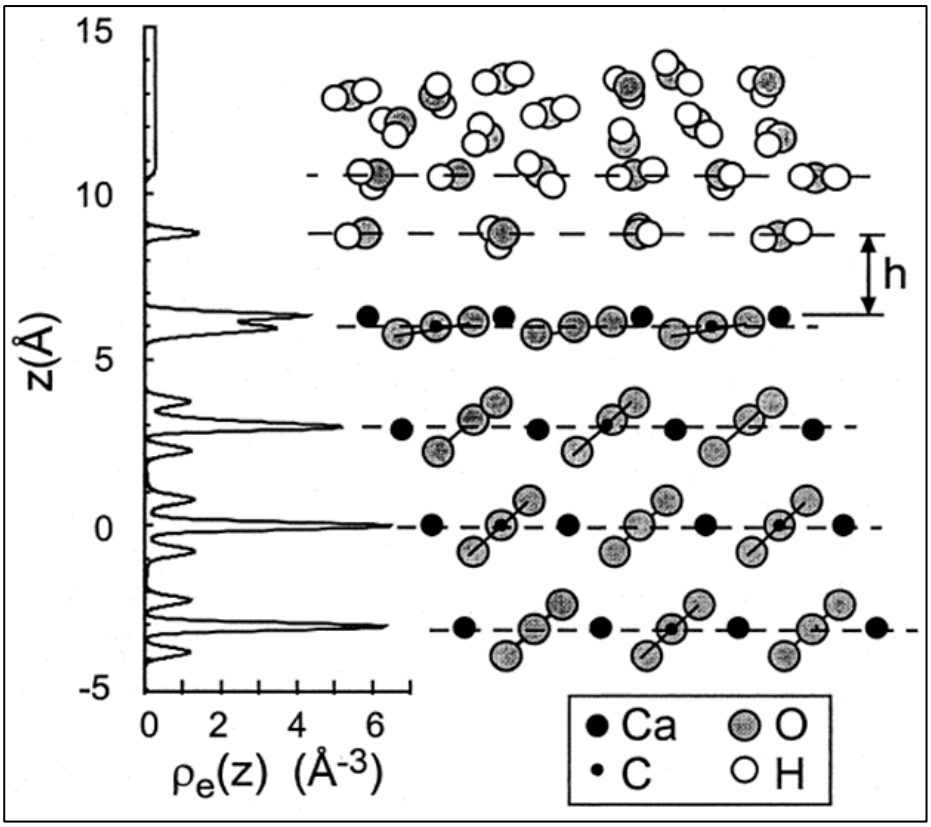

Figure 3.1: Calcite structure: The surface of calcite is relaxed (tilted) compared to its bulk, which causes the calcium sites to be hydrated. The electron density is $\rho_e(z)$ and h refers to the distance between the hydroxyl of the first water molecule and the calcium surface sites on the calcite. After Fenter el at. (2000).

However, there exists a discrepancy in opinion regarding calcite surface charge in the literature that might be attributed to a number of observations. First, different authors used calcite samples of different origins (natural versus synthetic) and different structures (powdered versus precipitate). At the same conditions, Vdovic (2001) found that synthetic calcite has a positive charge while the natural calcite was negatively charged. Similar observations were reported by Cicerone et al. (1992), where different zeta potential values were observed for organically and inorganically derived calcite powders.

The second observation is the attribution of Thompson and Pownall (1989) of the discrepancy in the literature to the dissolution and re-precipitation of new calcite material on the existing crystal surface as the solubility of calcite changes with pH. This suggests that the re-crystallized calcite

might have different electrical charge on its surface compared with the pre-existing crystal surface on which the new material precipitated.

The third observation is that most authors only considered the liquid phase equilibrium and the dissolved CO_2 interface was rarely taken into account (Moulin and Roques, 2003; Eriksson et al., 2008). Carbon dioxide (CO_2) plays an indirect role in the calcite electrical charging; CO_2-free water resulted in a negatively charged surface whereas it was positively charged where appreciable amounts (CO_2 partial pressure above $10^{-5.9}$ atm at room temperature) of CO_2 were present (Eriksson et al., 2007).

At the mineral/water interface, the surface charge is indirectly affected by the brine pH. This is because pH controls the crystal lattice ion concentrations on the surface in addition to the structural differences between the bulk and surface of the mineral. At lower pH (below 7), the Ca has the higher surface concentration and protonation is still predominant (higher H^+ concentration at low pH) giving the surface a positive charge. At higher pH (around 11), the CO_3 surface concentration is higher relative to Ca and the non-bridging oxygen is de-protonated giving the surface a negative charge (Gomari, 2009; Bortolotti et al., 2010).

It is clear that the surface charge is positive when the Ca concentration is relatively high (i.e., when Ca is more abundant than CO_3 at the mineral‟s surface). Similarly, the surface charge is negative when the CO_3 is more abundant at the mineral‟s surface. Hence, the pH is not considered to be a PDI for the carbonate minerals as it only controls the concentration of the PDIs, which are divalent ions Ca and CO_3 (e.g., Thompson and Pownall, 1989).

The calcite-water interface is electrically charged with the calcite crystal lattice constituents Ca and CO_3 being the main PDIs (Somasundaran and Agar, 1967). However, it is well known that divalent ions such as Mg and SO_4 are also PDIs as they are capable of altering the surface charge of the mineral (Pierre et al., 1990). In contrast to the metal oxides, H^+ and OH^- are not PDIs for calcite as they only regulate the Ca and CO_3 ion speciation on the mineral surface, and in aqueous solution, as a function of pH (Foxall et al., 1979). Hence, they have been excluded as having a direct impact on the surface charge of calcite (Thompson and Pownall, 1989). Despite this, it is still common to see zeta potential for natural and artificial calcite plotted as a function of pH as will be seen in Section 3.7.1. The broad range of zeta potential recorded for a given pH

demonstrates the indirect and relatively minor importance of pH in determining the surface charge of calcite.

The role of pH in affecting the surface charge in carbonate minerals is still confused as evidenced by the early literature and new studies (e.g., Mahani et al., 2015) that report zeta potential values in conditions where the pH was adjusted by adding an acid/base even though the application the study was examining (low salinity waterflooding in carbonates) does not involve any pH modification. This is discussed further in Section 3.7.1.

3.3. The Origin of Oil/Water Interfacial Charge

There exists an interfacial charge between crude oil and the water phase, which was first observed by Carruthers (1938) and Dickinson (1941) and later by Taylor and Wood (1957). The crude oil surface is not charged on its own but it becomes charged when it comes into contact with the charged surface of water.

The origin of the electrical charge at the oil-water interface is not fully understood and is a subject of debate. Marinova et al. (1996) considered a number of hypotheses, which included adsorption of hydroxyl ions, adsorption of other negatively charged ions, and depletion of hydrogen ions. The hypothesis of adsorption of other negative ions such as CO_3 and HCO_3 due to dissolved CO_2 was rejected because the authors found that adding Na_2CO_3 did not impact the charging process as similar zeta potential values were found the presence and absence of Na_2CO_3. The hypothesis of hydrogen ion depletion was also rejected as it does not physically explain the measured zeta potentials because it would require a 1 cm thick electrical double layer (EDL) at pH = 8 to explain the measured zeta potential.

Marinova et al. (1996) conclusion is that hydroxyl ions released by dissociation of the water phase specifically adsorb at the interface, which could result from the highly ordered water molecules at the interface (Israelachvili, 2011). Water molecules at the interface with a non-polar fluid are ordered so that the oxygen atom faces the hydrophobic phase (Conway, 1971). This explains the specific adsorption due to the strong dipole (i.e., the hydrogen bonding of the hydroxyl ions to the hydrogen ions).

The electrical description of the oil/water interface had been carried out using the Ionizable Surface Group (ISG) model, which was originally developed to explain the electrical double layer properties in clays in electrolyte solutions (Healy and White, 1978). This model accounts for charges resulting from surface dissociation of potential determining ions into the solution. Takamura and Chow (1985) applied the Ionizable Surface Group model to the bitumen/water interface, taking into account the polar component of the hydrocarbons, which dissociates at the interface as shown in Figure 2.14. This was later extended by Buckley et al. (1989) to incorporate the zwitterionic nature of the crude oil/water interface. Zwitterionic nature refers to a neutral molecule that retains a positive and a negative charge on different ends of the molecule, e.g., the positive charge on the head and the negative on the tail of the molecule, which might be activated as a function of pH (Schramm, 2000).

The oil/brine interface charge is pH dependent (Takamura and Chow, 1985; Buckley et al., 1989), where the charge is positive at low pH and negative at high pH (above 3-4). This was also observed by Marinova et al. (1996) who found the interface to be negatively charged at pH 4-10 (Marinova et al., 1996; see also Beattie and Djerdjev, 2004). Marinova et al. (1996) carried out electrophoretic mobility measurements on four types of non-polar oil-water suspensions. The results showed that the negative zeta potential increases in magnitude with increasing pH and with decreasing ionic strength of the brine. Also, the zeta potential was found to be independent of the type of oil used as the authors used polar and non-polar oils.

In low pH (lower than 4 for crude oil), the interface is positively charged since the basic end becomes protonated whereas for pH > 4 it is negatively charged as the carboxylic groups (RCOOH) in the acidic amino acids are negatively charged when they dissociate according to this reaction:

$$\mathbf{RCOOH + H_2O = RCOO^- + H_3O^+.} \qquad (3.1)$$

The polar head is oriented towards the water phase, in which it dissociates by losing H+ as in Figure 2.14 while the non-polar tail stays in the oil phase.

3.4. Electrical Double Layer (EDL)

The electric double layer (EDL) is formed in response to the surface charge, whose origin was discussed in the previous section. The formation of the EDL is in order to balance a charged interface between two phases and therefore to maintain electrical neutrality. An EDL arises between the water phase and both the mineral surface and the oil phase. The electrically charged interface causes an attraction of charges of the opposite sign (counterions), which screen the surface charge. This screening takes place by the formation of two layers of counterions (Figure 3.2). the first layer is termed the Stern layer, in which ions are firmly attached to the surface and immobile (Hunter, 1981). Usually, these ions do not fully balance the surface charge, therefore additional counterions are attracted towards the charged surface in order to have a complete compensation. This leads to the formation of the diffuse layer, which constitutes the second layer of an EDL where the counterion concentration gradually decreases away from the surface until it reaches equilibrium with the co-ions in the bulk solution. Similarly, coions are repelled by the surface and their concentration will increase with the distance away from it. The distribution of both counter- and co-ions is determined by the Poisson-Boltzmann distribution, which describes the interaction of electrostatic and diffusion forces (Hunter, 1981).

The Stern layer is divided further into an Inner and Outer Helmholtz planes. The Inner Helmholtz plane coincides with the centre of the unhydrated ions (Hunter, 1981) that are specifically adsorbed onto the surface. The Outer Helmholtz plane coincides with the centre of the hydrated ions and marks the beginning of the diffuse (mobile) layer and is thought to coincide with, or be very close to, the shear plane (Hunter, 1981). This is the plane along which excess mobile counterions move if a gradient (pressure, temperature, or concentration) is introduced. Figure 3.2 is a general schematic of the EDL.

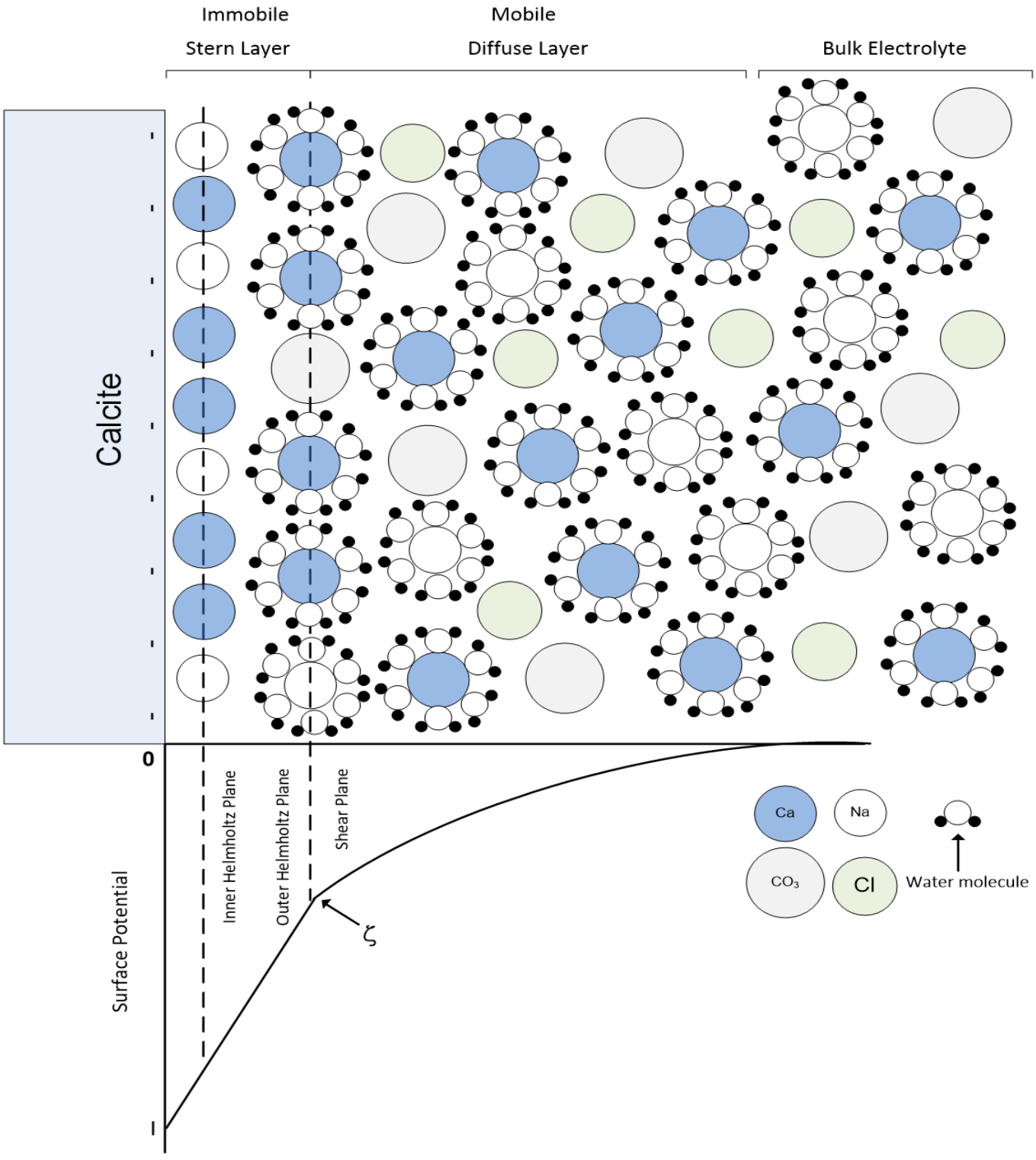

Figure 3.2: Electrical Double Layer formation in response to a negatively charged surface on calcite.

A very important characteristic measure of the surface charge is the zeta (ζ) potential. It corresponds to the potential at the shear plane, which is believed to coincide with the Outer Helmholtz plane (OHP) in Figure 3.2 (Hunter, 1981). The magnitude of this potential is related to the solid surface charge and to the aqueous phase characteristics such as the ionic strength and composition. It indicates the strength of the electrical force and the distance at which this force becomes significant. Thus, a higher zeta potential value reflects the presence of a high number of mobile ions in the diffuse layer. If these ions are of the same polarity in the two EDLs of both interfaces, then, a greater electrostatic repulsion is generated, which might result in the stability of the wetting film.

In sandstones (silica-dominated sands), Glover et al. (1994) developed a model of surface ion adsorption concentration because of the lack of a rigorous physicochemical theory of surface conduction. In this model, the fractional availability of positive and negative surface sites is calculated based on the fluid‟s pH and salinity. Revil and Glover (1997) presented a model for EDL that accounts for the matrix and the free electrolyte conductivities. The EDL is divided into a Stern plane (coincided with IHP in Fig. 3.2) and an electrical diffuse layer populated with hydrated counterions.

Revil and Glover (1998) described the surface conductance as the sum of three contributions from the diffuse layer, Stern layer, and a contribution associated with proton transfer on the silica‟s surface. They showed that the contribution from the diffuse layer is small and was neglected by Revil et al. (1999), which depicted the EDL at two different situations for silica. For pH 3-8, the shear plane coincides with the Stern plane (IHP in Fig. 3.2) with a thicker diffuse layer, while at pH >8, the shear plane is further from the surface because of the protruding filaments developed on the silica surface. In the latter case, the shear plane sits outside the OHP (Fig. 3.2).

As discussed in Section 2.6., $1/\kappa$ is the Debye length, which characterizes the thickness of the EDL where it is thicker for brines of low ionic strength and thinner for high ionic strength brines. The expansion of the EDL (DLE) was suggested to be the cause behind the increased oil recovery in LSW (Nasralla and Nasr-El-Din, 2014). This assumes that a thicker EDL will necessarily be reflected as a thicker and a more stable water film. This assumption is simplistic because it ignores the contribution of the different PDIs and certainly does explain the increased oil recovery when the ionic strength is actually increased.

3.5. Streaming potential Method (SPM)

The streaming potential is the electrical potential caused by the flow of ionic liquids through a charged capillary or porous medium under a pressure gradient (Figure 3.3). It is related to the current caused by the advection of electrical charges down the pressure gradient (Glover and Jackson, 2010). This method measures the electrical potential gradient at steady-state and electrical isolation conditions in 1-D, which insures the equivalence of the streaming current (I_s) and the opposing conduction current (I_c) (Glover, 2015). These currents and the corresponding potentials arise due to charge movement within the diffuse layer of the electrical double layer (EDL), which forms in response to the surface charge (e.g., Hunter, 1981):

$$I_c = -I_s = \frac{\pi r^2}{t}\frac{\Delta V}{L}(\sigma_f + \frac{2\sigma_s}{r}) = -\frac{\pi r^2}{\mu}\frac{\Delta P}{L_c}\varepsilon\zeta, \tag{3.2}$$

where t is the tortuosity, which defines the straightness of the flow path and is the ratio of the actual tortuous path L_c to the straight length of the capillary L of radius (r), bulk fluid conductivity σ_f , conductivity of the surface (fluid within the EDL) σ_s, incompressible fluid dynamic viscosity (μ), and DV and DP are the stabilized voltage and pressure measured across the capillary, which define the streaming potential coupling coefficient C_{SPM} (e.g., Glover and Dery, 2010):

$$C_{SPM} = \frac{\Delta V}{\Delta P} \tag{3.3}$$

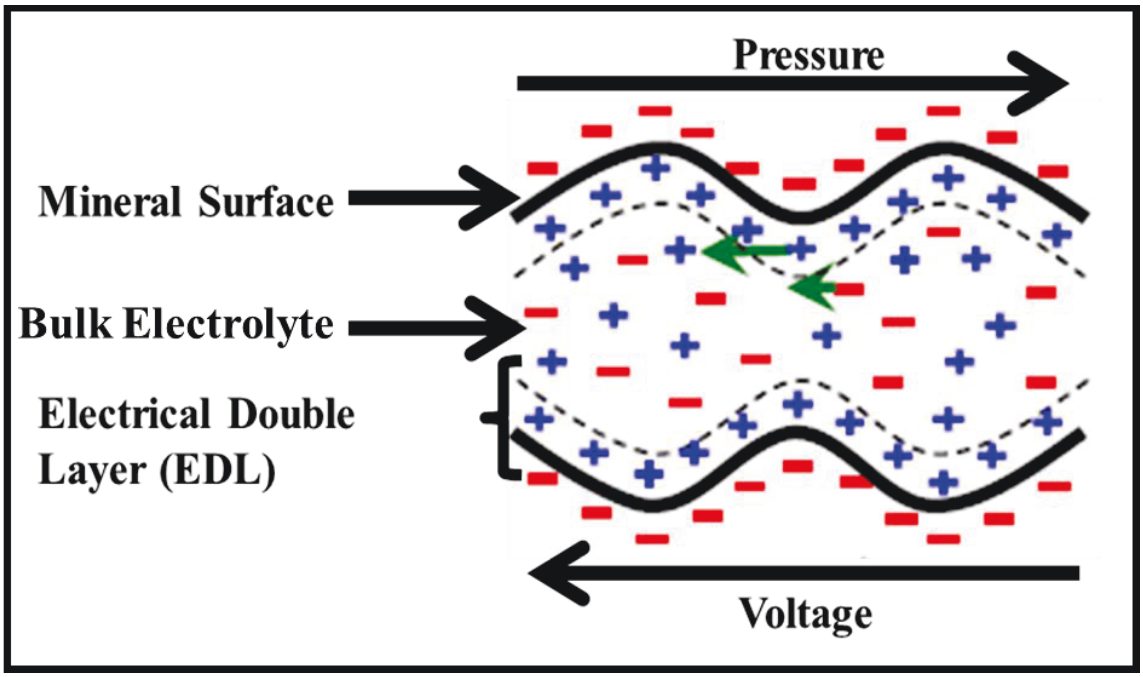

Figure 3.3: Streaming Potential generation due to a pressure gradient. After Jackson et al. (2010).

Measurements of DV and ΔP allow the determination of the coupling coefficient, which is an important parameter that helps to interpret the zeta potential using the Helmholtz-Smoluchowski equation (e.g., Jouniaux and Pozzi, 1995)

$$\zeta = \frac{C_{SPM}\mu\sigma_{rw}F}{\varepsilon} \tag{3.4}$$

where F is the formation factor, which is the ratio of the conductivity of the electrolyte to the conductivity of the saturated rock sample when surface conductivity is negligible, ε is the permittivity of the electrolyte, and σ_{rw} is the electrical conductivity of the saturated rock sample.

3.6. Electrophoretic Mobility (EPM)

Electrophoresis is the movement of charged colloidal particles submerged in a liquid, under the influence of an external electric field (e.g., Hunter, 1993). The electrophoretic mobility u_e of the suspension is related to the zeta (shear plane) potential using the Helmholtz-Smoluchowski equation for electrophoresis (Delgado et al., 2007):

$$\zeta = \frac{u_e \mu}{\varepsilon} \tag{3.5}$$

Electrophoresis can only be measured in suspensions of solid-liquid, liquid-liquid, and gas-liquid. The zeta potential obtained is an effective value because it reflects the average surface charge on all of the particles in suspension; at the particle level, the zeta potential may vary. Many, perhaps most, previous studies have used measurements of electrophoretic mobility (EPM) to determine the zeta potential (Madsen, 2002) because the measurement is quick, and because of the commercial availability of the zetameter, an electrophoresis measurement instrument. In this approach, the sample is crushed to a fine powder and suspended in a solution of the electrolyte of interest. An electrical potential field is applied across the suspension (the field typically oscillates at a controlled frequency, inducing an alternating current through the suspension) and the resulting movement of the solid particles is used to interpret the zeta potential via Eq. 3.5 (see Delgado et al., 2007). Electrophoretic mobility measurements may not reflect the natural conditions of interest for several reasons. First, the samples are crushed, which creates „fresh" mineral surfaces that may have different properties to „aged" surfaces that have been previously exposed to fluids in the pore-space. Second, the ratio of electrolyte volume to mineral surface area is changed significantly compared to the natural porous medium, which may be important in systems such as carbonates where dissolution and precipitation and/or adsorption and desorption may simultaneously modify surface charge and electrolyte composition (Thompson and Pownall, 1989; Pierre et al., 1990). Third, the EPM method is limited to representing only one fluid phase. Hence, it cannot be used to obtain multiphase measurements when both non-aqueous phase liquids (NAPLs) and water are present within the pore-space, as is often the case in subsurface carbonates.

3.7. Previous Zeta Potential Measurements

In this section, a survey of what has been reported in the literature on the zeta potential for both the calcite mineral and the oil interfaces with water is presented. The EPM was the method used to obtain most of the reported data. It is conducted on powder that is suspended in the solution of interest, which means that the porous medium; the pore bodies and throats are not preserved since the sample is crushed and powdered. Also, the majority of the experiments were conducted using

dilute electrolytes that have much lower ionic strength than formation and saline aquifer brines. These make it a limited representation of real subsurface settings. Moreover, EPM does not account for the presence of a third phase (e.g., crude oil), which means it does not represent rocks of variable wettability states. Hence, we were motivated to conduct this study in order to represent the porous medium in presence of realistic brine compositions to represent hydrocarbon reservoirs and saline aquifers.

3.7.1. Calcite/Water Zeta Potential

Here is a summary of the various experimental results reported in the literature, which should highlight some of the discrepancy mentioned in Section 3.2. The calcite surface was found to be positively charged at neutral pH (around 7) (Tabrizy et al., 2011, Anderson, 1986, Hirasaki, 2003). Somasundaran and Agar (1967) measured streaming potential and determined the point of zero charge (PZC) of calcite to range from pH 8 to 9.5. Somasundaran and Agar (1967) hypothesized the electrical charge is related to the preferential adsorption of ions from solution and desorption of surface ions as the pH changes. Thompson and Pownall (1989) found that zeta potential interpreted from streaming potential measurements was positive in pH 7-12 implying positive surface charge. Vdovic and Biscan (1998) found synthetic calcite was positively charged (pH 9.5) with a PZC around pH 9.5, whereas natural calcite was always negatively charged (no PZC) in the range of pH 6-11. Eriksson et al. (2007) found that calcite had a positive charge at pH 7.5-11, which was due to the preferential dissolution of surface CO_3.

Figure 3.4 shows that there are numerous papers reporting measurements of the zeta potential on calcite. These have highlighted the difference between natural and artificial calcite samples (e.g. Cicerone et al., 1992, Vdovic, 2001), the importance of controlling CO_2 partial pressure (pCO_2) in open or closed-system experiments (Thompson and Pownall, 1989; Heberling et al., 2011), the impact of wetting state in the presence of NAPLs (e.g. Jackson and Vinogradov, 2012; Kasha et al., 2015), and the effect of PDI concentration (Pierre et al., 1990; Zhang and Austad, 2006; Strand et al., 2006; Alotaibi et al., 2011; Chen et al., 2014; Mahani et al., 2015). However, few report measurements of zeta potential in carbonates at conditions relevant to natural subsurface systems. Most explore only dilute electrolytes, with much lower total ionic strength and PDI concentration than subsurface brines. Moreover, most do not employ an experimental method that establishes equilibrium conditions of pH, pCO_2 and PDI concentration relevant to subsurface carbonates.

Many use artificial calcite, open system measurements with uncontrolled pCO_2, or vary pH and/or pCO_2 over a broad range not relevant to subsurface brines.

Most of the above results presented in Figure 3.4 save those for Somasundaran and Agar (1967) and Thompson and Pownall (1989) were done using electrophoretic mobility measurements (EPM), from which zeta potential is calculated. They were conducted with electrolytes of variable compositions, i.e., different concentration of potential determining ions (PDIs).

The data spread in Figure 3.4 highlights a very important issue, which is the complex behavior of water-wet calcite and also dolomite (carbonate rocks). This complexity must be investigated as function of brine chemistry and temperature. The results of such investigation will serve as a reference to which measurements on crude-oil-aged samples of limestone are compared.

Studying the surface charge of metal oxide minerals as function of pH is required because the proton is a PDI for these minerals. However, the proton is not a PDI for calcite (e.g., Foxall et al., 1979; Thompson and Pownall, 1989) or other carbonate minerals, and we hypothesize that the difference in PZC reported by different studies stems from the fact that Ca and CO_3 concentration change by modifying the pH. Moreover, the brine pH in hydrocarbon reservoirs during, e.g., CSW does not change as the formation brine pH=7-8 (Yousef et al., 2011) and seawater has pH=8 (Stumm and Morgan, 1996). Hence, measuring the zeta potential by changing the concentration of divalent ions (e.g., Ca, Mg, and SO_4) is more representative of CSW and other applications where the water composition is being changed by flooding the reservoir with water of a different chemical composition.

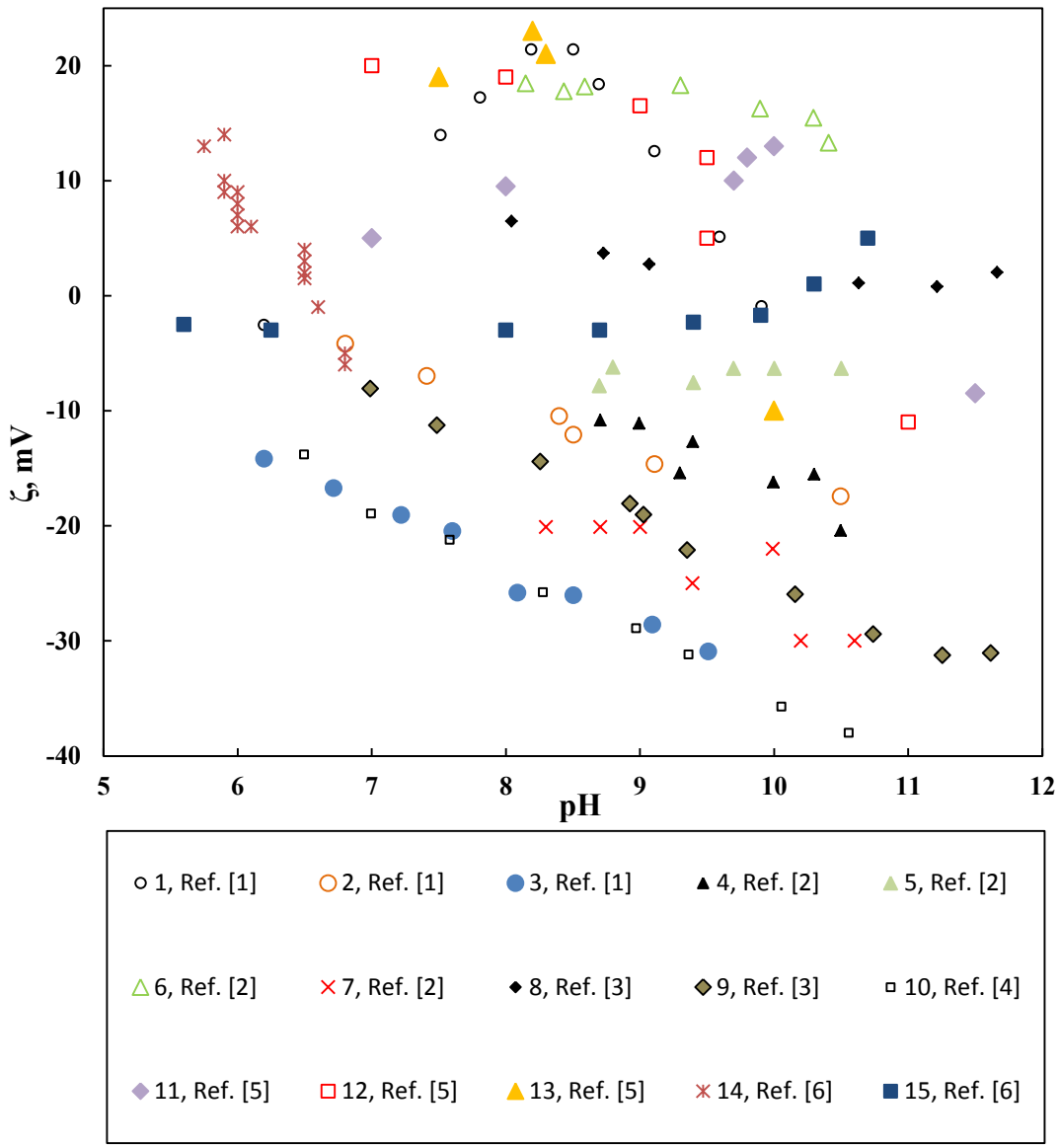

Figure 3.4: Zeta potential as a function of pH reported on various artificial and natural calcite and limestone for various electrolyte compositions and ionic strengths. Vdovic (2001) (Ref. 1) used synthetic calcite (labelled 1), natural limestone (2), and lake sediments (3) in 10^{-3}M NaCl electrolyte. Cicerone et al. (1992) (Ref. 2) used synthetic calcite in 0.03M KCl (4), 0.001M $CaCl_2$ (5) and 0.01M $CaCl_2$ (6) electrolytes, and natural calcite in 0.03M KCl electrolyte (7). Thompson and Pownall (1989) (Ref. 3) used synthetic calcite in $5x10^{-4}$M $CaCl_2$ (8) and 0.005M NaCl (9) electrolytes. Sondi et al. (2009) (Ref. 4) used natural calcite in 0.001M NaCl electrolyte (10). Somasundaran and Agar (1967) (Ref. 5) reported measurement of calcite in deionized water after no mixing (11), mixing for one week (12), and mixing for two months (13). Heberling et al. (2011) (Ref. 6) used calcite in 0.1M NaCl in equilibrium with $p(CO_2)$=1 bar (14) and non-equilibrium 0.01M NaCl with 0.005M $CaCl_2$ (15).

More recent studies have employed natural calcite that was derived from chalk (e.g., Zhang and Austad, 2006) and reservoir limestone (Chen et al., 2014). The salinity range that the EPM zetameter is reported to reach (e.g., Zhang and Austad, 2006) is (~1 M), which the authors were able to do (Figure 3.5). This is representative of seawater salinity but still well below the formation brine salinity of hydrocarbon reservoirs and the associated saline aquifers (above 2 M). Figure 3.5 shows two series of experiments where either calcium or sulfate were added to a 0.573 M NaCl background electrolyte, which is equivalent to seawater in ionic strength.

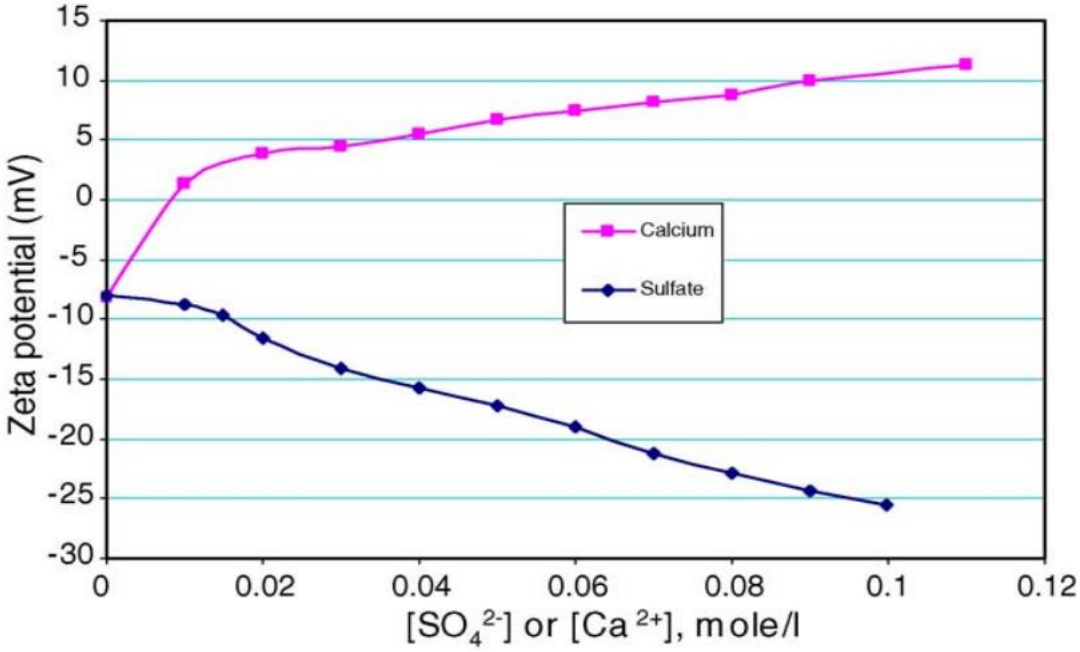

Figure 3.5: Zeta potential measurements for calcium and sulfate on chalk using a 0.573M NaCl background electrolyte. After Zhang and Austad (2006).

The starting NaCl point (Fig. 3.5) shows a negative zeta potential but becomes positive as calcium is added. When sulfate is added, the zeta potential becomes more negative. The authors assumed that the zeta potential measured represent the Stern plane potential and that the distance between the calcite surface and the shear plane is constant. They concluded that the average charge on the chalk surface appeared to be dictated by the relative concentration of the two PDIs.

Yousef et al. (2012) reported zeta potential measurements for carbonate reservoir samples on a number of seawater dilutions (from twice up to a hundred times) notated as normal dilution in

Figure 3.6 whereas the common ion dilution refers to diluting the NaCl but not the salts containing PDIs. It is clear that diluting seawater leads to a more negative zeta potential, which is comparable to the increase in the zeta potential noticed in the common ion dilutions (except at 100x dilution). Their conclusion is that these measurements confirmed that increased oil recovery from diluted seawater they observed were related to changes in the surface charge towards more negative, which lead to more interactions with water molecules, and eventually alter the rock wettability. This is the only work to date that used the same brines to relate increased oil recovery to changes in the surface charge as measured by the zeta potential. Yousef et al.‟s (2012) measurements are limited to room temperature and were done on cleaned samples of the rock in absence of an oil phase. Moreover, they could not obtain any measurements for seawater or formation brine compositions.

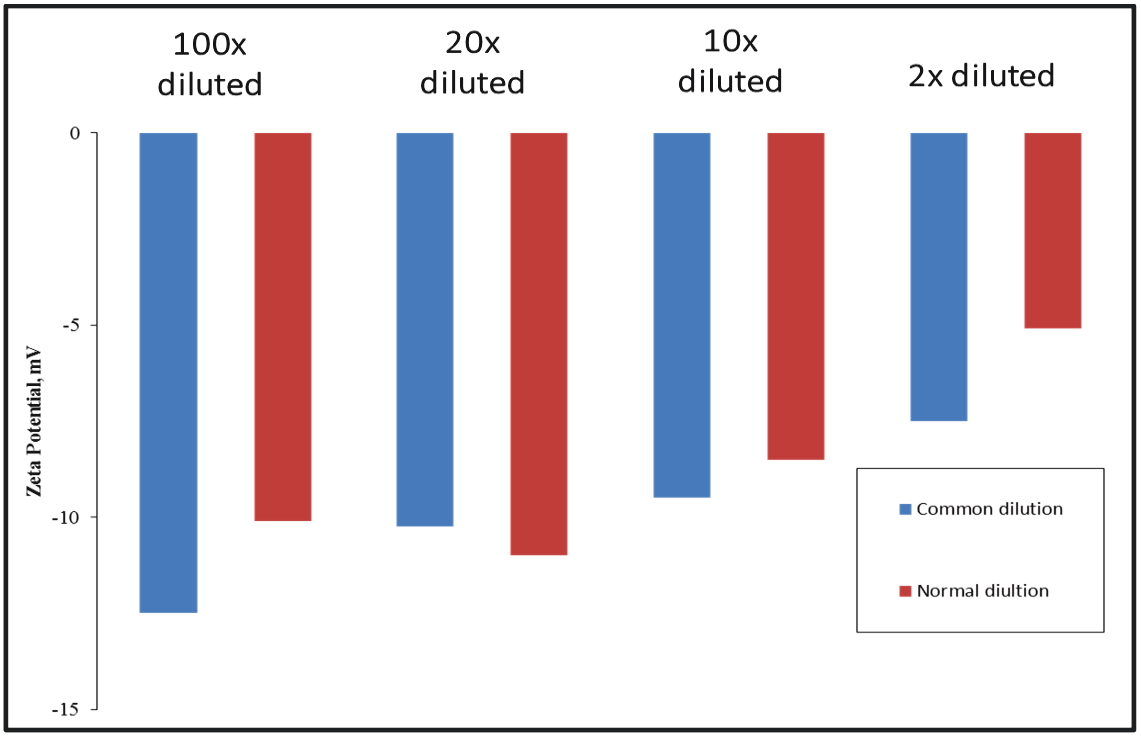

Figure 3.6: Zeta potential measurements for reservoir carbonate rocks for seawater derived dilution of 2x, 10x, 20x, and 100x. Common ions dilution refers to the dilution of Na^+ and Cl^- alone. After Yousef et al. (2012).

Chen et al. (2014) reported zeta potential measurements of a synthetic formation brine of high salinity on four reservoir rocks as shown in Figure 3.7, which shows that the zeta potential can be

either positive or negative depending on the limestone‟s mineralogy. Table 3.1 shows the composition of each rock as derived from XRD analysis. At full formation brine, all the rocks show a positive zeta potential except sample S86 with a negative zeta potential. Sample S86 has the least amount of calcite (Table 3.1). The zeta potential gets more negative as the formation brine is diluted for all the rock samples except AD, which only gets a negative zeta potential at 1/16 formation brine dilution. Sample AD has the highest amount of calcite (98%). Hence, the zeta potential is also dependent on the mineralogical composition of the rock.

Table 3.1. XRD analysis for carbonate rock powders from Chen et al. (2014)

Sample/ mineral %	Quartz	Feldspar	Plagioclase	Calcite	Ankerite	Siderite	Pyrite	Clays
TP	9	-	-	82	4	-	1	4
AD	1	-	-	98	-	-	-	1
AO	16	1	-	71	-	1	2	9
S86	19	2	9	47	14	-	1	8

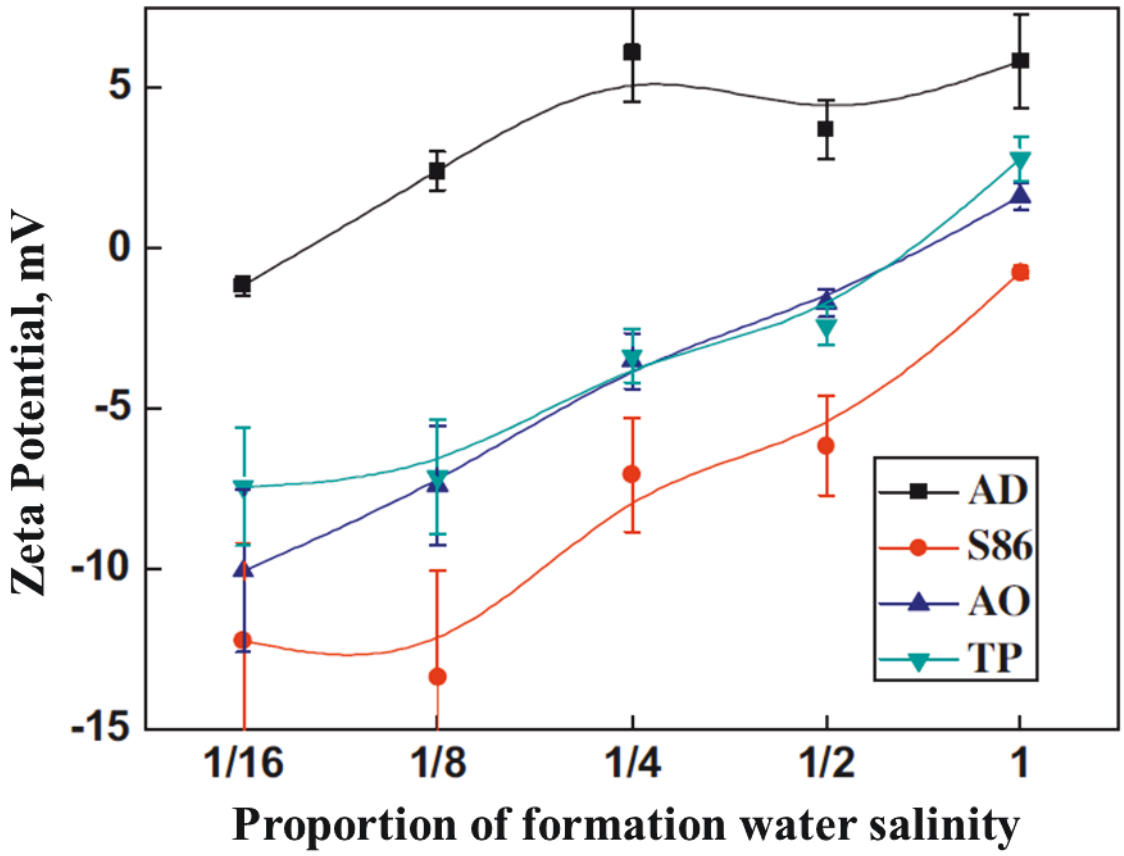

Figure 3.7: Zeta potential measurements of different ratios of a synthetic formation brine. The data is shown for four reservoir limestone rock samples from Table 3.1. After Chen et al. (2014).

Also, they report zeta potential measurements on a wide concentration range of sodium, calcium, and magnesium salts on one of the reservoir limestone rocks, as shown in Figure 3.8. The zeta potential decreases dramatically up to 1 wt% of added salts. At higher concentrations, it decreases very slowly up to 10 wt%, where it turns positive for the calcium and magnesium salts. The authors believe the inflection point at 1 wt% is probably caused by the completion of monolayer adsorption. However, it is not possible to compare the effect of each ion (Na, Ca and Mg) on the zeta potential because the salt concentration was reported in wt% rather than molar concentrations. Also, this means that the effect of total salinity versus PDI can not be determined.

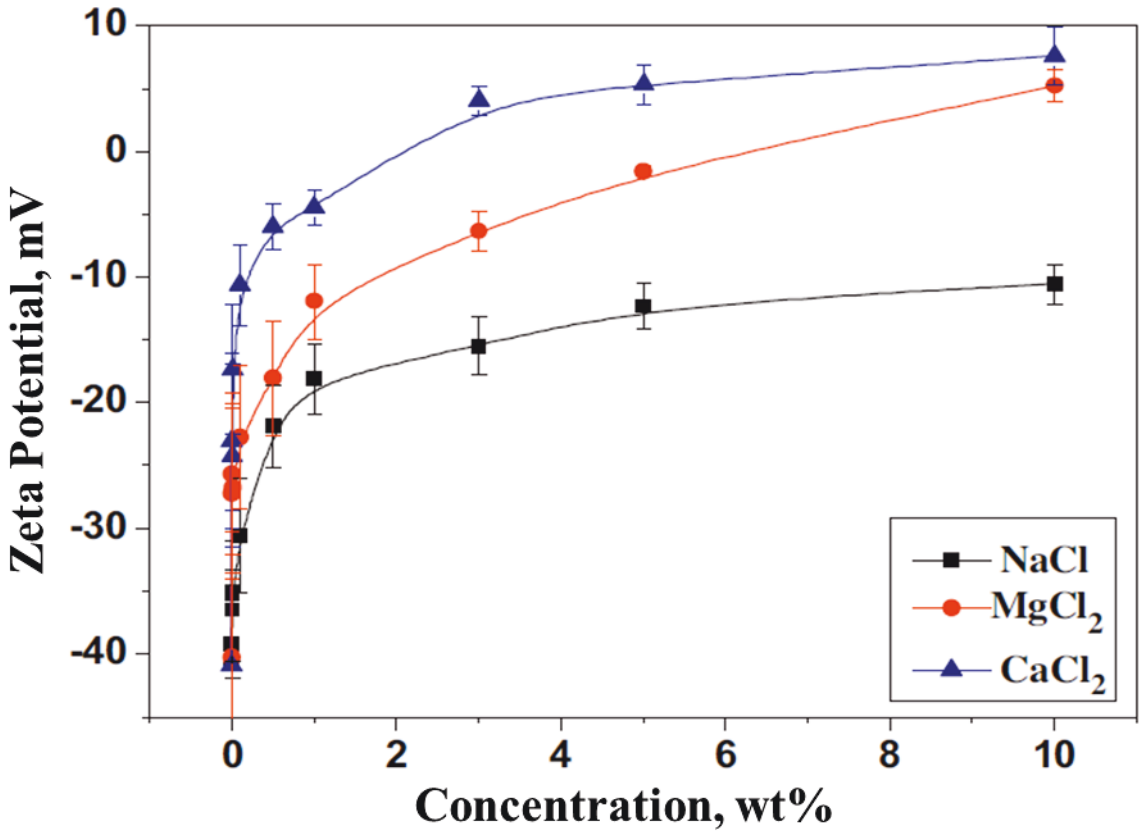

Figure 3.8: Zeta potential measurements of three salts for reservoir limestone. After Chen et al. (2014).

Mahani et al. (2015) measured the zeta potential on formation brine, seawater, and seawater diluted 25 times for a Middle Eastern reservoir limestone. This was done in order to show how the electrostatic interaction changes during low salinity waterflooding from one extreme (FW) to the other (25dSW). Formation brine always resulted in a positive zeta potential throughout the pH range as seen in Figure 3.9. Seawater is negative at its default pH=8 but shows a PZC at pH = 9.4, above which it becomes positive. The seawater dilution (25dSW) was more negative than seawater throughout the pH range and showed a higher PZC at pH = 10.3. However, it is not realistic to modify the pH in this range because the low salinity effect was never shown to cause any pH change. Hence, the most reasonable thing to do was to leave the system at its current equilibrium without modifying the pH (with acid and/or base).

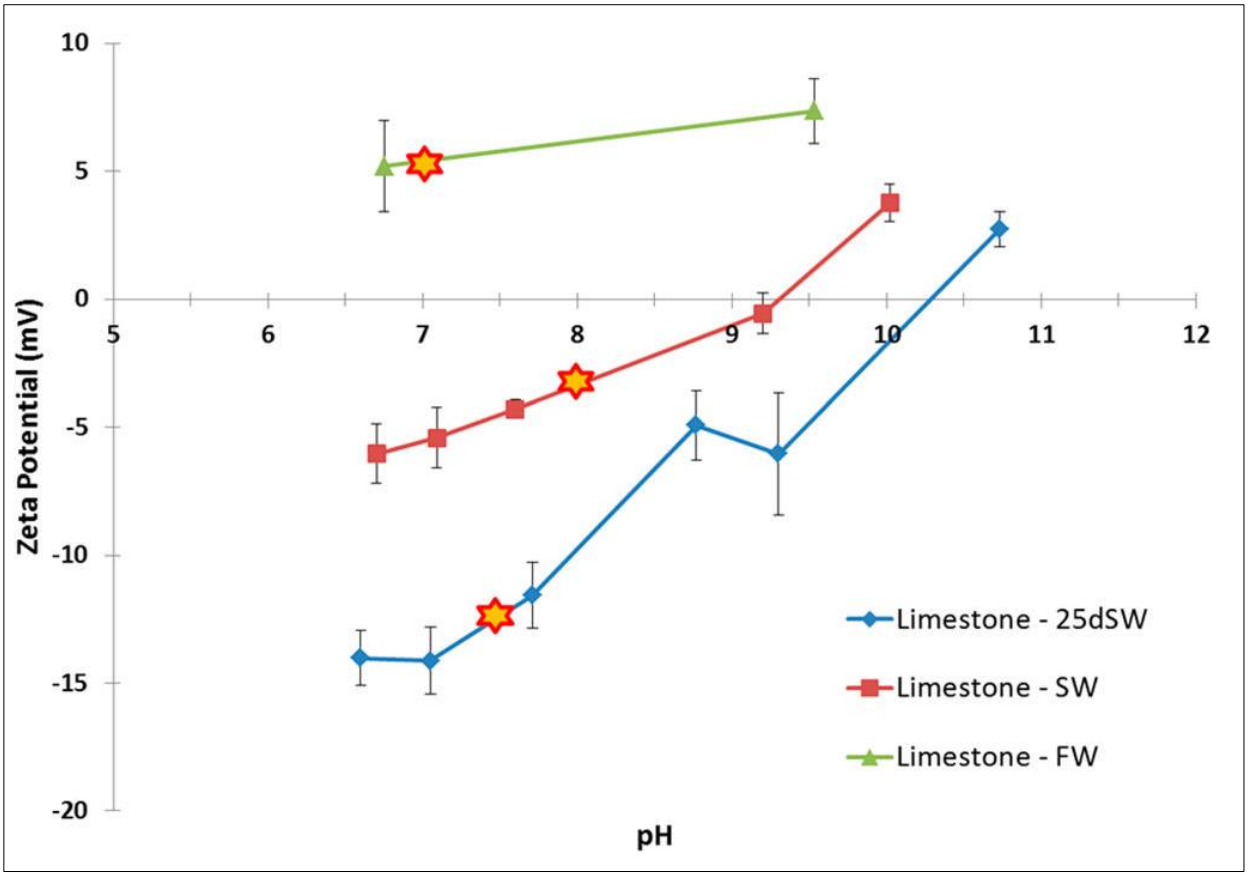

Figure 3.9: Zeta potential of limestone particles in formation brine (FW), seawater (SW), and seawater diluted 25 times (25dSW) in the pH range of 6.5−11 (yellow stars represent the natural pH of the brines). After Mahani et al. (2015).

The measurements of zeta potential have improved from using very dilute electrolytes and synthetic (e.g., Iceland spar) calcite to using real reservoir rocks and synthetic formation brines that represent the salinity and composition encountered in real reservoirs. However, these measurements are still of limited relevance to the real subsurface settings because EPM is conducted on powder, which means that the porous medium; the pore bodies and throats are not preserved since the sample is crushed and powdered. Also, EPM does not account for the presences of a third phase (e.g., crude oil), which means it does not represent rocks of variable wettability states. There is confusion as to what controls the surface charge of calcite as evidenced by continuing the usage of acids/bases to cause pH modification and to measure the corresponding zeta potential. Out of the studies that varied the PDI concentration and kept the pH constant, none considered the effect of the total ionic strength on the effect of the PDI on the zeta potential. For

example, calcium effect on the zeta potential might be different for a NaCl background electrolyte of different concentrations.

3.7.2. Oil/Water Surface Charge

Much less attention has been given to the oil-brine interfacial charge. This might be related to the its uncertain origin but more likely because the force at this interface is mainly characterized by the interfacial tension (IFT) measurements, which serves in other areas of enhanced oil recovery (EOR) such as polymer flooding.

Buckley et al. (1989) was the first work to systematically measure the zeta potential at crude oil-brine interface in order to understand how adhesion of oil to glass plates relate to how the zeta potential changes with ionic strength and pH. Figure 3.10 shows zeta potential measurements for Moutray crude oil/water interface at different salinities and pH values. The main point to highlight is that the charge is only positive at pH below 4 and the zeta potential is higher for lower NaCl concentrations as seen in Figure 3.10. However, their study was not adequate for petroleum reservoirs as the highest salinity they experimented with was 0.1M NaCl.

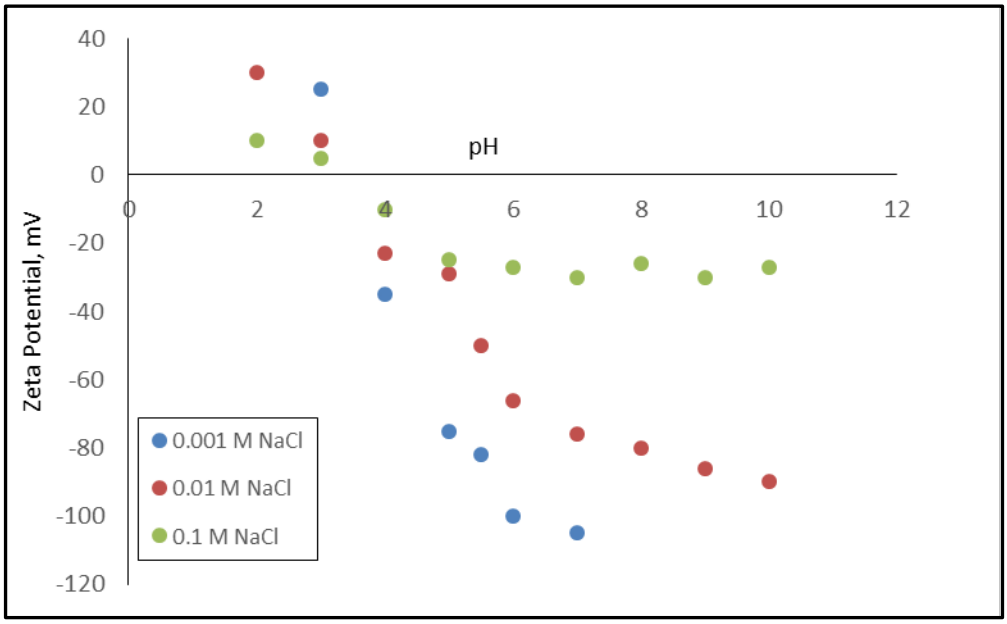

Figure 3.10: Oil/Water interface zeta potential measurements on Moutray crude as a function of brine's pH and salinity. After Buckley et al. (1989).

Nasralla and Nasr-El-Din (2014) measured zeta potential for two crude oil-brine emulsions. Table 3.2 shows the oils properties. Three salts were used including two multivalent ions (calcium and magnesium) at three concentrations (Figure 3.11). The higher the salinity, the lower the zeta potential because of the thinned EDL. Also, the divalent ions were able to lower the zeta potential much better than the monovalent sodium ion. Actually, calcium lead to polarity reversal from negative to positive at 50,000 mg/L for both oils. Their conclusion is that lowering the total salinity and the calcium concentration leads to a more negative zeta potential at the oil-brine interface, which should add to the electrostatic repulsion.

Table 3.2 Oil properties from Nasralla and Nasr-El-Din (2014)

Sample	Density (kg/m^3)	Viscosity (Pa.s)	AN (mg KOH/g)	BN (mg KOH/g)
Oil A	886	0.0322	0.18	1.65
Oil B	828	0.0204	0.11	0.62

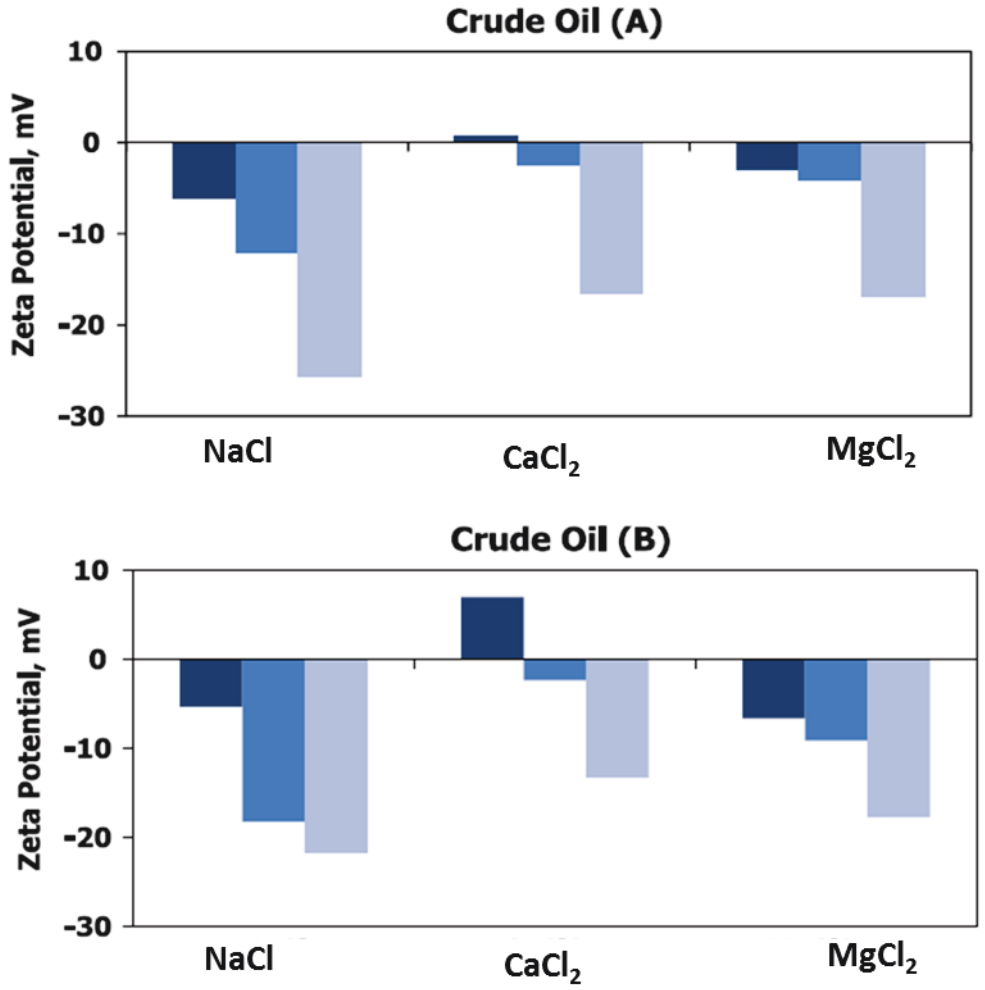

Figure 3.11: Zeta potential of oil-in-water emulsion for two crude oils. Three salts (NaCl, $MgCl_2$, $CaCl_2$) were used at 2000 (light blue), 10000, and 50000 (dark blue) ppm concentrations. After Nasralla and Nasr-El-Din (2014).

Mahani et al. (2015) measured the zeta potential for a Middle Eastern crude oil in formation brine, seawater and seawater diluted 25 times (25dSW). The oil-brine interface was negatively charged for all brines throughout the investigated pH range of 3−10.5 as seen in Figure 3.12. The authors could only note that the lower the ionic strength the higher the zeta potential of the oil-in-water emulsion, and were not able to conclude if, for example, Ca in the formation brine was able to lower the measured zeta potential. Thus, a switch from attraction to repulsion is expected when formation brine is displaced with seawater and even more repulsion should result when displacing with seawater diluted 25 times (25dSW). As discussed in the previous section, modifying the pH is

not practical since it does not change when considering the application studied (i.e., low salinity waterflooding).

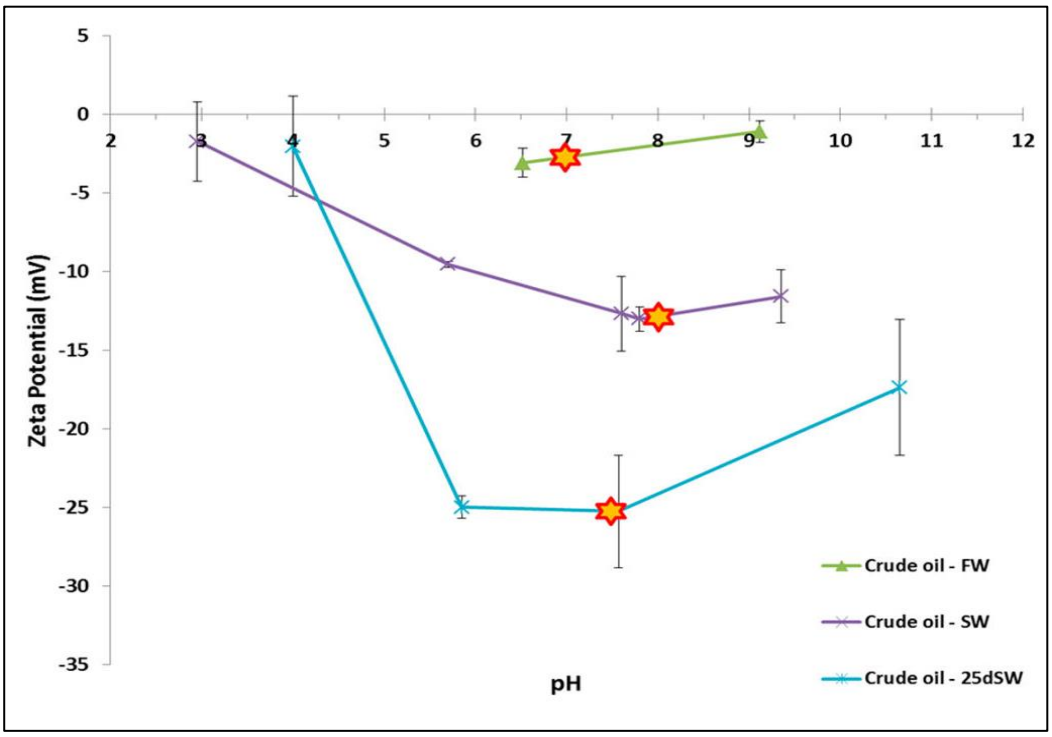

Figure 3.12: Zeta potential of oil-in-water emulsion for formation brine (FW), seawater (SW), and seawater diluted 25 times (25dSW) in the pH range of 6.5−11 (yellow stars represent the natural pH of the brines). After Mahani et al. (2015).

3.7.3. Wettability Effect on the Surface Charge

We have seen the effect of the water chemical composition on both the surface charge of calcite and the oil recovery, and hence, the wetting state of the system. A natural conclusion we might draw is that there must be a relationship between the surface charge and the wetting state. Preliminary results reported in Jackson and Vinogradov (2012) demonstrated the existence of such a relationship between the wetting state and electrokinetic (streaming potential) measurements. These initial results make the basis and motivation for starting this work.

The excess charge density transported by the flow (Q_w) can be calculated from the coupling coefficient as (Jackson and Vinogradov, 2012):

$$Q_w = -\frac{C_{SPM}\sigma_{rw}\mu_w}{k_w}, \tag{3.6}$$

where σ_{rw} is the conductivity of the saturated rock, μ_w and k_w are the viscosity and relative permeability of the brine. It was shown (Jackson and Vinogradov, 2012) that the excess charge density is different for samples of different wetting states. This is related to the two interfaces (oil-brine, brine-mineral) having charges of opposite sign (Figure 3.13b and 3.13c). This difference in charging because of the different wetting state is reflected in differences in the measured C_{SPM}. Thus, this difference in charging is not transient as C_{SPM} was found to be consistent for each sample indicating that the measurements reflect the true redistribution of the counterions of each interface and that the excess charge density is effectively an average of the counterions of both interfaces.

This excess charge density was much higher in magnitude for the water-wet case when the fully saturated sample was flooded to residual oil saturation. In comparison, the aged sample that became more oil-wet had zero excess charge density (Figure 3.13a).

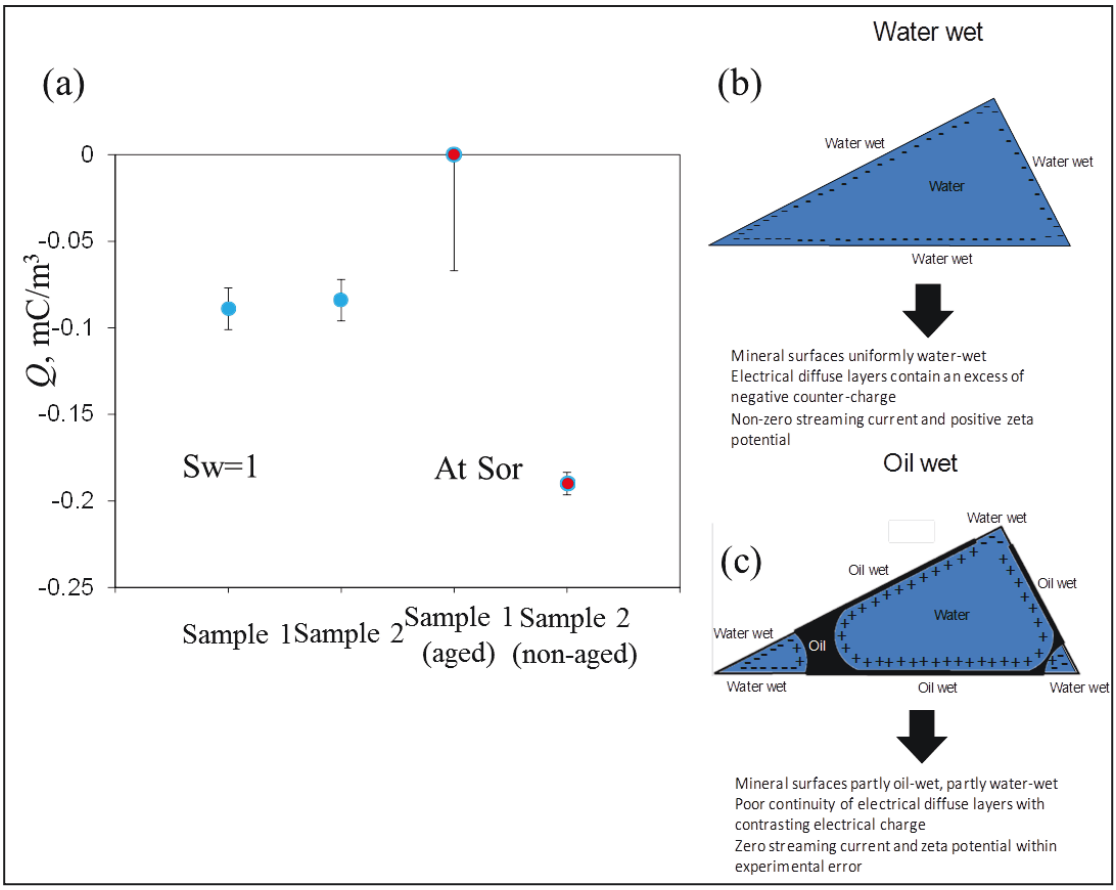

Figure 3.13: Excess charge density of the 2 samples at 100% water saturation versus at residual oil saturation after aging one sample. After Jackson and Vinogradov (2012).

More recently, Kasha et al. (2015) have reported zeta potential values using electrophoretic mobility measurements on clean and stearic-acid aged calcite and dolomite particles. Figure 3.14a shows the zeta potential dependence on pH in deionised water (DIW) for both clean and aged calcite crystals whereas Figure 3.14b shows the same comparison for the dolomite crystals. For each mineral, it is clear that the trend of zeta potential vs pH observed is the same for both pure and aged. The exception for calcite is at pH 8 and 9.5 and for dolomite at pH 5.5, 6.5, and 11.5 where the aged particles showed a more negative zeta potential when compared to pure powder.

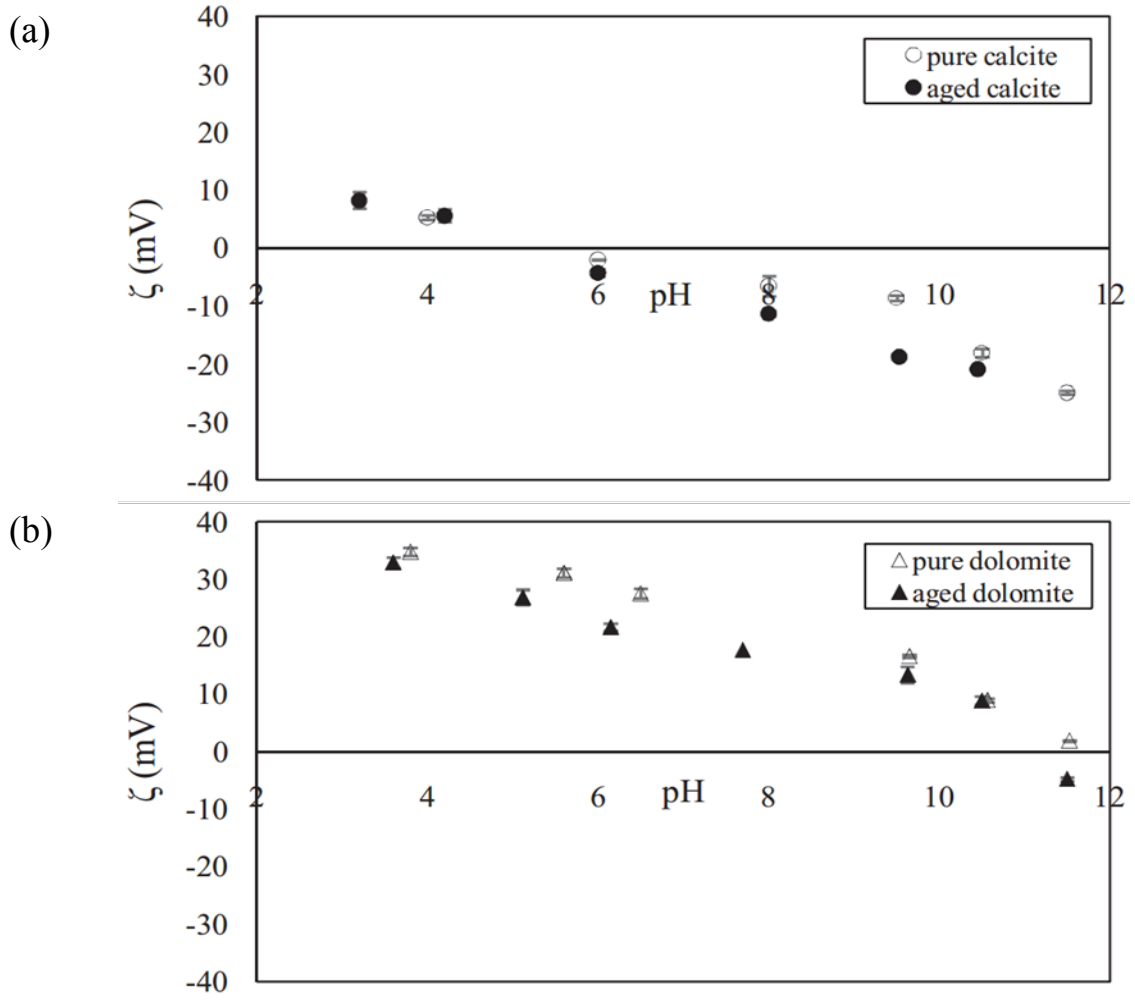

Figure 3.14: The effect of aging on the zeta potential dependence on pH in deionized water for a) pure vs aged calcite b) pure vs aged dolomite. After Kasha et al. (2015).

Figure 3.15 shows the effect of the PDIs (Ca, Mg, SO_4) on the zeta potential of the aged particles of calcite and dolomite. Figure 3.15a shows the default zeta potential for both minerals in absence of any added PDIs in a NaCl background electrolyte with a seawater equivalent ionic strength.

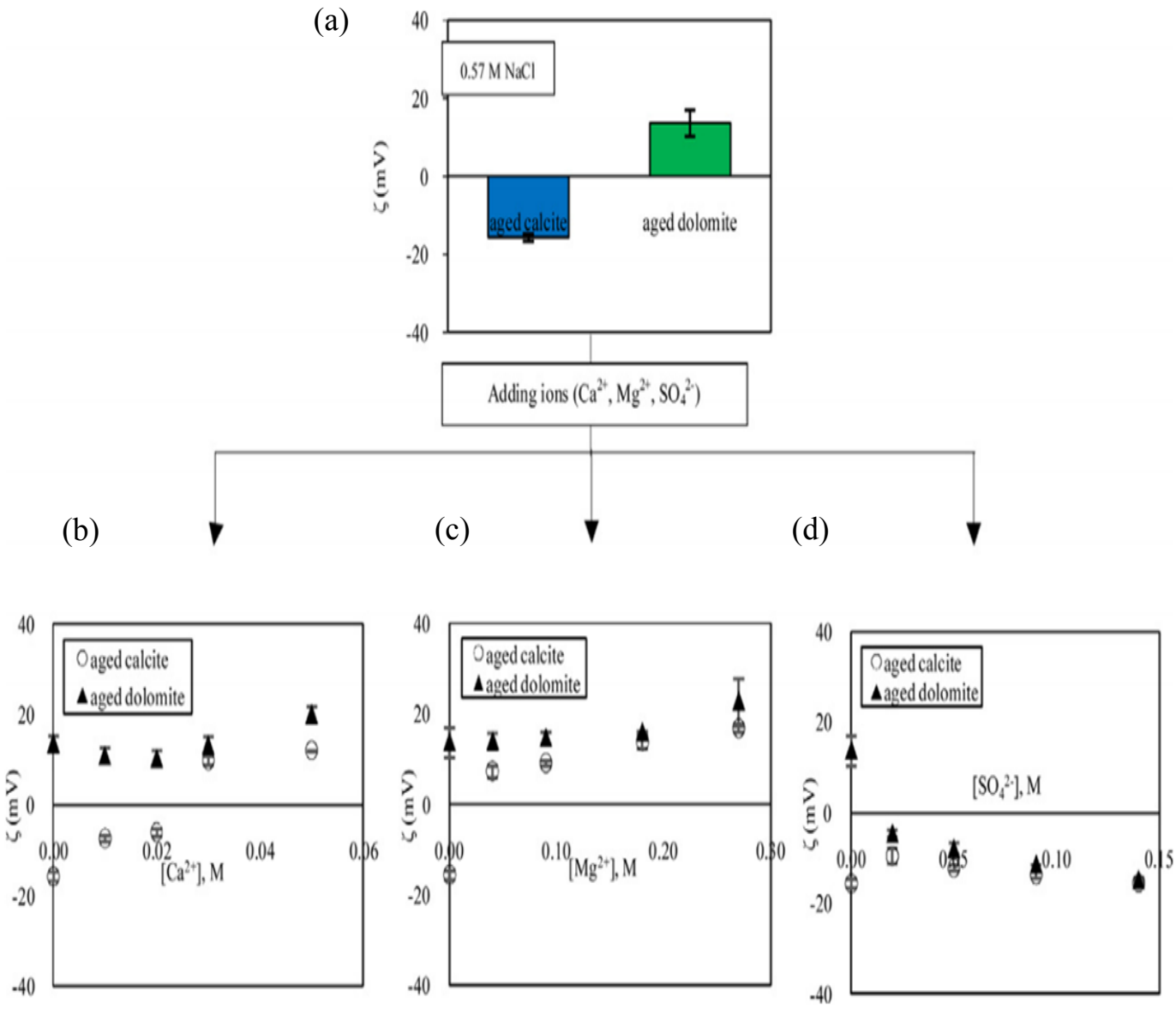

Figure 3.15: The effect of the three PDIs on the zeta potential for both aged calcite and dolomite in 0.574 M NaCl, a) aged calcite and dolomite in 0.574 M NaCl b) the effect of calcium concentration on both minerals c) Magnesium effect and d) sulfate effect. After Kasha et al. (2015).

Figure 3.15b-3.15d show the effect of adding calcium, magnesium and sulfate, respectively. An interesting observation is that calcite (negatively charged in NaCl) seems to responds to the addition of Ca and Mg while the addition of SO_4 showed little effect on the zeta potential. Another interesting observation is that the addition of Ca and Mg had little effect on the zeta potential for

dolomite, which is positively charged in NaCl, whereas the addition of SO_4 resulted in the polarity reversal of the dolomite‟s surface charge.

3.8. Focus Area

Water chemistry affects both the surface charge and the wettability as was discussed in Chapters 2 and 3. The relationship between the surface charge and wettability is expected to be affected by water chemistry. Hence, an understanding of the surface charge of clean calcite in various brines especially, formation brine and seawater become a pre-requisite for understanding the relationship of wettability and surface charge. Thus, the work was divided into two broad areas where streaming potential measurements are conducted in order to:

1. Understand the effect of the PDI (Ca, Mg, and SO_4) and total salinity on the zeta potential (Chapter 4)
2. Understand the effect of the wettability (as S_{wi} or 1-S_{or}) on the zeta potential (Chapter 5)

4. Zeta Potential of Intact Natural Limestone: Impact of Potential-Determining Ions Ca, Mg and SO_4

4.1. Introduction

The aim of this chapter is to determine the zeta potential in intact natural carbonate samples saturated with aqueous electrolytes containing PDIs at similar concentration to natural brines, and with total ionic strength similar to natural brines. We are particularly interested in determining how the zeta potential is affected by the concentration of PDIs such as Ca, Mg and SO_4 over the range found in natural brines. Several previous studies have investigated the relationship between Ca concentration and zeta potential, but these typically probed concentration ranges much lower than natural brines (see Sections 3.6 and 3.7.1). Much less attention has been paid to the role of Mg and SO_4 as PDIs, yet these ions are also abundant in natural brines such as seawater (e.g., Zhang and Austad, 2006). We also wish to determine how the zeta potential is affected by the concentration of these PDIs in the presence of Na and Cl ions over the range found in natural brines. Sodium and chloride are by far the most common ionic species found in such brines and are not thought to act as PDIs for carbonate minerals; nonetheless, it has not yet been determined whether the effect of the known PDIs (Ca, Mg and SO_4) on carbonate surface charge is modified by the presence of Na and Cl at high concentration.

Our approach contrasts with many previous studies because the experimental method is specifically designed to ensure the equilibrium achieved between sample and electrolyte is consistent with natural processes, which was found to be important even with sparingly soluble minerals such as quartz (Walker et al., 2014). The results are directly applicable to a wide variety of natural subsurface carbonates.

4.2. Methodology

4.2.1. Materials and sample preparation

The rock samples used in the experiments are Portland limestone from the Portland quarry on the South Coast of the UK (Table 4.1). We used two different types of electrolyte. The first comprised reagent-grade NaCl, $CaCl_2.2H_2O$, Na_2SO_4 (Sigma-Aldrich), $MgCl_2.6H_2O$ (Fluka Analytical) solutions in deionized water (DIW) from a Thermo Scientific filtered system with electrical conductivity below 1 μS/cm. In these electrolytes, the maximum concentration probed was 2 M for NaCl, 0.42 M for $CaCl_2$ and $MgCl_2$, and 0.13 M for Na_2SO_4. The second comprised natural seawater (SW) from the Arabian Gulf, collected from Dammam, Saudi Arabia. The natural seawater sample was treated with UV light and then filtered through 5 μm filter paper. Table 4.2 lists the compositions of the electrolytes used, including the natural seawater and synthetic formation brine (FMB) typical of oil reservoirs and deep saline aquifers (e.g., Romanuka et al., 2012).

Table 4.1. Properties of Portland rock samples used in this study.

Sample	Porosity (%)	Permeability (10^{-15}, m^2)	Formation Factor (F)
P1	20±0.4	2.96±0.48	21.3±0.8
P2	19.5±0.4	2.17±0.3	22.4±1
P3	21±0.4	3.45±0.55	20.6±0.9

Table 4.2. Composition of the synthetic formation brine (FMB) and natural seawater (SW) and derived compositions used in this study. The seawater was twice (½SW), ten times (1/10SW), and twenty times (1/20SW) diluted, and also had SO_4 added to yield twice (2SW), three times (3SW), and four times (4SW) the natural concentration.

Concentration M	FMB	SW	1/2SW	1/10SW	1/20SW	2SW	3SW	4SW
Na	2	0.5	0.25	0.05	0.025	0.5	0.5	0.5
Ca	0.42	0.012	0.006	0.0012	0.0006	0.012	0.012	0.012
Mg	0.07	0.05	0.025	0.007	0.00025	0.05	0.05	0.05
SO4	0.0033	0.033	0.016	0.0033	0.0016	0.066	0.099	0.13
Total	2.49	0.615	0.107	0.061	0.0107	0.648	0.681	0.715

Figure 4.1 shows a flowchart of all the steps leading to the measurement of the coupling coefficient C_{SPM} including brine and rock sample preparation and equilibration.

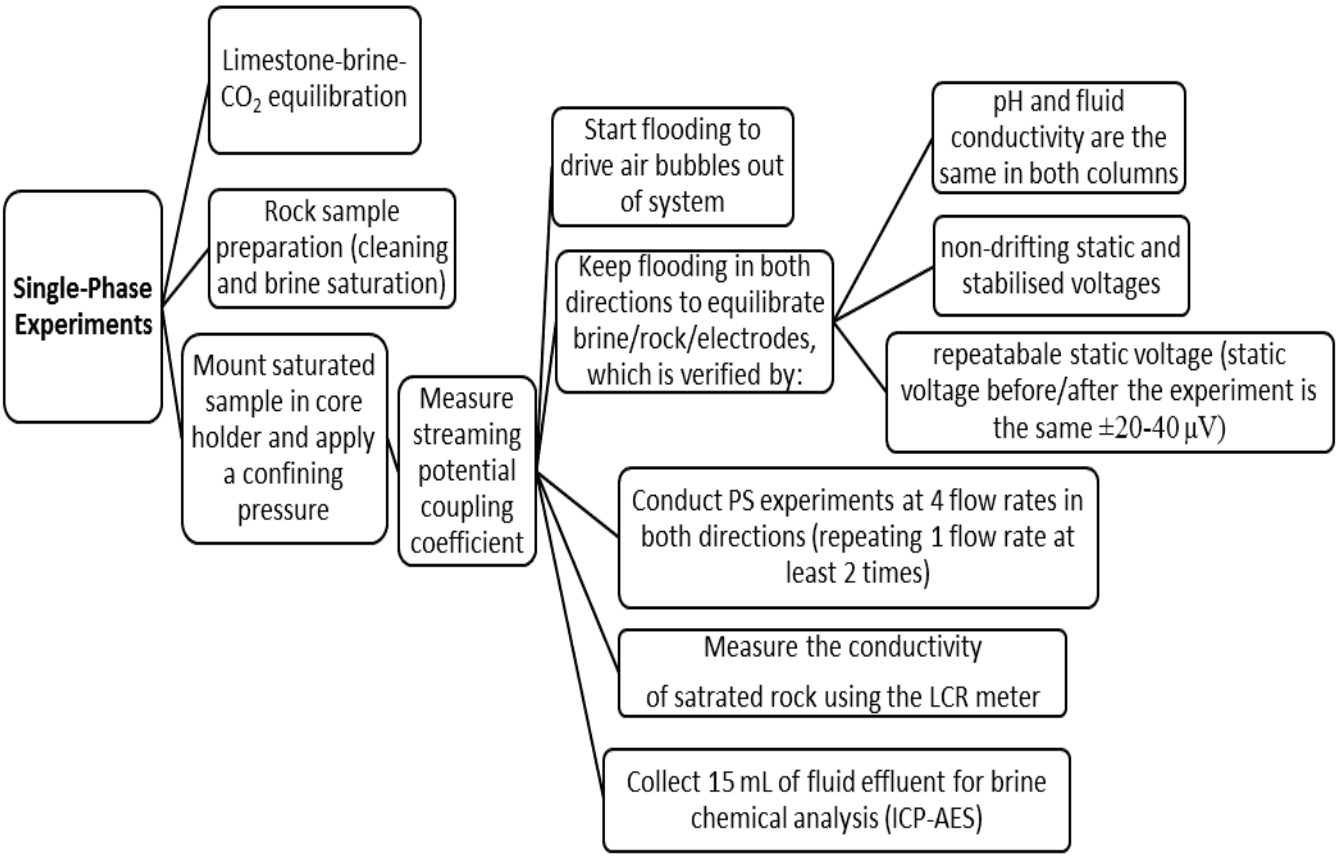

Figure 4.1: Flowchart showing the steps taken in single-phase streaming potential experiments including brine and rock preparation and voltage repeatability establishment.

The majority of limestone formations are directly deposited in seawater (Morse, 1986; Morse and Mackenzie, 1990) and the seawater is in equilibrium with both calcite and CO_2 (Stumm and Morgan, 1996). Any factor, such as organic activity, CO_2 partial pressure, or temperature that modifies the equilibrium will result in precipitation or dissolution of calcite. Carbonate minerals are soluble in water, with calcite having a solubility product $K_{sp} = 10^{-8.48}$ (Plummer and Busenberg, 1982). Dissolution yields carbonate ions (CO_3) that can react to form bicarbonate (HCO_3) and hydroxide (OH) ions according to the equilibrium reactions

$$\mathbf{CaCO_{3\,(s)} \leftrightarrow Ca^{2+} + CO_3^{2-}, \text{ and}}$$
$$\mathbf{CO_3^{2-} + H_2O \leftrightarrow HCO_3^{-} + OH^{-}.} \quad (4.1)$$

If the system is open, atmospheric CO_2 dissolves into the water, reacting directly with hydroxide to form bicarbonate and hence reducing the pH according to the equilibrium reaction

$$\mathbf{CO_{2(aq)} + OH^- \leftrightarrow HCO_3^-.} \quad (4.2)$$

Equilibrium between calcite and water in the presence of CO_2 is reached when most of the carbonate ions are turned into bicarbonate (Krauskopf, 1989); this corresponds to a minimum aqueous concentration of carbonate and carbonic acid, and a maximum for bicarbonate (Figure 4.2a). The equilibrium pH is 8.3-8.4 (Garrels and Christ, 1965; Stumm and Morgan, 1996; Figure 4.2a).

These conditions of carbonate/water/CO_2 equilibrium were replicated here in the following way. For DIW-based electrolytes, we began by preparing a NaCl solution of the desired concentration in DIW. This solution was then placed in a beaker with offcuts of the Portland limestone, maintaining an air layer in the beaker to provide a source of atmospheric CO_2 but sealing the beaker to prevent evaporation. Monitoring of the pH (using a Five-Go Mettler-Toledo pH meter) and Ca concentration (described below) confirmed the dissolution of calcite and associated pH changes discussed above (Figure 4.2b). The initial increase in pH reflects the formation of hydroxide ions according to the equilibrium reaction (4.1). The subsequent decrease in pH reflects the formation of bicarbonate according to the equilibrium reaction (4.2). The final pH of the equilibrated solution was *c.* 8.2, consistent with the predicted value for an open system (Figure 4.2a). Dissolution of calcite is demonstrated by the increase in Ca concentration from zero to *c.* 0.001M (Figure 4.2b). The resulting equilibrated NaCl solution was termed NaCl-EQ. For the experiments reported below, equilibrated solutions of three different NaCl concentrations (0.05 M, 0.5 M, and 2 M) were prepared. Equilibrium was assumed to have been reached at a measured pH of 8.2±0.2. The NaCl-EQ solution was then used directly in zeta potential measurements, or was modified by addition of PDIs. This preparation step is essential to ensure equilibrium between calcite, water and atmospheric CO_2 defined by constant ionic strength and pH. Also, it prevents calcite dissolution and associated changes in formation factor and surface charge during measurements of zeta potential.

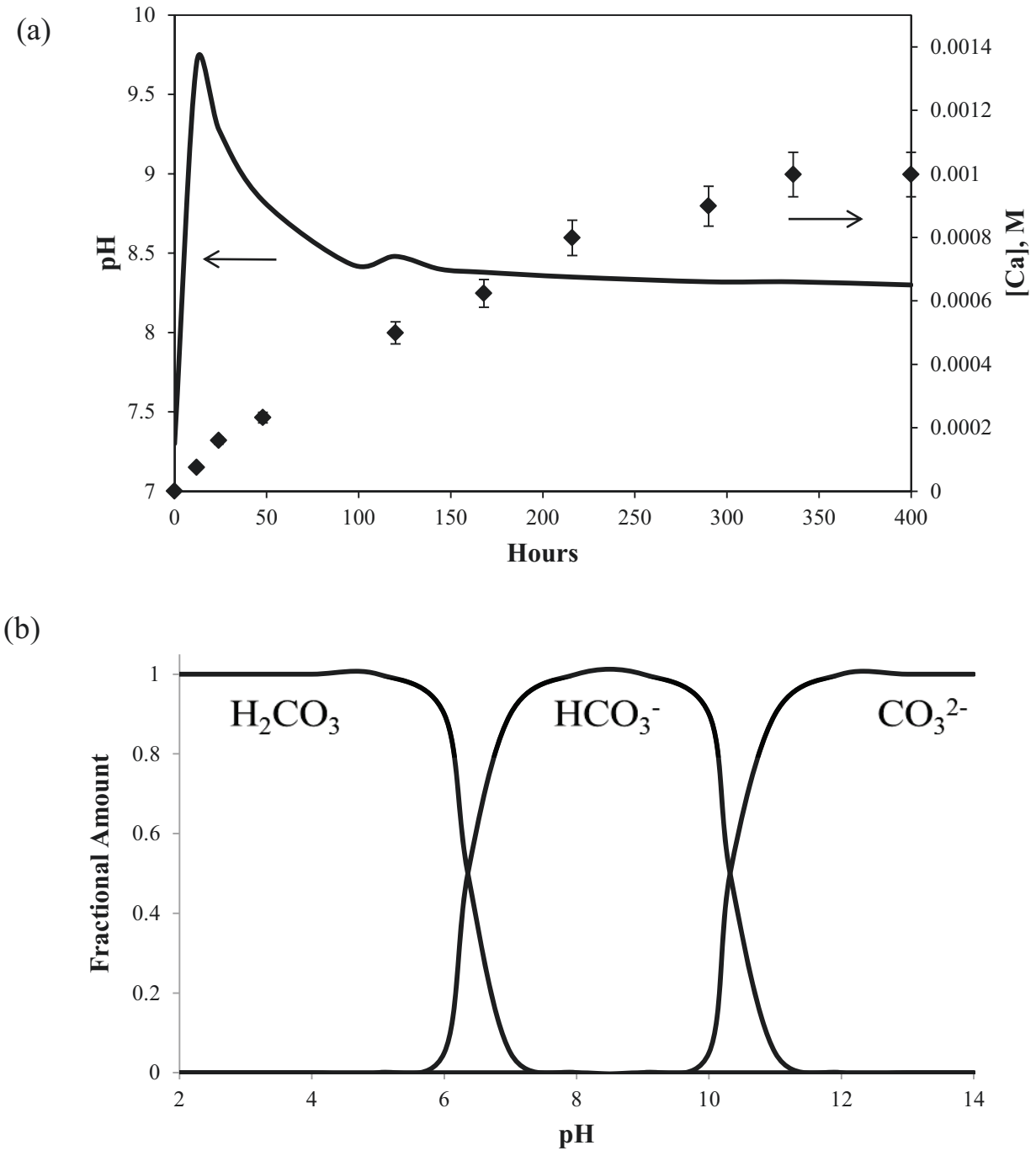

Figure 4.2: Calcite-water-CO_2 equilibrium. (a) Calcium concentration and pH measured here as a function of time during equilibration of the natural Portland rock samples with DIW. pH was measured every 12 hours for the first 96 hours, and every 24 hours thereafter. Ten milliliter samples were taken from the beaker for calcium concentration analysis. (b) Calculation of the carbon speciation into H_2CO_3, HCO_3^-, and CO_3^{2-} as a function of pH (modified after Stumm and Morgan, 1996).

The core flooding apparatus used to measure the zeta potential in the SPM (described below) is closed to the atmosphere, and the final equilibration step prior to measuring the zeta potential was to ensure equilibrium between the electrolyte of interest (NaCl-EQ after the addition of any PDIs to be studied) and the rock sample at the closed-system conditions pertaining to a rock-brine system at depth. The rock sample was pre-saturated with the selected electrolyte at open-system conditions and then confined in the core holder at closed-system conditions, and the electrolyte was pumped through the sample from the (closed) inlet reservoir to the (closed) outlet reservoir and back again. At regular intervals, the electrical conductivity and pH of the electrolyte in the reservoirs was measured, and equilibrium was assumed to have been reached when the conductivity and pH of the electrolyte in each reservoir differed by <5%. Addition of Ca or Mg reduced the pH to the range 7-7.5 while addition of SO_4 caused a smaller change, yielding pH in the range 7.9-8.1. These are consistent with reported values for natural brines in carbonate rocks (pH ~ 7-8; Yousef et al., 2012).

Prior to a given experiment, the rock sample was cleaned in a Soxhlet apparatus with methanol for 48 hours. It was then dried for at least 12 hours in a vacuum oven at 80^{o} C. Then, it was allowed to cool at room temperature for a minimum of 6 hours. The rock sample was saturated with the brine of interest for 24 h in the vacuum oven. Then, the sample was loaded into the core holder and a confining pressure *c.* 3500 kPa was applied. At least 2 flow rates were used to drive the brine from one reservoir column to the other in order to insure no air was trapped. Each flow rate experiment consists of flooding the brine from the right column through the core holder to the left column for a minimum 30 minutes and flooding back from the left column to the right column. The flow rate chosen is slightly higher than the other flow rates, which are used for the streaming potential measurements. Air bubble are visually monitored and pushed out of the flow lines by tapping on the part where the bubble is stuck.

This is a standard core sample cleaning procedure used in many previous studies and was used with fresh samples here (e.g., Jaafar et al., 2009). However, for reasons discussed later in the chapter, after a series of experiments using electrolytes with elevated PDI concentration, the rock samples were flooded with at least 2 pore-volumes (PV) of deionized water (DIW) prior to the methanol cleaning step, and were then flooded with a further 4 PV of 0.05 M NaCl-EQ electrolyte. The conductivity of the effluent electrolyte was measured in order to confirm it was the same as that obtained on the fresh samples using the same electrolyte within a 5% tolerance.

For comparison, the zeta potential of one selected sample was also measured using the EPM method (described below). Off-cuts of fresh Portland Limestone were cleaned for 48 hours in methanol and then crushed using a jaw crusher. A Tema Mill with an agate vessel was then used to obtain a fine powder of the sample. NaCl-EQ was used to prepare solutions with different Ca content. Suspensions of 0.05g of Portland powder in 50 ml (1 wt %) of the desired electrolyte were prepared and left for a minimum of 1 hour, to allow the fraction of larger suspended particles to settle out of solution. For each sample, the suspension was injected via a syringe into a capillary cell in order to obtain the zeta potential measurement. Care was taken to ensure no air bubbles were left in the cells.

4.2.2. Measurement of Zeta Potential

4.2.2.1. Streaming Potential Measurement (SPM)

The zeta potential was measured using the SPM described by Vinogradov et al. (2010). Only a brief summary of the method is provided here. The carbonate core samples were tightly confined within an embedded rubber sleeve in a stainless steel core holder with non-metallic end caps. A syringe pump was used to induce a fluid pressure difference across the sample, causing the electrolyte to flow through the sample from reservoirs connected to each side of the core holder (Figure 4.3). Synthetic oil was used to translate the induced pressure from the pump to the brine in the inlet reservoir, which maintains closed-system conditions by preventing exposure of the electrolyte to atmosphere. The pump maintains a constant rate, high accuracy, and flow can be directed in either direction through the sample.

The pressure difference across the sample was measured using a pair of pressure transducers (calibrated Druck PDCR 810 with accuracy 0.1% of measured value, resolution 70 Pa) and the voltage across the sample was measured using in-house-made non-polarizing Ag/AgCl electrodes and an NI9219 voltmeter (internal impedance >1 GΩ, accuracy 0.18%, resolution 50 nV). The noise level of the measurements is dictated by the stability of the electrodes, rather than the performance of the voltmeter. The electrodes were positioned out of the flow path, in an electrolyte reservoir of a NaCl solution of the same ionic strength as that used in the experiments.

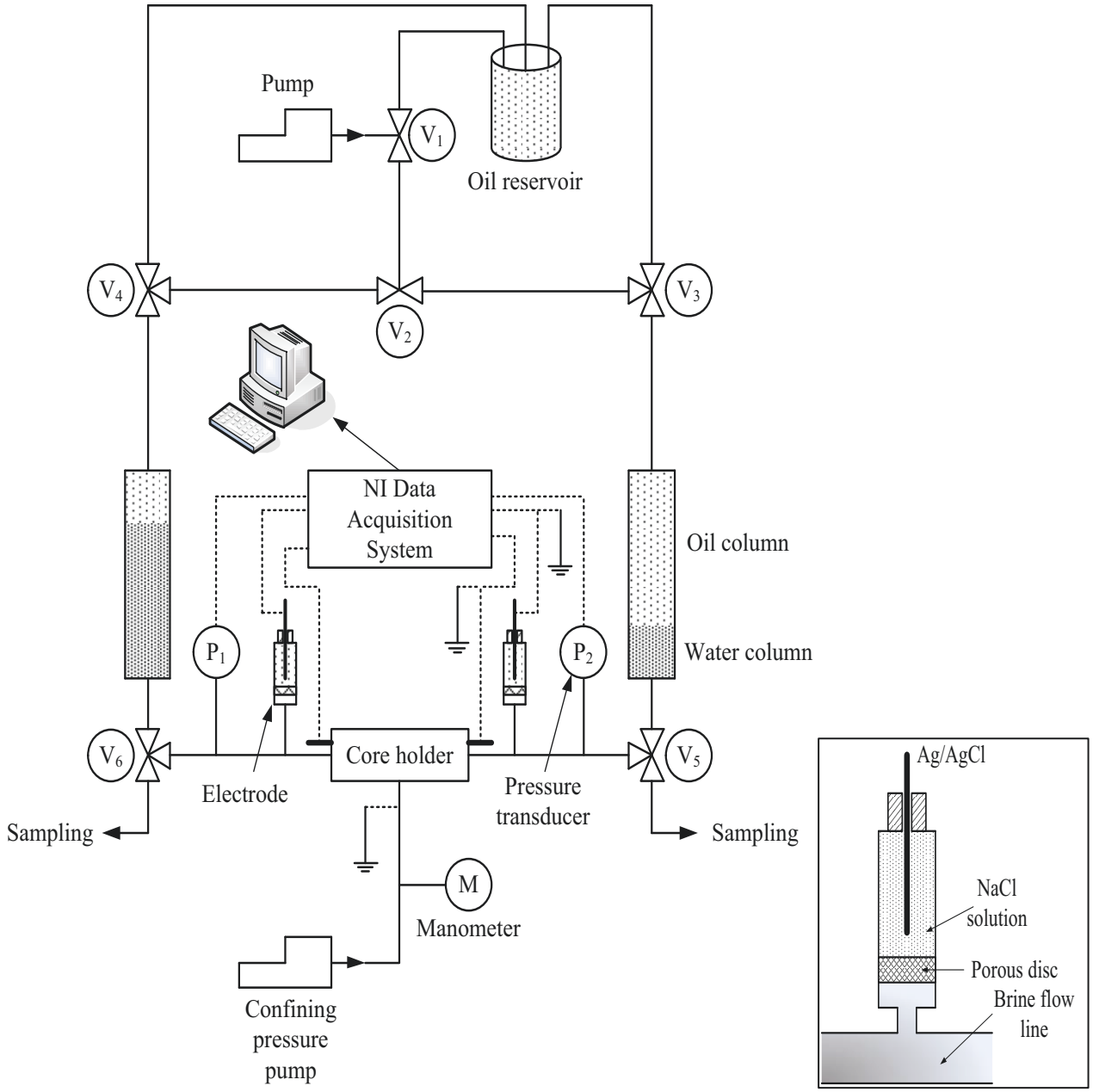

Figure 4.3: Experimental apparatus for measuring the streaming potential, which consists of a pressure vessel (core holder), electrolyte reservoirs, pump, flow lines (solid lines) and electrical connections (dashed lines). The oil column in the electrolyte reservoirs serves to isolate the electrolyte from the atmosphere (closed-system). The flow valves V1 – V6 allow the pump the flow electrolyte through the sample in opposing directions. The box in the right bottom corner represents a close-up of the in-house electrodes. Modified from Jaafar et al. (2009).

We used the „paired-stabilization" or PS method of Vinogradov et al. (2010) to measure the streaming potential across the sample, in which flow is induced through the sample at the same rate but in opposing directions. The method eliminates the effect of temporal variations in the

static voltage and demonstrates that electrode polarization effects that might arise from imperfect AgCl layers (of variable thicknesses) coating the silver rods are negligible through confirmation that the change in potential induced by flow in one direction is equal and opposite to the change in potential induced by flow in the opposite direction. To ensure that exclusion-diffusion potentials were eliminated during measurements of the streaming potential, uniform and constant electrolyte conductivity and pH in each reservoir, and uniform and constant temperature (23°C), were maintained within a 5% tolerance. Redox potentials were minimized by ensuring that the Ag/AgCl electrodes were the only metal in contact with the samples and electrolyte. The fluid flow path consisted of Perspex columns, plastic flow lines and the core-holder caps were non-metallic.

Interpretation of the results from the PS experiments follows from the observation that at steady-state, the streaming current induced by the flow is balanced by a conduction current to maintain overall electrical neutrality. It is reasonable to assume that the currents follow approximately the same 1-D path along the samples, in which case the streaming potential coupling coefficient can be determined using Eq. 3.3.

The coupling coefficient is given by the slope of a linear regression through a plot of voltage against pressure difference obtained for a number of different flow rates (e.g., Figure 4.4e, f). An effective value for the zeta potential for the sample was obtained using a modified version of the Helmholtz-Smoluchowski equation that accounts for surface electrical conductivity by applying the Overbeek correction, which is the ratio of the formation factor at high salinity (>0.5 M NaCl) to that of any given experiment where the surface conduction might be significant.

The formation factor and electrical conductivity were measured following the methodology of Vinogradov et al. (2010) (Table 4.1). Note that the zeta potential obtained is an effective value because it reflects the average streaming charge density transported by the flow of the electrolyte; at the pore-level, the zeta potential may vary. The viscosity and permittivity of the electrolyte as a function of ionic strength were also determined using the approach of Vinogradov et al. (2010). Uncertainty in the reported value of zeta potential reflects the range of possible regressions that can be fitted to the measured streaming potential data within experimental error (Figure 4.4).

(a)

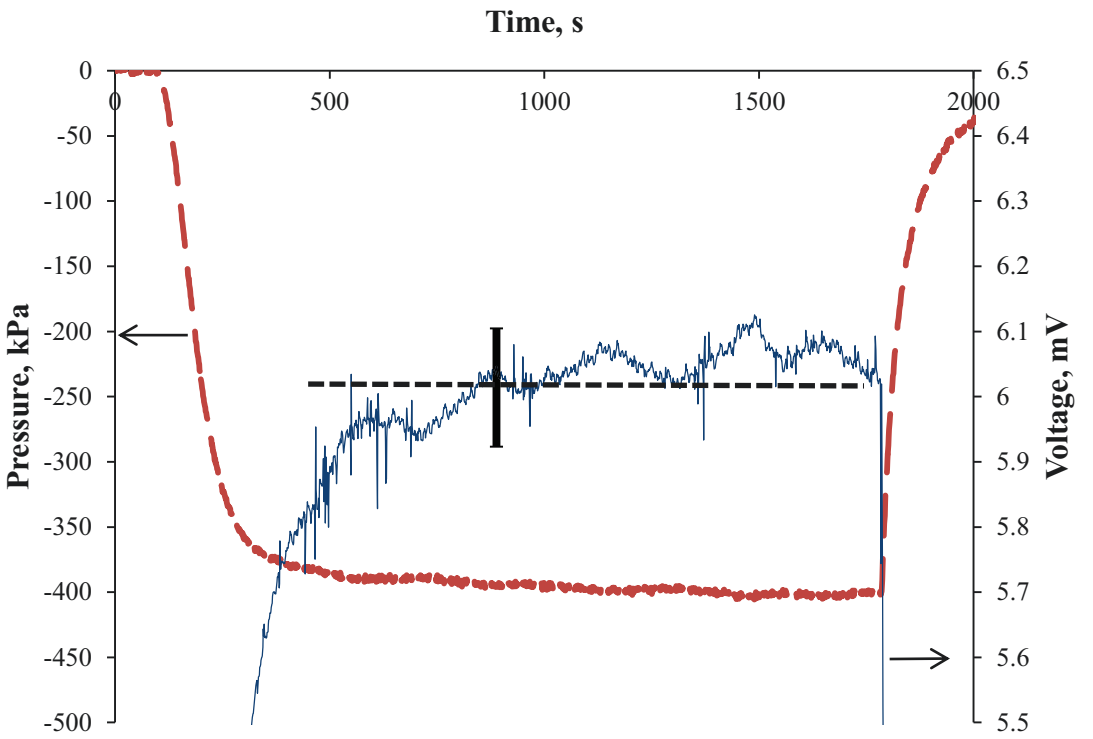
Time, s
Pressure, kPa
Voltage, mV
0
-50
-100
-150
-200
-250
-300
-350
-400
-450
-500
0
500
1000
1500
2000
6.5
6.4
6.3
6.2
6.1
6
5.9
5.8
5.7
5.6
5.5

(b)

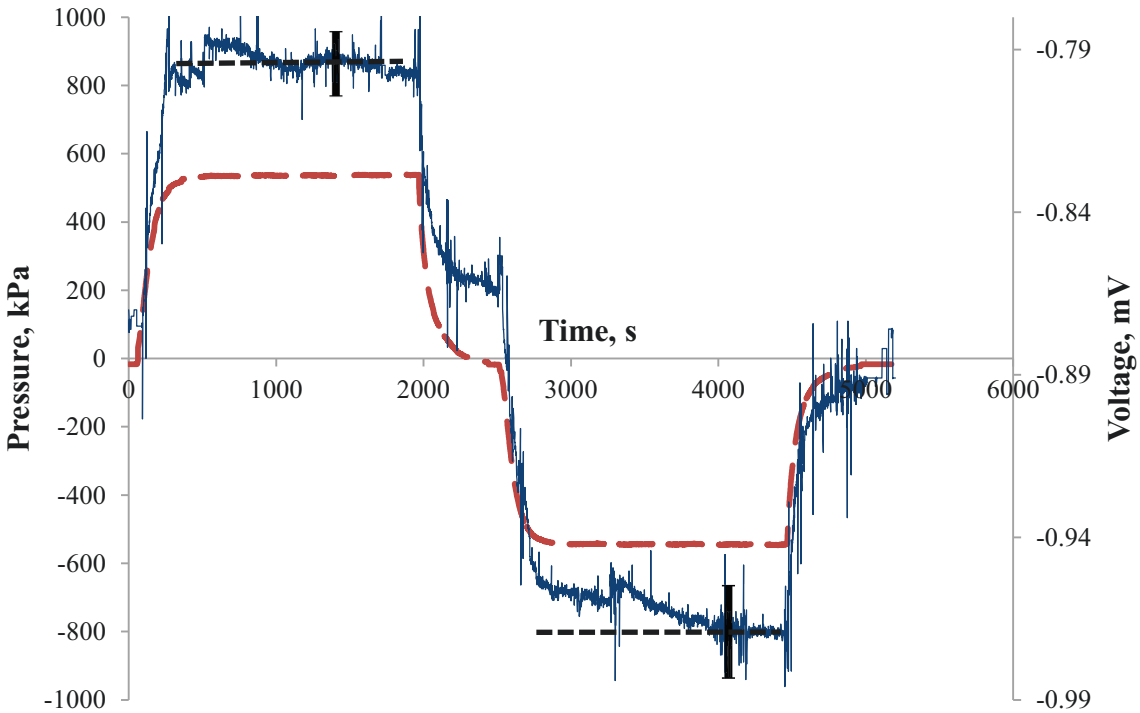
Pressure, kPa
Time, s
Voltage, mV
1000
800
600
400
200
0
-200
-400
-600
-800
-1000
0
1000
2000
3000
4000
5000
6000
-0.79
-0.84
-0.89
-0.94
-0.99

(c)

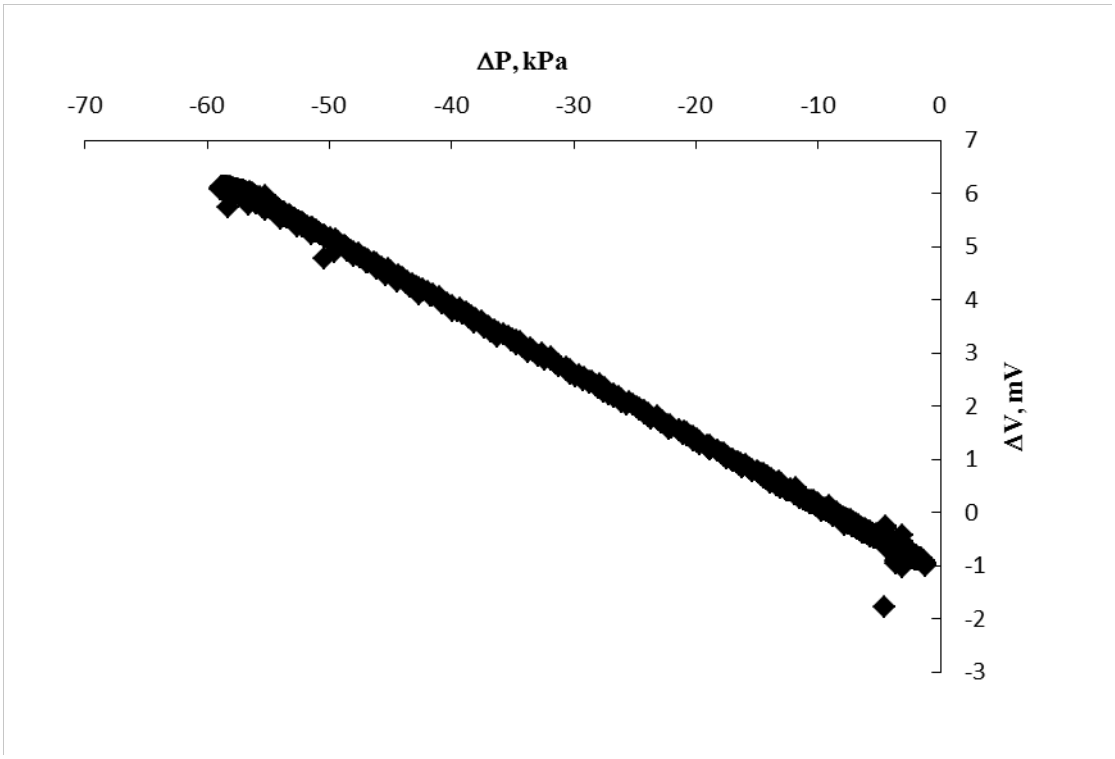
ΔP, kPa
-70
-60
-50
-40
-30
-20
-10
0
7
6
5
4
3
2
1
0
-1
-2
-3
ΔV, mV

(d)

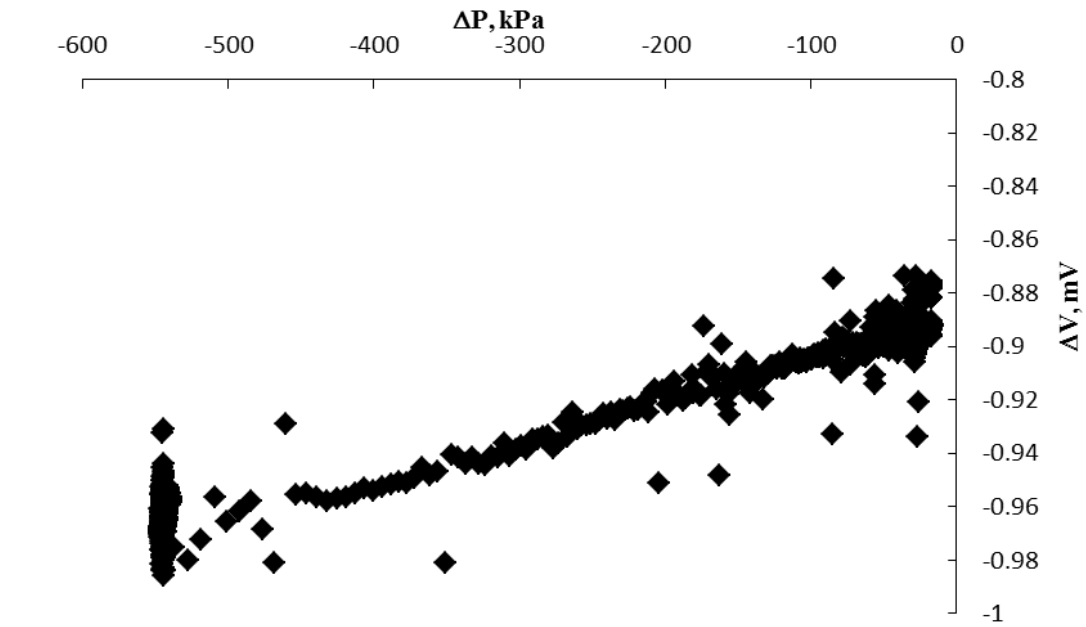
ΔP, kPa
-600
-500
-400
-300
-200
-100
0
-0.8
-0.82
-0.84
-0.86
-0.88
-0.9
-0.92
-0.94
-0.96
-0.98
-1
ΔV, mV

(e)

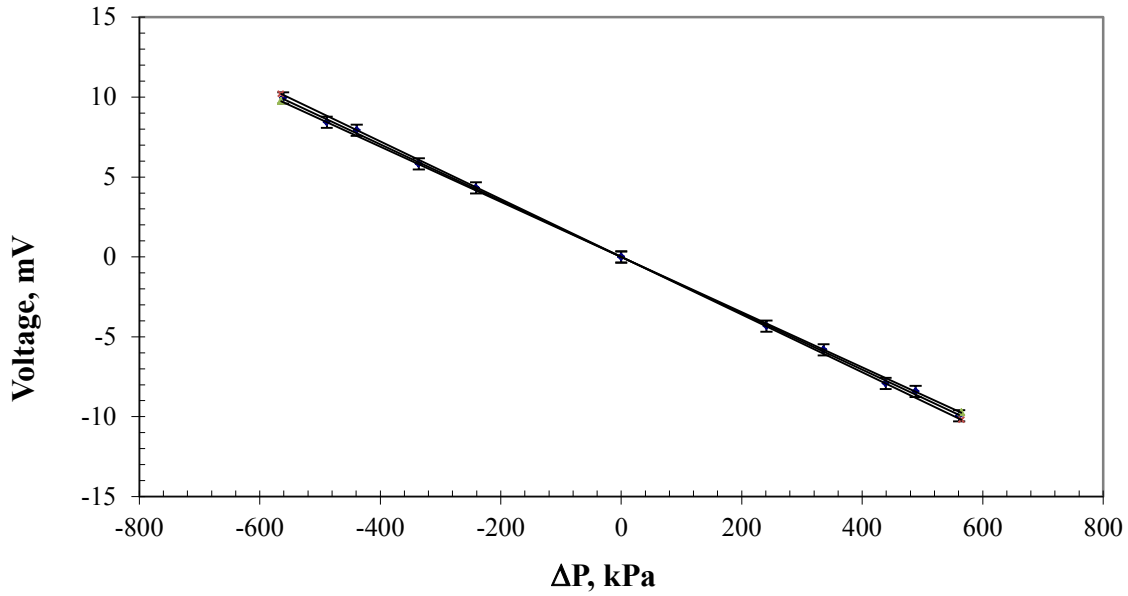

(f)

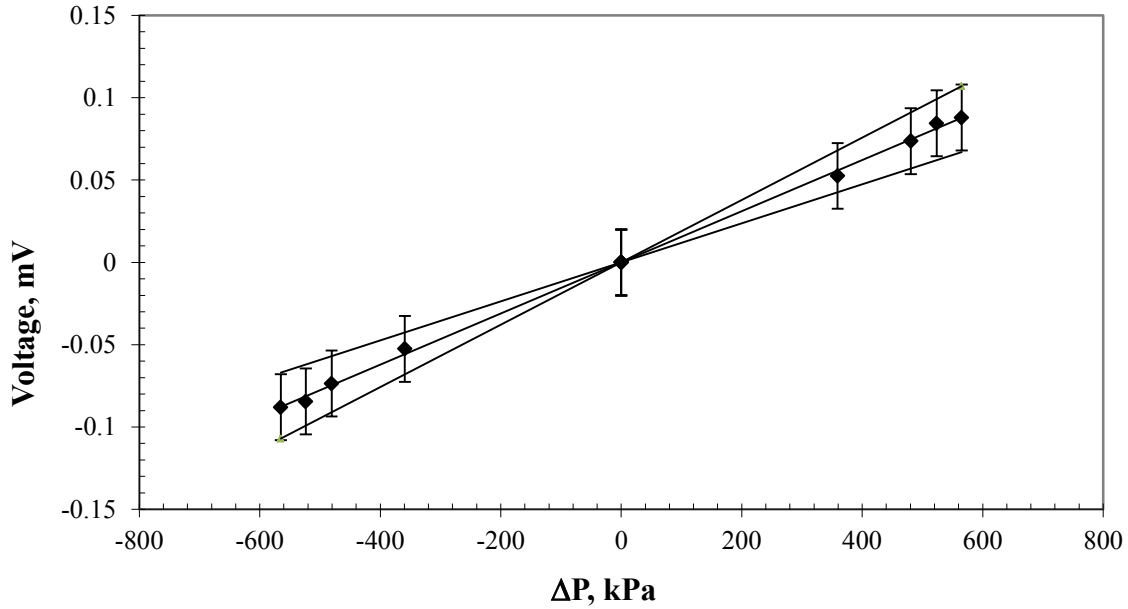

Figure 4.4: Typical experimental results used to determine the streaming potential coupling coefficient. Plots (a) and (b) show the voltage and pressure variation in experiments at a given flowrate using (a) low ionic strength 0.05 M NaCl-EQ electrolyte and (b) high ionic strength synthetic formation brine (FMB) (see Table 4.2). The horizontal dashed lines show the stabilized voltage and pressure for a minimum 17 minutes, and the error bar denotes the spread in these values. The sample rate was 1 per second. Plots (c) and (d) show voltage against pressure difference for a single flow rate experiment shown in (a) and (b). The gradient represents C_{SPM} for that flow rate and the spread represents the error associated. Plots (e) and (f) show the stabilized voltage plotted against stabilized pressure for 5 different flow rate experiments shown in (a) and 4 different flow rates experiments shown in (b). The gradient of a linear regression through these data yields C_{SPM}.

4.2.2.2. Electrophoretic Mobility Measurement (EPM)

The zeta potential for one powdered sample in suspension was also obtained for comparison with the SPM using a Brookhaven ZetaPALS zetameter to measure the electrophoretic mobility u_e of the suspension; this is related to the zeta (shear plane) potential using the Helmholtz-Smoluchowski equation for electrophoresis as in Eq. 3.5.

As noted above, the zeta potential obtained is an effective value because it reflects the average surface charge on the particles in suspension; at the particle level, the zeta potential may vary. The measurement of each sample consisted of 5 runs; each run consisted of 10 cycles. The mean of all the runs for each sample is reported as the zeta potential and the error bars represent the standard deviation.

4.2.3. Measurement of Electrolyte Composition

Electrolyte composition was determined using inductively coupled plasma atomic emission spectroscopy (ICP-AES). The analysis was carried out in the Analytical Chemistry Laboratory at the Natural History Museum, London.

Electrolyte samples from the SPM measurements were collected from the core holder *via* a valve on the outlet flow line at the end of a given suite of zeta potential measurements for the chosen electrolyte; each effluent sample had therefore interacted with the rock sample for a minimum volume of 10 PV spread over a minimum of two days. These samples are referred to as the final effluent electrolytes. Appropriate dilutions were prepared for each sample prior to analysis depending on the total ionic strength and relative abundance of the PDIs of interest. All samples were acidified with 2% HNO_3 to prevent formation of complexes that might affect the interpreted concentrations.

Reference standard solutions at concentrations ranging from 0.5-200 ppm containing all the ions of interest (Na, Ca, Mg, and S) were prepared to represent the ion matrix of the effluent samples. The accuracy of the method was determined using certified check solutions and the repeatability

by conducting 5 repeat measurements on all the samples whose standard deviation is represented by the error bars.

4.2.4. Design of Experiments

In this work, we investigated the effect of three key PDIs (Ca, Mg and SO_4) on the zeta potential of natural limestone in two ways. The first approach was to systematically vary the concentration of each PDI over the range found in natural brines to establish its effect on the zeta potential. For each range of PDI concentrations, we tested three different NaCl (0.05M, 0.5M and 2M) concentrations to determine whether this changes the relationship between the PDI concentration and surface charge. The 0.5 M NaCl concentration represents seawater and is similar to the „ZP brine" of Zhang and Austad (2006) and Zhang et al. (2007) which contained 0.573 M NaCl, allowing direct comparison of results. The 0.05 M NaCl concentration represents a tenfold dilution of seawater and approximates the injection brine used in controlled salinity waterflooding (CSW) for enhanced oil recovery (Yousef et al., 2010), while the 2 M NaCl concentration represents the saline brines found in many deep saline aquifers. The second approach was to combine all three PDIs in the proportions and total concentration typical of (i) natural saline brines, and (ii) natural seawater, and compositions derived from seawater similar to those used in CSW.

4.3. Results

4.3.1. Measurements of streaming potential and interpretation of zeta potential

Figure 4.4 (a, b) shows typical results for the pair-stabilised (PS) experiments for low and high ionic strength electrolytes respectively. The pressure response to pumping is clear and the pressure difference across the samples reached a stable value (fluctuations <500 Pa around an induced pressure difference of *c.* 500 kPa) in all experiments. The voltage response is also clear and reached a stable value with fluctuations typically below ±5 μV at high ionic strength (e.g., FMB) and below ±50 μV at low ionic strength (<0.5 M NaCl) in all experiments. The interpreted values of stabilized pressure and voltage are denoted by the dashed lines, while the error bars show the interpreted spread. The stabilized voltage was reproducible within ±25 μV across three repeat experiments at a given flow rate for high ionic strength and ±35 μV for low ionic strength. The

voltage fluctuations, and reproducibility of the stabilized voltage measurements, are similar to previous experiments conducted on limestone samples saturated with electrolytes of similar ionic strength (Jackson and Vinogradov, 2012). An important aspect of the SPM is that the polarity of the surface charge is very clear: if the polarity of the voltage response is in the opposite sense to the pressure response (i.e., a more positive pressure difference yields a more negative voltage difference relative to a common reference pressure and voltage at one end of the sample) then the surfaces are negatively charged, and vice-versa. This allows the iso-electric point (IEP) to be accurately determined even when the zeta potential is close to zero.

Figure 4.4 (c, d) shows voltage plotted against the corresponding pressure difference for a single PS experiment, which is the same flow rate shown in Figure 4.4 (a, b). The mean of the voltage and pressure difference for each single PS experiment represents a minimum of 17 minutes, in which >1000 bins were averaged and the standard deviation observed is represented by the error bars.

Figure 4.4 (e, f) shows typical plots of the stabilized voltage plotted against the corresponding stabilized pressure difference from each pair of PS experiments for 5 different flow rates for the 0.05 M NaCl-EQ and 4 different flow rates for the FMB case, respectively. The error bars represent the reproducibility of (typically) three repeat measurements at each flow rate. The streaming potential coupling coefficient, obtained from a linear regression through the measured data (Equation 3.3), is clearly negative in Fig 4.4 (c, e) and positive in Fig. 4.4 (d, f) and the linear regression is well constrained by the relatively small error bars associated with each value of stabilized voltage (Fig. 4.4 a,b). We calculate the associated zeta potential using Equation (3.4). The uncertainty in the streaming potential coupling coefficient arising from the range of linear regressions that can be forced through the stabilized voltage and pressure data was used to determine the associated uncertainty in zeta potential reported in the following sections.

4.3.2. Impact of Ca, Mg and SO_4 concentration on zeta potential

We begin by reporting experiments in which the concentration of each PDI was systematically varied in pre-equilibrated 0.05 M NaCl electrolytes (NaCl-EQ). Figure 4.5 shows the zeta potential as a function of calcium, magnesium and sulfate concentration. We plot concentration as

pPDI. Note that in all cases the lowest concentration (highest pPDI) investigated corresponds to the equilibrated concentration in the NaCl-EQ electrolyte. We notice first that a linear regression provides an excellent fit to the data for each PDI (R^2 >0.98) and that the gradient of the regression for Ca and Mg is identical within experimental error (-5.10 ± 0.47 mV/decade). Moreover, the zeta potential is negative at high pCa or pMg (i.e., low Ca or Mg concentration), becomes less negative with decreasing pCa or pMg, and becomes positive at low pCa or pMg. The IEP (defined as pPDI) appears to be the same within experimental error for Ca and Mg (pPDI = 0.60±0.03). However, the behaviour of SO_4 is very different. The zeta potential remains negative regardless of pSO_4 and becomes increasingly negative with decreasing pSO_4 (i.e., increasing SO_4 concentration). Moreover, the gradient of the linear regression that best fits the data is much smaller than that observed for Ca and Mg (1.9 ±0.3 mV/decade). These results suggest that Ca and Mg behave similarly as PDIs at room temperature and can have a significant impact on zeta potential, yielding positive zeta potential at pPDI < 0.60. However, the zeta potential is much less sensitive to pSO_4.

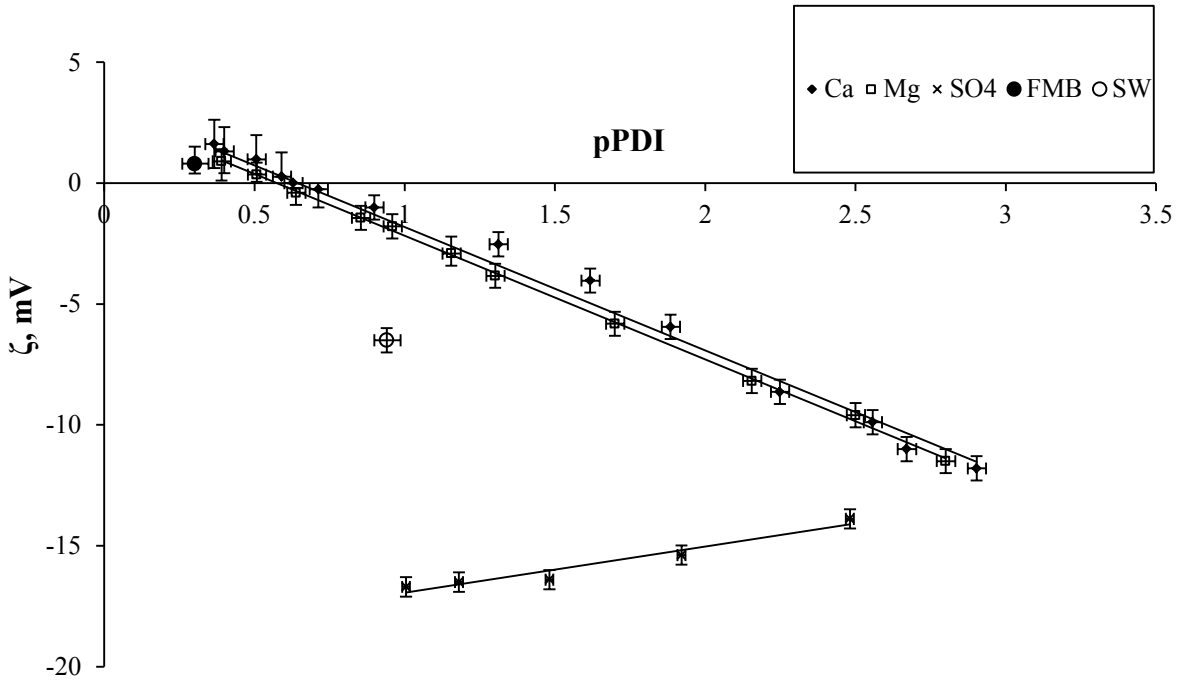

Figure 4.5: Effect of Ca, Mg and SO_4 concentration (expressed as pPDI) in 0.05 M NaCl electrolyte on the zeta potential of Portland limestone, where -5.10 ± 0.47 mV/decade is the gradient for both Ca and Mg whereas the gradient for sulfate was 1.9 ±0.3 mV/decade. Also shown are the results for the synthetic formation brine (FMB) and natural seawater (SW) plotted as a function of pCa + pMg.

4.3.3. Impact of varying the concentration of NaCl

Figure 4.6 shows the zeta potential as a function of Ca concentration for each of the three NaCl concentrations investigated (Figure 4.6a), and as a function of SO_4 concentration for two of the NaCl concentrations investigated (Figure 4.6b). Considering first the impact of Ca concentration, we again find that a linear regression provides an excellent fit to the data for each value of NaCl concentration ($R^2 > 0.98$) and that the gradient of the linear regression decreases with increasing NaCl concentration (Figure 4.6c). Thus, the zeta potential becomes less sensitive to pCa as the NaCl concentration increases. In all cases, the zeta potential is negative at high pCa (i.e., low Ca concentration), becomes less negative with decreasing pCa, and becomes positive at low pCa. The IEP, which is defined as pCa, was directly identified by measuring a zero C_{SPM} within experimental error and measuring the effluent for calcium concentration. We found that the IEP decreases with increasing NaCl concentration although the change only exceeds experimental error for the lowest NaCl concentration investigated (Figure 4.6c). Considering next the impact of SO_4 concentration, we observe similar behaviour. A linear regression again provides an excellent fit to the data, and the gradient of the regression decreases with increasing NaCl concentration (Figure 4.6b). However, the zeta potential remains negative over the range of pSO_4 investigated.

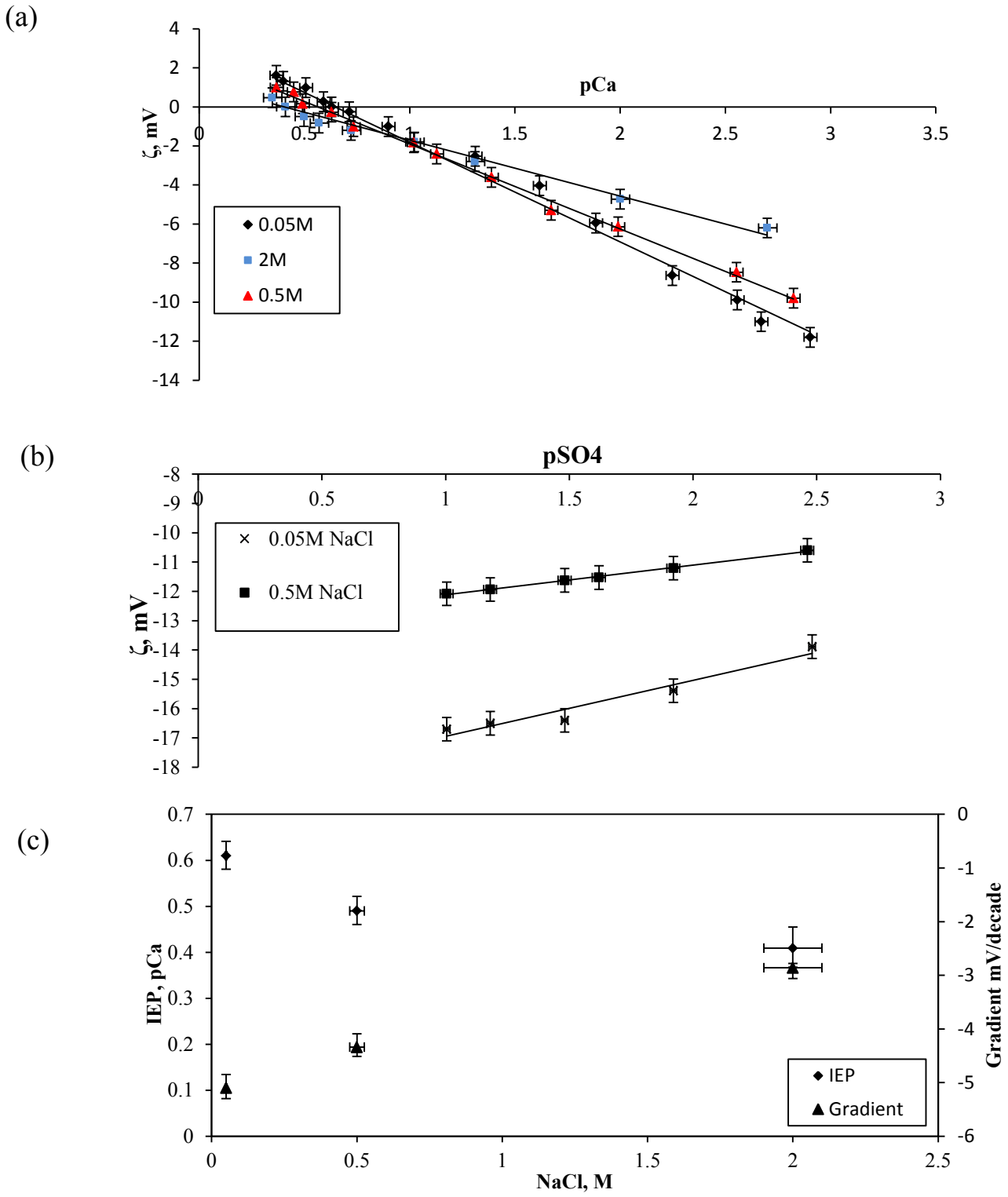

Figure 4.6: Effect of NaCl concentration on the relationship between PDI concentration and zeta potential of Portland limestone. (a) Effect of Ca concentration (expressed as pCa) in three different NaCl electrolytes (0.05 M, 0.5 M and 2 M) on the zeta potential of Portland limestone. (b) Effect of SO_4 concentration (expressed as pSO_4) in two different NaCl electrolytes (0.05 M, 0.5 M) on the zeta potential of Portland limestone. (c) Effect of NaCl concentration on the IEP (expressed as pCa) and zeta potential sensitivity to pCa (expressed as the gradient of the linear regressions shown in (a)). Temperature and pH are constant.

4.3.4. Effect of varying multiple PDIs

In this section, we report measurements of zeta potential using electrolytes containing all three PDIs (Ca, Mg, and SO_4) at the concentrations found in typical formation brine (FMB; Table 4.2) and seawater (SW; Table 4.2). The formation brine yields a positive zeta potential, which is the same within experimental error as the zeta potential obtained by adding a comparable amount of Ca to 0.05 M NaCl electrolyte (see the filled circle in Fig. 4.5). The natural seawater yields a negative zeta potential, which is more negative than the zeta potential obtained by adding a comparable amount of Ca to 0.05 M NaCl electrolyte (see the open circle in Fig. 4.5). Thus, the zeta potential in subsurface saline brine appears to be controlled primarily by the Ca content, with Mg and SO_4 playing a minor role; by contrast, the presence of SO_4 in seawater leads to a more negative zeta potential.

We also investigate the effect of diluting seawater and adding SO_4 to seawater. Both of these approaches to modifying the brine injected into carbonate oil reservoirs have been suggested to yield enhanced oil recovery (Zhang and Austad, 2006; Yousef et al., 2011). In the experiments conducted here, seawater (SW) was diluted twice (1/2SW), ten times (1/10SW) and twenty times (1/20SW), and SO_4 was added to yield twice (2SW), three times (3SW) and four times (4SW) the natural seawater concentration. In all cases, the measured zeta potential is negative (Figure 4.7a); however, the least negative (or smallest in magnitude) zeta potential is observed for seawater, and the zeta potential becomes increasingly negative (and larger in magnitude) as the seawater is diluted or SO_4 is added. Indeed, the response is identical within experimental error. The zeta potential increases in magnitude with both increasing and decreasing total ionic strength (Figure 4.7b); the ionic strength increases as SO_4 is added, but decreases as the seawater is diluted.

(a)

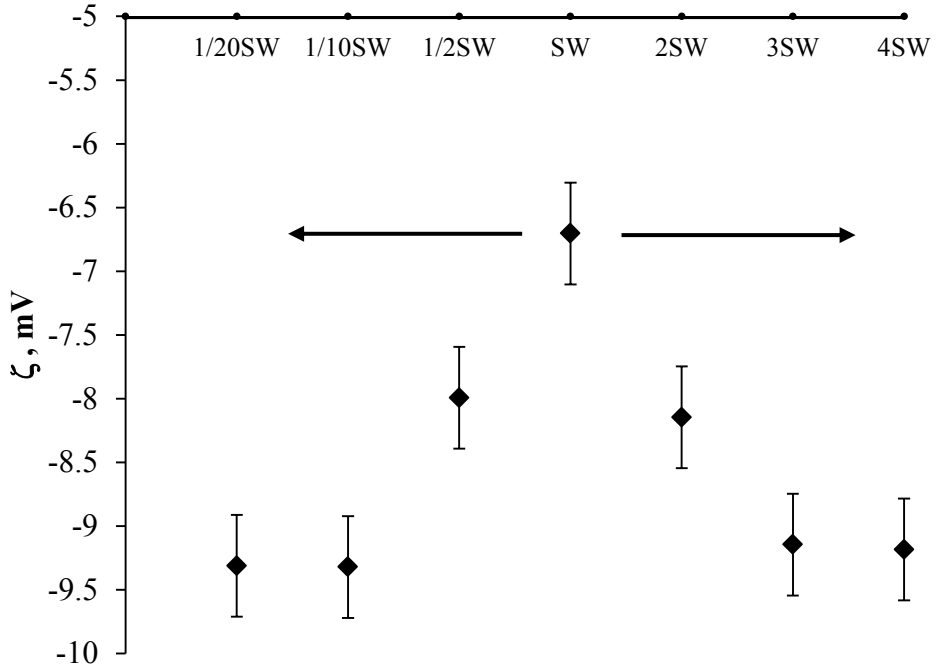

(b)

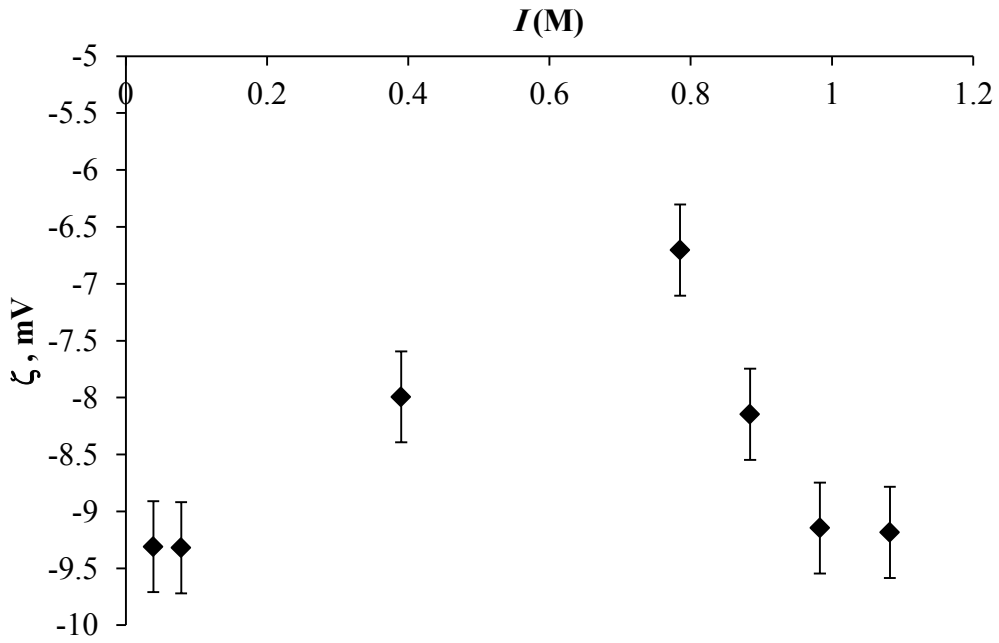

Figure 4.7: (a) Relationship between zeta potential and electrolyte compositions derived from seawater (SW). (b) Zeta potential of the same compositions plotted as a function of ionic strength (*I*).

4.3.5. Effect of sample preparation

Many experimental studies use a limited number of samples that are cleaned before each experiment. However, none have confirmed that the typical laboratory cleaning protocol (described here in the methodology) restores the zeta potential of natural carbonates to a consistent and repeatable value for a given electrolyte. To confirm the repeatability of zeta potential measurements obtained using the SPM, and determine the effect of sample cleaning, the zeta potential for three selected fresh samples was initially measured using 0.05 M NaCl-EQ electrolyte (circles in Fig. 4.8). The samples were then used in experiments in which the Ca or Mg concentration was increased (triangles in Fig. 4.8; these data are also shown in Fig. 4.5). The samples were then cleaned using a standard laboratory cleaning protocol and the zeta potential was measured again (diamonds in Fig. 4.8). Finally the samples were cleaned using the enhanced cleaning protocol reported here (squares in Fig. 4.8). It is clear that the standard cleaning procedure fails to return pMe (representing the Ca + Mg concentration) or zeta potential to their original fresh values after the samples are exposed to elevated PDI concentrations. It is important to use the enhanced cleaning procedure reported here to flush PDIs from the mineral surfaces and return the zeta potential to its pristine value.

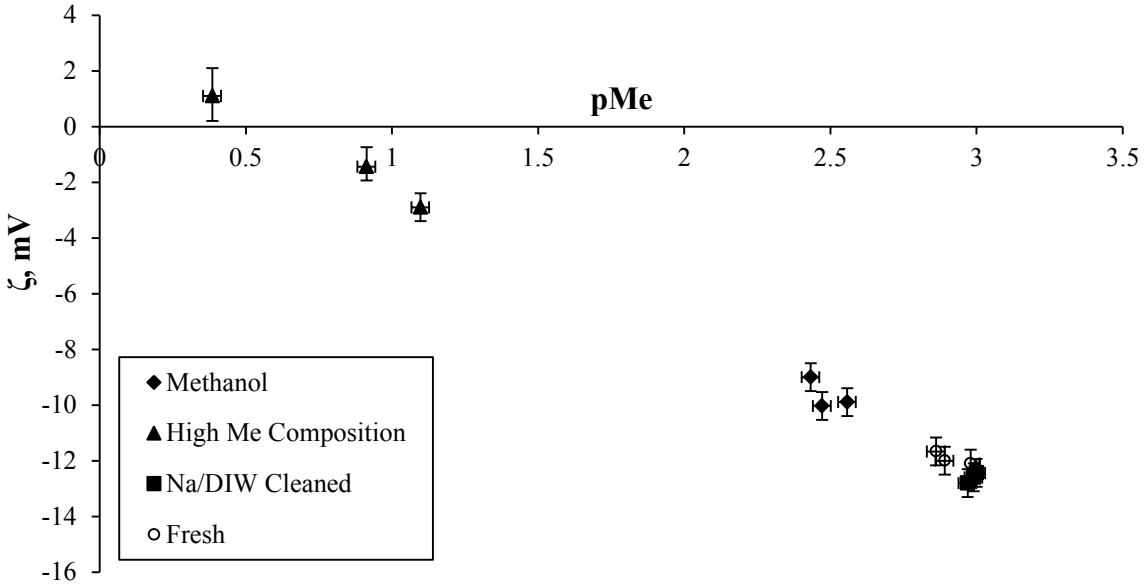

Figure 4.8: Zeta potential as a function of Ca + Mg concentration (expressed as pMe) for fresh samples (circles), experiments at elevated Ca and Mg concentration (triangles), after standard cleaning with methanol (diamonds), and after the enhanced cleaning with DIW used in this study (squares).

4.4. Discussion

4.4.1. Comparison with previous studies of the effect of PDI concentration on zeta potential in natural and synthetic calcite/carbonates

We have demonstrated here that Ca and Mg change the zeta potential of intact natural limestone samples, causing a linear decrease in the magnitude of the negative zeta potential with increasing concentration (expressed as pPDI), and causing polarity inversion to positive zeta potential at high concentration; moreover, the two PDIs behave identically within experimental error. Similarly, SO_4 changes the zeta potential of natural limestone, causing a linear increase in the magnitude of the negative zeta potential with increasing concentration (expressed as pPDI), but the gradient of the linear regression that best fits the data is lower than that of the cations. We have also demonstrated that the gradient of the zeta potential with respect to pCa and pSO_4 decreases with

increasing NaCl concentration. The relationship between zeta potential and pPDI is linear across the entire range of pPDI investigated.

No previous studies have determined the relationship between zeta potential and pMg, but several have reported a linear relationship between zeta potential (or its proxy, electrophoretic mobility) and pCa as observed here (e.g., Foxall et al., 1979; Thompson and Pownall, 1989; Pierre et al., 1990). However, these studies were conducted using electrolytes of much lower ionic strength than those considered here (e.g., Fig. 4.9a). Other studies have observed a non-linear relationship between zeta potential and pCa (e.g., Cicerone et al., 1992; Chen et al., 2014). Linear behaviour is expected if (i) the calcite surface behaviour is Nernstian, (ii) the lattice ions Ca and CO_3 are the PDIs, and (iii) the electrical double layer is described by the Gouy-Chapman-Grahame model (e.g., Hunter, 1981). Under these circumstances, the gradient of the zeta potential with respect to pPDI can be expressed as (e.g., Foxall et al., 1979)

$$\left.\frac{d\zeta}{dpPDI}\right|_{\zeta\to 0} = \frac{-2.303\frac{kT}{ze}}{\left(1+\frac{C_d}{C_s}\right)\exp(\kappa\Delta)} \tag{4.3}$$

where k is Boltzmann"s constant, T is the temperature, z is the valence of the PDI, e is the charge on an electron, C_d and C_s are the capacitance per unit area of the diffuse and Stern layers respectively, κ is the inverse Debye length, and Δ is the distance of the shear plane from the Stern plane. For low zeta potential, C_d is given approximately by $\kappa\varepsilon$ where ε is the permittivity. Cicerone et al. (1992) argued that the relationship between zeta potential and pPDI is linear only close to the IEP; away from the IEP, zeta potential values level off, because the Stern layer capacitance C_s varies, or because the Gouy-Chapman-Grahame model breaks down. We do not observe this levelling off, despite the broad range of pCa values investigated. Equation 4.3 can be used to fit our experimental data for pCa (and pMg). However, the decrease in gradient with increasing NaCl concentration can only be matched by adjusting the Stern capacitance (see Table 4.3; these values are discussed in more detail in the next section). Large values of Stern capacitance are required in the range 1.13-2.75 Fm^{-2}, which are at least twice those determined

previously (Foxall et al., 1979; Thompson and Pownall, 1989; Cicerone et al., 1992), but these values were obtained at considerably lower ionic strength. For the 0.05 M NaCl electrolyte (the lowest concentration investigated), the predicted diffuse layer thickness at the ionic strength corresponding to the IEP (0.8 M) is very small (the Debye length is 0.342 nm). Given that the calcium ion has a hydrated diameter of 0.59 nm (Diebler et al., 1969), it is not clear whether such a diffuse layer thickness is physically meaningful as it cannot accommodate even a single calcium ion. Vinogradov et al. (2010) suggested that the diffuse layer thickness decreases until it reaches the radius of the hydrated counter-ion, and then remains constant regardless of increasing ionic strength. However, their model does not account for changes in the Stern layer capacitance with changing ionic strength, and cannot explain the data reported here.

Figure 4.9b shows the effect of varying SO_4 concentration, comparing our data obtained for the 0.5 M NaCl electrolyte against that of Zhang and Austad (2006). These are the only comparable data for SO_4 reported previously. Both datasets yield a linear relationship between zeta potential and pSO_4, although the gradient of the linear regression is larger for the Zhang and Austad data than that obtained here. As discussed in the next section, we suggest this is a consequence of the differing measurement methods: Zhang and Austad used the EPM, in contrast to the SPM used here. Moreover, extrapolating the linear regression in each case to obtain the IEP suggests very different values in terms of pSO_4.

Table 4.3. Values of the Stern layer capacitance and shear plane location used to match the experimental data using Equation (4.3). The value of C_s was identified first for the EPM data using $\Delta = 0$, consistent with previous studies. The value of C_s was then fixed for the SPM data at the same NaCl concentration matched by adjusting Δ to account for the complex pore-space. It was not possible to match the other NaCl concentrations tested without further adjusting C_s. The shear plane location is not expected to be significantly affected by the increase in ionic strength.

Method	NaCl concentration (M)	Stern Layer capacitance C_s (F/m^2)	Shear plane location Δ (nm)
EPM	0.05	1.13	0
SPM	0.05	1.13	0.245
SPM	0.5	1.76	0.245
SPM	2	2.75	0.245

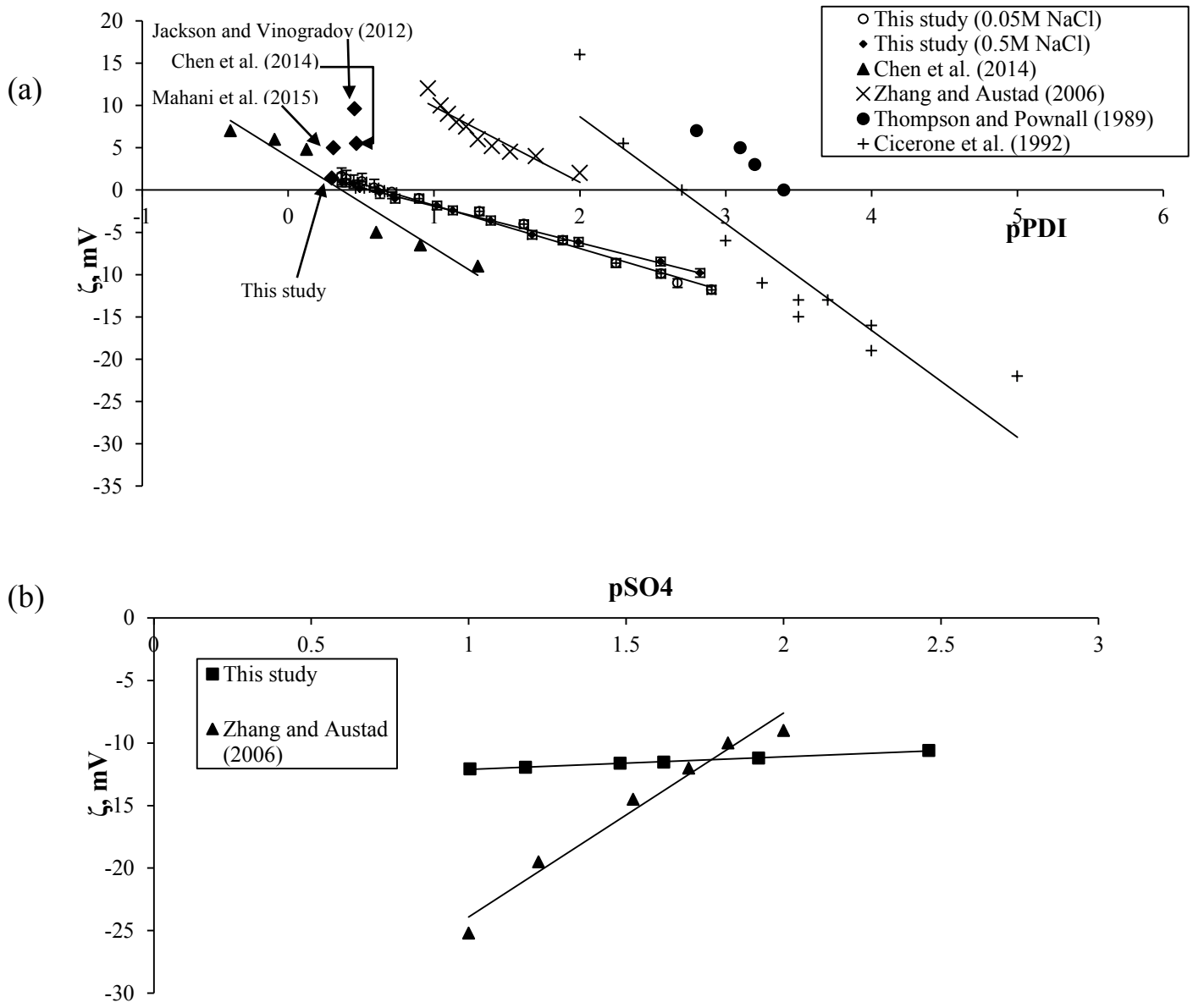

Figure 4.9: Comparison of the data obtained here and previously published measurements for the zeta potential sensitivity to (a) Ca and (b) SO_4. Thompson and Pownall (1989) used the SPM method, synthetic calcite and 0.002 M NaCl electrolyte over the pH range 7-11. All other published studies used the EPM method. Cicerone et al. (1992) used synthetic calcite and 0.03 M KCl electrolyte over the pH range 8.5-10.5. Zhang et al. (2006) used powered Stevns Klint chalk and 0.573 M NaCl electrolyte at pH = 8.4. These conditions are the most similar to those used here. Chen et al. (2014) used powdered natural limestone and DIW at pH = 8. The various labelled diamonds in (a) show data obtained using natural or synthetic formation brine (FMB).

4.4.2. Effect of electrokinetic measuring technique

A common difference between our data and that reported in previous studies is that we use the SPM to obtain the zeta potential, whereas previous studies have primarily used the EPM. Several studies have suggested that the two methods may yield different results (e.g. Vernhet et al., 1994; Delgado et al., 2007). To test this, we compare zeta potential measurements obtained using both methods on powdered derived from the Portland Limestone, varying pCa in 0.05 M NaCl electrolyte (Figure 4.10). We find that the IEP is identical within experimental error, although uncertainty in the IEP derived from the EPM data is significantly greater than for the SPM data, because positive and negative values of zeta potential were observed across a range of pCa (0.71-0.50). There was no such ambiguity in the SPM data.

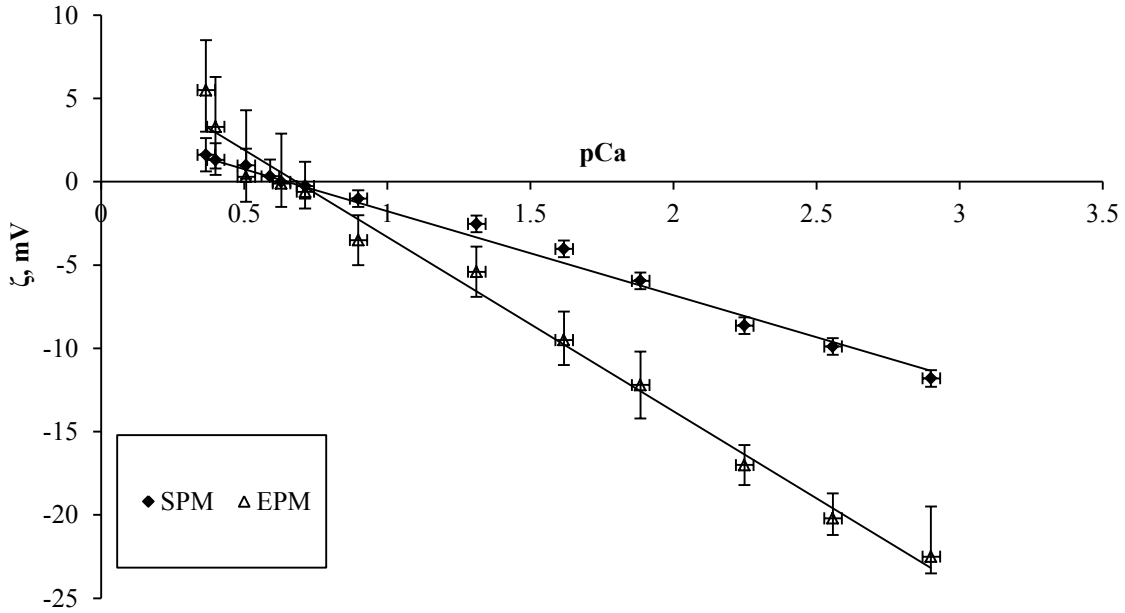

Figure 4.10: Comparison between zeta potential as a function of pCa obtained using the SPM and EPM method for the same natural Portland limestone and 0.05M NaCl electrolyte.

Both methods also yield a linear relationship between zeta potential and pCa, although the gradient of the linear regression obtained from the EPM data is twice that obtained from the SPM data (-10.45±0.55 mV/decade for the EPM versus -5.10 ± 0.47 mV/decade for the SPM). We fit the EPM

data using Equation 4.3 and the values are reported in Table 4.3, assuming $\Delta = 0$ (i.e., assuming the shear plane corresponds with the Stern plane) in common with previous studies using the EPM on calcite (Foxall et al., 1979; Thompson and Pownall, 1989; Pierre et al., 1990; Cicerone et al., 1992). We then fit our SPM data using the same parameters, but adjusting Δ to obtain a match, yielding a value of 0.245 nm. This is a very small offset for the shear plane, and reflects the very small thickness of the diffuse layer at the IEP as discussed in the previous section. Nonetheless, the difference in gradient is consistent with that expected when there are differences in the relative position of the shear plane in natural porous media and powder suspensions. The complex geometry of natural pore-spaces, including the presence of sharp-angled corners and crevices, means that the effective location of the shear plane lies further from the mineral surface than in powder suspensions. Measurements of SPM are more relevant when quantifying the zeta potential of natural samples, because the measurements reflect the mineral surfaces that predominantly interact with the adjacent fluids.

4.4.3. Effect of NaCl concentration on the IEP

No previous studies have determined the IEP for natural and artificial calcite expressed as pMg, but several have reported values of the IEP expressed as pCa (Table 4.4). The values observed are typically much higher (i.e., the IEP was observed at lower calcium concentration) than those determined here. Only Chen et al. (2014) have observed the IEP at a comparably low value of pCa; they investigated natural limestone, consistent with our study, but employed the EPM method and DIW electrolyte, rather than the SPM and NaCl electrolytes used here. It is not clear why the IEP for natural Portland limestone occurs at such low values of pCa compared to the majority of previous studies. Pierre et al. (1990) suggested that the IEP is governed by the relative magnitude of the equilibrium constants K_{Ca} and K_{CO3} governing the adsorption of Ca and CO_3 ions on the calcite mineral surface. The IEP shifts to lower pCa if $K_{CO3} > K_{Ca}$; that is, if the calcite surfaces show greater affinity for CO_3 than Ca. Pierre et al. (1990) found the IEP differed for synthetic and natural calcite and argued that this reflected the differing affinity for Ca and CO_3.

Table 4.4. Literature Compilation of the reported IEP, which include the used background electrolyte, type of calcite, pCa and whether the IEP was directly measured or extrapolated.

Reference	Background Electrolyte	Calcite	IEP, pCa	Determination
Somasundaran and Agar (1967)	DIW	Synthetic	3.72	extrapolated
Fuerstenau et al. (1968)	10^{-3} M (SiO_2/Na_2O)	Synthetic	4.1	extrapolated
Mishra (1978)	$2x10^{-3}$ M $NaClO_4$	Natural	3.09	extrapolated
Foxall et al. (1979)	0.01-.15 M NaCl	Synthetic	4.4	extrapolated
Amankonah and Somasundaran (1985)	$2x10^{-3}$ M KNO_3	Synthetic	4.08	extrapolated
Thompson and Pownall (1989)	$2x10^{-3}$-10^{-2} M (NaCl/HCl/NaOH)	Synthetic	2.02	direct
Thompson and Pownall (1989)	$2x10^{-3}$-10^{-2} M (NaCl/$NaHCO_3$/HCl/ NaOH)	Synthetic	1.92	direct
Thompson and Pownall (1989)	$2x10^{-3}$-10^{-2} M (NaCl/$CaCl_2$/HCl/Na OH)	Synthetic	2.16	direct
Thompson and Pownall (1989)	$2x10^{-3}$-10^{-2} M (NaCl/$CaCl_2$/HCl/Na OH)	Synthetic	3.4	direct
Thompson and Pownall (1989)	$2x10^{-3}$-10^{-2} M (NaCl/H_2CO_3)	Synthetic	4	direct
Thompson and Pownall (1989)	$2x10^{-3}$-10^{-2} M (NaCl/NaHCO3/$H_2C O_3$)	Synthetic	3.8	direct
Thompson and Pownall (1989)	$2x10^{-3}$-10^{-2} M (NaCl/NaHCO3/Ca($OH)_2$)	Synthetic	3.8	direct
Pierre et al. (1990)	10^{-2} M NaCl	Synthetic	3.37	direct
Pierre et al. (1990)	10^{-3}-10^{-1} M NaCl	Natural	4	direct
Pierre et al. (1990)	0.03 M NaCl (constant pH=8.3)	Natural	2	direct
Pierre et al. (1990)	10^{-2} M NaCl (constant pH=8.5)	Synthetic	3.9	direct
Huang et al. (1991)	DIW	Synthetic	4.35	extrapolated
Cicerone et al. (1992)	0.03 M KCl	Synthetic	2.7	direct
Chen et al. (2014)	DIW	Natural	0.2-0.48	extrapolated

The Pierre et al. model suggests that the natural Portland limestone investigated here has a much greater affinity for CO_3 than Ca. Thus, the difference may be related to sample type: most previous

studies used synthetic calcite or natural chalk, rather than the natural limestone used here. It may also be related to the pH and/or the establishment of the initial equilibrium conditions. Thompson and Pownall (1989) and Cicerone et al. (1992) conducted experiments over the pH range 7-11 and 8.5-10.5 respectively; the higher pH values do not represent equilibrium conditions. Zhang et al. (2006) and Chen et al. (2014) kept the pH fixed at 8.4 and 8 respectively, but do not report the pre-equilibration steps used here. The pH was fixed in our experiments by the procedure used to ensure the sample was in equilibrium with the electrolyte prior to starting the experimental measurements.

We have also found that the IEP for Portland limestone decreases with increasing NaCl concentration over the range 0.05 M – 0.5 M. Previous studies have argued that the IEP is independent of NaCl concentration, as Na and Cl are indifferent ions to the calcite surface (e.g., Pierre et al., 1990). We suggest that the difference in IEP between the 0.05 M and 0.5 M/2 M NaCl electrolytes observed here is due to the reduced ability of the calcium ions to interact with the calcite surface, owing to (i) the collapse of the double layer and (ii) increasing occupancy of the diffuse part of the double layer by hydrated sodium ions, which have a smaller radius than the calcium ions at 0.47 nm (Vinogradov et al., 2010). However, we note this hypothesis fails to explain the data of Chen et al. (2014), as they observed a comparable IEP to ours at much lower NaCl concentration.

4.4.4. Implications for controlled salinity waterflooding (CSW)

We have shown that the zeta potential of intact natural limestone samples is positive at elevated Ca and Mg concentration below the IEP (pCa ~ pMg ~ 0.63 – 0.41 as discussed above) and becomes negative as the Ca and or Mg concentration is decreased; it also becomes increasingly negative as the SO_4 concentration is increased. We have also shown that the zeta potential of natural limestone saturated with formation brine, rich in Ca ions, is positive, consistent with previous studies (Jackson and Vinogradov, 2012; Chen et al., 2014; Mahani et al., 2015; see Figure 4.9a). In such formations, an attractive electrostatic force will act between the positively charged mineral surfaces and the negatively charged oil-brine interface, promoting wettability alteration to oil-wet conditions (e.g., Buckley et al., 1989). However, if the concentration of Ca or Mg in the injection

brine during controlled salinity waterflooding (CSW) is decreased below the IEP, the zeta potential changes polarity to negative leading to electrostatic repulsion, which may lead to wettability alteration to more water-wet conditions, releasing previously adsorbed crude oil from the calcite mineral surfaces and therefore improving oil recovery. It has been shown by Jackson and Vinogradov (2012) that more water-wet conditions in natural carbonate samples correlate with a more positive zeta potential.

Previous reported values of the IEP expressed as pCa suggest that considerable reduction in Ca concentration is required to change the polarity of calcite (Table 4.4; see also Fig. 4.9a); however, our results suggest that reducing the concentration of Ca in the injection brine (selectively or by bulk dilution) by a factor of only 2 relative to the formation brine can lead to inversion of the surface charge. Injection of seawater will also cause inversion of the calcite surface charge, because of the lower Ca concentration and higher SO_4 concentration. This can explain why improved recovery in carbonates during CSW has been observed in response to relatively minor levels of injection brine dilution, compared to sandstones in which improved recovery is only observed for very low salinity injection brines (<0.05 M; see Jackson et al., 2015 for a review).

Previous studies have also suggested that improved oil recovery in corefloods or spontaneous imbibition (SI) experiments can be observed by either diluting seawater as the injection fluid (Yousef et al., 2011), or adding SO_4 to seawater as the imbibing fluid (Zhang and Austad, 2006). In one case, the total ionic strength is simply decreased; in the other, the ionic strength is increased but the relative concentration of ions is changed. Here we show the change in zeta potential is almost identical; diluting seawater and adding SO_4 causes the negative zeta potential to increase in magnitude, i.e., become more negative (Figure 4.7). As discussed above, this can cause wettability alteration to more water-wet conditions and release previously trapped oil in coreflooding experiments, or cause increased imbibition in SI experiments. Simple dilution causes expansion of the double layer and hence a more negative zeta potential (Ligthelm et al., 2009; Nasralla and Nasr-El-Din, 2014); addition of SO_4 yields a more negative zeta potential by increasing the negative charge on the calcite mineral surface (e.g., Fig. 4.5). Figure 4.11 shows the incremental recovery observed by diluting seawater, or adding SO_4 to seawater, in the experiments reported by Yousef et al. (2011) and Zhang and Austad (2006), plotted against the change in zeta potential we observed here by modifying the composition of seawater in the same way. There is a clear

correlation between increasingly negative zeta potential change and improved recovery, irrespective of the how the seawater composition is changed.

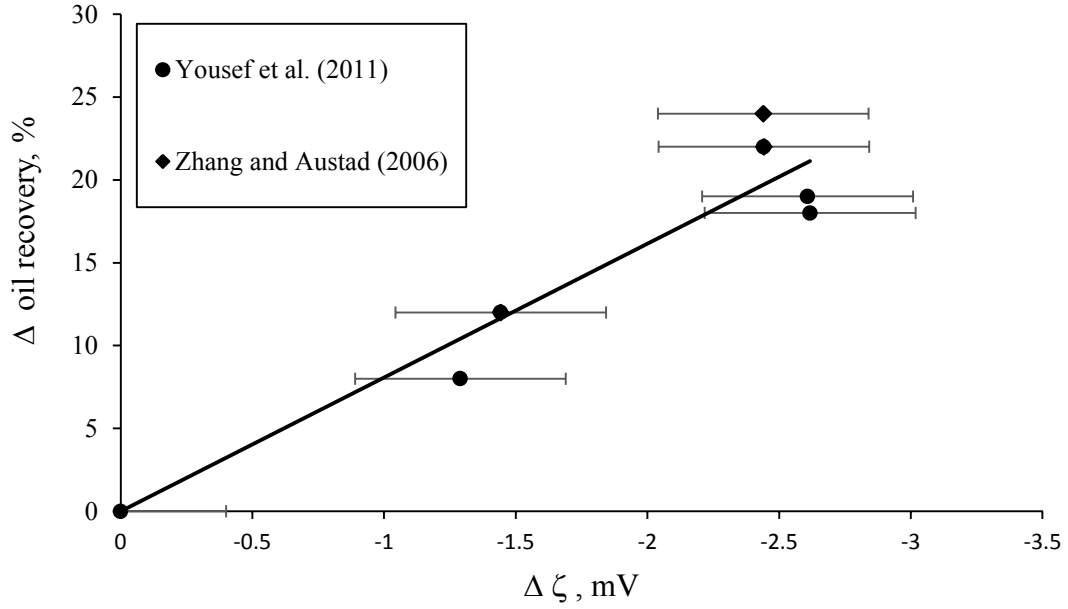

Figure 4.11: Comparison of the change in incremental oil recovery and zeta potential referenced to that of seawater for both controlled salinity (CSW) approaches: seawater dilution (Yousef et al., 2011) and sulfate addition to seawater (Zhang and Austad, 2006).

One final point relevant to CSW relates to the repeatability of laboratory coreflooding experiments. In many studies, a small number of samples are used repeatedly and are cleaned in between experiments. The cleaning protocol typically focuses on ensuring that crude oil is removed from the pore-space. However, we show here that standard cleaning protocols does not restore the zeta potential to its pristine state. This may impact on how the surfaces interact with PDIs in the aqueous phase, and polar species in the oil phase, during aging and subsequent waterfloods. If the zeta potential is not returned to its pristine state then the experiments may not be repeatable. We recommend the zeta potential is measured on intact samples before, during and after controlled salinity waterflooding experiments to constrain the behaviour of this key surface property.

4.5. Conclusions

We report here measurements of the zeta potential on intact Portland limestone obtained primarily using the streaming potential method (SPM), supplemented by a smaller number of measurements of the more widely applied electrophoretic mobility method (EPM). The experiments were designed to determine how the zeta potential is affected by the concentration of Ca, Mg and SO_4 over the range found in natural brines, and also how the zeta potential is affected by the concentration of these potential-determining ions in the presence of Na and Cl over the range found in natural brines. Our approach contrasts with many previous studies because the experimental method is specifically designed to ensure the equilibrium achieved between rock and electrolyte is consistent with natural processes. The results are directly applicable to a wide variety of natural systems including carbonate oil reservoirs and deep saline aquifers. The key findings can be summarized as follows:

- Ca and Mg change the zeta potential of intact natural limestone samples, causing a decrease in magnitude of the negative zeta potential with increasing concentration and causing polarity inversion to positive zeta potential at high concentration. We show that the two PDIs behave identically within experimental error, and the zeta potential varies linearly with both pCa and pMg over the broad range found in natural brines.
- SO_4 changes the zeta potential of natural limestone, causing an increase in the magnitude of the negative zeta potential with increasing concentration, and the zeta potential varies linearly with pSO_4 over the broad range found in natural brines. However, the gradient of the liner regression is lower than for Ca and Mg.
- We show that the IEP (expressed as pCa or pMg) decreases with increasing NaCl concentration. We report considerably lower values of IEP than most previous studies of calcite and chalk, and suggest that this may result from differences in the mineral surfaces (synthetic and natural calcite, natural chalk) compared to the natural limestone investigated here, and the careful method used to establish the initial equilibrium conditions between sample and electrolyte. We recommend this method in all studies of natural carbonates.
- We show that the IEP (expressed as pCa) obtained using SPM and EPM measurements on the same Portland Limestone are identical within experimental error, but the error is much larger for the EPM method. Both methods show a linear relationship between zeta potential

and pCa, but the gradient is a factor of two larger for the EPM method, consistent with a change in the location of the shear plane. SPM measurements are more relevant when quantifying the zeta potential of natural porous samples, because the measurements reflect the mineral surfaces that predominantly interact with the adjacent fluids.

- Standard laboratory cleaning protocols do not return carbonate mineral surfaces to a repeatable „pristine" state, which may affect the repeatability of subsequent experiments on the same sample, including the coreflooding/spontaneous imbibition experiments used to investigate controlled salinity waterflooding.
- Changes in wettability and oil recovery during controlled salinity waterflooding are consistent with the changes in zeta potential observed here. Carbonates saturated with formation brine rich in Ca are likely to have positively charged mineral surfaces (electrostatic attraction), encouraging wettability alteration to oil-wet conditions. Injecting seawater or diluted formation brine can reduce the Ca and/or Mg concentration below the IEP; note that the lower IEP observed here suggests that much less dilution is required than predicted previously. This yields negatively-charged mineral surfaces (electrostatic repulsion), increasing recovery by releasing previously trapped oil. Diluting seawater, or adding SO_4, both yield increasingly negative zeta potential, consistent with experimental studies that report improved recovery in both cases.

5. Quantification of Carbonate Rock Wettability Using Zeta Potential Measurements

5.1. Introduction

We have seen in Chapter 2 what wettability is, how it is traditionally measured, and discussed the main advantages and disadvantages of each method. The aim of this chapter is to determine whether wettability can be characterised from measurements of zeta potential on intact carbonate rock samples, obtained using the streaming potential method (SPM; see Jaafar et al., 2009). This chapter includes the preliminary results of the Portland limestone using synthetic and crude oil.

It has previously been shown that SPM measurements in carbonates saturated with brine and crude oil are sensitive to the wetting state (see Section 3.7.3) and it is well known that surface charge plays a key role in wettability alteration (Buckley et al., 1989; Hirasaki, 1991a; Buckley and Liu, 1998; Buckley, et al., 1998). However, there has been no attempt to relate systematically variations in wettability to variations in zeta potential. The potential advantage of the SPM to characterise wettability in laboratory experiments is that it is much quicker than traditional Amott or USBM tests, and the data can be obtained during the conventional coreflooding experiments used to measure (for example) permeability and relative permeability.

The SPM can be used to measure zeta potential at reservoir conditions of high salinity brine (Vinogradov et al., 2010), multiphase flow (Vinogradov and Jackson, 2011) and elevated temperature (Vinogradov and Jackson, 2015). However, most significantly, the SPM could be used to determine zeta potential *in-situ* using, for example, a modified version of any formation tester (FMT) tool, by inducing flow in the reservoir and measuring the pressure and voltage response. Such a tool would be of great utility in reservoir characterisation. There is, therefore, the potential to develop a new method to characterise wettability both in the laboratory, and *in-situ* in the reservoir, if a quantifiable and predictable relationship can be demonstrated between wettability and zeta potential obtained using the streaming potential method.

5.2. Methodology

5.2.1. Materials and Sample Preparation

The rock samples used in the experiments were Portland limestone from the Portland quarry on the south coast of the UK (Table 4.1). We used two different types of brine. The first were synthetic solutions of reagent-grade NaCl, $CaCl_2$, Na_2SO_4 and $MgCl_2$ salts in deionized water (DIW) from a filtered system with electrical conductivity below 1 μS/cm. These brines comprised synthetic formation brine (denoted FMB) typical of oil reservoirs and with a total ionic strength of 3.5 M (e.g., Romanuka et al., 2012; note the same FMB was used in Chapter 4), and a simple NaCl brine (denoted NaB) with a total ionic strength of 2 M. The second comprised natural seawater (SW) from the Arabian Gulf, collected from Dammam, Saudi Arabia. The natural seawater sample was treated with UV light and then filtered through 5 μm filter paper. Seawater diluted 10 times, and seawater with twice the natural SO_4 content, was also tested. Modifying the composition of injected brine in this way has been suggested as a mechanism for improved oil recovery (e.g. Austad et al., 2005; Strand et al., 2006; Yousef et al., 2012). Table 5.1 lists the compositions of the brines used. Two different types of oil were also used. The first was a synthetic oil comprising cyclohexane-pentanoic acid mixed in *n*-decane (see also Wu et al., 2008). The second was a crude oil containing asphaltenes (Table 5.2). The source and detailed composition of the dead crude oil cannot be reported for commercial reasons.

Appropriate initial conditions of carbonate/water/CO_2 equilibrium were replicated here following the approach described in Chapter 4. Each brine was prepared and then placed in a beaker with offcuts of the Portland limestone, maintaining an air layer in the beaker to provide a source of atmospheric CO_2 but sealing the beaker to prevent evaporation. Equilibrium was assumed to have been reached at a measured pH of 8.2±0.2 (see Section 4.2.1). The pH does not change regardless of the composition.

The core flooding apparatus used to measure the zeta potential in the SPM (described below) is closed to the atmosphere, and the final equilibration step was to ensure equilibrium between the

brine of interest and the rock sample at the closed-system conditions pertaining to a rock-brine system at depth.

The rock sample was pre-saturated with the selected brine at open-system conditions and then confined in the core holder at closed-system conditions, and the brine was pumped through the sample from the (closed) inlet reservoir to the (closed) outlet reservoir and back again. At regular intervals, the electrical conductivity and pH of the brine in the reservoirs was measured, and equilibrium was assumed to have been reached when the conductivity and pH of the brine in each reservoir differed by <5%. As discussed in Section 4.2.2, this preparation step is essential to ensure equilibrium between calcite, brine and atmospheric CO_2, and to prevent calcite dissolution and associated changes in surface charge during measurements of zeta potential.

The rock samples were cleaned following the enhanced cleaning procedure outlined in Chapter 4. In this process, each sample was flooded with at least 2 pore-volumes (PV) of deionized water (DIW) prior to cleaning with methanol in a Soxhlet apparatus for 48 hours and then dried for at least 12 hours in a vacuum oven at 80^{o}C. It was then allowed to cool at room temperature for a minimum of 6 hours, and flooded with a further 4 PV of 0.05 M NaCl brine that had been equilibrated with the carbonate samples. During this step, the conductivity of the effluent brine was measured in order to confirm it was the same as that obtained in Section 4.3.5 on fresh samples using the same brine within a 5% tolerance. We have seen in Chapter 4 that this enhanced cleaning procedure was essential to flush elevated concentrations of multivalent ions such as Ca, Mg and SO_4 from the pore-space of samples used in previous experiments.

Table 5.1. Composition of the synthetic Formation Brine (FMB) and natural seawater (SW) and derived compositions used in this study. The seawater was twice ten times (1/10SW) and also had SO_4 added to yield twice (2SW) the natural concentration.

Concentration M	NaB	FMB	SW	1/10SW	2SW
Na	2	2	0.5	0.05	0.5
Ca	-	0.42	0.012	0.0012	0.012
Mg	-	0.07	0.05	0.007	0.05
SO4	-	0.0033	0.033	0.0033	0.066
Total	2	2.49	0.615	0.061	0.648

Table 5.2. Properties of the oils used in this study.

Oil	Acid Number (AN)	Base Number (BN)	Asphaltene, %
Synthetic	4.57	-	-
Crude	0.37	2.02	3.49

Figure 5.1 outlines the step taken in order to establish the different wetting states and the Amott index (I_w) measurement. Once this is completed, the single phase experiments protocol (Figure 4.1) is followed in order to measure the coupling coefficient C_{SPM} and interpret the zeta potential.

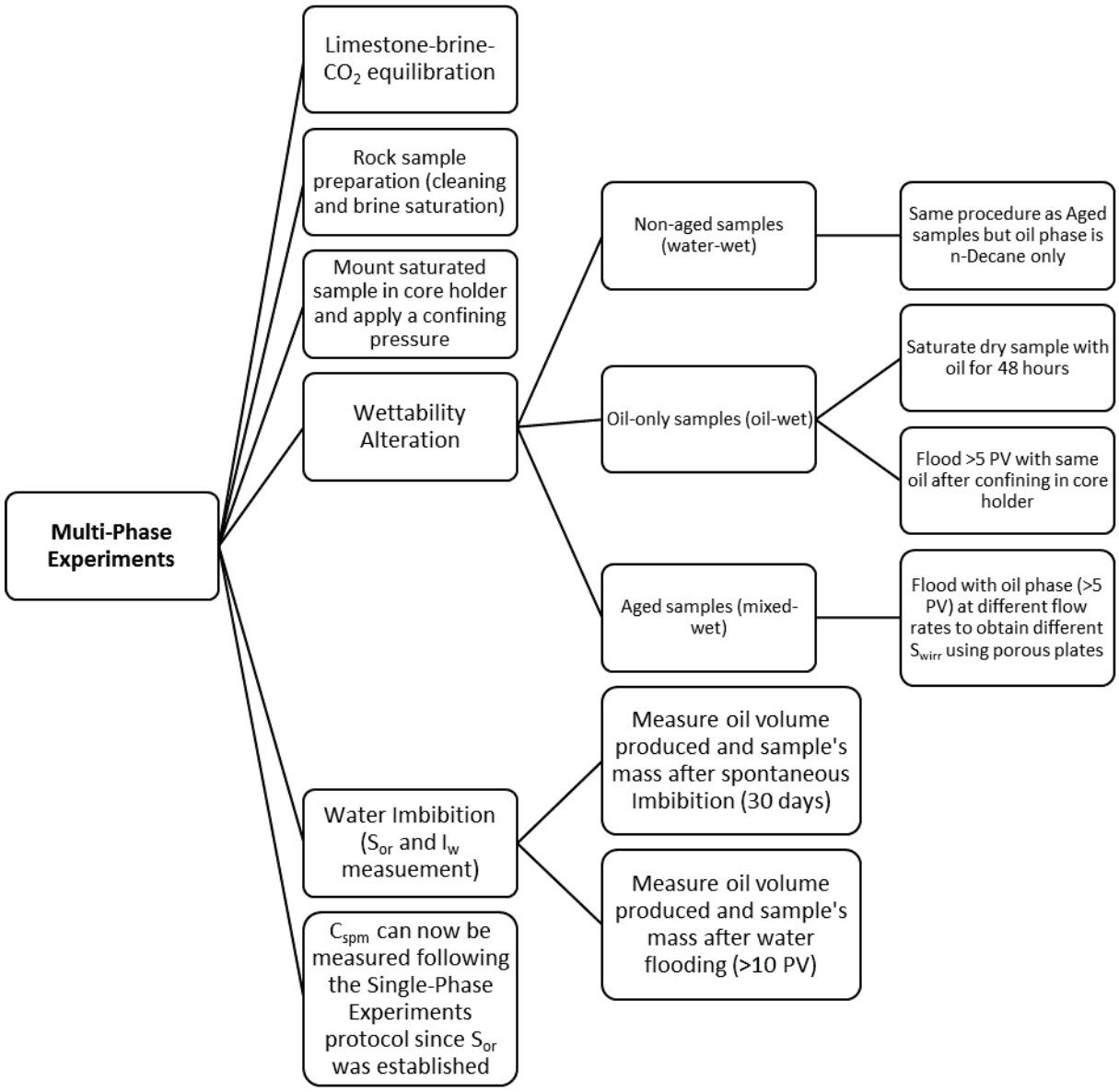

Figure 5.1 Flowchart showing the establishment of residual oil saturation and Amott index measurement for the multi-phase experiments for three different wetting states. Measurement of C_{SPM} is, then, measured according to the single-phase protocol presented in Figure 4.1.

5.2.2. Aging to Alter Wettability

Initially, brine-saturated samples were confined in the core-flooding apparatus and then flooded with >5 pore volumes (PV) of the oil at different flow rates to vary the balance of capillary and viscous forces and establish different values of initial water saturation (S_{wi}) using the porous plate method. The samples were then aged for four weeks in oil-filled containers, at room temperature for the synthetic oil samples and at 70°C for the crude oil samples. After aging, the remaining oil saturation (S_{or}) was established by first allowing spontaneous imbibition, leaving the samples in cells filled with pre-equilibrated brine for four weeks, and then mounting the samples in the core-flooding apparatus and flooding with >10 PV of the same brine. This approach allowed the wettability to be determined (see below).

In one suite of experiments, oil was injected into dry samples and the oil-saturated samples were aged to induce wettability alteration. The dry samples were saturated with the oil phase in a vacuum oven for 48 hours. Then, the oil-saturated samples were flooded with >5 PV of the same oil. This was done to ensure that no air bubbles were trapped in the sample. The rest of the aging procedure, and the establishment of S_{or}, was the same as described above.

5.2.3. Amott Index to Water (I_w) Measurement

The Amott method for wettability evaluation is based on spontaneous imbibition and forced displacement of oil and water from cores (Amott, 1959). It depends on capillary pressure and microscopic displacement efficiency. This method measures how easily the wetting phase spontaneously displaces the non-wetting phase, and then, compares that to the total displacement after forced imbibition is finished (Anderson, 1986b). The Amott wettability index for water is expressed as:

$$I_w = \frac{V_{wsp}}{V_{wt}} \tag{5.1}$$

where V_{wsp} is the volume of water spontaneously imbibed and V_{wt} is the total volume of water produced, which includes the volumes of water produced during spontaneous and forced imbibition. This index ranges from 1 for water-wet samples to 0 for oil-wet samples.

For the spontaneous imbibition part, after the aging process was done, each sample was placed in a water-filled Amott cell and left for 30 days. The volume of water produced was recorded for each sample. Then, the samples were removed from the Amott cell and transferred into a core holder for the forced imbibition part, where each sample was flooded with a minimum of 10 PV of water and the volume of produced oil was recorded.

5.2.4. Measurement of Zeta Potential using the Streaming Potential Method (SPM)

The zeta potential of brine saturated samples, and of samples saturated with brine and oil at the irreducible saturation (S_{or}), was measured using the SPM as described by Jackson and Vinogradov (2012). Only a brief summary of the method is provided here. The carbonate core samples were confined within an embedded rubber sleeve in a stainless steel core holder with non-metallic end caps. A syringe pump was used to induce a fluid pressure difference across the sample, causing brine to flow through the sample from reservoirs connected to each side of the core holder. Synthetic oil was used to translate the induced pressure from the pump to the brine in the inlet reservoir, which maintains closed-system conditions. The pump maintains constant rate to high accuracy and flow can be directed in either direction through the sample.

The pressure difference across the sample was measured using a pair of pressure transducers and the voltage across the sample was measured using non-polarizing Ag/AgCl electrodes and a high impedance voltmeter. The noise level of the measurements is dictated by the stability of the electrodes, rather than the performance of the voltmeter. To ensure that exclusion-diffusion potentials were eliminated during measurements of the streaming potential, uniform and constant brine conductivity and pH in each reservoir, and uniform and constant temperature (23°C), were maintained within a 5% tolerance. Redox potentials, which affect the measured voltage, were minimized by making the flow path electrically isolated from metals by ensuring that the Ag/AgCl electrodes were the only metal in contact with the samples and electrolyte. The stainless steel core

holder end caps were replaced by ones made of plastic and the core sample was enclosed in a rubber sleeve inside the core holder.

Interpretation of the results from the pair-stabilised (PS) experiments follows from the observation that at steady-state, the streaming current induced by the flow is balanced by a conduction current to maintain overall electrical neutrality. It is reasonable to assume that the currents follow approximately the same 1-D path along the samples, in which case the streaming potential coupling coefficient can be determined using

$$C_{SPM} = \frac{\Delta V}{\Delta P} \tag{5.2}$$

where ΔV and ΔP are the stabilized voltage and pressure measured across the plug, respectively. An effective value for the zeta potential for the sample was obtained using the Helmholtz-Smoluchowski equation (e.g. Jackson, 2015)

$$\zeta = \frac{C_{SPM}\mu\sigma_w F}{\varepsilon} \tag{5.3}$$

where F is the formation factor, which is the ratio of the conductivity of the brine to the conductivity of the saturated rock sample when surface conductivity is negligible (e.g. Jouniaux and Pozzi, 1995), ε is the permittivity of the brine, μ is the brine viscosity and σ_{rw} is the electrical conductivity of the saturated rock sample. The formation factor and electrical conductivity were available from a previous study (Table 4.1). Note that the zeta potential obtained is an effective value because it reflects the average streaming charge density transported by the flow of the brine; at the pore-level, the zeta potential may vary. Uncertainty in the reported value of zeta potential reflects the range of possible regressions that can be fitted to the measured streaming potential data within experimental error.

5.2.5. Determination of Water Composition

Brine composition was determined using inductively coupled plasma atomic emission spectroscopy (ICP-AES). As was seen in Chapter 4, the analysis was carried out in the Analytical Chemistry Laboratory at the Natural History Museum, London.

Brine samples from the SPM measurements were collected from the core holder *via* a valve on the outlet flow line at the end of a given suite of zeta potential measurements. Appropriate dilutions were prepared for each sample prior to analysis depending on the total ionic strength. All samples were acidified with 2% HNO_3 to prevent formation of complexes that might affect the interpreted concentrations. The accuracy of the method was determined using certified check solutions and the repeatability by conducting 5 repeat measurements on all the samples whose standard deviation is represented by the error bars.

5.2.6. Design of Experiments

The wettability of the samples was varied by aging the samples with different initial brine saturations after drainage, for each oil type and brine composition investigated, following the approach of Jadhunandan and Morrow (1995). These samples are termed „aged" throughout the results section. It is likely that mixed wettability here corresponds to the mixed-wet-small (MWS) condition of Dixit et al. (1999), in which the largest pores are occupied by oil and have the potential to become oil-wet, while the smallest pores remain occupied by water and hence water-wet. Mixed wettability is also likely to include some fractional wettability, with the mineral faces of the oil-filled pores having the potential to become oil-wet, and the corners remaining occupied by water and hence water-wet (Brown and Fatt, 1956; Kovscek et al., 1993). For comparison, samples were also drained to establish S_{wi} but were not aged. These samples are termed „non-aged". The most water-wet samples were not exposed to oil and the results obtained here correspond to those reported in Chapter 4 for brine-occupied samples. These samples are termed „brine-only". The most oil-wet samples were saturated only with oil prior to aging, and these samples are termed „oil-only" although it should be noted that the zeta potential in all samples containing oil was measured at the residual oil saturation, i.e., with the brine of interest flowing in the pore-space. Table 5.3 summarizes the experiments conducted.

Table 5.3. Summary of experiments, which includes the sample name, wettability, water saturation, and the water compositions used.

Sample	Wettability	S_{wi}	$1-S_{or}$	I_w	NaB	FMB	SW	1/10SW	2SW
P1	Brine-only	1	1	1	x	x	x	x	x
$\mathbf{P_{ww}}$	Non-aged	0.57	0.79	0	x	x	x	x	x
$\mathbf{P_{syn}}$	Oil-only	0	0.51	0	x	x	x	x	x
$\mathbf{P_{syn,a}}$	Aged	0.51	0.73	0	x	x			
$\mathbf{P_{syn,b}}$	Aged	0.62	0.79	0	x	x			
$\mathbf{P_{syn,c}}$	Aged	0.75	0.84	0	x	x			
$\mathbf{P_{cr}}$	Oil-only	0	0.30	0.04	x	x	x	x	x
$\mathbf{P_{cr,a}}$	Aged	0.71	0.88	0.13	x	x			
$\mathbf{P_{cr,b}}$	Aged	0.39	0.75	0.17	x	x			
$\mathbf{P_{cr,c}}$	Aged	0.17	0.53	0.09	x	x			

5.3. Results

5.3.1. Samples Saturated with Synthetic Oil

Figure 5.2 shows the zeta potential as a function of water saturation (1-S_{or}) after waterflooding for the synthetic oil and the two synthetic brines investigated (Table 5.2): NaB (Figure 5.2a) and FMB (Figure 5.2b). The values for the „water-only" and „non-aged samples" are identical within experimental error for each brine (compare empty diamonds and solid squares), suggesting that the lack of aging caused the oil to fail to adhere to the mineral surfaces, leaving them water-wet so the measurement records the zeta potential developed at the mineral-brine interface. The aged samples yield a consistently more negative zeta potential with decreasing 1-S_{or} for both brines (follow the open square symbols) and the „oil-only samples" show a strongly negative zeta potential, although the value is larger in magnitude for the NaB brine than for the FMB (compare circles in Fig. 5.2a and Fig. 5.2b).

Values of zeta potential for the aged samples and a given brine lie consistently between the „oil-only" and „brine-only"/„non-aged" sample values. For the NaB, the zeta potential is negative irrespective of 1-S_{or}, but for the FMB, the water-only, non-aged, and aged sample with the highest 1-S_{or} all yield positive zeta potentials. However, both brines show a similar trend between 1-S_{or} and zeta potential. The FMB brine values are shifted towards more positive potential by approximately 7±1 mV on average, compared to the NaB values. This voltage difference is consistent with the difference in zeta potential for the „brine-only" (most water-wet) samples saturated with each brine (-5.5 mV for the NaB versus 1 mV for the FMB, yielding a difference of 6.5 mV). Thus, there is a clear and consistent relationship between 1-S_{or} and zeta potential irrespective of brine composition, so long as the difference in zeta potential between water-wet samples is accounted for.

However, the Amott index to water (I_w) was zero for all samples, except the (assumed) value for the „brine-only" sample, because none of the oil-bearing samples imbibed any water. This would be interpreted to be consistent with strongly oil-wetting behaviour, irrespective of aging or 1-S_{or}. Thus, no relationship between I_w and zeta potential can be identified for the synthetic oil.

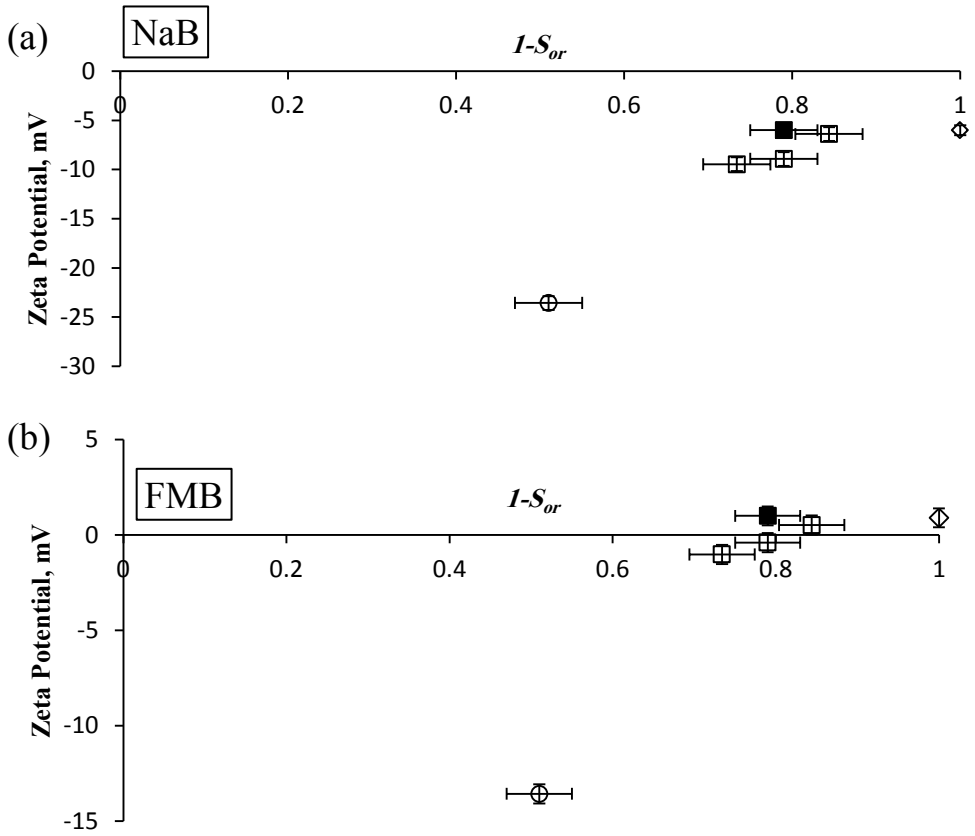

Figure 5.2: The zeta potential of samples aged with synthetic oil for, a) NaB, and b) formation brine FMB as a function of 1-S_{or}. Hollow circle represents aging in the absence of water, hollow squares represent aged samples in presence of water, filled square represents the water-wet case (no aging) and the diamond represents the single phase (S_w = 1).

5.3.2. Samples Saturated with Crude Oil

Figure 5.3 shows the zeta potential as a function of water saturation (1-S_{or}) after waterflooding (Figure 5.3a and 5.3b) and the inverted Amott water index (Figure 5.3c and 5.3d) for the crude oil and the two synthetic brines investigated: NaB (Figure 5.3a,b) and FMB (Figure 5.3c,d). Note that we plot the zeta potential against an inverted Amott index to water expressed as $I_{inv} = (1\text{-}I_w)/I_w$. In this scheme, a water-wetting sample ($I_w \rightarrow 1$) yields $I_{inv} \rightarrow 0$; conversely, a non-water-wetting sample ($I_w \rightarrow 0$) yields $I_{inv} \rightarrow \infty$. The rationale for this is explained below.

Similar to the synthetic oil case, we find that zeta potential values for the „brine-only" and „non-aged samples" (i.e., the strongly water-wet samples) are identical within experimental error for each brine (compare empty and solid diamonds in all plots). Moreover, the „oil-only" samples show a strongly negative zeta potential, although the value is again larger in magnitude for the NaB brine than for the FMB (compare circles in Figs. 5.3a,b with those in Figs. 5.3c,d). However, in contrast to the synthetic oil, there is a consistent linear trend between zeta potential and $(1-I_w)/I_w$, which can be expressed as

$$\zeta = A\left(\frac{1-I_w}{I_w}\right) + B, \tag{5.4}$$

where A denotes the sensitivity of the zeta potential to $(1-I_w)/I_w$, and B denotes the zeta potential in strongly water-wetting conditions, when $(1-I_w)/I_w = 0$. Equation (5.4) yields a good fit to the measured data ($R^2 > 0.97$) with A = -0.65 mV irrespective of the brine used, B = -5.95 mV for the NaB, and B = +0.49 mV for the FMB. Increasing $(1-I_w)/I_w$ (i.e., decreasing water-wettability) consistently yields more negative zeta potential for both brines (follow all symbols in Figs. 2c,d). Indeed, the trend between zeta potential and $(1-I_w)/I_w$ is clearer and more consistent than that between zeta potential and $1-S_{or}$ (compare circles in Figs. 5.3a,b with those in Figs. 5.3c,d). Both brines show an identical relationship between zeta potential and I_w, expressed by Equation (5.4), so long as the intercept B is adjusted to yield the zeta potential in strongly water-wetting conditions. Thus, there is a clear and consistent relationship between wetting behaviour and zeta potential irrespective of brine composition.

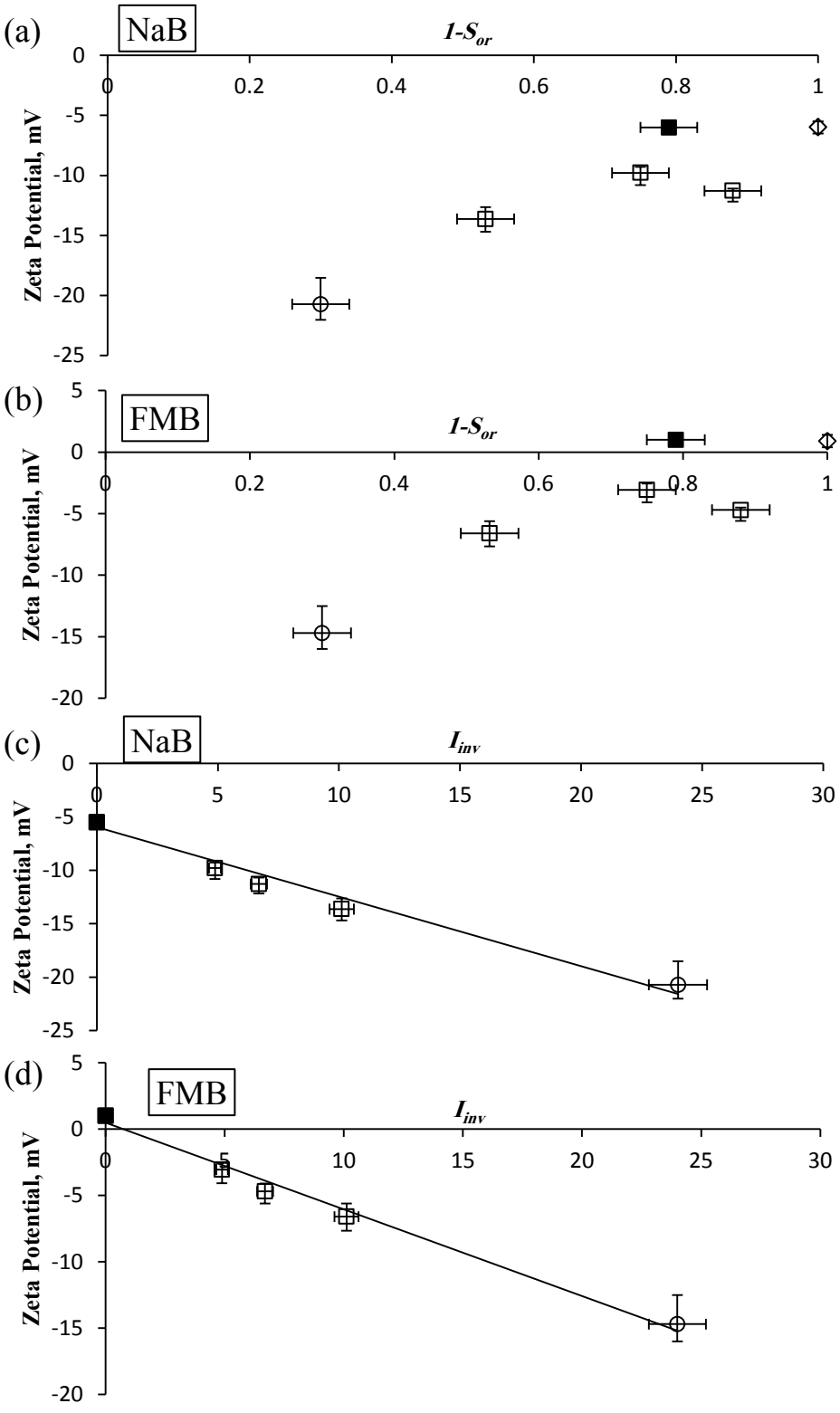

Figure 5.3: The zeta potential of samples aged with crude oil for, a) NaB, and b) formation brine FMB as a function of 1-S_{or}. Hollow circle represents aging in the absence of water, hollow squares represent aged samples in presence of water, filled square represents the water-wet case (no aging) and the diamond represents the single phase (S_w=1), c) and d) show the inverse of the Amott index as a function of the zeta potential for NaB and FMB, respectively.

5.3.3. Impact of Brine Composition

Brine composition and ionic strength are well known to impact the zeta potential of carbonates, and here we find the FMB yields a positive zeta potential in the „brine-only" samples which demonstrate the pristine brine-mineral interface; all the other brine compositions tested yield negative zeta potential (Fig. 5.4a). The most negative zeta potential values are for seawater (SW) with twice the natural SO_4 content, and SW diluted 10 times; the zeta potential values for these two modified SW compositions are identical within experimental error (compare circle and square for the „brine-only" samples in Fig. 5.4a). The SW and NaB also yield a negative zeta potential, which is identical within experimental error but smaller in magnitude than that observed for the modified SW compositions.

The relationship between zeta potential and brine composition is markedly different for the „oil-only" samples. All recorded zeta potential values are negative, and the most negative values are for the NaB. The least negative values are for the natural SW and SW-derived compositions, which yield similar zeta potential to the SW-derived compositions in the „brine-only" samples. By contrast with the „brine-only" samples, the FMB yields a strongly negative zeta potential in the „oil-only" samples.

5.3.4. Impact of Oil Composition

Figure 5.4b shows the zeta potential in the „oil-only" samples for the natural SW and FMB. Also shown for comparison are the zeta potential values obtained by Mahani et al. (2015), using a commercial zetameter. They prepared crude-oil suspensions in seawater, and formation brine of a similar composition to that used here, and the reported zeta potentials represent the pristine oil-brine interface. We find the zeta potential values obtained here are identical for a given brine composition, irrespective of the oil type, with the FMB yielding a negative zeta potential that is larger in magnitude than the natural SW. Moreover, the zeta potential obtained for the „oil-only" sample using SW, is identical to the value obtained by Mahani et al. (2015) for the crude-oil-seawater interface. However, the zeta potential obtained by Mahani et al. (2015) using formation

brine was much smaller in magnitude than that obtained using seawater, in contrast to the values obtained here.

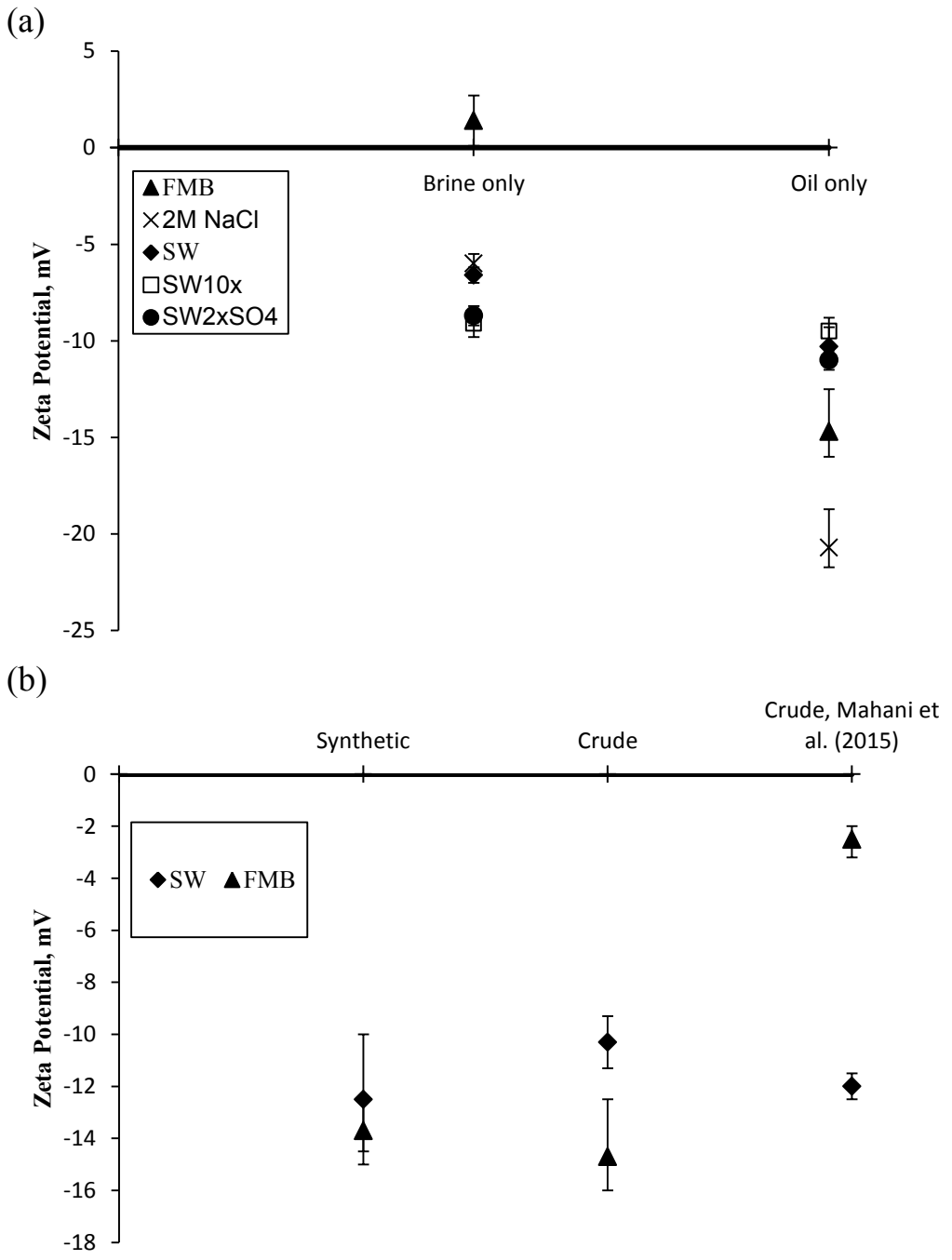

Figure 5.4: a) A comparison between the brine-only and the oil-only (aged in water absence) limestone samples as shown by the zeta potential for 2M NaCl, FMB, SW, seawater diluted ten times (SW10x) and seawater with twice the sulfate content ($SW2xSO_4$) for both cases b) zeta potential for formation brine FMB and seawater SW for the synthetic and the crude oils and that of Mahani et al. (2015).

5.4. Discussion

5.4.1. Wettability impact on the Zeta Potential

We observe a clear and consistent relationship between 1-S_{or} and zeta potential for the synthetic oil tested here, and wettability (expressed as (1-I_w)/I_w) and zeta potential for the crude oil tested. In each case, the observed sensitivity of the zeta potential is identical within experimental error, irrespective of the brine composition, so long as the influence of brine composition on the zeta potential in strongly water-wet conditions is accounted for. For the crude oil, the relationship between zeta potential and I_w is given by Equation (5.4), with A fixed regardless of brine composition and B adjusted to match the zeta potential at strongly water-wet conditions. The zeta potential is identical for the „brine only" samples, and „non-aged" samples saturated with brine and oil. These samples are strongly water-wet and the zeta potential reflects the pristine mineral-brine interface. Thus, introducing oil into the pore-space without aging does not affect the electrical properties of the mineral-brine interface, as observed by Vinogradov and Jackson (2012), because the oil does not replace the brine at the mineral surface.

The „oil-only" samples were aged with no brine present prior to measurement of the zeta potential, and we hypothesize that the oil in these samples wets all of the mineral surfaces. If this is the case, the measured zeta potential corresponds to the oil-brine interface rather than the mineral-brine interface (Fig. 5.4a). Evidence to support this hypothesis is provided by the differing response of the „brine-only" and „oil-only" samples to changes in brine composition. The brine-only samples show the expected behaviour for the calcite-brine interface, with Ca-rich formation brine yielding positive zeta potential, and SO_4 enriched or Ca-poor diluted seawater yielding the largest negative zeta potential (Fig. 5.4a). Both the Ca and SO_4 ions are known to be key potential-determining-ions (PDIs) for the calcite mineral surface, with increasing Ca concentration yielding increasingly positive zeta potential, and increasing SO_4 yielding increasingly negative zeta potential (e.g., Pierre et al., 1990; Zhang and Austad, 2006; Chapter 4). The „oil-only" samples show different behaviour, yielding negative zeta potential irrespective of brine composition and consistent with previous studies of the pristine oil-brine interface (e.g., Mahani et al. 2015) and calcite particles aged with stearic acid (Kasha et al., 2015). Moreover, in the „oil-only" samples the SW and related compositions yield the least negative zeta potential, and the NaB the most negative zeta potential, which is different to the brine-calcite interface and cannot be explained in terms of

Ca and SO_4 concentration. Nor can it be explained by simple double layer expansion which, for a given concentration of PDIs, yields the largest magnitude of zeta potential for the lowest ionic strength and vice-versa (e.g., Glover, 2015; Jackson, 2015). This aspect of the observed behaviour of the „oil-only" samples remains poorly understood.

The „brine-only"/„non-aged" samples reflect water-wet conditions and yield the most positive (or least negative) zeta potential values for a given brine composition. The „oil-only" samples reflect the most oil-wet conditions and yield the most negative zeta potential values for a given brine composition. Given this, the relationship between wettability and zeta potential observed here can be explained by the varying proportions of water-wet and oil-wet surfaces encountered by the flowing brine during a streaming potential measurement. In water-wet conditions, the brine encounters only water-wet surfaces, and the resulting zeta potential reflects the pristine mineral-brine interface. As the wetting state becomes mixed-wet, the brine encounters some oil-wet mineral surfaces in the pore-space, yielding a measured zeta potential that is more negative in value, reflecting the zeta potential at the oil-brine interface. Increasingly oil-wet surfaces yield increasingly negative values of zeta potential, reflecting the increasing proportion of oil-wet mineral surfaces encountered by the flowing brine.

Zeta potential measurements obtained using the streaming potential measurements are therefore sensitive to the wetting state if two conditions are met. First, the zeta potential at the mineral-brine and oil-brine interfaces must differ in magnitude and/or polarity. Second, variations in wettability must reflect differing proportions of water-wet and oil-wet mineral surfaces in the pore-space. These conditions are typically met in carbonate reservoirs, where the mineral-brine interface is often positively charged (e.g., Jackson and Vinogradov, 2012; Chen et al., 2014), and those parts of the pore-space contacted by oil become oil-wet (Kovscek et al., 1993). Thus, streaming potential measurements, yielding zeta potential data sensitive to the pore-level proportion of oil- and water-wet mineral surfaces, offer a new route to determine wettability in carbonate reservoirs. The streaming potential measurements may be conducted in the laboratory, as part of modified core-flooding experiments that are conducted routinely to measure permeability, or *in-situ* using a modified wireline formation testing tool.

5.4.2. The impact of the Electrostatic Interaction on the wetting thin film thickness

Strong water-wetting conditions are characterized by the presence of a stable thin film that wets and separates the mineral surface from the oil phase (Buckley et al., 1989; Hirasaki, 1991a; Buckley et al., 1998). Thin wetting films are described by their pressure, which is termed the disjoining pressure (Π) and is a function of the film‟s thickness (*h*) (Israelachvili, 2011):

$$\Pi_{total}(h) = \Pi_{VdW}(h) + \Pi_{EDL}(h) + \Pi_s(h) \quad (5.5)$$

where Π_{Vdw} is the van der Waals or the molecular component (between dipoles), Π_{EDL} is the electrostatic component (between ions), and Π_s is the component of structural forces, which is also referred to as solvation or hydration.

The Van der Waals dispersion force is always attractive, which means that its component is negative in the total disjoining pressure. Also, Van der Waals force is not affected by the solvent‟s properties such as the ionic strength (Hunter, 1993). The structural force is very short-range of around 0.02-0.06 nm (Hirasaki, 1991b) and is always repulsive.

As such, the electrostatic force is the only factor that assesses the overall change in the disjoining pressure as a function of water chemistry. This is because the zeta potential, which is a reflection of the surface charge, is directly affected by the brine‟s total ionic strength and composition during controlled salinity waterflooding.

The electrostatic component of the disjoining pressure is calculated when the zeta potential at both interfaces (mineral-water and water-oil) and the total ionic strength are known (Israelachvili, 2011):

$$\Pi_{EDL} = 64n^0 kT\, tanh(ze\zeta_1 /4kT)\, tanh(ze\zeta_2 /4kT)\, exp(-\kappa x) \quad (5.6)$$

where n^0 is the number density, *k* is the Boltzmann constant, *T* is the temperature, *z* is the valence, *e* is the elementary charge, ζ_1 is the zeta potential at the mineral-water interface, ζ_2 is the zeta

potential at the oil-water interface, and x is the distance separating the two interfaces, and the Debye parameter is κ, which is given by:

$$\kappa = \sqrt{\frac{2n^0 z^2 e^2}{\varepsilon kT}} \tag{5.7}$$

The Debye length is $1/\kappa$ and characterizes the electrical double layer (EDL) thickness. At higher electrolyte concentrations it is shorter reflecting a thinner EDL and vice versa. The electrostatic energy of interaction per unit area (W_{EDL}) in J/m^2 (Israelachvili, 2011) is:

$$W_{EDL} = \frac{64n^0 kT}{\kappa} tanh(ze\zeta_1 /4kT)\ tanh(ze\zeta_2 /4kT)\ exp(-\kappa x) \tag{5.8}$$

We have shown how that the zeta potential is affected by the wetting state and how the brine composition affects both the oil-brine and the calcite-brine interfaces. Now, we assess the impact of surface charge on the electrostatic interaction between the two interfaces and how that might reflect on the stability of a wetting film.

Figure 5.5 shows the energy of interaction at the four compositions, formation brine, seawater, seawater diluted ten times (SW10x), and seawater with twice the amount of sulfate added (SW2xSO_4). The interaction favours oil-wetting conditions in the formation brine case as the high calcium concentration results in a positive zeta potential at the mineral-water interface while the oil-brine interface is still negatively charged, which leads to electrostatic attraction favouring the collapse of the wetting film.

For the seawater case, the electrostatic interaction becomes repulsive as both interfaces are negatively charged since the polarity of the calcite surface charge is reversed. The range at which this repulsion operates is larger (1.8 nm) than that of the attraction experienced in the formation brine case (0.5 nm) because of the lower ionic strength of seawater. Hence, a greater possibility for the stability of a range of thin film thicknesses exists, which should lead to the re-mobilization of trapped oil.

Further repulsion is observed when comparing the seawater to the seawater dilution and the sulfate addition approaches. The range of interaction (film thickness in Figure 5.5) for SW10x is about

doubled from 1.8 nm to 4 nm, which might lead to the stability of much thicker wetting film thicknesses. The seawater with added sulfate $SW2xSO_4$ shows higher repulsion (energy of interaction) compared to the seawater case (0.36 and 0.23 mJ/m^2, respectively).

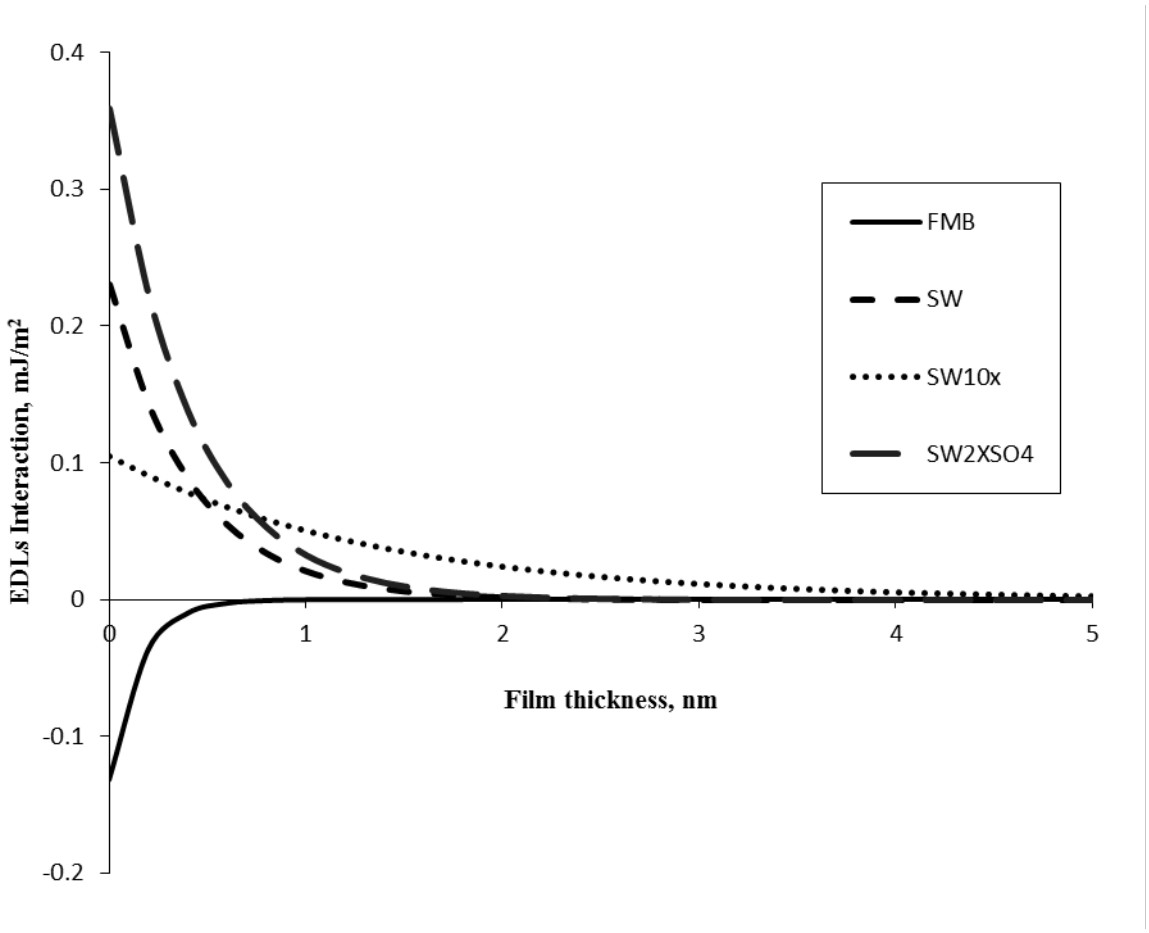

Figure 5.5: Electrostatic interaction energy and the possible film thicknesses for typical brine compositions used in controlled salinity waterflooding. FMB (solid line), SW (dashed line), SW10x (dotted line), and $SW2xSO_4$ (long-dashed line).

5.5. Conclusions

We report here preliminary measurements of the zeta potential on intact Portland limestone containing synthetic and natural crude oil aged at various values of initial brine saturation. The zeta potential was measured using the streaming potential method (SPM). We observed a clear correlation between zeta potential and initial brine saturation regardless of the oil or brine composition used. Aging with the synthetic oil yielded strongly oil-wet conditions regardless of initial brine saturation, so no correlation between wettability and zeta potential could be obtained. However, the natural crude oil yielded a variety of wetting states depending upon the initial brine saturation, and a clear relationship was observed between the wetting state, quantified by the Amott water index (I_w), and the zeta potential. A linear regression provided an excellent match to the data when the wetting state was expressed as $(1 - I_w)/I_w$. The gradient of the regression was independent of the brine composition; the only parameter that needed to be adjusted to obtain a match was the zeta potential observed in strongly water-wetting conditions.

These results suggest that zeta potential data, obtained using the SPM, can be used to determine wettability in carbonates. The SPM can be applied in laboratory core-flooding experiments, yielding a more rapid approach to characterise wettability than current methods and allowing wettability to be determined whilst simultaneously measuring permeability, relative permeability or other rock properties of interest. More significantly, the SPM could be applied downhole to determine wettability *in-situ*. However, further data are required, probing a wider range of crude oil and brine composition, carbonate rock samples, and temperature, before the results obtained here can be generally applied.

6. Conclusions and Future Work

6.1. Summary

In the first part of this study, measurements of the zeta potential on intact Portland limestone obtained primarily using the streaming potential method (SPM), supplemented by a smaller number of measurements of the more widely applied electrophoretic mobility method (EPM) were reported. The second part of this study was concerned with the presence of oil in the rock where measurements of zeta potential were reported as a function of the Amott index (I_w) and the remaining saturation of oil. Streaming potential method was used to measure the changes to the zeta potential as a function of wettability where different rocks were aged with a range of initial water saturation. In addition, the most oil-wet case was considered by aging some sample in the absence of a brine phase.

The experiments were designed to determine how the zeta potential is affected by the concentration of Ca, Mg and SO_4 over the range found in natural brines, and also how the zeta potential is affected by the concentration of these potential-determining ions in the presence of Na and Cl over the range found in natural brines. Our approach contrasts with many previous studies because the experimental method is specifically designed to ensure the equilibrium achieved between rock and electrolyte is consistent with natural processes. The results are directly applicable to a wide variety of natural systems including carbonate oil reservoirs and deep saline aquifers. The key findings can be summarized as follows:

- We show that the two PDIs (Ca and Mg) behave identically within experimental error, and the zeta potential varies linearly with Ca and Mg concentration when expressed as pCa or pMg. Here we follow the procedure used in metal oxides where the proton is the PDI and zeta potential is plotted against pH. We recommend plotting concentration as pPDI in all studies.
- SO_4 changes the zeta potential of natural limestone, causing an increase in the magnitude of the negative zeta potential with increasing concentration, but the sensitivity is lower than that of Ca and Mg. The zeta potential varies linearly with SO_4 concentration when expressed as pSO_4.

- We show that the sensitivity of the zeta potential to PDI concentration in natural limestone (expressed as the gradient of the linear regression between zeta potential and pPDI) decreases with increasing NaCl concentration.
- We show that the IEP (expressed as pCa or pMg) decreases with increasing NaCl concentration. We report considerably lower values of IEP than most previous studies of calcite and chalk, and suggest that this may result from differences in the mineral surfaces (synthetic and natural calcite crystals, natural chalk) compared to the natural limestone investigated here, and the careful method used to establish the initial equilibrium conditions between sample and electrolyte. We recommend this method in all studies of natural carbonates.
- The sensitivity of the zeta potential to pPDI is much lower (by a factor of approximately two in the measurements obtained here) when measured using the SPM compared to the EPM. The sensitivity of the zeta potential to pCa obtained in historical EPM measurements is consistent with the EPM data we report in this study, despite the broad range of calcite/carbonate sample types and electrolytes used, and we suggest that the measurement technique dominates the observed sensitivity. Streaming potential method measurements are more relevant when quantifying the zeta potential of natural porous samples, because the measurements reflect the mineral surfaces that predominantly interact with the adjacent fluids.
- Standard laboratory cleaning protocols may not return carbonate mineral surfaces to a repeatable „pristine" state, which may affect the repeatability of subsequent experiments on the same sample, including the core-flooding/spontaneous imbibition experiments used to investigate controlled salinity waterflooding.
- Changes in oil wettability and recovery during controlled salinity waterflooding are consistent with the changes in zeta potential observed in this study. Carbonates saturated with formation brine rich in Ca are likely to have positively charged mineral surfaces, encouraging wettability alteration to oil-wet conditions. Injecting seawater or diluted formation brine can reduce the Ca and/or Mg concentration below the IEP; note that the lower IEP observed here suggests that much less dilution is required than predicted previously. This yields negatively charged mineral surfaces, increasing recovery by releasing previously trapped oil. Diluting seawater, or adding SO_4, both yield increasingly

negative zeta potential, consistent with experimental studies that report improved recovery in both cases.

- Understanding the surface charge of the mineral is important in understanding the underlying mechanisms for the controlled salinity effect, especially, because of the lack of other surface chemistry tools that address them. The measurement of streaming potential method is a powerful tool in understanding the zeta potential, which we show correlates with the wetting state.
- Streaming potential method is the only tool to measure zeta potential in intact porous media and, hence, is able to give representative values that reflect the wetting state and fluid distribution in pores.
- The mineral‟s wetting state affects its surface charge. The more oil-wet the system is, the more negative the zeta potential gets with the oil-wet case being the most negatively charged. For the crude oil samples, there is a strong correlation between the Amott Index (as I_{inv}) and the zeta potential.
- When compared to the mineral-brine interface, the oil-brine interface is less sensitive to the presence of PDIs as the zeta potential of SW, SW10x, and SW2xSO_4 were the same within experimental error.
- The oil-brine interface yields the same negative zeta potential for both synthetic and crude oil as shown in FMB and NaB. However, more work needs to be done in order to understand the contribution of oil properties such as (acid and base numbers, amounts of resins and asphaltene) to the measured zeta potential.
- The calcite-brine interface reversed polarity from positive in FMB to negative in SW, SW10x, and SW2xSO_4 while the oil-brine interface was always negative, which indicates a shift from an initial electrostatic attraction in FMB to electrostatic repulsion when the formation brine is replaced with SW and/or other common compositions in controlled salinity waterflooding. This is consistent with observed wettability alteration towards more water-wet conditions and increased oil recovery reported.
- The type (repulsive/attractive), magnitude, and range of the electrostatic interaction are all important factors affecting the stability of a wetting-thin film. All three can be characterized knowing the zeta potential and the brine ionic strength.

6.2. Challenges Faced

- Unlike quartz (and other metal oxides), calcite (and other carbonate minerals) is soluble. This was challenging because SPM experiments had to be at constant ionic strength and pH.
- Calcite dissolution poses another challenge as the formation factor also needs to be constant in order to correctly interpret the zeta potential from SPM. This is related to the permeability reduction as the mineral dissolves, which leads to a higher cementation factor leading to a higher formation factor when compared to a fresh rock sample.
- The solution was to equilibrate the brine with pieces of the same rock block (not the plug itself). The calcium concentration and pH were monitored regularly for a long time (more than 2 months) in order to insure equilibrium conditions.
- Low permeability rock samples
- The oil phase is a complex parameter when considering the resulting wettability alteration. Thus, using the synthetic oil in order to represents an oil phase of a different acid number

6.3. Implications

- Petrophysics/Reservoir Engineering application: Incorporating the surface charge (coupling coefficient and the zeta potential) into reservoir models by establishing a relation between the zeta potential and multiphase flow characteristics such as the relative permeability.
- Laboratory application: SPM can be part of a rapid protocol for wettability measurement when compared to traditional capillary dependent methods (e.g., the Amott-Harvey index).
- Field application: a simple modification for the MDT tool can lead to SPM data acquisition. Thus, a possible in-situ measurement of wettability within different parts of the same reservoir as well as different parts of the same field.
- Moreover, regular SPM data acquisition in a field will lead to real-time monitoring of EOR processes such as CSW.

6.4. Future Work

Some insights that resulted from this work point towards the need to developing a better understanding of what really takes place at the surface of calcite during the processes of aging, controlled salinity waterflooding and indeed to any other process that involve changing the wetting state and/or the water chemistry of the reservoir.

- In order to represent the reservoir temperature, the values of the zeta potential must reflect that specific temperature, which should be conducted using the newly-developed elevated temperature streaming potential apparatus.
- Different reservoirs have different formation brine compositions. This study only considered one composition. Hence, there is a need for obtaining SPM measurements using different FMB compositions.
- Conducting streaming potential experiments where both increased oil recovery and the corresponding zeta potential are measured. The correlation of the change in increased oil recovery and the change in zeta potential presented in Chapter 4 was of three different rocks, two different oil phases, and at three different temperatures. Moreover, the increased oil recovery reported was done spontaneously for the study of Zhang and Austad (2006) while Yousef et al. (2011) conducted waterflooding experiments.
- Conducting streaming potential experiments with other carbonate rocks in addition to the Portland limestone used in this study. Also, there is a need for obtaining data using different crude oils in order to better delineate the SPM and wettability relationship.
- Varying the aging process by changing the brine composition in order to maximise/minimise the electrostatic interaction, which should result in different states of wettability.
- In this study, the only mobile phase was water, which is not the case in real reservoirs as both phases flow. Hence, a better understanding of the streaming potential coupling coefficient during multiphase flow is highly beneficial. Once such understanding is established, measurements of streaming potential would be of immense usefulness as they would be directly applicable to the understanding of the in-situ default wetting state as well as the understanding of the efficacy of the controlled salinity waterflooding and other processes that might impact the wetting state of the reservoir.

- Extending the measurement of SPM to other applications such as the addition of supercritical CO_2, surfactants, polymers, alkali to the water phase during waterflooding in order to understand the effect of each on the zeta potential, which should shed light on how these EOR processes work.

References

Akbar, M., Vissarpragada, B., Alghamdi, A. H., Allen, D., Herron, M., Carnegie, A., Dutta, D., Olesen, J.-R., Chourasiya, R. D., Logan, D., Steif, D., Netherwood, R., Russell, S. D. and Saxena, K. "A snapshot of carbonate reservoir evaluation" Oilfield Review, Vol. 12, pp. 20-41. (2001)

Al-Maamari, R.S.H. and Buckley, J.S.: "Asphaltene Precipitation and Alteration of Wetting: The Potential for Wettability Changes during Oil Production," SPE REE, Vol. 6, pp. 210-214. (2003)

Al-Mahrooqi, S.H., Grattoni, C.A., Moss, A.K., Jing, X.D. "An investigation of the effect of wettability on NMR characteristics of sandstone rock and fluid systems" J. Pet. Sci. Eng. Vol. 39, pp. 389–398. (2003)

Al-Mahrooqi, S.H., Grattoni, C.A., Muggeridge, A.H. and Jing, X.D. "Pore-scale Modelling of NMR Relaxation for the Characterization of Wettability", J. Pet. Sci. Eng. Vol. 52, p.172-186. (2006)

Alotaibi MB, Nasr-El-Din HA, Fletcher JJ. "Electrokinetics of limestone and dolomite rock particles" SPE Reserv Eval Eng. Vol 14, pp. 594–603. (2011)

Amankonah, J. O., and Somasundaran, P. "Effects of dissolved mineral species on the electrokinetic behavior of calcite and apatite" Journal of Colloids and Surfaces, Vol. 15, pp. 335-353. (1985)

Amott, E., "Observations relating to the wettability of porous rocks" Petroleum Transactions of AIME 216, 156– 162. (1959)

Amyx, J.W., Bass Jr., D.M., and Whiting, R.L. "Petroleum Reservoir Engineering - Physical Properties" McGraw Hill, New York. (1960)

Andersen, MA, Thomas, DC and Teeters, DC. "A New Formation Wettability Test: The Dynamic Wilhelmy Plate Wettability Technique" SPE 17368 (1988)

Anderson, W. G. “Wettability Literature Survey- Part 1: Rock/Oil/Brine Interactions and the Effects of Core Handling on Wettability” SPE 13932. (1986a)

Anderson, W.G., “Wettability Literature Survey – Part 2: Wettability Measurement”, J. Pet. Tech., Nov. (1986b)

Andrew, M., Bijeljic, B., Blunt, M. J. “Pore-scale contact angle measurements at reservoir conditions using X-ray microtomography” Advances in Water Resources. Vol. 68, pp. 24–31. (2014)

Appelo, C.A.J. “Cation and proton exchange, pH, variations, and carbonate reactions in a freshening aquifer” Water Resources Research, Vol 30, pp. 2793–2805. (1994)

Archie, G.E. ”Electrical Resistivity Log as an Aid in Determining Some Reservoir Characteristics” Trans. AIME. Vol. 146, pp 54-61. (1942)

Austad, T, Strand, S and Puntervold, T. “Is Wettability Alteration of Carbonates by Seawater Caused by Rock Dissolution?” SCA2009-43. (2009)

Austad, T., Strand, S., Høgnesen, E.J., and Zhang, P. “Seawater as IOR fluid in fractured chalk” SPE 93000. (2005)

Bakiewicz, W., Milne, D.M., Noori, M. “Hydrogeology of the Umm Er Radhuma aquifer, Saudi Arabia, with reference to fossil gradients” Q. J. Eng. Geol., Vo. 15, pp. 105–126 (1982)

Beattie, JK and Djerdjev, AM. “The Pristine Oil/Water Interface: Surfactant-Free Hydroxide-Charged Emulsion” Angew. Chem. Int. Ed. 43, pp. 3568–3571. (2004)

Berg, C. J. “An Introduction to Interfaces and Colloids: The Bridge to Nanoscience” World Scientific Publishers, Singapore. (2010)

Bortolotti, V, Mancini, P and Srisuriyachai, F. “Wettability Index of Carbonatic Reservoirs and EOR: Laboratory Study to Optimize Alkali and Surfactant Flooding” SPE 131043 (2010)

Briant, J. and Cuiec, L. “title not available!” Rev. Inst. Fr. Pet. Ann. Combust. Liq. 26: pp. 591-616. (1971)

Brown, C.E. and Neustadter, E.L. “The Wettability of Oil/Water/Silica Systems With Reference to Oil Recovery” J. Canadian Pet. Tech. Sept. 19, No. 3, pp. 10-110. (1980)

Brown, R.J.S. and Fatt, I. “Measurements of Fractional Wettability of Oilfield Rocks by the Nuclear Magnetic Relaxation Method.” Trans. AIME. 207, 262-264. (1956)

Buckley, J.S. and Liu, Y. “Some mechanisms of crude oil/brine/solid interactions” Journal of Petroleum Science and Engineering vol. 20, pp. 155–160. (1998)

Buckley, J.S., Bousseau, C, and Liu, Y. “Wetting Alteration by Brine and Crude Oil: From Contact Angle to Cores” SPE 30765. (1995)

Buckley, J.S., Liu, Y. and Monsterleet, S., “Mechanisms of Wetting Alteration by Crude Oils”, SPE Journal, Vol. 3, pp. 54-61. (1998)

Buckley, J.S., Takamura, K. and Morrow, N.R., “Influence of Electrical Surface Charges on the Wetting Properties of Crude Oils”, SPE Res. Eng. Vol. 4, pp. 332-40. (1989)

Busireddy, C, Rao, D. “Application of DLVO Theory to Characterize Spreading in Crude oil-Brine-Rock Systems” SPE 89425 (2004)

Carruthers, J. C. “The electrophoresis of certain hydrocarbons and their simple derivatives as a function of pH” Trans. Faraday Soc. Vol. 34, pp. 300-307. (1938)

Chen, L, Zhang, G, Wang, L, Wu, W, Ge, J “Zeta potential of limestone in a large range of salinity” Colloids and Surfaces A: Physicochem. Eng. Aspects, Vol. 450, pp. 1-8. (2014)

Chilingar GV, Yen, TF “Some notes on wettability and relative permeability of carbonate rocks” Energy Sources 7 (1) pp. 67-75. (1983)

Chung, F, Sarathi, P and Jones, R. “Modelling of Asphaltene and Wax Precipitation” NIPER-498, January DOE Topical Report, Bartlesville, OK. (1991)

Cicerone, DS, Regazzoni, AE, Blesa, MA ”Electrokinetic properties of the calcite/water interface in the presence of magnesium and organic matter” Colloids and Surfaces A: Physicochem. Eng. Aspects, Vol. 154, pp. 423–433. (1992)

Conway B. E. “The State of Water and Hydrated Ions at Interfaces” Adv. in Colloid Interface Science. Vol. 8, p 91. (1971)

Corelab “Fundamentals of Core Analysis” Houston, Tx. (1983)
Craig, F.F. Jr. ”The Reservoir Engineering Aspects of Waterflooding”, Monograph series, Soc. Pet. Eng., Dallas, 3. (1971)

Cuiec, L. “Restoration of the natural state of core samples” SPE 5634 Dallas (1975)

Cuiec, L.E. “Evaluation of reservoir wettability and its effect on oil recovery.” In: Morrow, N.R. (Ed.), Interfacial Phenomena in Oil Recovery. Marcel Decker, New York, pp. 375–391. (1991)

Delgado, AV, González-Caballero, F, Hunter, RJ, Koopal, LK and Lyklema, J. “Measurement and interpretation of electrokinetic phenomena” Journal of Colloid and Interface Science, Vol. 309, pp.194–224. (2007)

Derjaguin, B.V., Churaev, N.V. and Muller, V.M. “Chapter 8: The Derjaguin-Landau-Verwey-Overbeek (DLVO) theory of stability of lyophobic colloids” In: J.A. Kitchener (Editor), Surface Forces. Consultans Bureau, New York. (1987)

Dickinson, W. “The effect of pH upon the electrophoretic mobility of emulsions of certain hydrocarbons and aliphatic halides” Trans. Faraday Soc. Vol. 37, pp. 140-148. (1941)

Diebler, H., Eigen, M., Ilgenfritz, G. Maas, G., Winkler, R. “Kinetics and mechanism of reactions of main group metal ions with biological carriers” Pure Appl. Chem. Vol. 20, pp. 93–115. (1969)

Dixit, AB, Buckley, JS, McDougall, SR, and Sorbie, KS. "Empirical Measures of Wettability in Porous Media and the Relationship between them Derived from Pore-Scale Modelling" Transport in Porous Media, Vol. 40: pp. 27-54. (2000)

Donaldson, E.C., Thomas, R.D., Lorenz, P.B. “Wettability determination and its effect on recovery efficiency.” SPEJ, 13– 20 (March). (1969)

Drummond, C and Israelachvili, J. “Fundamental studies of crude oil-sruface water interactions and its relationship to reservoir wettability” J. Petroleum Science and Engineering, Vol. 45: pp. 61-81. (2004)

Dubey, ST and Waxmann, M.H. “Asphaltene adsorption and desorption from mineral surfaces” SPERE 6: pp. 389– 395. (1991)

Eriksson, R, Merta, J and Rosenholm, JB. “The calcite/water interface I. Surface charge in indifferent electrolyte media and the influence of low-molecular-weight polyacrylate” J. of Colloid and Interface Science. Vol. 313, pp. 184-193. (2007)

Eriksson, R, Merta, J and Rosenholm, JB. “The calcite/water interface II. Effect of added lattice ions on the charge properties and adsorption of sodium polyacrylate” J. of Colloid and Interface Science. Vol. 326, pp. 396–402. (2008)

Fenter, P., Geissbühler, P., DiMasi, E., Sörensen, L.B., and Sturchio, N.C. “Surface speciation of calcite observed in situ by high- resolution X-ray reflectivity” Geochimica et Cosmochimica Acta, Vol. 64, pp. 1221–1228. (2000)

Fleury, M., Deflandre, F. “Quantitative evaluation of porous media wettability using NMR relaxometry” Magn. Reson. Imaging, Vol. 21, pp. 385–387. (2003)

Fox, H W and Zisman, W A “The spreading of liquids on low-energy surfaces. III. Hydrocarbon surfaces” J. of Colloid Science. Vol. 7, pp. 428-442. (1952)

Foxall, T, Peterson, GC, Rendall, HM, Smith, AL “Charge determination at the calcium salt/aqueous solution interface” J. Chem. Soc. Faraday Trans. Vol. 75, pp. 1034-1039. (1979)

Fuerstenau, M. C., Gutirrrez, G., and Elgillani, D. A. “The influence of sodium silicate in non-metallic floatation systems” Trans. AIME 241, pp. 319-323. (1968)

Garrels, R and Christ C “Solutions, Minerals, and Equilibria” Jones and Bartlett Publishers International, London, pp. 450. (1990)

Glover, P.W.J., Meredith, P.G., Sammonds, P.R., Murrell, S.A.F. “Ionic Surface Electrical Conductivity in Sandstone” J. Geophys. Res., Vol. 99, pp. 21635-21650. (1994)

Glover, P.W.J. “Geophysical Properties of the Near Surface Earth: Electrical Properties,” in: Treatise on Geophysics (editor in chief: G. Schubert), 2nd edition, volume 11, chapter 4, Elsevier. (2015)

Glover, P.W. J., Dery, N. “Dependence of streaming potential on grain diameter and pore radius for quartz glass beads” Geophysics. Vol. 75, pp. 225–241. (2010)

Glover, P.W.J., Jackson, M.D. “Borehole Electrokinetics” The Leading Edge, pp. 724-728. (2010)

Gomari, K. A. “Different Approaches to Understand Mechanism of Wettability Alteration of Carbonate Reservoirs” SPE 121952 (2009)

Gomari, KAR, Hamouda, AA, Denoyel, R “Influence of sulfate ions on the interaction between fatty acids and calcite surface” Colloids and Surfaces A: Physicochem. Eng. Aspects, Vol. 287. (2006)

Guan, H., Brougham, D., Sorbie, K.S., Packer, K.J. “Wettability effects in a sandstone reservoir and outcrop cores from NMR relaxation time distributions” J. Pet. Sci. Eng. Vol. 34, pp. 35–54. (2002)

Gulamali M.Y., Leinov E., and Jackson M. D. “Self-potential anomalies induced by water injection into hydrocarbon reservoirs” Geophysics, Vol. 76, pp. 283–292. (2011)

Hall, A.C., Collins, S.H., and Melrose, J.C.: “Stability of Aqueous Wetting Film in Athabasca Tar Sands” SPEJ. Vol. 23, pp. 249-258. (1983)

Hamon, G., “Field-wide variations in wettability” SPE ATCE, Dallas, Tx. (2000)

Hamouda, AA and Gomari, KAR. “Influence of Temperature on Wettability Alteration of Carbonate Reservoirs” SPE 99848. (2006)

Healy, TW and White, LR. “Ionizable Surface Group Models of Aqueous Interfaces” Adv. In Colloid and Interface Science. Vol. 9, pp. 303-345. (1978)

Heberling, F, Trainor, TP, Lutzenkirchen, J, Eng, P, Denecke, MA, Bosbach, D "Structure and reactivity of the calcite-water interface" Journal of Colloid and Interface Science. Vol. 354, pp. 843–857. (2011)

Hirasaki, G. J., "Shape of Meniscus/Film Transition Region," In: Interfacial Phenomena in Oil Recovery. Edited by Morrow, N.R. Marcel Decker, New York. (1991b)

Hirasaki, G. J., and Zhang, D. L. "Surface chemistry of oil recovery from fractured, oil-wet, carbonate formation" SPE 80988. (2003)

Hirasaki, G.J. "Wettability: Fundamentals and Surface Forces" SPEFE, Tran. AIME, June (217) 291. (1991a)

Hoeiland, S, Barth, T, Blokhus, AM and Skauge, A. "The effect of crude oil acid fraction on wettability as studied by interfacial tension and contact angles" J. Petroleum Science and Engineering, Vol. 30: pp. 91-103. (2001)

Huang, YC, Fowkes, FM, Lloyd, TB, Sanders, ND "Adsorption of calcium ions from calcium chloride solutions onto calcium carbonate particles" Langmuir, Vol. 7, pp. 1742-1748. (1991)

Hunter, R. J. "Introduction to Modern Colloid Science" Oxford University Press, UK. (1993)

Hunter, R. J. "Recent developments in the electroacoustic characterisation of colloidal suspensions and emulsions" Colloids and Surfaces A: Physicochem. Eng. Aspects. Vol. 141, pp. 37-66. (1998)

Hunter, R. J. "Zeta Potential in Colloid Science" Academic Press, New York. (1981)

Israelachvili, J.N. "Intermolecular and Surface Forces" Academic Press. (2011)

Jaafar, M. Z., Vinogradov, J. and Jackson M. D. "Measurement of streaming potential coupling coefficient in sandstones saturated with high salinity NaCl brine" Geophys. Res. Lett., Vol. 36, L21306. (2009)

Jackson, M.D., Valvatne, P.H. and Blunt, M.J. "Prediction of wettability variation within an oil-water transition zone and its impact on production", SPEJ. Vol. 10, pp. 184–195. (2005)

Jackson, M.D. “Self-potential: Tools and techniques” in: Treatise on Geophysics (editor in chief: G. Schubert), 2nd edition, volume 11, chapter 9, Elsevier. (2015)

Jackson, M.D. and Vinogradov, J. “Impact of wettability on laboratory measurements of streaming potential in carbonates” Colloids and Surfaces A: Physiochem. Eng. Aspects. Vol. 393, pp. 86-95. (2012)

Jackson, M.D., Butler, A.P., Vinogradov, J. “Measurements of spontaneous potential in chalk with application to aquifer characterization in the southern UK” Quarterly Journal of Engineering Geology and Hydrogeology, vol. 45, pp. 457 –471. (2012b)

Jackson, M.D., Gulamali M.Y., Leinov E., Saunders, J. H., Vinogradov, J. “Spontaneous Potentials in Hydrocarbon Reservoir during Waterflooding: Application to Water-Front Monitoring” Society of Petroleum Engineers Journal. Vol. 17, pp. 53-69. (2012)

Jackson, MD, Gulamali, MY, Leinov, E, Saunders, JH, Vinogradov, J “Real-Time Measurements of Spontaneous Potential for Inflow Monitoring of Intelligent Wells” SPE 135146. (2010)

Jadhunandan, P. and Morrow, N. R. “Spontaneous imbibition of water by crude oil/brine/rock systems” In Situ, Vol. 15, pp. 319–345. (1991)

Jadhunandan, P.P. and Morrow, N.R.: „„Effect of Wettability on Waterflood Recovery for Crude Oil/Brine/Rock Systems,““SPEFE February (1995)

Jouniaux, L., and J. P. Pozzi “Streaming potential and permeability of saturated sandstones under triaxial stress: consequences for electro-telluric anomalies prior to earthquakes” J. Geophys. Res., Vol.100 (B6), pp. 10,197–10,209. (1995)

Kasha, A, Al-Hashim, H, Abdallah, W, Taherian, R, Saurerer, B “Effect of Ca, Mg and SO4 ions on the zeta potential of calcite and dolomite particles aged with stearic acid” Colloids and Surfaces A: Physicochem. Eng. Aspects, Vol. 482, pp. 290-299. (2015)

Kennedy, HT, Burja, EO, Boykin, RS. “An Investigation of the Effects of Wettability on the Recovery of Oil by Water Flooding” J. Phys. Chem., vol. 59, 867. (1955)

Kovscek, A.R., Wong, H and Radke, CJ "A Pore-Level Scenario for the Development of Mixed Wettability in Oil Reservoirs" AIChE Journal. Vol. 39, pp. 1072-1085. (1993)

Krauskopf, Konrad B. “Introduction to Geochemistry” 2nd Edition. McGraw-Hill International, New York. (1982)

Ligthelm, D.J.,Gronsveld, J., Hofman, J.P. ”Novel waterflooding strategy by manipulation of injection brine composition” EUROPEC/EAGE Conference and Exhibition, Amsterdam. SPE119835 (2009)

Liu, Y and Buckley, JS “Evolution of Wetting Alteration by Adsorption from Crude Oil” SPEFE, March 5, pp. 5-11. (1997)

Looyestijn, W.J. “Wettability Index Determination from NMR Logs” SPWLA 48th Annual Symposium, Austin, TX, published in Petrophysics, Vol. 49, pp. 130-145. (2008)

Lowe AC, Philips, MC and Riddiford, AC “On the Wetting of Carbonate Surfaces by Oil and Water” J. Can. Pet. Tech. Vol. 2, pp. 33-40. (1973)

Lucia, F. J. “Carbonate reservoir characterization” Springer, Berlin. (1999)

Ma, SM, Morrow, NR, Zhang, X, and Zhou, X. “Characterization of Wettability from Spontaneous Imbibition Measurements” Special Edition. J. Can. Pet. Tech. Vol. 38, No. 13, pp. 94-47. (1999)

Madsen, L “Surface Charge of Calcite” Encyclopedia of Surface and Colloid Science, Marcel Dekker Inc., New York, Vol. 4, pp. 3978-3992. (2002)

Mahani, H, Keya, AL, Berg, S, Bartels, WB, Nasralla, R, and Rossen, WR “Insights into the Mechanism of Wettability Alteration by Low-Salinity Flooding (LSF) in Carbonates” Energy Fuels, Vol. 29, pp. 1352–1367. (2015)

Mannhardt, K, Schramm, LL and Novosad, JJ. “Effect of Rock Type and Brine Composition on Adsorption of Two Foam-Forming Surfactants” SPE Advanced Technology Series, Vol. 1, pp. 212-218 (1993)

Mao, Y and Siders, PD. “Molecular Hartree–Fock model of calcium carbonate” Journal of Molecular Structure. Vol. 419, pp.173–184. (1997)

Marinova, KG, Alargova, RG, Denkov, ND, Velev, OD, Petsev, DN, Ivanov, IB and Borwankar, RP. “Charging of Oil-Water Interfaces Due to Spontaneous Adsorption of Hydroxyl Ions” Langmuir, Vol. 12, No. 8. (1996)

McGuire, P.L., Chatham, Jr. “Low Salinity Oil recovery: An Exciting New Opportunity for Alaska's North Slope” SPE 93903. (2005)

Meece, DE, Benninger, LK “The coprecipitation of Pu and other radionuclides with CaCO3” Geochim. Cosmochim. Acta, Vol 57, pp. 1447-1458. (1993)

Melrose, J. C., “Interpretation of Mixed Wettability States in Reservoir Rocks,” SPE 10971, SPE Tech. Conference, New Orleans. (1982)

Mishra, SK “The electrokinetics of apatite and calcite in inorganic electrolyte environment” International Journal of Mineral Processing, Vol. 5, pp. 69-83. (1978)

Moore, C. H. “Carbonate reservoirs porosity evolution and diagenesis in a sequence stratigraphic framework” Elsevier, Amsterdam. (2001)

Morrow, N “The Effects of Surface Roughness on Contact Angle with Special Reference to Petroleum Recovery” J. Can. Pet. Tech. pp. 42-53. (1975)

Morrow, N.R., Buckley, J.S. “Improved Oil Recovery by Low-Salinity Water-flooding” JPT, Distinguished Author Series, pp.106–112. (2011)

Morrow, NR, Ma, S, Zhou, X and Zhang, X. “Characterization of Wettability from Spontaneous Imbibition Measurements” J. Can. Pet. Tech. Vol. 38, pp. 94-47. (1994)

Morse, JW and Mackenzie, FT “Geochemistry of sedimentary carbonates” Elsevier, Amsterdam. (1990)

Morse, JW. “The Surface Chemistry of Calcium Carbonate Minerals in Natural Waters: An Overview” Marine Chemistry, 20, pp. 91-112. (1986)

Moulin, P and Roques, H. “Zeta potential measurement of calcium carbonate” Journal of Colloid and Interface Science 261, pp. 115–126. (2003)

Nasralla RA, Nasr-El-Din HA. “Double-layer expansion: is it a primary mechanism of improved oil recovery by low-salinity waterflooding?” SPE Res. Eva. Eng. Vol. 17, pp. 49–59. (2014)

Okasha, TM, Funk, JJ and Al-Rashidi, HN. “Fifty Years of Wettability Measurements in the Arab-D Carbonate Reservoir” SPE 105114 (2007)

Owens, WW and Archer, D.L. “The Effect of Rock Wettability on Oil-Water Relative Permeability Relationships” JPT (July) 873-78; Trans., AJME, 251. (1971)

Parker, A.R. and Rudd, J.M. “Understanding and Modelling Water-Free Production in Transition Zones: A Case Study” SPE 59412. (2000)

Pierre, A, Lamarche, JM, Mercier,RFoissy, A and Persello, J. “Calcium As Potential Determining Ion in Aqueous Calcite Suspensions” J. of Dispersion Science and Technology, Vol.11: pp. 611-635. (1990)

Plummer, L. N. and Busenberg, G. E. “ The solubilities of calcite, aragonite and vaterite in CO2 H2O solutions between 0 and 90 C and an evaluation of the aqueous model for the system CaCO3-CO2–H2O.” Geochim. Cosmochim. Acta. Vol. 46, pp. 1011–1040. (1982)

Pokrovsky, O.S., Golubev, S.V., Schott, J.“Dissolution kinetics of calcite, dolomite and magnesite at 25 C and 0 to 50 atm pCO2.” Chemical Geology. Vol 217, pp. 239–255. (2005)

Puntervold, T., Strand, S. and Austad, T. “Water flooding of carbonate reservoirs: Effects of a model base and natural crude oil bases on chalk wettability” Energy and Fuels, Vol. 21, pp. 1606-1616. (2007)

Reeder, RJ Nugent, M Tait, CD Morris, DE Heald, SM Beck, KM Hess, WP and Lanzirotti, A “Coprecipitation of Uranium(VI) with Calcite: XAFS, micro-XAS, and luminescence characterization” Geochim. Cosmochim. Acta. Vol. 65, pp. 3491–350. (2001)

Revil, A., and P. W. J. Glover, “Theory of ionic surface electrical conduction in porous media” Phys. Rev. B , Vol. 55, pp. 1757-1773. (1997)

Revil, A., and P. W. J. Glover, “Nature of surface electrical conductivity in natural sands, sandstones, and clays” Geophys Res. Lett., Vol. 25, pp. 691-694. (1998)

Revil, A., P. A. Pezard, and P. W. J. Glover, “Streaming potential in porous media, 1, Theory of the zeta potential” J . Geophys Res., Vol. 104, pp. 20021-20031. (1999)

Riley, Jason “Charge in Colloidal Systems” in: Colloid Science Principles, Methods and Applications. Edited by: Cosgrove, Terrance Department of Chemistry University of Bristol, UK. Blackwell Publishing. (2005)

Riley, Nick. “Geological storage of carbon dioxide.” In: Hester, R.E.; Harrison, R.M., (eds.) Carbon capture: sequestration and storage. Cambridge, UK, Royal Society of Chemistry, 155-178. (2010) (Issues in environmental science and technology, 29).

Robins, N.S., Jones, H.K., Ellis, J. “An aquifer management case study: the Chalk of the English South Downs” Water Resources Management, Vol. 13, pp. 205-218. (1999)

Roehl, P.O., Choquette, P.W. “Carbonate Petroleum Reservoirs” Spring-Verlag, New York. (1985)

Romanuka, J., Hofman, J.P., Ligthelm, D.J., Suijkerbuijk, B.M.J.M. Marcelis, A.H.M., Oedai, S., Brussee, N.J., van der Linde, H.A., Aksulu, H., Austad, T “Low Salinity EOR in Carbonates" SPE Improved Oil Recovery Symposium, 14-18 April 2012, Tulsa, Oklahoma, USA. (2012)

Rosenbauer JR, Koksalan T, Palandri JL. “Experimental investigation of CO2–brine–rock interactions at elevated temperature and pressure: Implications for CO2 sequestration in deep-saline aquifers.” Fuel Process Tech. Vol. 86, pp.1581–97. (2005)

Salathiel, R.A.: „„Oil Recovery by Surface Film Drainage in Mixed-Wettability Rocks,““ JPT October 1216; Trans., AIME, 255. (1973)

Saunders, J. H., M. D. Jackson, and C. C. Pain “Fluid flow monitoring in oil fields using downhole measurements of electrokinetic potential” Geophysics, 73(5). (2008)

Schembre, J.M., Akin, S., Castanier, L.M., Kovscek, A.R. “Spontaneous water imbibition into diatomite” In: SPE Western Regional Meeting. (1998)

Schramm, L.L. “Surfactants: Fundamentals and Applications in the Petroleum Industry” Cambridge University Press: Cambridge, UK. (2000)

Sjostrom, L. “the stability of charged colloids” in: Interfacial Forces and Fields: Theory and Applications (edited by: Jyh-Ping Hsu), Surfactant Science Series Vol. 85, chapter 11, Marcel Dekker, Inc. (1999)

Somasundaran, P and Agar, GE. “The Zero Point of Charge of Calcite” J. Colloid Interface Science Vol. 24: pp. 433-440. (1967)

Sondi, I., Biscan, J., Vdovic, N., Skapin, S. D. “The electrokinetic properties of carbonates in aqueous media revisited” Colloids and Surfaces A: Physicochem. Eng. Aspects, Vol. 342, pp. 84-91. (2009)

Speight, J.G. “The chemistry and technology of petroleum” 3rd Edition. Marcel Dekker, New York. (1999)

Standnes, D.C. and Austad, T. “Wettability alteration in chalk. 1. Preparation of core material and oil properties” Journal of Petroleum Science and Engineering, Vol. 28, pp. 111-121. (2000)

Stipp, SLS, Eggleston, CM and Nielsen, BS. “Calcite surface structure observed at micro-topographic and molecular scales with atomic force microscopy (AFM)” Geochim. et Cosmochim. Acta, Vol. 58, pp. 3023-3033. (1994)

Strand, S, Høgnesen, EJ, Austad, T. “Wettability alteration of carbonates-Effects of potential determining ions (Ca and SO4) and temperature” Colloids and Surfaces A: Physicochem. Eng. Aspects Vol. 275, pp. 1–10. (2006)

Stumm, W. and Morgan, J. “Aquatic Chemistry, Chemical Equilibria and Rates in Natural Waters” 3rd edition, John Wiley & Sons, New York, pp. 1022. (1996)

Suicmez, S.V., Piri, M. and Blunt, M.J. “Surprising Trends on Trapped Hydrocarbon Saturation with Wettability” SCA2007-51. (2007)

Tabrizy, VA, Denoyel, R, and Hamouda AA. “Characterization of Wettability Alteration of calcite, quartz and kaolinite: Surface energy analysis” Colloids and Surfaces A. Vol. 384, pp. 98-108. (2011)

Takamura, K and Chow, RS. “The Electric Properties of the Bitumen/Water Interface. Part II. Application of TheIonizable Surface-Group Model” Colloids and Surfaces, 15: pp. 35-48. (1985)

Tang, G. Q., Morrow, N.R. “Salinity, temperature, oil composition and oil Recovery by waterflooding” SPERE November, pp. 269–276. (1997)

Tang, G.Q., Morrow, N. R. “Influence of brine composition and fines migration on crude oil brine rock interactions and oil recovery” Journal of Petroleum Science & Engineering, Vol. 24, pp. 99–111. (1999)

Taylor, A. J., Wood, F. W. “The electrophoresis of hydrocarbon droplets in dilute solutions of electrolytes” Trans. Faraday Soc. Vol. 53, pp. 523-529. (1957)

Thompson, DW and Pownall, PG. “Surface Electrical Properties of Calcite” J. of Colloid and Interface Science, Vol. 131, No. I, pp. 74-82. (1989)

Tiab, D., Donaldson E.C. “Petrophysics: Theory and practice of measuring reservoir rock and fluid transport properties.” 2nd Edition. Gulf Publishing Company. (2004)

Tokunaga, TK. “DLVO-based estimates of adsorbed water film thicknesses in geologic CO2 reservoirs” Langmuir, Vol. 28, pp. 8001–8009. (2012)

Vdovic, N, Biscan, J. “Electrokinetics of natural and synthetic calcite suspensions” Colloids and Surfaces A: Physicochem. Eng. Aspects, A. Vol. 137, pp. 7–14. (1998)

Vdovic, N. “Electrokinetic behaviour of calcite - the relationship with other calcite properties” Chemical Geology, 177, 241–248 (2001)

Vernhet, A, Bellon-Fontaine, MN, Doren, A “Comparison of Three Electrokinetic Methods to Determine the Zeta Potential of Solid Surfaces” J. Chim. Phys. Vol. 91, pp. 1728-1747. (1994)

Vinogradov, J and Jackson, MD “Multiphase streaming potential in sandstones saturated with gas/brine and oil/brine during drainage and imbibition” Geophys. Res. Lett. 38 (2011)

Vinogradov, J, Jaafar, MZ, Jackson, MD “Measurement of streaming potential coupling coefficient in sandstones saturated with natural and artificial brines at high salinity” J. Geophysical Research, Vol. 115, B12204. (2010)

Vinogradov, J. and Jackson, M.D. “The effect of brine composition, concentration, temperature and rock texture on zeta potential and streaming potential coupling coefficient measured in sandstones and sandpack” presented at the Annual Meeting of the American Geophysical Society. (2014)

Walker E., Glover P.W.J., Ruel J. “A transient method for measuring the DC streaming potential coefficient of porous and fractured rocks” J. Geophys. Res.: Solid Earth, Vol. 119, pp. 957-970. (2014)

Webb, K.J., Black, C.J.J., Al-Jeel, H. “Low Salinity Oil Recovery –Log-Inject-Log” SPE 89379. (2004)

Wu, Y, Shuler, PJ, Blanco, M, Tang, Y and Goddard, WA. “An experimental study of Wetting Behavior and Surfactant EOR in Carbonates with Model Compounds” SPEJ, Vol. 13, pp. 26-34. (2008)

Yildiz, H. O. and Morrow, N. R., “Effect of brine composition on recovery waterflooding of Moutray crude oil by waterflooding” Petroleum Science & Engineering, vol., 14, pp. 159–168. (1996)

Yousef AA, Al-Saleh S, Al-Kaabi A, Al-Jawfi MS. “Laboratory investigation of the impact of injection-water salinity and ionic content on oil recovery from carbonate reservoirs” presented

at the Canadian Unconventional Resources and International Petroleum Conference, Calgary, Canada, 19-21 October. (2010)

Yousef AA, Al-Saleh S, Al-Kaabi A, Al-Jawfi MS. “Laboratory investigation of the impact of injection-water salinity and ionic content on oil recovery from carbonate reservoirs” SPE Reserv Eval Eng. Vol. 14, pp. 578–93. (2011)

Yousef, A A, Al-Saleh, S and Al-Jawfi, M. “Improved/Enhanced Oil Recovery from Carbonate Reservoirs by Tuning Injection Water Salinity and Ionic Content” SPE 154076 (2012)

Yousef, A A, Al-Saleh, S and Al-Jawfi, M. “Smart WaterFlooding for Carbonate Reservoirs: Salinity and Role of Ions” SPE 141082 (2011)

Yuan, Y and Lee, T. R. “Contact Angles and Wetting Properties" In Surface Analytical Techniques; Editors: G. Bracco and B. Holst; Springer Series in Surface Sciences 51. (2013)

Zhang, P and Austad, T “Wettability and oil recovery from carbonates: Effects of temperature and potential determining ions.” Colloids and Surfaces A: Physicochem. Eng. Aspects, Vol. 279. (2006)

Zhang, P., Tweheyo, M.T. and Austad, T. “Wettability alteration and improved oil recovery by spontaneous imbibition of seawater into chalk: Impact of the potential determining ions: Ca2+, Mg2+ and SO4” Colloids and Surfaces A: Physicochem. Eng. Aspects, Vol. 301, pp. 199-208. (2007)

Zhou, X, Morrow, NR, and Ma, S. “Interrelationship of Wettability, Initial Water Saturation, Aging Time, and Oil Recovery by Spontaneous Imbibition and Waterflooding” SPE 62507 (2000)

Zhou, X, Torsaeter, O, Xie, X and Morrow, NR. “The Effect of Crude-Oil Aging Time and Temperature on the Rate of Water Imbibition and Long-Term Recovery by Imbibition” SPE 26674. (1995)

Appendix A: Brine-saturated Rock Sample Conductivity Measurement

The saturated rock conductivity is measured at the end of every experiment in order to correct for the surface conductivity and to calculate the formation factor. This was done using a QuadTech7600 Precision LCR meter which supplies AC current to the rock sample over a frequency range of 10 Hz to 2 MHz. The frequency (f), the total impedance (Z), and the resistance in series (R_s) were the measured parameters. The resulting reactance (X) is calculated as:

$$X = \sqrt{(Z^2 - {R_s}^2)} \tag{A.1}$$

Figure A.1 shows these parameters: the calculated reactance (X), the resistance (R_s) and the total impedance (Z) as a function of the frequency whereas Figure A.2 shows the reactance (X) as a function of the resistance (R_s) where the minimum value of X corresponds to the resistance of the rock sample to DC current.

The resistivity of the brine-saturated rock sample (R_o) is calculated by:

$$R_o = R_s \frac{A}{L} \tag{A.2}$$

where A is the cross-sectional area and L is the sample‟s length. The conductivity of the sample (σ_{rw}) is the reciprocal of R_o.

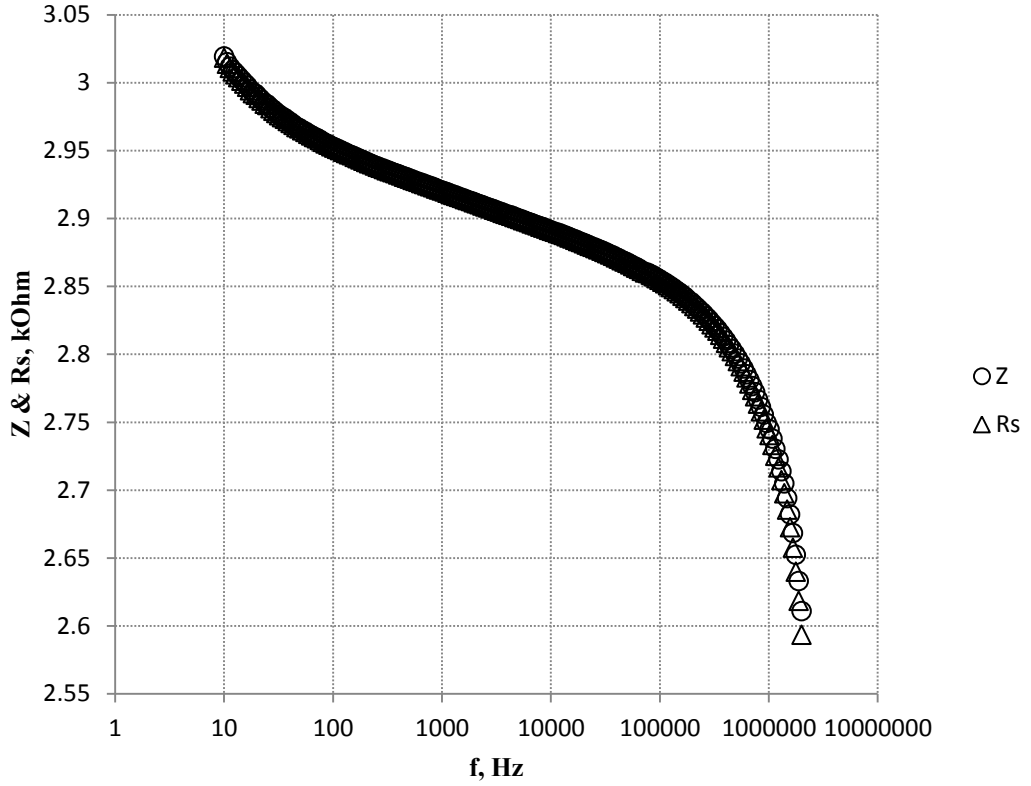

Figure A.1. The measured impedance and electrical resistance of 0.05 M NaCl saturated sample of the Portland limestone as a function of the frequency range 10 Hz-2 MHz.

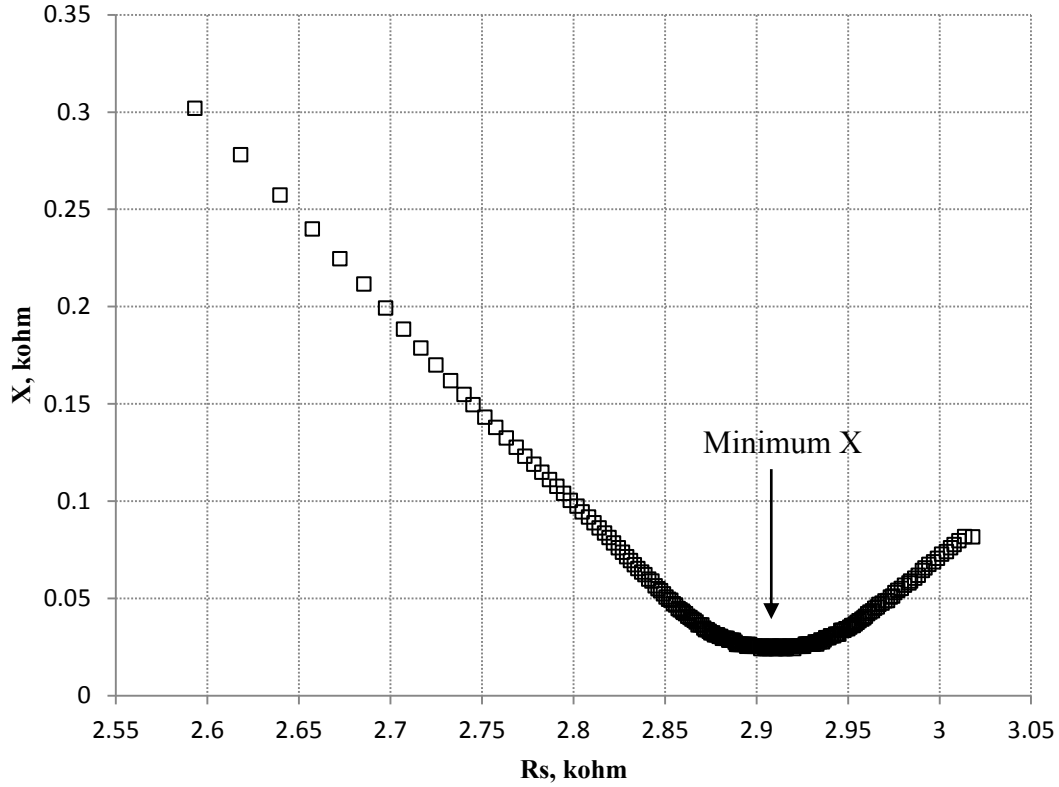

Figure A.2. The calculated reactance (X) as a function of the meausred electrical resistance of 0.05 M NaCl saturated sample of the Portland limestone. The minimum reactance corresponds to 2.9 kohm.

Appendix B: Formation Factor Measurement

Knowledge of the formation factor (F) is important in order to correct the zeta potential interpreted from SPM measurements for the surface conductivity as seen in Eq. 4.4. It is defined as (Archie, 1942):

$$F = \frac{R_o}{R_w} = \frac{\sigma_f}{\sigma_{rw}} \tag{B.1}$$

where R_w is the resistivity of the brine, which is the reciprocal of the brine‟s conductivity s_f. Figure B.1 shows the plot of both conductivities and the reciprocal of the slope of the linear relationship defines the formation factor.

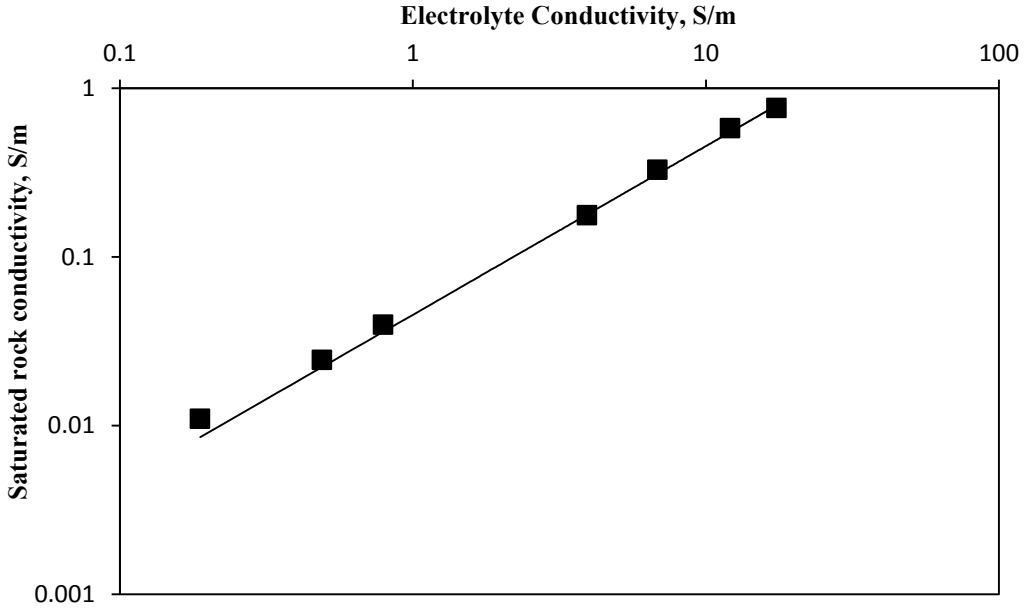

Figure B.1. Saturated rock conductivity against the electrolyte conductivity. The relationship is linear through most of the salinity range except the 0.01 M NaCl (0.18 S/m) point.

The streaming potential measurements were conducted for salinities in the range (0.01 M-3.5 M NaCl) and are plotted in Figure B.2. We noticed that the higher the salinity, the lower the zeta potential is, which reflects a thinning EDL.

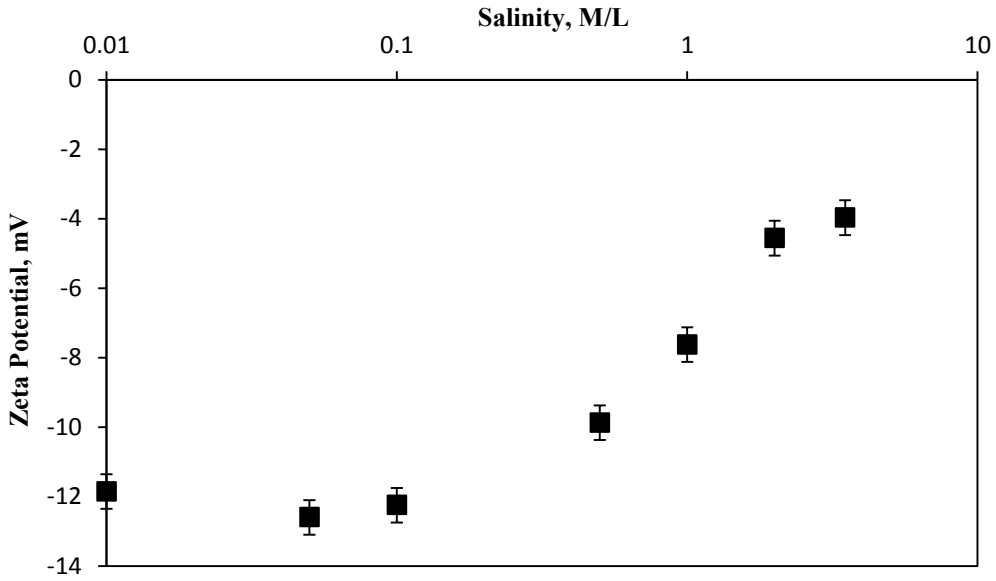

Figure B.2. A plot of the zeta potential as a function of salinity for the Portland limestone.

Appendix C: Brine Chemical Analysis (ICP-AES)

Inductively Coupled Plasma-Atomic Emission Spectrometry (ICP-AES) is one of the common techniques for elemental analysis. It was used to analyze the samples in this study in order to quality check the ion content of the prepared NaCl-EQ, FMB, seawater and the seawater modified compositions. In addition, it was used to monitor any dissolution and adsorption/desorption during the core flooding experiments.

The samples were prepared by acidizing each sample with 2% HNO_3. A quality check was conducted on the machine using 6 standard solutions that were prepared with the specific ions that were expected to be in the samples in the concentration range 0.5-200 ppm. Then, the measurements were conducted and the data was collected based on the different light intensity counts gathered at any wavelength. An example for Na is shown in Figure C.1, where Na has a characteristic wavelength that peaks at 589.59nm. The peak of a standard solution of a known concentration (50 ppm) is highlighted in brown. The software was instructed to use the light intensity value corresponding to that peak in the linear regression in Figure C.2. This was done for all 6 standard solutions (blue squares) in order to establish a correlation between gathered light intensities and concentration.

Also shown in Figure C.1 are the curves of different samples with elevated Na concentrations, where each sample will have the peak occurring at the same wavelength but at a different light intensity depending on the concentration present. The same process was conducted for the other elements of interest (Ca, Mg, and S).

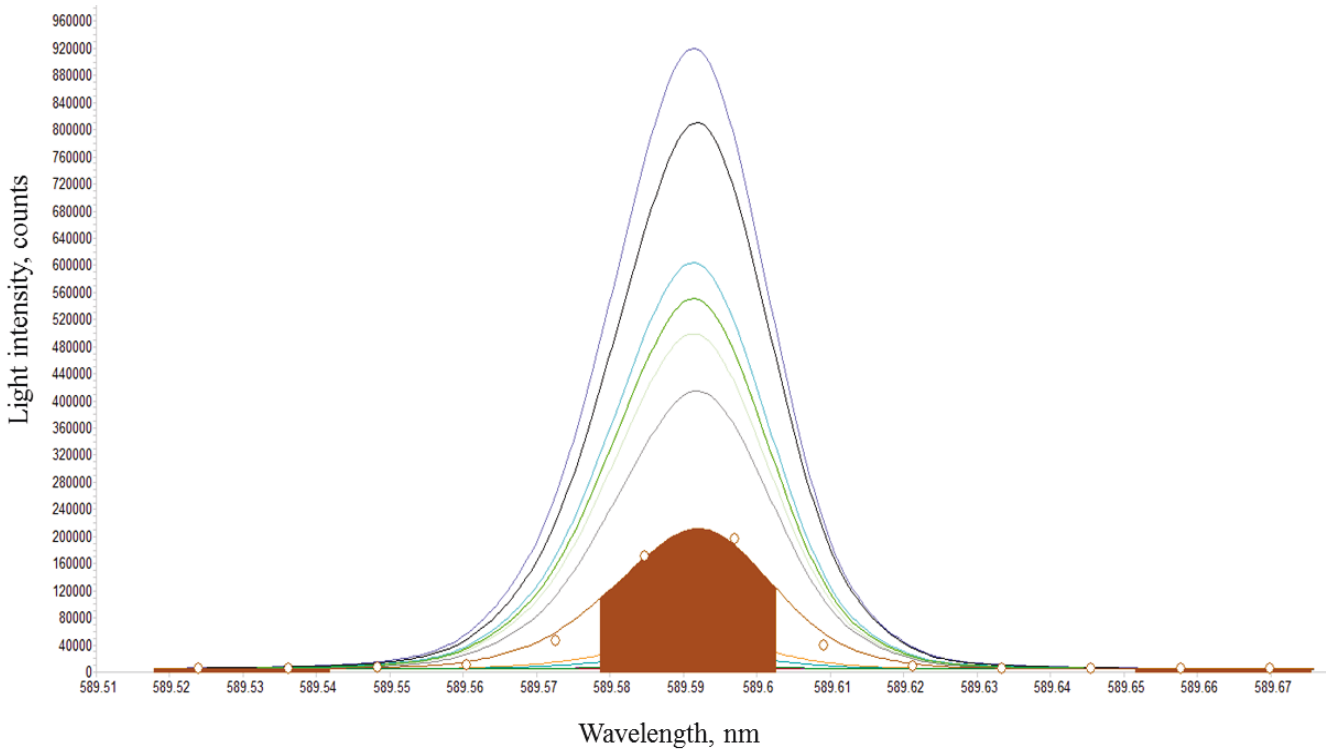

Figure C.1. An example result from ICP-AES measurements, where different samples will show different light intensities based on the element concentration present (sodium in this case).

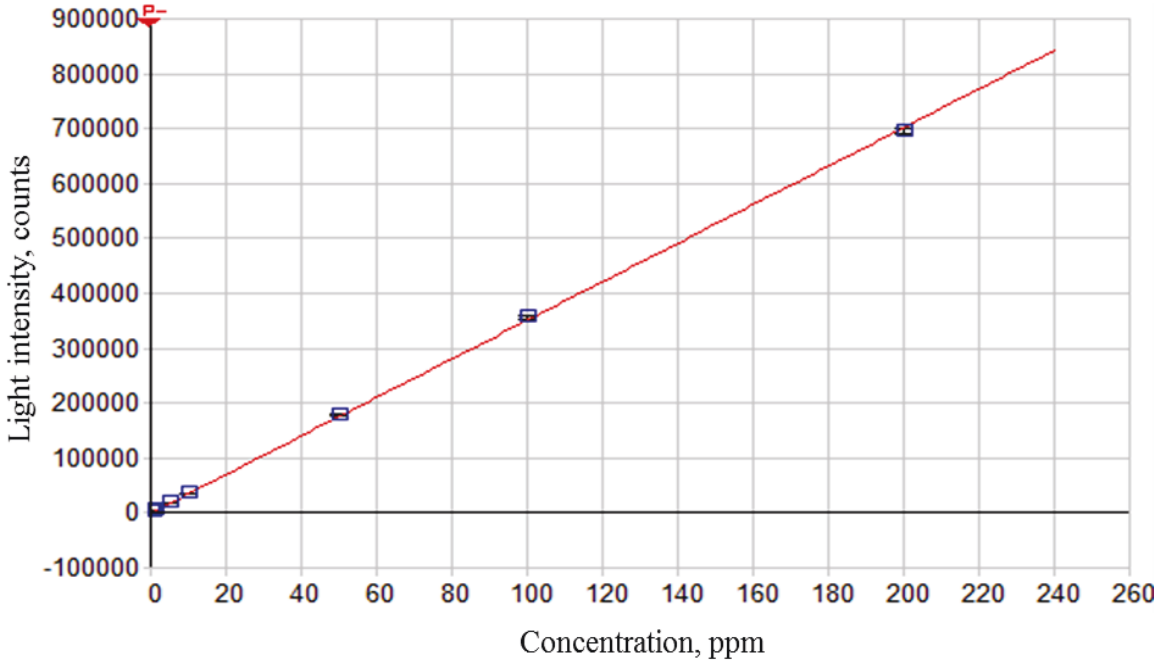

Figure C.2. A linear regression obtained from 6 standard solutions in order to relate the light intensity to the element concentration.

Appendix D: Determination of Fluid Saturation

The initial saturation of water (S_{wi}) and the remaining saturation of oil (S_r) were determined by both mass and volume methods. Knowing the pore volume (PV) of the rock sample and the produced volumes of water and oil allows for saturation measurement:

$$S_{wi} = 1 - S_{oi} = \frac{V_{wi}}{PV} \tag{D.1}$$

where S_{oi} is the initial saturation of oil, V_{wi} is the volume of water displaced by oil during the primary drainage process. This saturation can also be determined using the mass method:

$$S_{wi} = \frac{m_{dy} - m_{dg}}{PV * \Delta\rho} \tag{D.2}$$

where m_{dy} is the mass of the dry sample, m_{dg} is the mass of the sample after primary drainage, and Dr is the difference between the oil and water densities. The remaining oil saturation (S_r) is determined volumetrically by:

$$S_r = \frac{V_{wi} - V_{owf}}{PV} \tag{D.3}$$

where V_{wi} is the volume of water displaced by oil during the primary drainage and V_{owf} is the volume of oil displaced by water during water flooding. The remaining oil saturation (S_r) can also be determined using the mass method by:

$$S_r = \frac{m_{dy} - m_{owf}}{PV * \Delta\rho} \tag{D.4}$$

where m_{dy} is the mass of the dry sample and m_{owf} is the mass of the sample after the completion of the water flooding process.

Appendix E: Compilation of Streaming Potential Results

Table E.1. Portland sample #1 (P1) acquired results

Salinity, M	C_{EK}, mV/psi	C_{EK}, V/Pa	σ_f, S/m	σ_b, S/m	FF	C, M/L	μ, Pa-s	ε, F/m	ζ, mV	ζ_c, mV
0.05 Na	0.1295	1.87823E-08	0.024385	0.4318	17.70783	0.039296322	0.000949	7.03493E-10	-10.9459	-12.7337
0.001 Ca	0.1149	1.66647E-08	0.024378	0.4655	19.09545	0.042332051	0.00095	7.03147E-10	-10.4784	-11.304
0.5SW Ca	0.076	1.10228E-08	0.028671	0.53265	18.57816	0.04846353	0.00095	7.02446E-10	-7.9438	-8.80831
DI	0.984	1.42716E-07	0.002599	0.0314	12.08317	0.002569387	0.000946	7.07704E-10	-5.9881	-10.2088
SW Ca	0.0405	5.87399E-09	0.030197	0.652	21.59124	0.059592662	0.000952	7.01177E-10	-5.19724	-4.95864
2SW Ca (0.02M Ca)	0.0191	2.7702E-09	0.039727	0.85515	21.52562	0.079074311	0.000953	6.98961E-10	-3.23152	-3.09256
4SW Ca	0.0082	1.1893E-09	0.061169	1.231	20.12471	0.127710754	0.000958	6.9346E-10	-2.02296	-2.07073
nacl_after_Ca	0.1184	1.71724E-08	0.024385	0.4315	17.69553	0.039269433	0.000949	7.03497E-10	-10.0007	-11.6421
0.007M Mg	0.0754	1.09358E-08	0.024385	0.5562	22.80939	0.05063754	0.000951	7.02198E-10	-8.23434	-7.43674
0.02M Mg	0.0482	6.99078E-09	0.024385	0.66275	27.17894	0.060607819	0.000952	7.01062E-10	-6.28906	-4.76673
0.04M Mg	0.0277	4.01752E-09	0.056382	0.968	17.2415	0.090131508	0.000955	6.97707E-10	-5.32063	-6.27158
0.14M Mg	0.0082	1.1893E-09	0.107047	2.1915	20.47231	0.240485925	0.000969	6.80873E-10	-3.70806	-3.73119
nacl_after_Mg	0.1017	1.47502E-08	0.02365	0.456	19.28132	0.041473303	0.00095	7.03245E-10	-9.08323	-9.70445
.1SW SO4	0.1151	1.66937E-08	0.023689	0.45575	19.23855	0.041450736	0.00095	7.03247E-10	-10.2743	-11.0014
.5sw SO4	0.1014	1.47067E-08	0.03039	0.5845	19.2331	0.053264967	0.000951	7.01899E-10	-11.6454	-12.4731
.02M SO4	0.0982	1.42426E-08	0.034657	0.6685	19.28903	0.061151605	0.000952	7.01E-10	-12.926	-13.8045
SW_SO4	0.0828	1.20091E-08	0.04181	0.8028	19.20095	0.073998083	0.000953	6.99538E-10	-13.1335	-14.0905
2SW_SO4	0.0593	8.60068E-09	0.057767	1.25	21.63856	0.129699667	0.000958	6.93236E-10	-14.863	-14.1496
3SW_SO4	0.0447	6.48315E-09	0.079	1.582	20.02532	0.166310806	0.000962	6.89125E-10	-14.3155	-14.7263
0.05M NaCl	0.0412	5.97552E-09	0.069029	1.38	19.99151	0.143633979	0.00096	6.91669E-10	-11.442	-11.7903
.05_pre_SW	0.125	1.81296E-08	0.024	0.459	19.125	0.04174424	0.00095	7.03214E-10	-11.2385	-12.1053
.1SW_3pdi	0.07	1.01526E-08	0.031848	0.62	19.46743	0.056582597	0.000951	7.0152E-10	-8.53512	-9.03167
.5SW_3pdi	0.028	4.06103E-09	0.058714	1.17	19.92717	0.121412163	0.000958	6.9417E-10	-6.5545	-6.77581
SW_3pdi_.1Na	0.0149	2.16105E-09	0.088466	1.8035	20.38643	0.192398466	0.000964	6.86212E-10	-5.47682	-5.5342
SW_3pdi	0.009	1.30533E-09	0.135	2.96	21.92593	0.341217416	0.000978	6.6983E-10	-5.63922	-5.2982
.5M_Na_pre_SO4	0.0114	1.65342E-09	0.186	3.74	20.10753	0.446284641	0.000987	6.58509E-10	-9.26597	-9.49291
2M	0.0015	2.17555E-10	0.595	11.9	20	1.69090636	0.001112	5.39123E-10	-5.34126	-5.5015
.24M Ca_.5M_Na	0.0002	2.90074E-11	0.268	6.2	23.13433	0.774492743	0.001015	6.24425E-10	-0.29244	-0.2604
.28M Ca_.5M_Na	-0.0001	-1.4504E-11	0.317	6.4	20.18927	0.801233472	0.001018	6.21732E-10	0.151948	0.15504
.36M Ca_.5M_Na	-0.0004	-5.8015E-11	0.3619	7.536	20.82343	0.95681554	0.001032	6.06314E-10	0.744289	0.736303
.42M Ca_.5M_Na	-0.0005	-7.2518E-11	0.37	8.11	21.91892	1.039200819	0.00104	5.9832E-10	1.022432	0.960909
.24M_Mg	0.0005	7.25184E-11	0.17	3.39	19.94118	0.399040684	0.000983	6.63574E-10	-0.36405	-0.37607
.32M Mg	-0.0005	-7.2518E-11	0.2066	4.155	20.11133	0.502200974	0.000992	6.52565E-10	0.457831	0.468956
.42M Mg	-0.0009	-1.3053E-10	0.255	5.09	19.96078	0.627115929	0.001002	6.39491E-10	1.041389	1.074738
2m	0.0016	2.32059E-10	0.59	12.2	20.67797	1.751024617	0.00112	5.34015E-10	-5.93648	-5.91409
sw ca 2m	0.0012	1.74044E-10	0.59	12.7	21.52542	1.85353795	0.001133	5.25438E-10	-4.76537	-4.56049
4SW Ca	0.0008	1.16029E-10	0.58	12.91	22.25862	1.897385276	0.001138	5.2182E-10	-3.26817	-3.02464
.11M ca	0.00055	7.97703E-11	0.56	13.24	23.64286	1.967144093	0.001148	5.16127E-10	-2.34853	-2.04627

Table E.2. Portland sample #2 (P2) acquired results

Salinity, M	C_{EK}, mV/psi	C_{EK}, V/Pa	σ_{rf}, S/m	σ_b, S/m	FF	C, M/L	μ, Pa-s	ε, F/m	ζ mV	ζ_c, mV
0.05	0.1245	1.80571E-08	0.020985	0.4204	20.03349	0.038276269	0.000949	7.0361E-10	-10.2426	-10.5323
0.05_post_Ca	0.1036	1.50258E-08	0.021731	0.4435	20.40871	0.040346899	0.00095	7.03373E-10	-8.99655	-9.08087
DI	0.8993	1.30432E-07	0.002217	0.0282	12.72114	0.002303506	0.000946	7.07735E-10	-4.91458	-7.95843
0.5SW Ca	0.0688	9.97853E-09	0.025729	0.5357	20.82077	0.048744432	0.00095	7.02414E-10	-7.23295	-7.15626
SW Ca	0.0362	5.25033E-09	0.030197	0.647	21.42567	0.059121165	0.000951	7.01231E-10	-4.60923	-4.43161
nacl_pre_Ca	0.133	1.92899E-08	0.022933	0.45	19.62204	0.040932123	0.00095	7.03307E-10	-11.7208	-12.3049
1/10 sw ca	0.1086	1.5751E-08	0.023933	0.477	19.93031	0.0433746	0.00095	7.03027E-10	-10.1514	-10.4925
0.5SW Ca	0.0763	1.10663E-08	0.025711	0.5175	20.12757	0.047071208	0.00095	7.02605E-10	-7.74541	-7.92721
SW Ca	0.0426	6.17857E-09	0.031606	0.6497	20.55592	0.05937572	0.000952	7.01202E-10	-5.44713	-5.45881
2SW Ca	0.0229	3.32134E-09	0.039727	0.80225	20.19404	0.073944943	0.000953	6.99544E-10	-3.6298	-3.70277
4SW Ca	0.0092	1.33434E-09	0.056382	1.2	21.28345	0.124493056	0.000958	6.93823E-10	-2.21063	-2.13965
10SW Ca	0.0022	3.19081E-10	0.099483	2.062	20.72712	0.224150178	0.000967	6.82682E-10	-0.93215	-0.92643
15SW Ca	0.0004	5.80147E-11	0.134321	2.904	21.61983	0.333731403	0.000977	6.70644E-10	-0.24543	-0.23385
0.21M Ca	-0.0001	-1.4504E-11	0.152178	3.3075	21.73439	0.387914934	0.000982	6.64773E-10	0.07084	0.067142
20SW Ca	-0.0002	-2.9007E-11	0.171821	3.6	20.95204	0.42738598	0.000985	6.6053E-10	0.155739	0.153123
25SW Ca	-0.001	-1.4504E-10	0.197906	4.2775	21.61385	0.518657356	0.000993	6.50827E-10	0.946525	0.902126
30SW Ca	-0.0011	-1.5954E-10	0.234688	5	21.30487	0.615155563	0.001001	6.40731E-10	1.246591	1.205348
35SW Ca	-0.0012	-1.7404E-10	0.258691	5.688	21.98759	0.706433368	0.001009	6.31335E-10	1.582593	1.482719
35SW Ca+ SW Mg	-0.0012	-1.7404E-10	0.27886	6.22	22.3051	0.777161565	0.001016	6.24155E-10	1.761451	1.626798
FM	-0.0012	-1.7404E-10	0.284911	6.35	22.2877	0.794536647	0.001017	6.22405E-10	1.806104	1.66934
FM_.55M Nacl	-0.0005	-7.2518E-11	0.397	8.68	21.86398	1.124522718	0.001049	5.90164E-10	1.118488	1.053827
FM_2M Nacl	-0.0002	-2.9007E-11	0.682	15.19	22.27273	2.396275849	0.001208	4.82769E-10	1.102253	1.019472
.05 nacl_pFM	0.1231	1.7854E-08	0.023	0.46	20	0.041834603	0.00095	7.03203E-10	-11.0921	-11.4248
.1sw Mg	0.061	8.84725E-09	0.027	0.543	20.11111	0.049417558	0.00095	7.02337E-10	-6.5015	-6.65955
.02M Mg	0.0305	4.42362E-09	0.0357	0.73	20.44818	0.067000964	0.000952	7.00334E-10	-4.39091	-4.42351
.05M Mg	0.0124	1.79846E-09	0.054597	1.13	20.69695	0.117356167	0.000957	6.94628E-10	-2.80048	-2.78736
SW_Mg	0.0078	1.13129E-09	0.0656	1.39	21.18902	0.144728405	0.00096	6.91546E-10	-2.18253	-2.12185
Ca_Mg_SW	0.0067	9.71747E-10	0.064471	1.35	20.93974	0.140369501	0.000959	6.92035E-10	-1.81871	-1.7892
SW_.1Na	0.0116	1.68243E-09	0.081	1.82	22.46914	0.1943864	0.000964	6.8599E-10	-4.30505	-3.94693
SW	0.008	1.16029E-09	0.132	2.84	21.51515	0.325194656	0.000976	6.71574E-10	-4.79004	-4.5863
.55M Nacl	0.0105	1.52289E-09	0.164612	3.87	23.50981	0.463822668	0.000988	6.56638E-10	-8.8698	-7.77198
Ca_SW	0.0072	1.04427E-09	0.173797	3.91	22.49748	0.469215681	0.000989	6.56064E-10	-6.15328	-5.6343
2Ca_SW	0.006	8.70221E-10	0.179	4.072	22.7486	0.49103641	0.000991	6.53747E-10	-5.36928	-4.86216
4Ca_SW	0.0039	5.65644E-10	0.186	4.33	23.27957	0.5257018	0.000994	6.50084E-10	-3.74331	-3.31244
.08M_Ca	0.0024	3.48088E-10	0.199749	4.67	23.37933	0.571196907	0.000997	6.45309E-10	-2.51272	-2.21401
.11M_Ca	0.0017	2.46563E-10	0.211976	4.94	23.30451	0.607175918	0.001001	6.4156E-10	-1.89966	-1.6792
0.18M_ca (15sw)	0.0008	1.16029E-10	0.243229	5.76	23.68139	0.715983383	0.00101	6.3036E-10	-1.07096	-0.93161
0.21M Ca	0.0002	2.90074E-11	0.268741	6.24	23.21939	0.779831462	0.001016	6.23886E-10	-0.29472	-0.26147
0.24M Ca	0.0002	2.90074E-11	0.283895	6.49	22.86053	0.813309983	0.001019	6.2052E-10	-0.3091	-0.27854
0.28M Ca	0.001	1.45037E-10	0.317	7	22.08202	0.882431508	0.001025	6.13633E-10	-1.69619	-1.58235
.5M Na	0.012	1.74044E-09	0.167	3.73	22.33533	0.44493502	0.000987	6.58653E-10	-9.7243	-8.96877
.5M Na_.012M_SO4	0.0127	1.84197E-09	0.18	3.9	21.66667	0.467867597	0.000989	6.56208E-10	-10.8223	-10.2895
.5M Na_.024M_SO4	0.0126	1.82746E-09	0.186325	3.94	21.14581	0.473259211	0.000989	6.55634E-10	-10.8618	-10.5814
.5M_NA_SW_SO4	0.0122	1.76945E-09	0.186658	4.05	21.6974	0.488075295	0.00099	6.54061E-10	-10.8506	-10.3018
.5M_NA_2SW_SO4	0.0118	1.71143E-09	0.203549	4.3	21.12517	0.521677028	0.000993	6.50508E-10	-11.2362	-10.9569
.5M_NA_3SW_SO4	0.0112	1.62441E-09	0.2149	4.6	21.4053	0.561848125	0.000997	6.46287E-10	-11.5234	-11.0899
SW_CaMg_3SW_SO4	0.006	8.70221E-10	0.242	5.22	21.57025	0.644375562	0.001004	6.37707E-10	-7.15054	-6.82891

Table E.3. Portland sample #3 (P3) acquired results

Salinity, M	CEK, mV/psi	CEK, V/Pa	σrf, S/m	σb, S/m	FF	C, M/L	μ, Pa-s	ε, F/m	ζ mV	ζc, mV
0.01	0.2699	3.91454E-08	0.010954	0.18775	17.1396	0.018504333	0.000947	7.05874E-10	-9.8636	-11.855
0.1	0.08	1.16029E-08	0.039614	0.7914	19.97765	0.072897469	0.000953	6.99663E-10	-12.5055	-12.8951
0.55	0.0114	1.65342E-09	0.176648	3.931	22.25328	0.472046268	0.000989	6.55763E-10	-9.80193	-9.0737
1	0.0047	6.81673E-10	0.328012	6.7335	20.52819	0.846149989	0.001022	6.17237E-10	-7.59889	-7.62547
2	0.001469	2.13059E-10	0.497971	12.11	24.31866	1.732874568	0.001117	5.35551E-10	-5.38376	-4.56051
3.5	0.000677	9.81899E-11	0.676314	17.445	25.79422	2.933244214	0.001291	4.4491E-10	-4.97029	-3.96942
0.05	0.1297	1.88113E-08	0.023004	0.4238	18.42251	0.038580118	0.000949	7.03575E-10	-10.7576	-12.0291
0.05	0.1156	1.67663E-08	0.023174	0.4395	18.96545	0.039987315	0.00095	7.03415E-10	-9.94712	-10.8044
0.05	0.1321	1.91594E-08	0.023615	0.4842	20.50432	0.044028968	0.00095	7.02953E-10	-12.5367	-12.5952
0.5	0.0122	1.76945E-09	0.19	3.68	19.36842	0.4381861	0.000986	6.59374E-10	-9.73743	-10.3566
.21M_Ca_2M_Na	0.0003	4.35111E-11	0.426978	12.8	29.97811	1.874362438	0.001135	5.23716E-10	-1.20754	-0.82978
.28M_Ca_2M_Na	0.0002	2.90074E-11	0.59	13	22.0339	1.916309812	0.001141	5.20268E-10	-0.82699	-0.77317
.32M_Ca_2M_Na	0.0002	2.90074E-11	0.59	13	22.0339	1.916309812	0.001141	5.20268E-10	-0.82699	-0.77317
.37M_Ca_2M_Na	0	0	0.62	13.4	21.6129	2.00131679	0.001152	5.13367E-10	0	0
.42M_Ca_2M_Na	-0.0001	-1.4504E-11	0.64	14	21.875	2.131281352	0.00117	5.03034E-10	0.472254	0.444729
FM_2M_Na	-0.0001	-1.4504E-11	0.68	14.13	20.77941	2.159785843	0.001174	5.00802E-10	0.480382	0.476234
0.05	0.13	1.88548E-08	0.025	0.47	18.8	0.042739616	0.00095	7.031E-10	-11.9714	-13.1176
.07M_Mg	0.0078	1.13129E-09	0.0736	1.33	18.07065	0.138209113	0.000959	6.92278E-10	-2.08476	-2.37656
.1sw_nat	0.0627	9.09381E-09	0.0366	0.685	18.71585	0.062715056	0.000952	7.00822E-10	-8.46042	-9.31214
.05SW_nat	0.1056	1.53159E-08	0.0219	0.415	18.94977	0.037794352	0.000949	7.03665E-10	-8.57503	-9.32178
FM_0.05M_Na	-0.0015	-2.1756E-10	0.2945	6.165	20.93379	0.769824789	0.001015	6.24896E-10	2.178343	2.14361
0.05	0.126	1.82746E-08	0.0263	0.485	18.44106	0.044101752	0.00095	7.02944E-10	-11.9777	-13.38
.11M_Mg	0.0047	6.81673E-10	0.095692	1.875	19.59414	0.201053454	0.000965	6.85248E-10	-1.80009	-1.8925
.14M_Mg	0.0029	4.20607E-10	0.1167	2.237	19.16881	0.246283339	0.000969	6.80233E-10	-1.3406	-1.44069
0.5sw_nat	0.0124	1.79846E-09	0.1401	2.75	19.62884	0.313228469	0.000975	6.7288E-10	-7.16759	-7.52222
SW	0.0056	8.12206E-10	0.259708	5.06	19.48341	0.623130282	0.001002	6.39904E-10	-6.43518	-6.80398
.5sw	0.013	1.88548E-09	0.14194	2.764	19.47302	0.315086652	0.000975	6.72677E-10	-7.55621	-7.99352
2so4_sw_nat	0.0064	9.28236E-10	0.2704	5.25	19.41568	0.648356261	0.001004	6.37296E-10	-7.67868	-8.14707
3so4_sw_nat	0.0066	9.57243E-10	0.291509	5.545	19.02171	0.687473609	0.001008	6.33274E-10	-8.44544	-9.14618
4so4_sw_nat	0.0065	9.42739E-10	0.2952	5.752	19.48509	0.71492208	0.00101	6.30468E-10	-8.6872	-9.18427
0.05_pMg	0.09	1.30533E-08	0.027	0.53	19.62963	0.048219629	0.00095	7.02474E-10	-9.35971	-9.8224
0.05M	0.119	1.72594E-08	0.025	0.5	20	0.045469253	0.00095	7.02788E-10	-11.6665	-12.0165
.1so4	0.12	1.74044E-08	0.0276	0.55	19.92754	0.050064069	0.000951	7.02264E-10	-12.957	-13.3942
.012M so4	0.107	1.55189E-08	0.032	0.66	20.625	0.060347942	0.000952	7.01091E-10	-13.9023	-13.8854
.02M so4	0.097	1.40686E-08	0.039	0.7762	19.90256	0.071432757	0.000953	6.9983E-10	-14.8659	-15.3868
2sw so4	0.0622	9.02129E-09	0.065	1.294	19.90769	0.134353305	0.000959	6.92712E-10	-16.1583	-16.7202
sw ca 2m	0.0014	2.03052E-10	0.61	12.7	20.81967	1.85353795	0.001133	5.25438E-10	-5.55959	-5.50093
2sw ca 2m	0.0011	1.59541E-10	0.61	12.81	21	1.87645046	0.001136	5.23544E-10	-4.43361	-4.34916
4sw ca 2m	0.0008	1.16029E-10	0.61	12.97	21.2623	1.909993016	0.00114	5.20786E-10	-3.29465	-3.19202
.11m ca 2m	0.0007	1.01526E-10	0.64	13.3	20.78125	1.979933145	0.001149	5.15092E-10	-3.01308	-2.9868

Table E.4. Multiphase Experiments results

Salinity, M	C_{EK}, mV/psi	C_{EK}, V/Pa	σ_{rf}, S/m	σ_b, S/m	FF	C, M/L	μ, Pa-s	ε, F/m	ζ, mV	ζ_c, mV
PA_mw_2M	0.0026	3.77096E-10	0.373	11.92	31.9571	1.694879831	0.001113	5.38784E-10	-9.28367	-10.1676
PB_mw_2M	0.0018	2.61066E-10	0.3557	11.88	33.39893	1.686937915	0.001112	5.39463E-10	-6.39191	-6.69832
P2_si_ww_2M	0.0016	2.32059E-10	0.4	12.05	30.125	1.720828497	0.001116	5.36574E-10	-5.81588	-5.79174
PS3_si_cr_2M	0.0036	5.22133E-10	0.1658	12.16	73.34138	1.742946036	0.001119	5.34698E-10	-13.2843	-13.5847
P2_si_mw_cr_2M	0.0031	4.49614E-10	0.1345	12.15	90.33457	1.740929355	0.001118	5.34869E-10	-11.4236	-11.1284
Pow1_cr_2M	0.0057	8.2671E-10	0.099	12.05	121.7172	1.720828497	0.001116	5.36574E-10	-20.7191	-20.0141
Pmw_cr_uss_2M	0.0027	3.91599E-10	0.252407	12.03	47.66108	1.716822854	0.001115	5.36914E-10	-9.78742	-9.24096
Pmw_cpa_uss_2M	0.0024	3.48088E-10	0.459	12.06	26.27451	1.722833146	0.001116	5.36403E-10	-8.73578	-8.64451
Pow1_cr_FMB	0.0031	4.49614E-10	0.118	14.9	126.2712	2.330870429	0.001198	4.87671E-10	-16.4595	-16.2276
PS3_si_cr_FM	0.002	2.90074E-10	0.2177	15.04	69.0859	2.36237792	0.001203	4.85302E-10	-10.8122	-10.9553
P101_OW_4.5AN_2M	0.0064	9.28236E-10	0.121	12.22	100.9917	1.755070982	0.00112	5.33673E-10	-23.8109	-21.4337
P101_OW_4.5AN_FMB	0.0024	3.48088E-10	0.169	14.6	86.39053	2.263768762	0.001189	4.92768E-10	-12.2579	-12.3418
Pa_CPA_FMB	0.0002	2.90074E-11	0.46	14.6	31.73913	2.263768762	0.001189	4.92768E-10	-1.02149	-1.06207
Pb_CPA_FMB	-0.0001	-1.4504E-11	0.43	14.6	33.95349	2.263768762	0.001189	4.92768E-10	0.510745	0.496402
Pmw_cpa_ussFM	-0.0002	-2.9007E-11	0.56	14.6	26.07143	2.263768762	0.001189	4.92768E-10	1.021489	1.018691
P101_ow_4.5AN_FMB	0.0026	3.77096E-10	0.163	14.88	91.28834	2.326379478	0.001198	4.8801E-10	-13.7692	-13.6258
P2_si_ww_FMB	-0.0003	-4.3511E-11	0.485	14.9	30.72165	2.330870429	0.001198	4.87671E-10	1.592859	1.555443
PS3_si_cr_FMB	0.0009	1.30533E-10	0.195	14.68	75.28205	2.281607621	0.001191	4.91407E-10	-4.64462	-4.75061
P2_si_mw_FMB	0.0013	1.88548E-10	0.16	14.6	91.25	2.263768762	0.001189	4.92768E-10	-6.63968	-6.54873
Pmw_cr_uss_FMB	0.0006	8.70221E-11	0.302	14.64	48.47682	2.272683197	0.00119	4.92087E-10	-3.08041	-3.05011
Pow1_FMB	0.0027	3.91599E-10	0.126	14.8	117.4603	2.308440756	0.001195	4.89368E-10	-14.1519	-14.6988
Pow1_sw	0.0083	1.20381E-09	0.06	5.29	88.16667	0.653662759	0.001005	6.36749E-10	-10.0474	-9.68655
P101_ow_4.5_sw	0.01	1.45037E-09	0.0551	5.1	92.55898	0.628444239	0.001002	6.39354E-10	-11.5976	-10.6504
Pow1_sw_r	0.0093	1.34884E-09	0.06	5.2	86.66667	0.641721331	0.001004	6.37981E-10	-11.0336	-10.8214
P101_ow_4.5_sw_R	0.007	1.01526E-09	0.058	5.2	89.65517	0.641721331	0.001004	6.37981E-10	-8.30485	-7.87364
P101_ow_4.5_0.5M_Na	0.0171	2.48013E-09	0.042	3.66	87.14286	0.435486225	0.000986	6.59663E-10	-13.565	-14.0098
pow1_.1sw	0.0576	8.35412E-09	0.0095	0.772	81.26316	0.071028601	0.000953	6.99876E-10	-8.77888	-9.18257
P101_ow_4.5_.1sw	0.0598	8.6732E-09	0.0092	0.783	85.1087	0.072087627	0.000953	6.99755E-10	-9.24666	-9.23485
p101_sw (2swso4)	0.0093	1.34884E-09	0.063	5.52	87.61905	0.684159425	0.001007	6.33614E-10	-11.837	-11.4831
pow1_sw (2swso4)	0.008	1.16029E-09	0.062	5.495	88.62903	0.680845243	0.001007	6.33954E-10	-10.1279	-9.71315